Understanding the Implications of Checkpoint Adaptation for Genome Stability and DNA Repair

Dissertation

zur Erlangung des Grades

Doktor der Naturwissenschaften

Am Fachbereich Biologie

der Johannes-Gutenberg-Universität Mainz

vorgelegt von

Olga Vydzhak

geboren am 12.02.1991

in Novoyavorivsk, Ukraine

Mainz, 2020

Dekan:

1. Berichterstatter:

2. Berichterstatter:

Tag der mündlichen Prüfung: 10 Juli 2020

Table of Contents

Table of Contents

List of Publications

Vydzhak O, Luke B, Schindler N. Non-coding RNAs at the eukaryotic rDNA locus: RNA-DNA hybrids and beyond [published online ahead of print, 2020 May 21]. *J Mol Biol. 2020;S0022-2836(20)30351-X.*

Vydzhak O*, Bender K*, Klermund J, Busch A, Reimann S, and Luke B. Checkpoint adaptation in repair-deficient cells drives aneuploidy and resistance to genotoxic agents. *Submitted.*

*shared first-autorship.

List of Publications

Summary

To study the relationship between checkpoint adaptation (CA), genotoxin resistance, and aneuploidy, I have employed yeast as a model system and generated homozygous diploid *rad52* deletion cells. These cells have a strong defect in homology-directed repair (HDR). Additionally, diploid budding yeast actively suppress their non-homologous end joining (NHEJ) pathway. Therefore, diploid *rad52* mutants are defective in HR and NHEJ. The diploid state of the mutant allowed us to study genomic instability that occurs following CA. Yeast Rad52 participates in Rad51 filaments assembly and ssDNA strand exchange, wich in mammalian cells is executed by the BRCA2. This allowed me to use *rad52* yeast mutants to model the response to genotoxins in BRCA2-deficient cancers.

Despite a strong DNA repair defect, *rad52* mutants were eventually able to form viable colonies following treatment with double-strand break-inducing genotoxins, X-rays and CPT (Figure 12). The colony formation required CA, as the re-growth of the adaptation-defective mutants was significantly impaired (Figure 12). These adapted colonies gained genotoxin resistance to the second round of genotoxic treatment (Figure 13). The adapted *rad52* mutants underwent drastic genome alterations and became aneuploid. In this work, I have further analysed the relationship between the ploidy and genotoxin resistance, and conclude that the near-haploid phenotype confers resistance to CPT and X-rays in *rad52* mutants.

So far, the aneuploidy-associated phenotypes in budding yeast were studied using controlled experimental systems. I aimed to exploit aneuploidy-associated physiological disadvantages in checkpoint-adapted cells. I have characterized the aneuploidy-associated phenotypes in HDR-defective mutants that became aneuploid following the genotoxic treatment. I show that these genotoxin-resistant *rad52* aneuploids can be targeted pharmacologically (Figures 19-24).

Furthermore, I employed the *rad52* model to determine genetic requirements for the DNA repair and genotoxin resistance formation in repair-defective cells. I have analysed genetically the involvement of the genes that belong to the *RAD52* epistasis group (Figure 26), and the genes required for the microhomology-medated end joining pathway in the post-adaptation DNA repair (Figure 30). I have found that the Mre11-Rad50-Xrs2 (MRX) complex confers the chemoresistance to CPT in naïve and checkpoint adapted *rad52* mutants (Figures 27-29). These results suggest that the inhibition of Mre11 could potentially sensitize HDR-deficient human cells to CPT. Together, my results provide a connection between CA, aneuploidization, and genotoxin resistance in HDR-deficient yeast model. This provides a rationale to target genotoxin resistant cells based on their aneuploidy-associated stresses, and the genetic requirements for the MRX complex for the DNA repair.

Summary

Zusammenfassung

Um den Zusammenhang zwischen Kontrollpunkt-Adaptierung („checkpoint adaptation“, CA), Genotoxin-Resistenz und Aneuploidie zu untersuchen, habe ich Hefe als Modellsystem genutzt und homozygot, diploide *rad52* Deletionsmutanten hergestellt. Diese Mutanten haben einen sehr großen Defekt in der Homologen Reparatur („homolgy-directed repair“, HR). Zusätzlich unterdrücken diploide, knospende Hefen die Nicht-homologe Endverknüpfung („non-homologous end joining“, NHEJ). Somit fehlt diploiden *rad52* Mutanten weitestgehend die Fähigkeit zu HR und NHEJ. Der diploide Zustand der Mutante erlaubte mir auch die genomische Instabilität nach CA zu untersuchen. Das Hefeprotein Rad52 partizipiert bei der Assemblierung von Rad51-Filamenten und beim Einzelstrang-DNA Austausch. Diese Funktionen werden in Säugerzellen von BRCA2 ausgeübt wird. Dies erlaubte mir *rad52* Hefemutanten als Modelsystem für BRCA2-negative Krebserkrankungen und die Antwort solcher Tumoren auf Genotoxine zu verstehen.

Trotz des starken DNA Reparaturdefektes konnten *rad52* Mutanten nach der Behandlung mit Röntgenstrahlung und CPT, was DNA-Doppelstrangbruch induzierende Genotoxinen sind, lebensfähige Kolonien ausbilden (Abbildung 12). Die Entstehung der Kolonien benötigte CA, weshalb das Wachstum von Adaptierung-defektiven Mutanten stark eingeschränkt war (Abbildung 12). Die ausgebildeten, adaptierten Kolonien waren bei einer zweiten Behandlung mit Genotoxin resistent (Abbildung 13). Die adaptierten *rad52* Mutanten erfuhren drastischen genomische Veränderungen und wurden aneuploid. In dieser Arbeit habe ich den Zusammenhang zwischen Ploidie und Genotoxin-Resistenz tiefergehend analysiert und schlussfolgere, dass ein fast-haploider Phänotyp die Resistenz gegen CPT und Röntgenstrahlen in *rad52* Mutanten vermittelt. Bisher wurden mit Aneuploidie zusammenhängende Phänotypen in der knospenden Hefe mittels kontrollierten experimentellen Systemen untersucht. Mein Ziel ist es die mit der Aneuploidie in Zusammenhang stehenden physiologischen Nachteile in Kontrollpunkt-adaptierten Zellen zu nutzen, um Krebstherapien zu entwickeln. Ich habe den aneuploiden Phänotyp der HR-defekten Mutanten charakterisiert, die nach einer Genotoxin Behandlung entstanden sind und davon aneuploid wurden. Ich zeige, dass diese Genotoxin-resistenten, aneuploiden *rad52* Zellen gezielt pharmakologisch bekämpft werden können (Abbildung 19-24).

Weiterhin habe ich das weitgehend Reparatur defekte *rad52* Model genutzt, um die genetischen Grundvoraussetzungen für DNA Reparatur und die Bildung der Genotoxin-Resistenz in diesen Zellen zu studieren. Ich habe genetisch untersucht inwiefern die Gene der *RAD52* Epistasisgruppe (Abbildung 26) und des MMEJ Weges (Abbildung 30) zur post-adaptiven DNA Reparatur beitragen. Ich habe herausgefunden, dass der MRX Komplex zur Chemoresistenz gegen CPT in

naiven und Kontrollpunkt adaptieren *rad52* Mutanten beiträgt (Abbildung 27-29). Diese Ergebnisse lassen darauf schließen, dass die Hemmung von Mre11 Potenzial hat, HR-defiziente Humanzellen gegen CPT zu sensibilisieren. Zusammenfassend zeigen meine Ergebnisse einen Zusammenhang zwischen CA, Aneuploidisierung und Genotoxin-Resistenz im HR-defizienten Hefemodel. Ich biete einen Ansatz, um Genotoxin-resistente Zellen auf der Grundlage des mit ihrer Aneuploidie zusammenhängenden Stresses anzugreifen und zeige die genetischen Notwendigkeiten des MRX-Komplex für die DNA Reparatur auf.

1. Introduction

Genomic integrity is constantly challenged by DNA damage that arises due to cellular metabolic processes, errors in DNA replication, and exogenous sources like UV irradiation and natural radioactivity. Therefore, cells have evolved elaborate pathways to detect and repair DNA damage, while coordinating these processes with DNA replication and cell cycle progression. A failure to repair DNA lesions due to either defects in DNA repair pathways or a difficult genomic context of the lesion, potentially results in genomic aberrations, aneuploidization, or cell death. In the introduction section, I will discuss the exogenous and endogenous sources of DNA damage, and how the repair of this damage is coordinated with cell cycle progression. I further discuss how aberrant cell cycle termination upon the DNA damage (checkpoint adaptation) induces genomic instability. I will continue with an overview of cellular states with high genomic instability, focusing on aneuploidy, and then connect the state with checkpoint adaptation and genotoxin resistance. Finally, I will discuss the mechanisms of genotoxin resistance in repair-defective tumors.

1.1 Endogenous and genotoxin-induced DNA lesions

DNA lesions arise constantly due to endogenous metabolic processes and exogenous naturally occurring sources that continuously challenge the integrity of our genome. Among them, the most mutagenic are single-strand breaks (SSBs) and double-strand breaks (DSBs), that occur with a frequency 55000 and twenty-five per cell per day, respectively (Tubbs and Nussenzweig, 2017). In this section, I will present an overview of different types of DNA lesions and their natural sources, as well as chemotherapeutic means to induce DNA damage.

1.1.1 Types of DNA lesions

DNA is a molecule composed of two polynucleotide strands that coil around each other to form a double helix. Each of the four nucleotides is composed of either a purine (guanine, G; adenine, A) or a pyrimidine (cytosine, C; thymine, T) base, a deoxyribose sugar, and a phosphate group. Multiple exogenous factors, such as UV light irradiation and radioactivity, and endogenously produced factors, such as reactive oxygen species (ROS), constantly damage cellular DNA (Lindahl and Barnes, 2000; Tubbs and Nussenzweig, 2017). It has been estimated that each human cell experiences approximately 70,000 lesions every day (Figure 1) (Lindahl and Barnes, 2000).

DNA SSBs are one of the most frequently occurring lesions, which account for approximately seventy-five percent of all DNA lesions (Tubbs and Nussenzweig, 2017). They arise as a result of spontaneous DNA base hydrolysis, due to the ROS-induced oxidative damage, or as a result of

abnormal topoisomerase activity of Top1 (Jakobsen et al., 2019). These lesions interfere with DNA replication and transcription processes, and could potentially be converted into deleterious DSBs (Cristini et al., 2019; Lin et al., 2020).

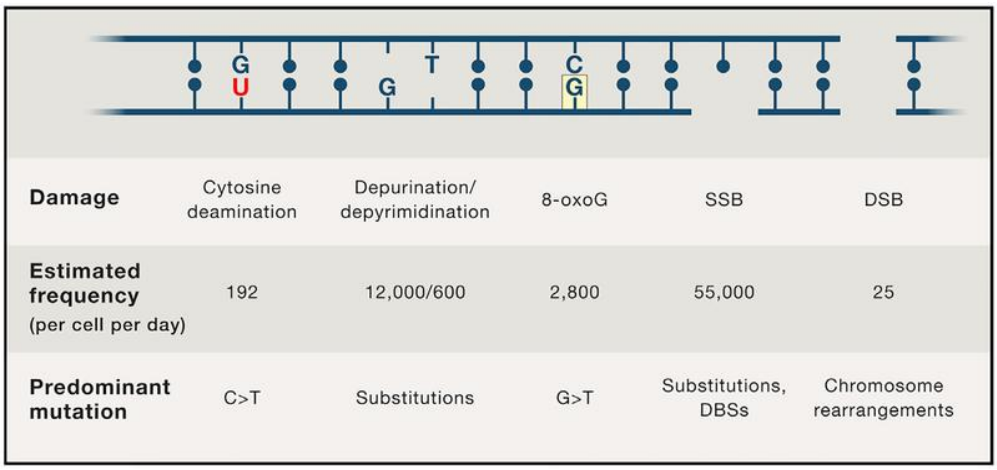

Damage	Cytosine deamination	Depurination/ depyrimidination	8-oxoG	SSB	DSB
Estimated frequency (per cell per day)	192	12,000/600	2,800	55,000	25
Predominant mutation	C>T	Substitutions	G>T	Substitutions, DBSs	Chromosome rearrangements

Figure 1. Different types of DNA lesions, their estimated frequency, and mutations associated with their abnormal repair. Of note, this estimation accounts for the human genome. Figure taken from (Tubbs and Nussenzweig, 2017).

DSBs are the most toxic DNA lesions that occur with an estimated frequency of twenty-five per cell per day (Tubbs and Nussenzweig, 2017). Spontaneously occurring DSBs can form as a result of natural radioactivity, conversion of a SSB into a DSB due to transcription or replication, replication stress, or abnormal SSB processing (Cristini et al., 2019; García-Muse and Aguilera, 2016). Programmed DSBs are formed by the expression of endonucleases and are utilized by cells to induce complex genomic changes during meiosis, mating type switch in yeast, and V(D)J recombination during B cell receptor development in humans (Coopera et al., 2016; Lee and Haber, 2015; Yeap and Meng, 2019). The mechanisms of DSB repair are summarized in section 1.5 of this thesis.

Spontaneous hydrolysis of the glycosidic bonds that connect DNA bases to the backbone, which occurs due to the aqueous environment of the nucleus, represent another source of DNA damage (Gates, 2009). This process results in depurination or depyrimidination, depending on the nucleotide base, which leads to the creation of abasic sites. Each cell experiences approximately 13,000 of these potentially mutagenic events daily (Tubbs and Nussenzweig, 2017). Abasic sites are repaired by the nucleotide excision repair (NER) pathway.

Hydrolytic deamination of DNA bases, which happens with a frequency of 200 events per cell daily, is another source of hydrolysis-induced DNA damage. The cytosine deamination reaction leads to the formation of a uracil residue, which is a potentially mutagenic source of the C to T

conversion. Deamination of guanine and cytosine residues, as well as methylcytosine residues, represent another potential source of base substitutions (Gates, 2009). The mismatch repair pathway (MMR) targets these deaminated residues, thereby preventing base substitutions (Tubbs and Nussenzweig, 2017).

ROS, which are generated as metabolic by-products in the mitochondria, can cause oxidative damage to virtually all cell molecules, including DNA. The ROS-induced lesions include purine 5′,8-cyclonucleosides, DNA intra- and interstrand crosslinks, and DNA-protein crosslinks (reviewed in (Lee and Kang, 2019)). The oxidation of guanine leads to the formation of 8-oxoG, which can pair with adenine and generate G to T conversions (Tubbs and Nussenzweig, 2017). The 8-oxoG lesion is repaired by DNA glycosylases OGG1 and MUTYH (Majumdar et al., 2018; Sampath and Lloyd, 2019). 5′,8-cyclo-2′-deoxyadenosine (cdA) and 5′,8-cyclo-2′-deoxyguanosine (cdG) are other oxidative DNA lesions that occur rather frequently in cells, and are repaired by the NER pathway (Krokidis et al., 2017). The ROS-induced intra- and interstrand crosslinks, as well as DNA-protein crosslinks are extremely dangerous DNA lesions that block transcription and DNA replication (Stingele et al., 2017). These hard-to-repair lesions are processed by NER members XPA, XPG, and XPF, and then further repaired by either translesion synthesis polymerases or the homology-directed repair pathways (Enoiu et al., 2012). It is important to note that DNA and DNA-protein cross-links are not exclusively induced by ROS, but also by UV light and multiple chemotherapeutic drugs (Andreassen and Ren, 2009).

The non-enzymatic methylation of DNA bases is another source of DNA damage. The methyl group donor S-adenosylmethionine can serve as an endogenous donor for the spontaneous methylation of adenine, which leads to the formation of 3´-methyladenine, a strong replication impediment (reviewed in (Lindahl, 1993)). Another potentially mutagenic base amination reaction leads to the formation of O^6-methylguanine, which also impairs DNA replication (Warren et al., 2006).

1.1.2 Genotoxic drugs induce DNA lesions

Tumor cells are actively replicating their DNA, while frequently harboring mutations in key DNA repair and DNA damage checkpoint genes. Therefore, targeting tumor cells using DNA damaging agents is a widespread strategy in clinics (Hurley, 2002). Mechanistically, the genotoxic agents used in cancer treatment interfere with DNA replication, modify DNA bases, or directly cause DNA SSBs and DSBs.

One class of genotoxins that block DNA replication include alkylating agents, such as nitrogen mustards, nitrosourea, and temozolomide. These agents induce DNA bases' alkylation and lead to the formation of DNA intra- and interstrand crosslinks, as well as DNA-protein crosslinks

(reviewed in (Diethelm-Varela et al., 2019) and (Swift and Golsteyn, 2014)). Widely used in cancer therapy, platinum drugs, such as cisplatin and oxaliplatin, similarly block DNA replication by inducing DNA intra- and interstrand crosslinks, and DNA-protein crosslinks (reviewed in (Swift and Golsteyn, 2014)).

Another class of DNA replication inhibitors, which includes hydroxyurea, affects ribonucleoside diphosphate reductase (RNR), thereby limiting *de novo* DNA synthesis (Madaan et al., 2012). Gemcitabine is another RNR inhibitor commonly used in cancer therapy, and its mechanism of action is not limited to the reductase inhibition (Mini et al., 2006). The RNR inhibition leads to the depletion of deoxyribonucleotide (dNTP) pools necessary for DNA synthesis, which therefore leads to replication stress and subsequent replication forks collapse (Poli et al., 2012).

Antimetabolites is a class of genotoxic agents that mimic the chemical structure of nucleotides and exhibit genotoxin activity by either inhibiting nucleotide biosynthesis or by misincorporation into nucleic acids (Huehls et al., 2016; Swift and Golsteyn, 2014). 5-Fluorouracil is an antimetabolite commonly used in cancer therapy. The drug exhibits its genotoxic activity in a dual way: it is metabolically converted both into thymidine synthase inhibitor FdUMP and into FdUTP, the latter is misincorporated into DNA. Treatment with 5-Fluorouracil results in an impairment of DNA replication, cell cycle arrest, and activation of the HR pathway (Huehls et al., 2016).

A variety of anticancer genotoxins do not impair DNA replication, but rather act directly via the induction of DNA damage. For example, bleomycin, a commonly used radiomimetic drug, directly induces SSBs, DSBs, and abasic sites (reviewed in (Bolzán and Bianchi, 2018)). The direct delivery of DNA damage using ionizing radiation and inducing DSBs by inhibiting topoisomerases are other strategies commonly used in clinics. I will discuss their mode of action in more detail in sections 1.1.2.1 and 1.1.2.2 below, as they are two major genotoxin treatments used in this study.

1.1.2.1 The mode of action of Camptothecin

Topoisomerases are evolutionarily conserved enzymes that carry out the essential function of relaxing DNA supercoiling. There are two major types of topoisomerases, which are differentiated based on their mechanism of action: type I topoisomerases relieve topological stress by transiently nicking one strand of the DNA, allowing strand rotation, and resealing the break; the type II topoisomerases induce a transient DSB, transport another DNA stretch through the break and reseal the DSB (reviewed in (Pommier, 2006)). Type I topoisomerases are further subdivided into two classes based on the site of the break to which the cleavage complex (cc) becomes covalently bound: type 1A topoisomerases form 5′-DNA tyrosyl adducts, while type 2A topoisomerases form 3′-DNA tyrosyl adducts (reviewed in (Pommier, 2006)). DNA topoisomerases are essential for

cellular processes of transcription and replication, as their inactivation leads to the accumulation of DNA supercoiling. The budding yeast genome harbors three genes that encode for topoisomerases: *TOP1* encodes for the type IB topoisomerase, *TOP2* encodes for type II enzyme, while *TOP3* encodes for type IA enzyme (reviewed in (Pommier, 2009)).

Camptothecin (CPT) is a natural compound that was isolated from the *Camptotheca acuminata* tree (Wall and Wani, 1995). CPT has only one cellular target: the type IB enzyme Top1 (Eng et al., 1988). Top1 executes DNA relaxation the following way: first, it carries out a transesterification reaction, in which catalytic tyrosine becomes covalently bound to the DNA 3' end (forming the Top1-cleavage complex, Top1-cc), resulting in DNA nicking; second, the enzyme allows the controlled rotation of the nicked strand around the intact strand; finally, the "nicking-closing reaction" leads to SSB ligation (Pommier, 2006). CPT is a Top1 poison that intercalates between DNA and Top1-cc, and stabilizes the latter, thereby also stabilizing otherwise transient SSB (reviewed in (Pommier et al., 2010)). The trapped Top1-cc leads to DSBs when the replisome hits Top1-cc during DNA replication (Figure 2). The DNA damage can also arise when Top1-cc collides with the RNA polymerase complex during transcription (reviewed in (Pommier, 2006)). Because these collisions with the replication machinery lead to the majority of CPT-induced DNA damage, CPT is considered an S-phase drug.

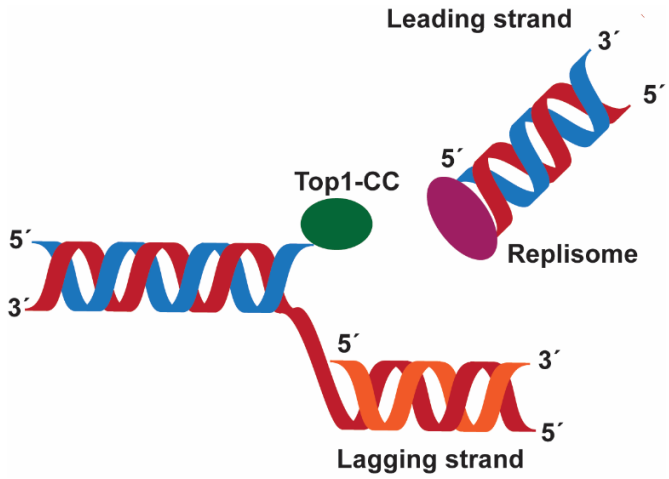

Figure 2. The replication-dependent generation of DSBs by CPT. Top1 is trapped on the leading strand by CPT. The leading strand polymerase synthesizes the nascent DNA strand up to Top1-cc, which results in the generation of a DSB. This figure is modified from (Pommier, 2006).

Although CPT is not used as cancer treatments due to the low stability of the drug and its high toxicity (Wall and Wani, 1995), different CPT derivatives (topotecan and irinotecan) are used clinically, while many non-CPT Top1 inhibitors (indenoisoquinolines) are being actively developed (reviewed in (Pommier, 2006) and (Pommier et al., 2018)).

1.1.2.2 The mode of action of X-Ray treatment

X-rays are a source of various types of single and clustered DNA lesions. Therefore, they are frequently used in clinically for targeted delivery of DNA damage (reviewed in (Sage and Shikazono, 2017)). X-rays are a type of ionizing radiation and the DNA damage produced by X-rays comes from the generation of ROS due to water radiolysis in DNA proximity, as well as from direct energy transfer to DNA molecules. In contrast to endogenous oxidative DNA damage, ionizing radiation-induced DNA damage is frequently more complex in its nature (reviewed in (Sage and Shikazono, 2017)). X-rays induce abasic sites, DNA base damages, SSBs, DSBs, intra- and interstrand crosslinks, DNA-protein crosslinks, and complex bulky lesions that are comprised of combinations of the aforementioned lesions within one or two DNA helix turns. These complex lesions could be further subdivided into DSB clustered lesions that carry DSBs and multiple base damages in proximity to each other and non-DSB clustered lesions that can have multiple SSBs, abasic sites, or other types of lesions in close proximity. Following X-ray treatment, complex lesions occur three to four times more frequently than DSBs (reviewed in (Sage and Shikazono, 2017)). X-ray-induced DNA damage includes cross-links DNA with chromatin-associated proteins, such as histones, which creates obstacles for DNA transcription and replication and leads to DNA damage (reviewed in (Nakano et al., 2017)). Both complex DNA lesions and bulky DNA-protein crosslinks are extremely difficult to repair; therefore, treatment with high dosages of X-rays induces genomic instability, senescence, and cell death in repair-deficient cells (Mortimer et al., 1981; Sage and Shikazono, 2017).

1.2 DNA damage checkpoints

In response to DNA damage, cells elicit elaborate signaling cascades that halt the cell cycle progression and allow time to repair the damage, known as a DNA damage checkpoint (DDC). The DDC is orchestrated by two key phosphatidyl inositol 3' kinase-related kinases (PIKK) checkpoint kinases, Mec1^{ATR} and Tel1^{ATM}. Checkpoint signaling cascades are highly conserved across organisms, from yeast to humans. The DDC operates via the apical checkpoint kinases, their effector kinases, and multiple adaptor proteins that modulate the signaling cascade (reviewed in (Lanz et al., 2019)). The onset of the DDC results not only in cell cycle arrest, but also in regulation of dNTP pools, cellular transcriptome changes, repression of replication initiation, and many other physiological aspects. Budding yeast have two DDCs: the intra-S checkpoint that is activated in response to replication stress and the G2/M checkpoint that is activated by DSBs or dysfunctional telomeres. The DDCs are crucial for the maintenance of genome stability, as mutations in DDC genes are frequently found in cancers (Smith et al., 2010). In this section, I will present an overview of DDCs in budding yeast, with focus on DNA damage checkpoint proteins, intra-S and G2/M checkpoint signaling cascades, transcription response during the DDC, and the checkpoint recovery.

1.2.1 DNA damage checkpoint proteins

The DDC signaling in *Saccharomyces cerevisiae* is elicited by two apical checkpoint kinases that belong to the PIKK family, Mec1^{ATR} and Tel1^{ATM}. The activated kinases elicit a signaling cascade that involves multiple evolutionarily conserved proteins, whose major functions are summarized in Table 1 (modified from (Hustedt et al., 2013)).

Table 1. Key DDC proteins and their function (modified from (Hustedt et al., 2013)).

Protein or protein complex in *S. cerevisiae*	**Protein or protein complex homolog / orthologue in *H. sapiens***	**Major checkpoint function**
Ddc1-Rad17-Mec3 (9-1-1 complex)	RAD9-RAD1-HUS1	DNA damage checkpoint clamp that activates Mec1 (Parrilla-Castellar et al., 2004)
Rad24-RFC	RAD17-RFC	Loads the 9-1-1 checkpoint clamp onto the DNA (Majka et al., 2006)
Mre11-Rad50-Xrs2 (MRX complex)	MRE11-RAD50-NBS1 (MRN complex)	DSB recognition, Tel1^{ATM} recruitment (Clerici et al., 2004)
Dpb11	TOPBP1	Activation of Mec1^{ATR} (Navadgi-Patil and Burgers, 2009)
Dna2	DNA2	S-phase specific activation of Mec1^{ATR} (Kumar and Burgers, 2013)

Protein or protein complex in *S. cerevisiae*	**Protein or protein complex homolog / orthologue in *H. sapiens***	**Major checkpoint function**
Ddc2	ATRIP	Recruitment and activation of Mec1^{ATR} (Zou and Elledge, 2003)
Mec1	ATR	Apical checkpoint signaling kinase (Sanchez et al., 1996)
Tel1	ATM	Apical checkpoint signaling kinase (Morrow et al., 1995)
Chk1	CHK1	Checkpoint effector kinase (Furnari et al., 1997)
Rad53	CHK2	Checkpoint effector kinase (Allen et al., 1994)
Dun1	-	Checkpoint effector kinase (Zhou and Elledge, 1993)
Mrc1	Claspin	Replication fork associated checkpoint mediator that activates Rad53 (Alcasabas et al., 2001)
Rad9	53BP1, BRCA1	Checkpoint mediator that activates Rad53 (Weinert and Hartwell, 1988)

1.2.2 DNA damage checkpoint cascades

1.2.2.1 G2/M phase checkpoint

DNA damage, such as DSBs or unprotected telomeres, induce the activation of a DDC that arrests cells at the G2/M border (Klermund et al., 2014). The DDC is activated by two different DNA structures: DSBs with blunt ends activate Tel1 kinase, while, the resected 3' overhangs coated by the replication protein A (RPA) complex activate Mec1 (reviewed in (Oh and Symington, 2018)) (Figure 3). When a DSB occurs, it is rapidly bound by the Yku proteins and the Mre11-Rad50-Xrs2 (MRX) complex, which recruits and activates the Tel1^{ATM} checkpoint kinase (Cassani et al., 2019; Iwasaki et al., 2016). If the DSB is resected by the coordinated action of the MRX complex together with Exo1 and Dna2 helicases, the ssDNA becomes rapidly bound by the RPA complex, which consists of Rfa1, Rfa2, and Rfa3 subunits. This 3´ ssDNA overhang coated with RPA is a DNA structure that triggers the recruitment and activation of the Mec1-Ddc2 complex (Nakada et al., 2005; Saldivar et al., 2017). The following checkpoint proteins mediate the activation of Mec1: the Ddc1-Rad17-Mec3 (9-1-1 complex), the Dpb11 proteins, and the Dna2 proteins. The Rad24-RFC complex recognizes the ds-ssDNA junction and loads the checkpoint clamp-shaped complex that consists of Ddc1, Rad17, and Mec3 (9-1-1 checkpoint clamp) (Majka et al., 2006). The 9-1-1 checkpoint clamp recruits Dpb11, which is important for further Mec1 activation (Mordes et al., 2008).

The activated Mec1 and Tel1 kinases phosphorylate their downstream effector kinases, Rad53 and Chk1 (Figure 4a) (reviewed in (Lanz et al., 2019)). The Rad53 kinase is activated by the Mec1 kinase with the assistance of the Rad9 checkpoint adaptor protein, which is recruited to the DNA damage site by H2A-S129P and H3-K79Me histones, and serves as a scaffold for an efficient Rad53 autophosphorylation (Downs et al., 2000; Giannattasio et al., 2005; Ma et al., 2006). The full activation of Rad53 kinase activity requires phosphorylation by Mec1 together with multiple autophosphorylation events (Chen et al., 2017; Sanchez et al., 1996; Sun et al., 1996). The fully activated Rad53 kinase phosphorylates its downstream checkpoint kinase Dun1, a key regulator of cellular dNTP pools (Zhao and Rothstein, 2002). The activation of Chk1 effector kinase by Mec1 kinase also requires the Rad9 adaptor. Chk1 activation is modulated by cyclin-dependent kinase (CDK) phosphorylation of Rad9 in the S and G2/M phases of the cell cycle (Abreu et al., 2013; Blankley and Lydall, 2004). The activated checkpoint effector kinases Rad53, Chk1, and Dun1 phosphorylate their multiple downstream targets, which elicit DNA damage checkpoints. I discuss how cells halt the cell cycle progression and how the transcriptome is altered during the DDC onset in sections 1.2.3 and 1.2.4 respectively.

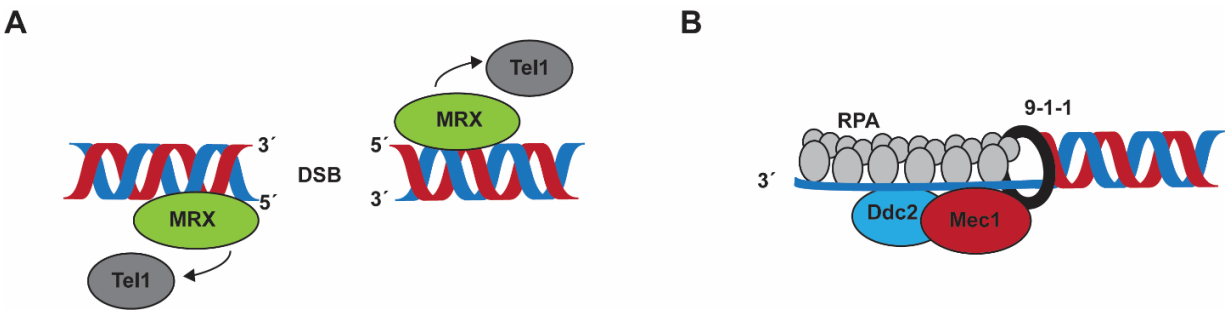

Figure 3. DNA structures that activate Tel1 and Mec1 checkpoint kinases. (a) Following the DSB formation, the break sites recruit the MRX complex, which is responsible for the recruitment and activation of the Tel1 checkpoint kinase. **(b)** When the DSB is resected, the 3´ DNA overhang is coated with the trimeric RPA complex. The ds-ssDNA junction recruits the 9-1-1 complex. Together, the RPA and 9-1-1 complexes recruit the Ddc2 checkpoint adaptor in complex with the Mec1 checkpoint kinase, which is activated at the structure. This figure is modified from (Oh and Symington, 2018).

In budding yeast, although Mec1 and Tel1 cooperate during the checkpoint activation, Mec1 seems to play a major role in the DDC. The fact that Mec1 and Tel1 are activated in response to different DNA structures suggests that the nature of a DSB can influence the degree of engagement of each kinase in the DDC (reviewed in (Gobbini et al., 2016). Tel1 hyperactivation can elicit Mec1-independent checkpoints when several DSBs are induced. When Mec1 is active, Tel1 positively regulates the resection of DSBs and further enforces Mec1 activation (Mantiero et

al., 2007). However, the deletion of the *TEL1* gene does not result in a strong checkpoint defect or sensitivity to genotoxins, while the deletion of the *MEC1* gene does (Mantiero et al., 2007). Despite the relatively minor role of the Tel1 kinase in the DDC in yeast, it is clear that the optimal DDC is achieved when Mec1 and Tel1 cooperate.

1.2.2.2 Intra-S phase checkpoint

The intra-S phase checkpoint, also known as a DNA replication checkpoint, is a surveillance mechanism that is activated upon the replication slow down or block. The intra-S checkpoint is an important mechanism that ensures faithful DNA replication (reviewed in (Hustedt et al., 2013)). The intra-S checkpoint is activated when the cell harbors long stretches of ssDNA that are coated by the RPA complex (Cortez, 2005; Hustedt et al., 2013). The ds-ssDNA junction structure is critical for the intra-S checkpoint activation (MacDougall et al., 2007). Long stretches of RPA-coated ssDNA can be generated by uncoupling the replicative MCM2-7 helicase complex from the DNA polymerase upon fork stalling (Cortez, 2005). Nucleotide excision repair and DSB resection also generate RPA-coated ssDNA structures that can trigger the intra-S phase checkpoint (Huang et al., 1992; Marini et al., 2019). The intra-S checkpoint is only initiated when a critical number of replication forks are stalled, indicating the presence of an S-phase-specific threshold (Shimada et al., 2002).

The intra-S phase checkpoint is elicited via an intricate cascade that ultimately results in Mec1 hyperactivation (Figure 4b) (reviewed in (Hustedt et al., 2013)). Similarly to the resected DSB ends, the long stretches of ssDNA and the ds-ssDNA junction recruit the 9-1-1 checkpoint clamp and Dpb11, which activate Mec1 (Navadgi-Patil and Burgers, 2009). At the same time, RPA-coated ssDNA tails serve as a recruitment signal for Ddc2, which is a critical event for Mec1 kinase activation (Zou and Elledge, 2003). Dna2 also facilitates Mec1 activation during the S-phase independent of its nuclease and helicase activity (Wanrooij and Burgers, 2015). These aforementioned events lead to the recruitment and hyperactivation of a key apical checkpoint kinase, Mec1, which is normally already active during unperturbed replication (Randell et al., 2010). The hyperactivated Mec1 further phosphorylates its downstream targets, Chk1 and Rad53. The activation of the Rad53 kinase is facilitated by two checkpoint mediators, Rad9 and Mrc1 (Bacal et al., 2018; Berens and Toczyski, 2012; Sweeney et al., 2005). Mrc1 is a replisome component that recruits Rad53 upon the replication fork stalling and promotes Rad53 activation by Mec1 (Katou et al., 2003). The Rad53 kinase is activated via an adaptor protein, Rad9, in response to DNA damage and via Mrc1 in response to replication stress.

The activated effector kinases, Rad53 and its downstream checkpoint kinase, Dun1, phosphorylate their multiple downstream targets and halt cell cycle progression. The checkpoint

leads to cell cycle arrest, giving the cell time to repair the DNA damage, and it simultaneously regulates the rates of origin firing, preventing the depletion of essential replication factors (reviewed in (Hustedt et al., 2013)). The intra-S phase checkpoint also elicits a transcriptional response, which is described in section 1.2.3.

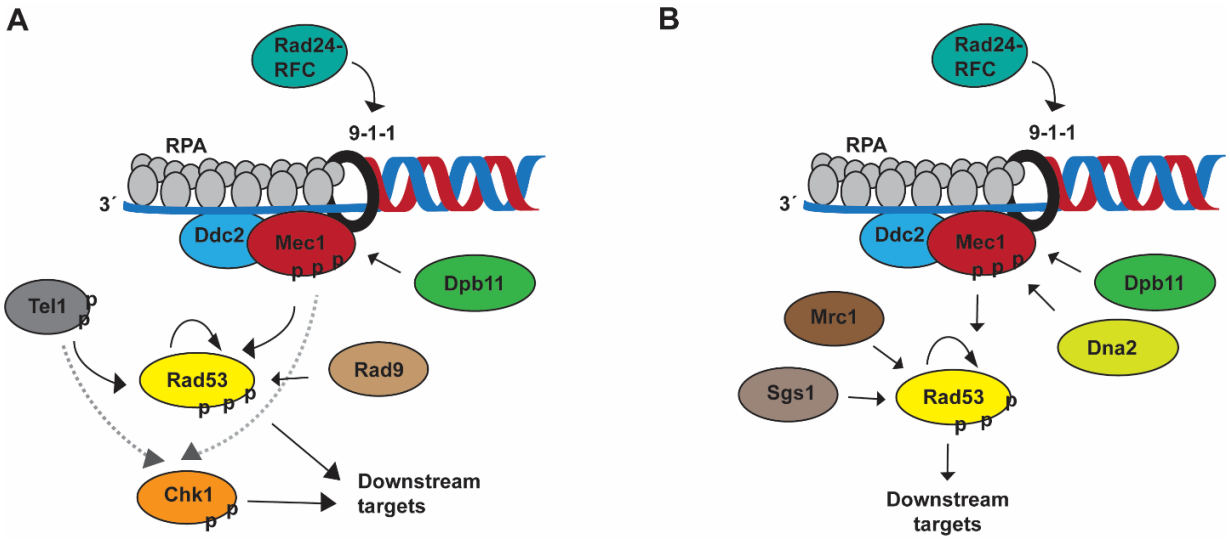

Figure 4. The G2/M and intra-S phase checkpoint signaling cascades. (a) The G2/M checkpoint signaling cascade is elicited in response to DSBs. Mec1 and Tel1 apical checkpoint kinases are recruited to the damage site and activated via hyperphosphorylation events. Mec1 is recruited by ssDNA-RPA structures and its full activation requires a Dpb11 adaptor. Both Mec1 and Tel1 phosphorylate downstream checkpoint kinases Rad53 and Chk1. The efficient Rad53 phosphorylation requires the adaptor protein Rad9. Chk1 and Rad53 kinases phosphorylate their downstream targets to elicit the DDC responses. **(b)** The intra-S phase checkpoint is elicited in response to replication stress and DSBs in the S phase. Mec1 is recruited to the ssDNA-RPA structures and its activation requires the adaptor proteins Dpb11 and Dna2. Mec1 phosphorylates Rad53, and Mrc1 and Sgs1 adaptor proteins assist with its activation. Rad53 phosphorylates its multiple downstream targets, which results in the DDC onset. p, phosphorylation. This figure is modified from (Hustedt et al., 2013).

1.2.3 Cell cycle control by checkpoints

Checkpoints lead to a cell cycle arrest, which ensures that the cell does not divide when DNA damage is unrepaired. The two major effector kinases, Chk1 and Rad53, coordinate the cell cycle arrest during the checkpoint. The cell cycle cessation at the G2/M border is achieved by inhibiting the only cyclin-dependent kinase in yeast, $Cdc28^{CDK}$, via multiple parallel mechanisms, and simultaneously inhibiting the onset of anaphase. In order to promote the cell cycle progression, Cdc25 phosphatase removes the inhibitory phosphorylation of Cdc28 on T19, as shown by studies in fission yeast, *Schizzosaccharomyces pombe,* and human cells (Furnari et al., 1997; Raspelli et al., 2015; Sanchez et al., 1997). Following DNA damage, Cdc25 is inhibited by

Chk1, thereby leading to an indirect inhibition of Cdc28 and cell cycle progression (Furnari et al., 1999; Zeng et al., 1998). In budding yeast, the Cdc25 homologue Mih1 also targets Cdc28; however, this happens during the morphogenesis checkpoint rather than the DDC (Sia et al., 1996). Cdc28 regulation in response to intra-S DDC in budding yeast is executed by the Swe1 kinase, which, when activated by the Rad53 and Mec1 kinases, phosphorylates Cdc28 (Palou et al., 2015). Importantly, Rad53 additionally phosphorylates Cdc28 upon genotoxic stress conditions, thereby inactivating Cdc28 in parallel to Swe1 (Palou et al., 2015).

In addition to Cdc28 inhibition, budding yeast checkpoints lead to the inhibition of anaphase onset and the mitotic exit network (MEN). First, Chk1 phosphorylates securin Pds1, which leads to the stabilization of the protein and the prevention of sister chromatid separation (Wang et al., 2001). Additionally, Rad53 inhibits a polo-like kinase, Cdc5, which halts MEN, because it prevents Cdc5-mediated phosphorylation of the MEN protein, Bfa1 (Sanchez et al., 1999; Valerio-Santiago et al., 2013). Rad53 can also regulate MEN in a Cdc5-independent pathway, by negatively regulation of the Tem1 kinase, which is a positive regulator of the mitotic exit (Liang and Wang, 2007). Together, Rad53 and Chk1 effector kinases ensure cell cycle arrest during the DDC.

1.2.4 Transcriptional response to DNA damage in yeast

The activation of either intra-S or G2/M checkpoints elicits dramatic transcriptional changes that lead to either repression or activation of different subsets of genes, aiming to coordinate the DNA repair with the cell cycle progression. In budding yeast, the transcriptional response to DNA damage is orchestrated by the apical checkpoint kinases Mec1 and Tel1, together with their downstream effector kinases Chk1, Rad53, and Dun1 (Jaehnig et al., 2013). In mammalian cells, DNA damage also elicits a similar transcriptional response that is orchestrated by ATM and ATR checkpoint kinases (reviewed in (Silva and Ideker, 2019)). In yeast, Mec1 is the major apical kinase that induces transcriptional changes in response to DNA damage, while Tel1 plays only a minor role. Downstream of Mec1, the Rad53 kinase activates another checkpoint kinase, Dun1 (Bashkirov et al., 2003), and these kinases orchestrate both Dun1-dependent and Dun1-independent transcriptional responses (Jaehnig et al., 2013). The transcriptome profiles differ depending on the DNA damaging agent used; for example, the changes following treatment with X-rays or methyl methanesulfonate (MMS) (Gasch et al., 2001) are not identical to the ones following treatment with radiomimetic drugs (Fry et al., 2006). Yet, the majority of transcriptional alterations overlap between the conditions.

The activation of intra-S DDC happens during replication stress, which can be induced by treatment with the replication inhibitor hydroxyurea. Under replication stress conditions, the activation of Rad53 checkpoint kinase leads to an inhibition of Nrm1, resulting in a prolonged

transcription of G1-specific genes, particularly MluI cell cycle box binding factor (MBF) targets. The MBF targets that are involved in DNA replication and nucleotide biosynthesis are upregulated ((De Oliveira et al., 2012; Travesa et al., 2012), reviewed in (Silva and Ideker, 2019)). The activated checkpoint kinases Chk1 and Rad53 also put an inhibitory phosphorylation on Ndd1 transcription factor, thereby repressing the transcription of the G2/M transcription cluster (*CDC5*, *CDC20*, *CLB1* and *CLB2* genes) (Yelamanchi et al., 2014). The transcriptional repressor Crt1 is another cellular target of the Rad53 kinase (together with Dun1) under DNA damage conditions (Huang et al., 1998; Zaim et al., 2005). When Ctr1 is phosphorylated by Rad53, the cellular transcription of ribonucleotide reductase genes (RNR) is upregulated to support cellular deoxyribonucleotide triphosphate (dNTP) pools. The activation of transcriptional responses at the intra-S checkpoint is important to support the cellular viability during DNA damage and to efficiently resume DNA replication.

The activation of G2/M checkpoints in response to DNA damage also leads to drastic changes in the cellular transcriptome, similarly to many other environmental stress responses. As a part of their transcriptional responses, cells generally inhibit RNA synthesis and ribosomal biogenesis (Gasch et al., 2000, 2001). The G2/M checkpoint activation upon treatment with alkylating agent MMS results in the differential expression of more than 900 genes. Among them, the genes that are involved in DNA repair, dNTPs biosynthesis and autophagy were upregulated, while genes involved in cell cycle progression and ribosomal biogenesis were downregulated (Jaehnig et al., 2013). It is important to note that the transcriptional responses to DNA damage that elicit either the intra-S checkpoint or the G2/M checkpoint seem to induce similar transcriptome changes, such as the upregulation of G1-specific genes, the downregulation of G2 transcription cluster, and the repression of ribosome biogenesis.

1.2.5 Checkpoint recovery

When DNA repair is successfully completed, cells terminate their DDC in order to resume cell cycle progression, which is known as a checkpoint recovery. A failure to terminate the DDC leads to permanent cell cycle arrest and cell death (Clerici et al., 2001). During the checkpoint recovery, both chromatin remodeling and dephosphorylation of checkpoint targets are key processes. The checkpoint recovery processes have been studied less extensively compared to DDC activation, and are therefore not yet fully understood.

Chromatin remodeling is extremely important during checkpoint recovery. The acetylation of histone H3 on K56 by histone acetyltransferase Rtt109 is the signal indicating the successful completion of DNA repair and also likely marks the start of the checkpoint recovery cascade (Chen et al., 2008). The dephosphorylation of histone H2A-S129P by the phosphatase Pph3, a subunit

of protein phosphatase 4 complex (PPH4), is crucial for the checkpoint recovery process (Keogh et al., 2006). Histone modifications are also involved in the control of Rad53 kinase activity. The phosphorylation of the histone H4-T80P leads to the recruitment of the Slx4-Rtt107 complex–an event that tips the balance towards the checkpoint recovery (Millan-Zambrano et al., 2018). Together with H4-T80P, the phosphorylated histone H2A-S129P interacts with the Slx4-Rtt107 complex, which counteracts Rad9-assisted Rad53 autophosphorylation, leading to the attenuation of the checkpoint (Cussiol et al., 2015; Ohouo et al., 2013). The chromatin remodeling complex, INO80, plays a role in the recovery from replication fork stalling, and the different mutants of the INO80 complex display defective resumption of replication following replication stress (Shimada et al., 2008). The loss of the DNA helicase Srs2 renders cells defective in the checkpoint recovery (Vaze et al., 2002). This happens due to the defective removal of Rad51 filaments and the chromatin persistence of Dpb11, which promotes checkpoint signals (Yeung and Durocher, 2011). Rad53 dephosphorylation is a key event that is required for checkpoint recovery following DSB repair, and for the resumption of replication during the recovery from replication stress (Clerici et al., 2001). The checkpoint recovery processes involve the action of multiple phosphatases, as DDC is a phosphorylation-mediated process. Rad53 is dephosphorylated by PP2C phosphatases, Ptc2 and Ptc3 (Leroy et al., 2003; Marsolier et al., 2000). Upon replication stress recovery, Rad53 is dephosphorylated by the Pph3-Psy2 phosphatase complex, which allows replication forks to restart (O'Neill et al., 2007). Curiously, phosphatases also play a role in DSB repair, as a deletion of all three phosphatases (Ptc2, Ptc3, Pph3) results in homologous recombination defect, characterized by a lack of repair-mediated DNA synthesis (Kim et al., 2011). The exact targets of these phosphatases and the order with which they dephosphorylate their targets during the checkpoint recovery has not yet been elucidated, to my knowledge.

1.3 Adaptation to the DNA damage checkpoint

When cellular genomic integrity is challenged with DNA damage, the cell elicits the DDC in order to repair the lesion before cell division occurs. When the lesion is successfully repaired, the cell terminates the DDC and resumes division. However, mitosis can occur also with unrepaired DNA damage, which is known as checkpoint adaptation (CA). CA happens either when the cell has mutations in the DNA repair genes and is repair-defective, or when the DNA damage is irreparable due to its nature, for example the deprotected telomeres. In this section, I discuss the molecular mechanisms of CA.

1.3.1 Checkpoint adaptation: not simply a checkpoint termination

The term “adaptation” describes a state when the initial stimulus becomes tolerable, or when the population changes in order to match its new environment. An adaptation to the DDC happens when the cell divides with unrepaired DNA damage because the checkpoint is overridden by proliferation signals. An adaptation to the DDC reflects this definition: when the cell adapts to the DNA damage-signaling stimuli, it tolerates them and continues the division. Although CA was initially described in budding yeast that had an irreparable loss of a telomere on a non-essential chromosome, the process is conserved in higher eukaryotes (Sandell and Zakian, 1993). The adaptation to the replication checkpoint was described in the egg extract of *Xenopus laevis* (Yoo et al., 2004). CA was also reported in human cell lines in response to treatment with X-rays and cisplatin (Swift and Golsteyn, 2016; Syljuåsen et al., 2006).

What is the difference between DDC termination and CA in terms of molecular mechanisms? DDC termination and CA seem to utilize the same molecular machinery. Yet, during checkpoint recovery, following the repair of DNA damage, an intricate cascade of phosphatases and chromatin remodelers fully reverse the modifications that happened during DDC activation (see section 1.2.5). During the adaptation process, the effector checkpoint kinases Chk1 and Rad53 are dephosphorylated, similarly to the checkpoint recovery scenario (Clémenson and Marsolier-Kergoat, 2009; Pellicioli et al., 2001). Yet, in the adaptation-promoting conditions of Cdc5 overexpression, the upstream checkpoint machinery, namely the 9-1-1 complex and Ddc2-Mec1 complex, are properly localized (Vidanes et al., 2010). This indicates that the adaptation can be triggered at the effector kinase level without affecting the apical players, which differs from the checkpoint recovery. However, recent work from the Haber lab demonstrated that Mec1-S1964-P autophosphorylation and Ddc2 degradation are the upstream events in CA (Memisoglu et al., 2019). The discrepancy between those studies might indicate that Cdc5 overexpression can drive adaptation without affecting the apical checkpoint kinases, while Mec1 autophosphorylation drives

CA during natural adaptation timing. These results indicate that CA likely affects the full DDC checkpoint cascade. Interestingly, the mutants in genes that are defective in CA are not defective in checkpoint termination, for example the *cdc5-ad* mutant, *mec1-ad* mutant, *sae2* mutant, or *ckb2* mutant (Clerici et al., 2014; Colombo et al., 2019; Toczyski et al., 1997). Vice versa, however, the checkpoint recovery mutants *ptc2* and *ptc3* are defective in CA (Leroy et al., 2003). Similarly, the *srs2* mutant is defective in both recovery and adaptation (Vaze et al., 2002). Yet, the precise differences between the substrates in CA and termination cascades remain elusive.

1.3.2 Mechanisms of adaptation to the DNA damage checkpoint

In a screen for mutants that affect CA, Toczysky and colleagues have identified a polo-like kinase, Cdc5, and Casein kinase II (CKII) as major regulators of adaptation to the DDC (Toczyski et al., 1997). Later studies revealed that many DNA repair proteins are involved in the regulation of the adaptation process, including RPA, Yku proteins, the Sae2 helicase, and many others (Colombo et al., 2019; Lee et al., 1998). In the section below, I discuss the molecular mechanisms underlying CA and the contribution of different pathways to this process (Figure 5). Although much is known about how CA occurs, the precise molecular mechanisms remain unknown.

1.3.2.1 The role of Cdc5 in unperturbed mitosis and checkpoint adaptation

Toczysky and colleagues discovered the polo-like kinase, Cdc5, as a key CA regulator (Toczyski et al., 1997). $Cdc5^{Plk1}$ kinase is a key regulator of the cell division cycle, and is conserved from yeast to humans. Cdc5 is a Ser/Thr kinase, which has a kinase domain on its N-terminus, and two polo box domains, which regulate the kinase localization and substrate specificity, on the C-terminus (reviewed in (Botchkarev and Haber, 2018)). Below I will discuss the role of Cdc5 in mitosis and CA.

1.3.2.1.1 The role of Cdc5 in mitosis

The Cdc5 kinase is expressed in the S and G2 phases of the cell cycle, and its kinase activity is regulated by Cdc28 (Mortensen et al., 2005). Cdc5 participates in a variety of mitosis-related processes, including the initiation of mitotic entry, the cleavage of cohesin, the maintenance of mitotic nucleus morphology, mitotic exit, and cytokinesis (reviewed in (Botchkarev and Haber, 2018)). To initiate mitotic entry, Cdc5 targets the Mcm1-Fkh2-Ndd1 transcription factor complex, which promotes the expression of a mitotic cyclin, Clb2 (Darieva et al., 2006). Additionally, Cdc5 targets the mitosis-inhibiting kinase, Swe1, for proteasome-mediated degradation (Asano et al., 2005). Cdc5 promotes sister chromatid separation by facilitating the cleavage of the cohesin ring subunit, Ssc1, by Esp1 separase (Alexandru et al., 2001; Hornig and Uhlmann, 2004). Cdc5 also

plays an important role in mitotic exit by participating in two crucial signaling cascades: Cdc Fourteen Early Anaphase Release (FEAR) and Mitotic Exit Network (MEN). Cdc5 has the following involvement in the FEAR network: the kinase interacts with the Esp1 and Slk19 network proteins and with Cdc14 phosphatase directly (Rahal and Amon, 2008). Furthermore, Cdc5 participates in the nucleolar release of Cdc14 by phosphorylating Net1, a protein that keeps the phosphatase inactive (Shou et al., 2002). Cdc5 also participates in MEN, which is executed by the Tem1 GTPase and its substrate kinase, Cdc15 (Asakawa et al., 2001). The Bfa1/Bub1 complex interacts with Tem1, regulating Tem1 activation, as Bfa1 inhibits Tem1 in the absence of Bub2 (Geymonat et al., 2002). When Bfa1 is phosphorylated by Cdc5, the Bfa1/Bub1 complex becomes inactivated, which allows further Tem1 activation and MEN execution (Hu et al., 2001). The activity of Cdc5 plays a critical role in chromosome condensation during anaphase by phosphorylating the condensin subunits Brn1, Ycg1, and Ycs4, thereby promoting condensin activation and DNA supercoiling activity (St-Pierre et al., 2009). Cdc5 also participates in spindle elongation during the progression of anaphase: the kinase targets the centrosome protein Sfi1 to prevent centrosome duplication (Elserafy et al., 2014). More functions of Cdc5 in MEN and the FEAR network are reviewed in detail in (Botchkarev and Haber, 2018). Finally, Cdc5 activity is important for cytokinesis, as the kinase activity towards the Rho1 guanidine exchange factors Tus1 and Rom2 is important for the assembly of a contractile actin ring (Yoshida et al., 2006).

1.3.2.1.2 The role of Cdc5 in the adaptation to the DNA damage checkpoint

During an unperturbed cell cycle, Rad53 is phosphorylated by the Cdc28 and Cdc5 kinases in the M phase at the C-terminal residues S774, S789 and S791. Mutations of these residues to alanine accelerate CA, indicating their role in checkpoint signaling (Schleker et al., 2010). Upon the induction of the DDC, Cdc5 activity is downregulated due to phosphorylation by Rad53, which indicates the intricate interplay between Rad53 and Cdc5 (Zhang et al., 2009). The adaptation happens following prolonged checkpoint arrest, when Cdc5 activity starts to rise again, actively overriding the DDC. During the G2/M transition in an unperturbed cell cycle, the activity of TORC1 regulates the activity of Cdc5, due to the nucleocytoplasmic shuffle of Cdc5 (Nakashima et al., 2008). During the prolonged checkpoint arrest, high TORC1 activity leads to a rise in Cdc5 activity, promoting adaptation (Figure 5) (Klermund et al., 2014). The overexpression of Cdc5 induces adaptation in a dose-dependent manner, indicating that the kinase plays a pivotal role in this process (Vidanes et al., 2010). The overexpression of Cdc5 overrides Mec1-mediated checkpoint signaling and drives Rad53 dephosphorylation (Figure 5) (Donnianni et al., 2010). During the overexpression course, the adaptation was driven by Rad53 dephosphorylation, while the localization of checkpoint sensors Ddc1 (thus, 9-1-1 complex) and Ddc2-Mec1 was not altered

and the upstream checkpoint adaptor Rad9 remained phosphorylated. Interestingly, the Ptc2 and Ptc3 phosphatases were not involved in Rad53 dephosphorylation, suggesting the involvement of the PP4 phosphatase complex (Vidanes et al., 2010). The overproduction of Cdc5 leads to impaired DSB resection and increased phosphorylation of Sae2, which directly interacts with Cdc5 (Donnianni et al., 2010). Cdc5 drives mitosis during DNA damage by the inhibition of the MEN proteins Bfa1-Bub2 (Valerio-Santiago et al., 2013). Importantly, Cdc5 promotes adaptation in a Bfa1-dependent and -independent manner, as it has other substrates. One of those substrates is a RSC chromatin remodeling complex, which consists of 17 subunits. Cdc5 targets Rsc1 and Rsc2; the deletions of *RSC1* or *RSC2* genes partially prevents adaptation during Cdc5 overexpression (Ratsima et al., 2016).

The mutants of Cdc5, which are CA defective, served as handy experimental tools to better understand the mechanisms of Cdc5-driven adaptation. The *cdc5-16* allele has a mutation in the polo-box domain and is defective in localizing to the centrosomes/spindle pole bodies (SPB). Using the *cdc5-15* allele, it was demonstrated that the localization of Cdc5 to the SPB is crucial for adaptation. The *cdc5-16* mutant is adaptation-defective, due to the altered substrate specificity of its polo-box domain, which also underlies the defective protein localization (Ratsima et al., 2016).

An adaptation-defective mutant of Cdc5, *cdc5-T238A*, has its mutation in the T-loop of the protein. The mutant has reduced kinase activity, defective localization to the SPB, and increased rates of chromosome loss (Rawal et al., 2016).

An adaptation-defective *cdc5-ad* allele, which harbors a single amino acid substitution (L251W) in the T-loop of the kinase domain, renders cells repair-defective with a penetrance of 89 percent (Toczyski et al., 1997). This allele does not have reduced kinase activity and its adaptation defect likely arises from an altered substrate specificity (Rawal et al., 2016). The overexpression of the phosphatases Ptc2 and Ptc3 rescues the CA defect of the *cdc5-ad* allele due to the dephosphorylation of Rad53 (Leroy et al., 2003). The overexpression of the nuclease Sae2 also rescues the *cdc5-ad* allele, presumably due to the decreased retention of the MRX complex and lower Tel1 and Mec1 activation (Clerici et al., 2006). However, the precise mechanism of how the *cdc5-ad* allele prevents adaptation remains elusive.

1.3.2.2 The apical kinases Mec1 and Tel1 during adaptation

The checkpoint maintenance following DSB induction depends on the activity of the apical checkpoint kinase Mec1, while Tel1 plays a relatively minor role (Pellicioli et al., 2001). The recent work from the Haber lab demonstrated that the Mec1-S1964-P autophosphorylation and Ddc2 degradation are the upstream events in the adaptation and the checkpoint recovery cascades

(Figure 5) (Memisoglu et al., 2019). Mec1-S1964A mutants fail to adapt, although the kinase activity of Mec1 seems unaffected during the initial checkpoint response. These mutants have increased recruitment of Ddc2 to the DSB, which likely correlates with persistent checkpoint signaling. The Mec1-S1964A adaptation defect depends on the activity of Chk1 and Mad2 proteins (Memisoglu et al., 2019). Another adaptation-deficient allele of Mec1, *mec1-ad*, has four mutations (D310G, K697T, Y944F and E961K) at the protein N-terminus. The adaptation defect of the *mec1-ad* allele stems from the increased recruitment and subsequent hyperactivation of Tel1 due to the increased persistence of the MRX complex at the DSB. Moreover, the allele displays defects in DNA ends resection, and many resection mutants are defective in CA (Clerici et al., 2014). The nature of the adaptation defect of the *mec1-ad* allele demonstrates that although Tel1 has a relatively minor role in the initial response to the DSB, the hyperactivation of Tel1 is sufficient to invoke the adaptation defect. The hyperactive alleles of Tel1, particularly *tel1-hy909*, not only compensate for the lack of Mec1 in response to DNA damage, but display a CA defect in response to a single irreparable DSB (Baldo et al., 2008). These results indicate that the adaption is likely initiated by the phosphorylation of Mec1-S1964, and that the hyperactivation of the apical kinases can prevent adaptation to the DDC.

1.3.2.3 The role of CKII in checkpoint adaptation

Toczysky and colleagues identified that the mutants in genes that encode for the regulatory Casein kinase II (CKII) subunits, *CKB1* and *CKB2*, are defective in CA (Toczyski et al., 1997). CKII is an essential pleiotropic kinase that is conserved from yeast to humans. The kinase is involved in the regulation of a variety of cell growth aspects, including cell cycle regulation, cytoskeleton organization, protein folding, and many other functions (reviewed in (D'Amore et al., 2019; Meggio and Pinna, 2003; Miyata, 2009)). CKII phosphorylates multiple substrates that are involved in DNA replication and the cell cycle, including Top1, Cdc28, and the START protein, Cdc27 (Meggio and Pinna, 2003). Guillemain and colleagues have partially uncovered the role of CKII in adaptation (Guillemain et al., 2007). To attenuate the DDC, hyperphosphorylated Rad53 needs to be dephosphorylated by the phosphatase Ptc2. CKII mediates the Rad53-Ptc2 interaction, and the mutant allele of Ptc2 (*PTC2-T376A)*, which abolishes the interaction, renders the cell defective in checkpoint recovery and adaptation (Figure 5). Yet, the adaptation defect of *PTC2-T376A* was less penetrant compared to the *ckb1* or *ckb2* deletion mutants, suggesting that CKII has additional functions in the adaptation process (Guillemain et al., 2007).

1.3.2.4 Other regulators of checkpoint adaptation

The adaptation process is influenced by the processing of the DSB, the chromatin state, autophagy induction, and other factors (Figure 5). The extent of DSB-end resection has a direct influence on adaptation kinetics (Clerici et al., 2006, 2014; Lee et al., 1998). An increased resection of DNA ends in *hdf1/yku70* mutants causes defective CA, which is suppressed by the deletion of *MRE11* or the mutation in the largest RPA subunit, *rfa1-t11* (Lee et al., 1998). While the *mre11* mutant has decreased resection, the *rfa1-t11* mutant is defective in the HDR pathway and in DDC activation. The latter likely explains the rescue of CA in *yku70 rfa1-t11* double mutants (Kim and Brill, 2001). Interestingly, the *sae2, dna2, sgs1* and *exo1 sgs1* mutants that are defective in DSB-end resection also display strong CA defects (Clerici et al., 2006, 2014; Eapen et al., 2012). The *sae2* mutant has increased retention of the MRX complex at DSBs, which triggers the hyperactivation of Tel1 (Clerici et al., 2006).

The Fun30 ATPase is a chromatin remodeler that facilitates the transfer of H2A-H2B histone dimers and promotes DNA end resection by both Exo1- and Sgs1 (Awad et al., 2010; Costelloe et al., 2012). The mutants lacking Fun30 display decreased resection of DNA ends, and has adaptation defect that could be rescued by the Exo1 overexpression, or the deletion of *MRE11* (Eapen et al., 2012). Ino80 and Swr1 are ATP-dependent chromatin remodeling enzymes, which were also implicated in the adaptation process (Papamichos-Chronakis et al., 2006). The deletion of the *INO80* gene leads to a CA defect due to the decreased levels of H2A-S129P around the DSB and increased incorporation of the Htz1p variant adjacent to a DSB (Papamichos-Chronakis et al., 2006). Mec1 cannot phosphorylate the Htz1 histone in response to DNA damage (Jackson, 2000). Yet, how this histone imbalance generates the adaptation defect is unclear.

Another chromatin remodeling protein, Rdh54 (a helicase, formerly Tid1), is required for CA (Lee et al., 2001). Rdh54 is a homolog of Rad54, and plays a role in Rad51-mediated strand exchange during homology-directed DSB repair as well as in meiotic recombination, as it dislocates Rad51 filaments from dsDNA (Petukhova et al., 2000; Shinohara et al., 2000). The loss of the *RDH54* gene does not alter DSB resection, and does not result in defective homology-directed repair. The adaptation defect of the *RDH54* deletion could be suppressed by the mutation in the largest RPA subunit, *rfa1-t11* (Lee et al., 2001). Following DNA damage, Rdh54 is phosphorylated by Mec1 and Rad53 and plays a role in attenuation of the checkpoint response in an unknown way (Ferrari et al., 2013).

The histone deacetylase complex, Sin3-Rpd3, is involved in the adaptation predominantly via the regulation of Rad53. The deacetylation of Rad53 at K22 and K213 by the Sin3-Rpd3 complex results in the reduced kinase activity of Rad53, which promotes adaptation. The inhibition of

histone deacetylase (HDAC) activity with valproic acid delays the adaptation due to Sin3-Rpd3 complex inhibition, but does not fully abolish it (Tao et al., 2013).

DNA damage signaling triggers autophagy, which was shown to potentially regulate the abundance of DNA repair proteins. For example, in cells experiencing DNA damage, the Sae2 protein is degraded by autophagy upon the HDAC inhibition (Robert et al., 2011). The deletions in the Golgi-associated retrograde protein (GARP) complex (*VPS51*, *VPS53*, and *YPT6*), which lead to increased autophagy, cause a CA defect (Dotiwala et al., 2013). The adaptation defect is triggered by the mislocalization of the separase Esp1 and its inhibitor securin Pds1 to the cytoplasm and the partial degradation of Pds1 (Eapen and Haber, 2013). In wild-type cells, hyperactivation of autophagy by overexpression of the dominant mutation of Atg13, Atg13-S8A, leads to an adaptation defect, although Rad53 becomes dephosphorylated during the prolonged checkpoint arrest (Dotiwala et al., 2013). Importantly, the inhibition of TORC1 activity with rapamycin prevents CA, although the autophagy induction is dispensable (Klermund et al., 2014). These results indicate that although autophagy can prevent adaptation, its induction is not required for the adaptation-induced cell cycle arrest.

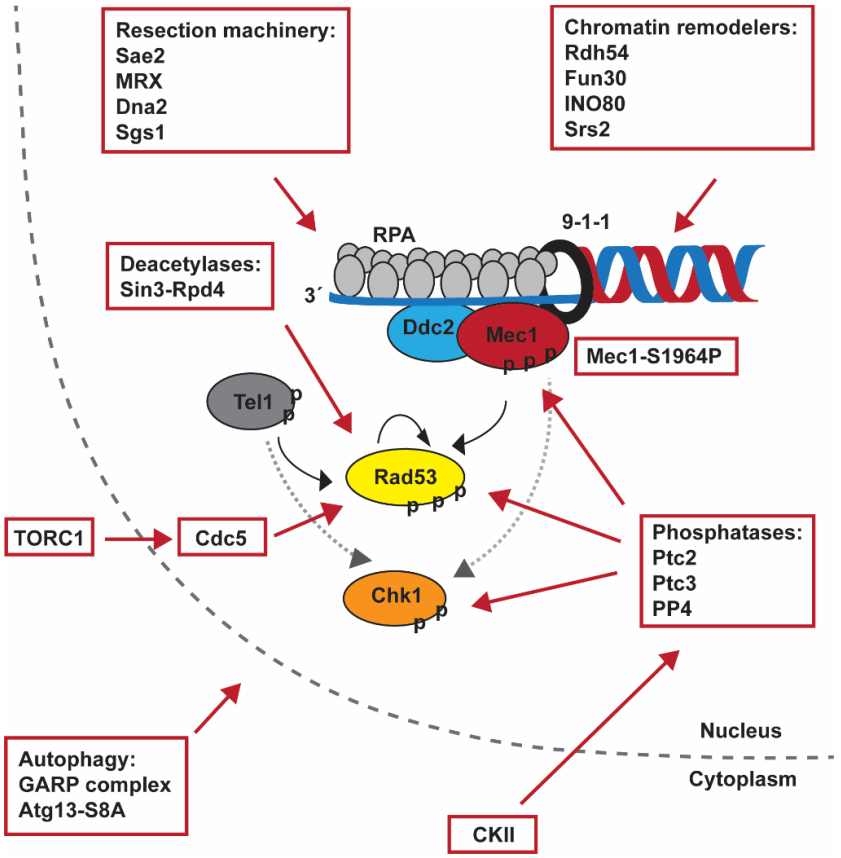

Figure 5. Mechanisms contributing to checkpoint adaptation. *Figure legend: see next page.*

Figure 5. Mechanisms contributing to checkpoint adaptation. Adaptation to the DDC likely affects the whole signaling cascade and is marked with the dephosphorylation of key effector kinases, Rad53 and Chk1, by Ptc2, Ptc3, or PP4 phosphatases. The autophosphorylation of Mec1 at S1994 is likely an initial step in CA. The nutrient-sensing TORC1 complex promotes CA via Cdc5 kinase, which drives Rad53 dephosphorylation. The dephosphorylation of Rad53 is a key step in adaptation. The Ptc2-mediated dephosphorylation of Rad53 is mediated by CKII. The deacetylation of Rad53 by the Sin3-Rpd4 complex also reduces the activity of the kinase. On the chromatin level, adaptation is regulated by the DNA-end resection rates by Sae2, the MRX complex, Dna2, and Sgs1. Both increased and decreased resection results in defective adaptation. The chromatin remodeling enzymes Rdh54, Fun30, INO80, and Srs2 also regulate adaptation by regulating the resection rates and histone modifications proximal to the DSB. Finally, the induction of autophagy prevents adaptation, and mutants in the GARP complex have strong adaptation defects. p, phosphorylation.

1.4 TOR as a central growth regulator

Cellular growth and division is tightly coupled to environmental conditions, such as the availability of nutrients or the presence of environmental stresses. The abundance of nutrients is sensed by the target of rapamycin complex 1 (TORC1). The two TOR kinases, TOR1 and TOR2, form two distinct multiprotein complexes that regulate cell growth. The TOR kinases are highly evolutionarily conserved proteins that belong to the PI kinase-related protein kinase (PIKK) family (reviewed in (Wullschleger et al., 2006)). In this section, I will review the structures of TORC1 and TORC2 complexes, their upstream activators, and downstream effectors. Additionally, I review how TOR signaling is influencing DNA repair and the cell cycle progression.

1.4.1 Structure and functions of TORC1 and TORC2 in budding yeast

The genome of budding yeast encodes for two highly conserved TOR kinases, TOR1 and TOR2. Both TOR1 and TOR2 are members of the PIKK family of Ser/Thr-specific kinases (Keith and Schreiber, 1995). All the TOR proteins have a similar domain structure (listed from N to C terminus): the two blocks of so-called HEAT repeats, the FAT domain that contains modified HEAT repeats, the FRB domain that binds to the FKBP12 protein, the kinase domain, and the C-terminal FATC domain that is indispensable for the kinase activity (reviewed in (Loewith and Hall, 2011)). The TOR kinases form two distinct multiprotein complexes: the TORC1 can contain either TOR1 or TOR2, while TORC2 always contains the TOR2 kinase (Loewith et al., 2002). TORC1, which is sensitive to rapamycin inhibition, is composed of either TOR1 or TOR2, Kog1, Tco89, and Lst8 proteins (Figure 6a). TORC2, which is rapamycin insensitive, is composed of TOR2, Avo1, Avo2, Avo3, Bit61, and Lst8 proteins (Figure 6b) (reviewed in (Wullschleger et al., 2006)).

Both of these complexes control cell growth via distinct signaling branches. Interestingly, the loss of TOR1 can be tolerated, while TOR2 is essential in budding yeast (Kunz et al., 1993). The TORC1 and TORC2 signaling branches majorly overlap and execute the control of ribosome biogenesis, mRNA synthesis, protein biosynthesis rates, autophagy, and nutrient transport (reviewed in (Schmelzle and Hall, 2000)). The TORC2 unique signaling branch regulates cytoskeleton organization, sphingolipid biosynthesis, and endocytosis (reviewed in (Loewith and Hall, 2011)). TORC1 is localized on the limiting membrane of the vacuole, while TORC2 is localized to the plasma membrane (Berchtold and Walther, 2009; Sturgill et al., 2008).

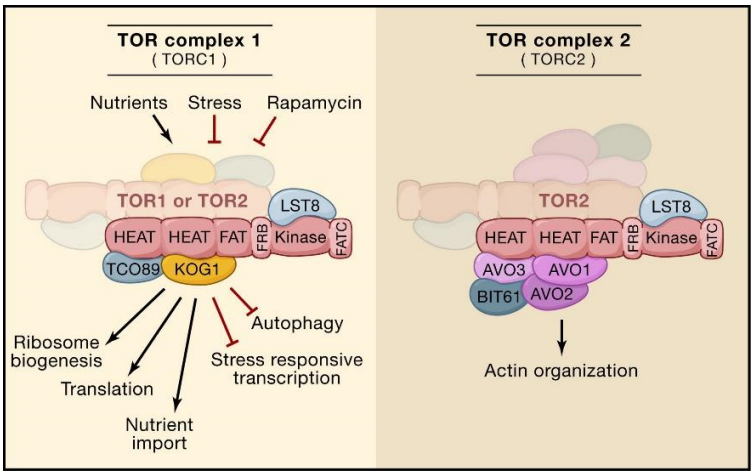

Figure 6. The structures of TORC1 and TORC2 and their major signaling functions. (a) TORC1 is composed of either TOR1 or TOR2, Kog1, Tco89 and Lst8 proteins. The complex is likely dimeric. The complex activity is promoted by high nutrients and downregulated by stressors or rapamycin. TORC1 signaling controls ribosome biogenesis, proteins translation rates, nutrient transport, and stress-induced cellular responses, including autophagy. **(b)** TORC2 is composed of TOR2, Avo1, Avo2, Avo3, Bit61, and Lst8 proteins, and is likely dimeric. The complex is rapamycin-insensitive. TORC2 majorly regulates cytoskeleton organization. Figure taken from (Wullschleger et al., 2006).

1.4.1.1 The mode of TORC1 inhibition with rapamycin

TOR signaling was uncovered due to the discovery of the anti-fungal lipophilic macrolide rapamycin, isolated from *Streptomyces hygroscopicus* in 1965 (reviewed in (Loewith and Hall, 2011)). Studies of antimicrobial activity of rapamycin, as well as studies using mammalian cells, demonstrated strong antiproliferative activity of the drug, suggesting that the drug targets the controller of cell growth. Rapamycin binds to the protein FKBP12 in the cell, which triggers the change in the behavior of the complex: it binds to the FRB domain of TOR1 and TOR2, and inhibits the catalytic activity of the kinases (Heitman et al., 1991). Deletions or mutations in the FKBP12-encoding gene and the point mutations in the TOR kinases (namely, S1972R or S1972N in TOR1 and S1975I in TOR2) render cells completely rapamycin-insensitive (Heitman et al., 1991; Helliwell et al., 1994). TOR1 and TOR2 form two distinct protein complexes, and only TORC1 is sensitive to rapamycin treatment. TORC2 is insensitive to rapamycin because one of its subunits, Avo3, masks the active site of TOR2, despite FKBP12 still binding to the complex (Gaubitz et al., 2015). Because I used rapamycin to inhibit TORC1 in this study, I will further focus on the overview of this complex.

1.4.2 Factors influencing the activity of TORC1

The activity of TORC1 is promoted by nutrient availability: different upstream factors activate TORC1 in response to free amino acids, nitrogen, and glucose. TORC1 signaling allows for the

integration of information about the abundance and quality of nutrients (reviewed in (Loewith and Hall, 2011)). TORC1 activity is downregulated by a variety of stresses like high salt or heat, via the factors upstream of TORC1 (Reinke et al., 2006; Wanke et al., 2008).

The availability of amino acids regulate the activity of TORC1 via the RAG family of small GTPases (reviewed in (Hatakeyama and De Virgilio, 2016)). There are two RAG small GTPases in budding yeast: Gtr1 and Gtr2. They are tethered to the vacuolar membrane by the EGO complex, which consists of Ego1, Ego2, and Ego3 (Zhang et al., 2012). The RAG small GTPases form a heterodimer, in which Gtr1 binds GTP and Gtr2 binds GDP. The RAG small GTPases bind the EGO complex and together activate TORC1 in response to amino acid abundance (Binda et al., 2009). In budding yeast, TORC1 activity is differentially regulated in response to different amino acids, and diverse sensing mechanisms are employed for sensing individual amino acids (reviewed in (González and Hall, 2017)).

Although glucose availability is primarily sensed by the AMP-activated protein kinase (AMPK), there is a cross talk between the two metabolic regulators ((Hardie, 2014), reviewed in (González and Hall, 2017)). In budding yeast, AMPK activity negatively regulates TORC1 activity in glucose-deprived cells. This is achieved via the activity of Snf1 kinase, which phosphorylates the Kog1 component of TORC1, leading to the disassembly of the complex (Hughes Hallett et al., 2015). Curiously, in response to glucose starvation, TORC1 is rapidly redistributed in the vacuole, forming oligomers that are important for the inactivation of TORC1 (Prouteau et al., 2017).

1.4.3 Downstream effectors of TORC1

In response to environmental cues, TORC1 signals through its multiple effector kinases to regulate ribosome biosynthesis rates, protein translation, macroautophagy, cell cycle progression, nutrient uptake, and cell wall integrity. The two major downstream effectors of TORC1 are Sch9 kinase and Tap42-PP2A phosphatase (reviewed in (Loewith and Hall, 2011)). Other substrates of TORC1 are the autophagy protein Atg13 (Kamada et al., 2010), the ion transporter Sfp1 (Lempiäinen et al., 2009), and many others (reviewed in (Loewith and Hall, 2011)).

The Sch9 kinase belongs to the AGC kinase family, and is directly phosphorylated by TORC1 at six different sites (Urban et al., 2007). This allows for the regulation of Ribi genes and therefore ribosome biogenesis, the G0 entry via Rim15 kinase, and protein translation rates (Urban et al., 2007). The regulation of ribosome biogenesis is achieved via Sch9-dependent inhibitory phosphorylation of Stb3, Dot6 and Tod6 transcriptional repressors, thereby promoting ribosome biogenesis and cell growth (Huber et al., 2011). The kinase Sch9 is also important for nitrogen metabolism, as it targets the ammonium permease MEP2, the amino acid permease GAP1, and the transcription factor Gcn4 that regulates biosynthesis of amino acids (Smets et al., 2008). Sch9

also plays an important role in TORC1-regulated autophagy: upon starvation, the inactivation of Sch9 induces autophagy by allowing the translocation of the transcription factors Msn2 and Msn4 to the nucleus in an Atg1-dependent manner (Beck and Hall, 1999; Yorimitsu et al., 2007). Finally, Sch9 regulates cell size, possibly via ribosome biogenesis regulation (Jorgensen et al., 2002). Together, TORC1 targets Sch9 to regulate nitrogen metabolism and amino acid biosynthesis, together with ribosome biogenesis and autophagy.

The phosphatases Tap42 and PP2A (the Pph21, Pph22, and Pph3 phosphatases are referred to as PP2Ac) are the other effector branches of TORC1 signaling. TORC1 regulates the interaction of PP2A phosphatases with the regulatory protein Tap42 (Di Como and Arndt, 1996). TORC1 regulates Tap42 phosphorylation presumably directly, as well as via the protein Tip41 ((Jacinto et al., 2001; Jiang and Broach, 1999), reviewed in (Loewith and Hall, 2011)). The Tap42-PP2A signaling axis regulates autophagy induction (Yorimitsu et al., 2009). Tap42-PP2A effectors also regulate the expression of genes that control the nitrogen discrimination pathway via the transcription factor, Gln3, under nitrogen limitation (Li et al., 2017). Additionally, Tap42 controls the expression of nitrogen catabolite repression (NCR)-sensitive genes, which allow growth on poor nitrogen sources, via transcription factor Gln3, Gat1, and Dal81 ((Beck and Hall, 1999; Georis et al., 2009), reviewed in (Loewith and Hall, 2011)). Yet another role of the Tap42-PP2A signaling branch is the control of gene expression by regulating histone acetylation. TORC1 signaling suppresses the sirtuin deacetylases Hst3 and Hst4, thereby promoting the acetylation of histone H3 and H4 N-terminal tails (Workman et al., 2016). The involvement of the Tap42-PP2A signaling branch in cell cycle control and DDR is discussed in the section below.

1.4.4 The role of TOR complex in cell cycle progression and DDC

Cell cycle progression is directly coupled to cell mass accumulation, and the central growth-promoting complex, TORC1, plays a direct role in these processes. Both Sch9 and Tap42-PP2A signaling branches are involved in cell growth and cell cycle regulation. Sch9 signaling majorly regulates the cell's entry into G0, as well as G1 progression in response to nutrient availability (Barbet et al., 1996). The inhibition of TORC1 with rapamycin leads to accumulation of the Cdc28 inhibitor, Sic1, thereby promoting G1 arrest (Zinzalla et al., 2007). Additionally, PP2A counteracts phosphorylation of the kinase, Whi5, by Cdc28, preventing the passage of the cell through START ((Talarek et al., 2017), reviewed in (Pérez-Hidalgo and Moreno, 2017)).

The Tap42-PP2A signaling branch regulates the G2/M cell cycle progression and is involved in the modulation of DDC (Ferrari et al., 2017; Nakashima et al., 2008). Although the inactivation of TORC1 with rapamycin leads to cell cycle arrest in G1, the addition of rapamycin to already cycling cells leads to a prolonged G2/M phase, indicating that TORC1 regulates cell division. Tap42-PP2A

regulates the nuclear re-localization of the polo-like kinase Cdc5, thereby promoting an entry into mitosis (Nakashima et al., 2008). Moreover, the inhibition of TORC1 leads to the inactivation of Cdc28 (CDK), because in the absence of nuclear Cdc5, the cell cycle inhibitor Swe1 is stabilized (reviewed in (Loewith and Hall, 2011)).

Besides positively regulating mitosis, TORC1 signaling plays an important role in the DNA damage response (Ferrari et al., 2017). The activation of PP2A attenuates Mec1-mediated DNA damage signaling, thereby attenuating the DDC (Ferrari et al., 2017). Moreover, the high activity of TORC1 promotes CA, while the inactivation of TORC1 with rapamycin rescues the checkpoint arrest by keeping Cdc5 inactive and by inducing autophagy (Klermund et al., 2014). In human cells, the hyperactivation of mTORC1 results in phosphorylation of the histone-targeting RNF168 ubiquitin ligase, and therefore impairment in DNA repair and entry into mitosis with unrepaired DNA (Xie et al., 2018). It is important to note that TORC1 activity is also downregulated by DNA damage, which is accompanied by the induction of autophagy (Eapen et al., 2017; Ueda et al., 2019). Yet, the precise mechanisms of how TORC1 signaling is integrated into mitotic exit and DDC remain to be determined.

1.5 Pathways to repair double strand DNA lesions

DNA double strand breaks (DSBs) are one of the most toxic DNA lesions and represent an extreme threat to genome stability and cellular survival. The failure to properly repair a DSB leads to mutations, genomic rearrangements, and loss of genetic material, ultimately resulting in cell death or oncogenic transformation (Gobbini et al., 2016). Strikingly, even a single unrepaired DSB is lethal in haploid budding yeast (Rudin and Haber, 1988). Therefore, cells have evolved multiple intricate mechanisms to recognize and repair their DSBs, and coordinate the repair process with cell cycle progression. The mechanisms of DDC are discussed in section 1.2. Here, I discuss the molecular pathways involved in DSB repair in yeast, such as homology-directed repair pathways, non-homologous end joining, microhomology-mediated end joining, and others. I also review the role of the Mre11-Rad50-Xrs2 complex in different pathways of DSB repair in detail.

1.5.1 Homology-directed repair pathways

1.5.1.1 Homologous recombination

Homologous recombination (HR) is a major DSB repair mechanism that utilizes homologous sequences as a repair template. In budding yeast, the vast majority of DSBs are repaired via HR mechanism, and it remains one of the most prevalent DSB repair mechanisms in mammalian cells. HR is a conserved process from yeast to humans, and is generally considered to be an error-free DSB repair pathway, with some particular exceptions. Due to the requirement for the homologous template, HR is restricted to the S and G2/M phases of the cell cycle (reviewed in (Symington et al., 2014)). HR is divided into the following critical phases: (I) the resection phase, in which DSBs are resected in the 5´ to 3´ direction, exposing 3´-ended single stranded DNA (ssDNA) molecules; (II) the ssDNA annealing phase, in which the search for the homologous template is carried out; (III) DNA strand exchange and D-loop formation; (IV) DNA synthesis using homologous sequence as a template; (V) ligation of the newly synthesized strand and Holliday junction resolution (Figure 7) (reviewed in (Prado, 2018)).

The resection phase (I) includes the degradation of the 5´ DNA strands on both ends of the DSB, which is initiated by the Mre11-Rad50-Xrs2 (MRX) complex together with the $Sae2^{CtiP}$ protein, and continued by the nucleases Exo1 and Dna2 together with the helicase Sgs1 (Cejka et al., 2010a; Gobbini et al., 2016; Mimitou and Symington, 2008). The ssDNA ends generated during the resection process are coated by RPA (Chen et al., 2013). The RPA complex is important for the prevention of secondary structures on the long 3´ DNA molecules, as well as for DDC activation (Brush et al., 1996; Chen et al., 2013). The second (II) phase of HR is the ssDNA annealing phase, which functions to carry out a search for the homologous template. On the ssDNA filament, RPA

is replaced with the ATP-dependent recombinase Rad51, which forms helical filaments that coat ssDNA (Morrical, 2015). This reaction is catalyzed by a key recombinase, Rad52, which interacts directly with RPA and Rad51, and thereby targets Rad51 to the RPA-coated ssDNA (New et al., 1998). Only polymerized Rad51 has efficient strand exchange activity. Rad51 filament assembly is mediated by the Rad55-Rad57 complex (Sugawara et al., 2003; Sung, 1997). The protein Srs2 promotes Rad51 filament disassembly and thereby prevents illegitimate recombination (Liu et al., 2011). In the third (III) phase of HR, the ssDNA coated with Rad51 filaments, the recombinase Rad52, and the DNA translocase Rad54 promote efficient strand exchange and invasion into homologous duplex DNA. Rad54 (as well as its paralog Rdh54) translocase exhibits dsDNA ATPase activity, and translocates on dsDNA, allowing for duplex opening and strand invasion (Van Komen et al., 2000; Symington et al., 2014). Next, in the fourth (IV) phase, DNA synthesis that extends the 3´ DNA end within the D-loop is carried out. The bulk of DNA synthesis within the D-loop is carried out by the DNA Pol δ, with the assistance of the DNA Pol ε (Hicks et al., 2010; Maloisel et al., 2008). In the fifth (V) and final phase of HR, the resolution of D-loop intermediates takes place. The displacement of the Rad51-coated invading strand is carried out by the helicase, Mph1 (Mazón and Symington, 2013). HR leads to the formation of Holliday junction intermediates, which must be resolved in order for the sister chromatids to segregate. These junctions are resolved in two ways: in a dissolution process by the activity of the Sgs1–Top3–Rmi1 complex (Cejka et al., 2010b) or in a resolution process by the activity of structure-specific nuclease complexes Mus81–Mms4, Yen1, and Slx1–Slx4 (Boddy et al., 2001; Fricke and Brill, 2003; Ip et al., 2008). Following the duplex resolution, when the sister chromatids were not exchanged, the HR results in non-crossover, whereas when they are exchanged, it results in crossover events. These HR events are error-free. If the HR event utilized misaligned templates (e.g. within the repetitive sequences), it results in unequal sister chromosome exchange, which is potentially mutagenic (Symington et al., 2014).

1.5.1.2 Break-induced replication

Break-induced replication (BIR) is a pathway to repair DSBs in a recombination-dependent replication process. Upon BIR, the 3´ ssDNA filament invades the homologous sequence in a Rad52-dependent manner and initiates DNA synthesis up to the end of the chromosome (reviewed in (Malkova, 2018) and (Symington et al., 2014)). BIR is utilized by a cell when the DSB is one-sided, the other side of the DSB fails to find homologous sequences, or when the two ends invade two different templates (reviewed in (Anand et al., 2013)). The first two steps of BIR, which are the resection of the DSB and the Rad52-assisted formation of Rad51-filaments that coat ssDNA, are similar to the HR pathway (Figure 7). BIR does not strictly require Rad51 because it

can utilize Rad59, but it strictly requires the recombinase Rad52 (Signon et al., 2001). The DNA synthesis step of BIR is drastically different from the HR pathway. Three different DNA polymerases (DNA Pol ε, DNA Pol α, and DNA Pol δ) participate in BIR, and the Pol32 subunit of DNA Pol δ is essential for the process (Lydeard et al., 2007). The unusual feature of BIR is that it progresses through the D-loop migration, which leaves the leading strand (that has invaded the homologous sequence) exposed as ssDNA (Wilson et al., 2013). Upon BIR, the lagging strand is synthesized utilizing the leading strand as a template (Donnianni and Symington, 2013). BIR can go through several rounds of strand invasion, DNA synthesis, and reaction resolution, therefore utilizing several different templates, which is extremely mutagenic (Smith et al., 2007; Štafa et al., 2014). Cells frequently utilize the BIR mechanism of DSBs repair upon replication stress to restart their replication forks ((Mayle et al., 2015), reviewed in (Malkova, 2018)), upon telomere erosion from alternative lengthening of telomeres (Min et al., 2017; Sobinoff and Pickett, 2020), and upon the breakage of common fragile sites ((Rosen et al., 2013), reviewed in (Malkova, 2018)).

1.5.1.3 Single strand annealing

Single strand annealing (SSA) is a DSB repair pathway that utilizes homologous sequences that are proximal to the DSB ends, and leads to the deletion of the sequences in between the annealed homologies (Bhargava et al., 2016). Following extensive DNA end resection, Rad52 promotes the annealing of homologous sequences that flank the DSB. To complete SSA repair, the 3´ ends of the resected DNA are degraded by the Rad1-Rad10 nuclease complex (Ivanov et al., 1996). The SSA pathway is independent of Rad51, Rad54, Rad55, and Rad57, but depends on Rad52, Rad59, Msh2, and the Msh3 mismatch repair proteins (Ivanov et al., 1996; Sugawara et al., 2000). The pathway is highly conserved from yeast to mammals. The repair of the DSB with SSA is mutagenic, because it leads to large deletions. This pathway of DNA repair is utilized (in parallel with the microhomology-mediated end joining pathway) by cells when the DSB is resected in the S phase, but the sister chromatid is not available yet (reviewed in (Bhargava et al., 2016)). Another scenario in which the cell utilizes the SSA pathway is in the case of a hyperresected DSB, because long stretches of ssDNA expose homologies ((Vaze et al., 2002), reviewed in (Bhargava et al., 2016)).

1.5.1.4 Synthesis-dependent strand annealing

The synthesis-dependent strand annealing (SDSA) pathway involves the invasion of 3´ ends of the DSB into the homologous duplexes (reviewed in (Symington et al., 2014)). During SDSA, the invading 3´ DNA end does not form a Holliday junction. The newly synthesized strand is annealed to the other DSB site. This type of HDR repair strictly produces non-crossover products (Figure

7). During SDSA repair, DNA synthesis is limited and the invading 3´ DNA end is frequently displaced by helicases, primarily Srs2 (Liu et al., 2017a).

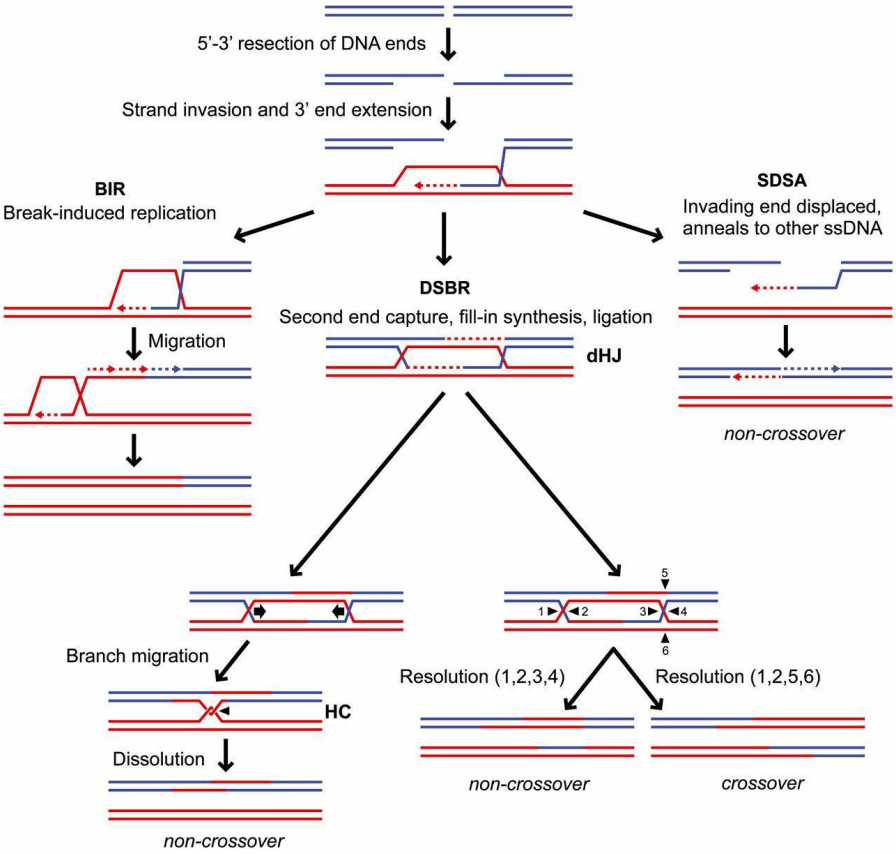

Figure 7. Models for classical DSB repair by homologous recombination, break-induced replication, and synthesis-dependent strand annealing. All the HDR pathways share the initial DNA end resection step and the 3´ DNA end invasion step. BIR progresses through the D-loop migration, which leaves the leading strand exposed as ssDNA, while the lagging strand is synthesized utilizing the leading strand as a template. During classic DSBR repair, the homologous sequence is utilized as a template for DNA synthesis. Following the branch migration, the D-loop could be resolved via either dissolution or Holliday junction resolution processes. The latter could produce gene crossovers. SDSA repair involves the invasion of the 3´ DNA end into a homologous sequence. The newly synthesized strand is annealed to the other site of the DSB, resulting in a non-crossover product. Figure taken from (Symington et al., 2014).

1.5.2 Non-homologous end joining

Non-homologous end joining (NHEJ) is a second key DNA repair pathway that is evolutionarily conserved from yeast to humans (reviewed in (Emerson and Bertuch, 2016)). NHEJ is a preferentially used DSB pathway in mammals, while haploid yeast utilize it in the G1 phase of the cell cycle. During NHEJ repair, the DNA ends are directly ligated and no homologies among them are required. The mechanism of NHEJ could be subdivided into three following steps: (I) DSB recognition and DNA end tethering by the MRX complex; (II) strand annealing and DNA end processing; (III) DNA end ligation (Figure 8) (Emerson and Bertuch, 2016). In the first (I) step,

when the DSB occurs, both DNA ends are rapidly bound by the ring-like structured Yku70-Yku80 complex and the MRX complex (Clerici et al., 2008); the latter provides a critical DNA end tethering function (Gobbini et al., 2016). The DNA end tethering allows the DSB ends to be spatially connected and further re-annealed. In the second (II) step of NHEJ repair, DNA ends are annealed and processed by the repair complex that is formed by scaffold Yku proteins, DNA ligase IV (Dnl4), Lif1, Nej1, and the MRX complex (Chen and Tomkinson, 2011; Gobbini et al., 2016; Zhang et al., 2007). After stabilization, the DNA ends are processed (either nucleolitically or by polymerases) for compatibility by the 5´ nuclease Rad27 or other DNA end processing factors like Exo1, Pol2, Pol3, and Tdp1 (reviewed in (Emerson and Bertuch, 2016)). In the final step (III), the processed DNA ends are ligated by Dnl4 ligase (Wilson et al., 1997).

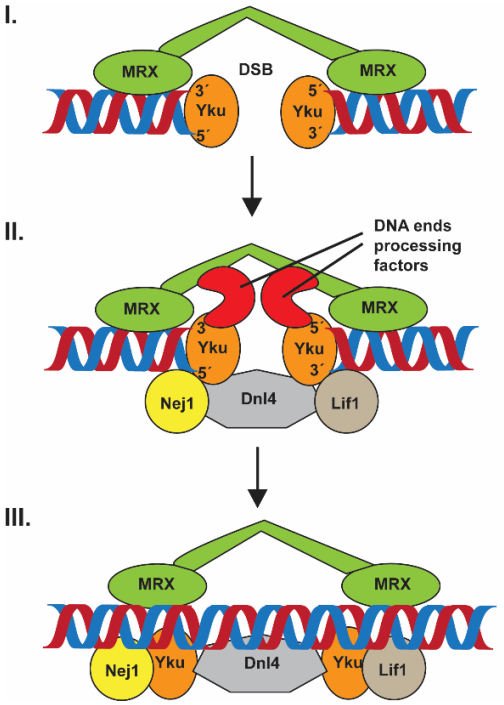

Figure 8. Mechanism of non-homologous end joining. Following DSB formation, the Yku proteins and the MRX complex instantly recognize the DNA ends. Later, the NHEJ factors Nej1, Lif1, and Dnl4 are recruited to the DSB. DNA ends are processed for the ligation step. Finally, the ligase Dnl4 seals the DSB, and the repair complex disassembles. This figure is modified from (Emerson and Bertuch, 2016).

In budding yeast, the NHEJ repair pathway is promoted in the G1 phase of the cell cycle, when resection is absent. The repair of the DSB via HDR is restricted to the S and G2 phases of the cell cycle, when the resection of the DSB is permitted (Symington and Gautier, 2011). In mammals, however, NHEJ is active throughout the cell cycle and accounts for the vast majority of the DSB

repair events (Pannunzio et al., 2018). Curiously, NHEJ is regulated by cellular ploidy in budding yeast. In diploid yeast, the a1–α2 repressor actively represses the transcription of Nej1 (Frank-Vaillant and Marcand, 2001; Kegel et al., 2001); therefore, the NHEJ pathway is actively suppressed in diploid budding yeast.

1.5.3 Microhomology-mediated end joining

Microhomology-mediated end joining (MMEJ), known as alternative non-homologous end joining (alt-NHEJ) in mammals, is a faulty, error-prone DNA repair pathway that operates in cells in a Ku- and Rad52-independent manner (Ma et al., 2003; Meyer et al., 2015; Sinha et al., 2016). The pathway utilizes the microhomologies (which are usually proximal to the DSB site) for end joining, resulting in deletions of the sequences in between the annealed microhomologies. DSB repair by the MMEJ pathway involves the following steps: (I) DSB recognition and 5´ to 3´ DNA end resection; (II) microhomology annealing ; (III) heterologous flap removal; (IV) gap filling by polymerases; and (V) DNA end ligation (Figure 9) (reviewed in (Sfeir and Symington, 2015)). In the first step of MMEJ repair (I), the DNA ends are bound by the MRX complex, which provides DNA end tethering and initial resection steps. The resection is further carried out by Dna2-Sgs1 and Exo1, similar to the HR pathway, and is important for exposing microhomologies (Ma et al., 2003; Xie et al., 2009). The next step (II) involves the annealing of exposed microhomologies, which is a Rad52-independent step for short microhomologies stretches. The minimal reported microhomologies utilized by the pathway is two base pairs (bp), and the optimal annealing sites are roughly 8-20 bp and contain no more than twenty percent mismatches (Lee et al., 2019). Next (III), the heterologous flap is removed by the action of the endonuclease Rad1-Rad10 (XPF-ERCC1 in mammals), which allows the polymerases to fill in the gap and permit DNA end re-ligation (Bennardo et al., 2008; Deng et al., 2014; Ma et al., 2003). In the fourth step (IV), DNA polymerases DNA Pol θ, DNA Pol δ, and DNA Pol λ perform a fill-in DNA synthesis (Black et al., 2019; Meyer et al., 2015). During this step in mammalian cells, DNA Pol θ can add a few extra nucleotides, resulting in insertions. Finally (V), the DNA ends are ligated. Although there is a slight decrease in the ligation efficiency upon *DNL4* deletion (Lee and Sang, 2007; Meyer et al., 2015), the ligation step is thought to be carried out by $Cdc9^{Lig1}$ in yeast, and Lig1 and Lig3 in mammals (Ma et al., 2003; Simsek et al., 2011; Wang et al., 2005).

MMEJ is a highly mutagenic pathway that is evolutionarily conserved from yeast to humans, and is frequently viewed as a back-up pathway that operates when the major HR or NHEJ repair pathways fail. MMEJ is actively suppressed by the recombinase Rad52 (Lee and Sang, 2007; Meyer et al., 2015; Sfeir and Symington, 2015). However, recent data have demonstrated that MMEJ is an active repair pathway that operates in parallel with the other pathways, particularly at

collapsed replication forks (Alexander et al., 2016; Truong et al., 2013; Wang et al., 2019). The MMEJ pathway depends on resection initiation, and is therefore executed in the S and G2/M phases of the cell cycle (Sfeir and Symington, 2015). This pathway is extremely mutagenic and leads to deletions, insertions, and translocations, thereby potentially inducing tumorigenesis (Seol et al., 2018; Sfeir and Symington, 2015). Besides potentially driving malignancy-inducing mutagenesis, the MMEJ pathway is frequently utilized by BRCA2-deficient cancers (Ceccaldi et al., 2015) and chronic myeloid leukaemia cells, which potentially drives genomic instability (Sallmyr et al., 2008).

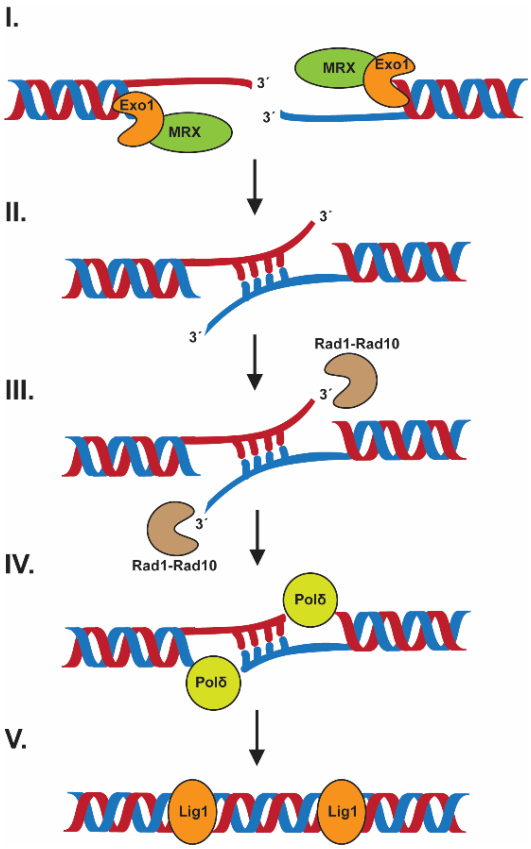

Figure 9. Mechanism of microhomology-mediated end joining. Following the DSB formation, the DNA ends are resected by the MRX complex and other nucleases, Exo1 and Dna2. The resection exposes microhomologies, which are annealed in a Rad52-independent manner. The heterologous flaps are removed by the Rad1-Rad10 nuclease complex. The ssDNA is filled-in majorly by Polδ-mediated DNA synthesis. The DNA strands are ligated presumably by Cdc9 (Ligase 1). The figure is modified from (Sfeir and Symington, 2015).

1.5.4 The role of the MRX complex in DNA repair

1.5.4.1 Structure of the MRX complex

MRX is a heterohexameric complex, which is formed by Mre11, Rad50, and Xrs2 (and Mre11. Rad50, and Nbs1 in mammals) in a 2:2:2 ratio. Mre11 is a nuclease, which forms the core of the complex by dimerization, and later interacts with and recruits both Rad50 and Xrs2 (reviewed in (Oh and Symington, 2018)). The N-terminal nuclease domain of Mre11 has five phosphodiesterase motifs, which provide endonuclease and 3´ to 5´ exonuclease activities of the protein. The nuclease domain of Mre11 is crucial for the dimerization of Mre11 (Hopfner et al., 2001). The C-terminus of the protein contains a capping domain, which is important for the DNA duplex unwinding (Gobbini et al., 2018), and the Rad50 interaction site (Figure 10a).

Rad50 belongs to the SMC protein family of ATPases (other members of the family include Cohesin and Condensin). The protein is composed of Walker A and Walker B domains, two coiled-coil arms, and a Zink hook domain (Figure 10a). The protein's N terminus has the Walker A domain and the C terminus has the Walker B domain, which, when juxtaposed, generate an ATP-binding domain (Hopfner et al., 2002). The ATP-binding and hydrolysis activity of Rad50 is important for binding to DNA and for DNA end tethering, as well as for the nuclease function of the MRX complex (Marsella et al., 2019). The N and C terminal Walker A and B domains are separated by two long coiled-coil domains, and an apical Zink hook that is located in between the coiled-coil domains (Hopfner et al., 2002). Upon ATP hydrolysis, the coiled-coil arms of Rad50 form a long antiparallel structure, which stabilizes the Rad50 dimer and allows intermolecular dimerization of the apical Zink hook domain (Hohl et al., 2010; Marsella et al., 2019). The Zink hook has one Cys-X-X-Cys motif, which binds Zn^{2+} ions and is crucial for the MRX complex dimerization (Hopfner et al., 2002). The ATPase activity of Rad50 triggers conformational changes of the complex.

Xrs2 in budding yeast has multiple protein-protein interaction motifs, which are important for the regulation of the MRX complex signaling activity (Oh and Symington, 2018). The protein is not conserved in mammals, where the functional analog Nbs1 executes its role in the complex. Xrs2 contains the N-terminal forkhead (FHA) domain adjacent to two BRCT domains, while the C terminus of the protein contains multiple motifs important for interaction with Mre11 and Tel1 (Figure 10a). The FHA domain of Xrs2 binds the phosphorylated form of Sae2 and the NHEJ protein Lif1 (Liang et al., 2015; Matsuzaki et al., 2008). Xrs2 mediates the nuclear import of Mre11, and the deletion of Xrs2 leads to a strong resection defect (Tsukamoto et al., 2005). Moreover, Xrs2 is important for the recruitment of the checkpoint kinase, Tel1, which initiates DDC (Iwasaki et al., 2016; Marsella et al., 2019).

The MRX complex exists in two distinct conformation states: the “closed” state, in which ATP is bound by the complex, and the “open” state, in which ATP is hydrolyzed (Figure 10b) (Oh and Symington, 2018). In the “closed” state, the dimerization of Rad50 blocks the nuclease-active site of Mre11 (Deshpande et al., 2014). The MRX complex in the “closed” state promotes DNA end tethering, NHEJ repair, and Tel1 activation. ATP hydrolysis by Rad50 induces the conformational change of the complex and results in an “open” state. This MRX conformation promotes DNA end resection by the nuclease Mre11 and HDR pathway repair ((Deshpande et al., 2014; Lim et al., 2011), reviewed in (Oh and Symington, 2018)).

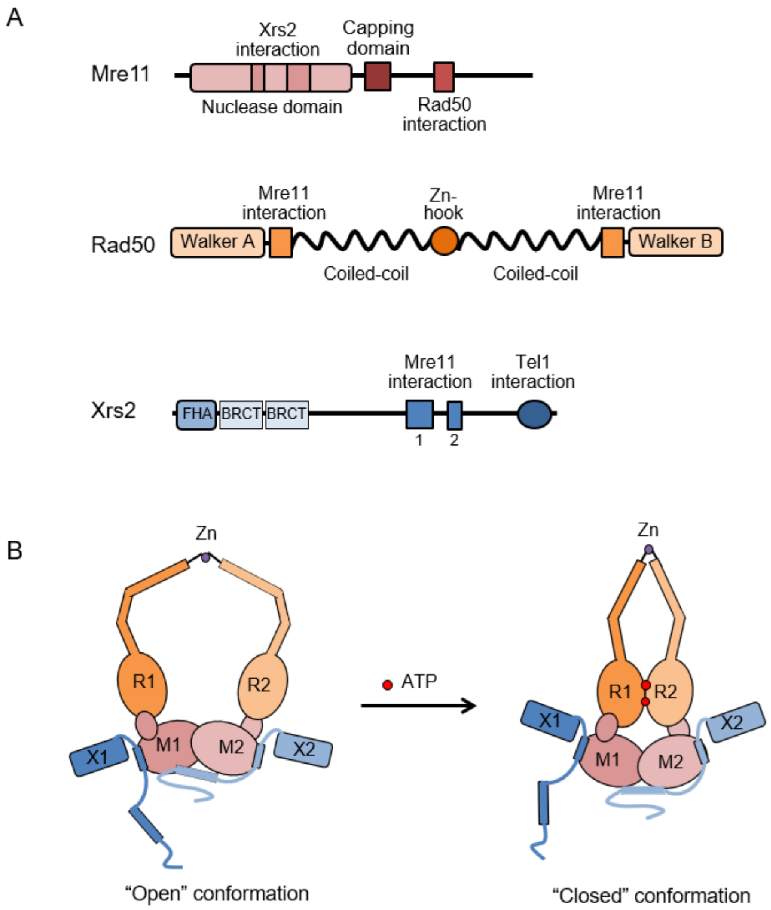

Figure 10. The domain structures of the Mre11, Rad50, and Xrs2 proteins, and the MRX complex conformation changes upon ATP hydrolysis. (a) The Mre11 protein has the N-terminal nuclease domain, the capping domain, and the C-terminal Rad50 interaction site. The Rad50 N and C termini Walker A and B domains are separated by two long coiled-coil arms. The apical Zink hook that is located in between the coiled-coil domains. The N terminus of Xrs2 has a forkhead domain (FHA) and two BRCT domains, while the C terminus is important for interaction with Mre11 and Rad50. **(b)** The two conformational states of the MRX complex. The “closed” state, in which ATP is bound by the complex, and the “open” state, produced by ATP hydrolysis. Figure taken from (Oh and Symington, 2018).

1.5.4.2 The role of MRX complex in DNA end resection and the HR pathway

The MRX complex is extremely important for the initial DNA end resection, a crucial step for all HDR pathways. The resection initiation by the MRX complex is controlled by CDK activity, and is therefore restricted to the S and G2/M phases of the cell cycle (Chen et al., 2011; Huertas et al., 2008). The nuclease Mre11 has multiple phosphodiesterase motifs on its N terminus and displays Mn^{2+}-dependent ssDNA endonuclease and dsDNA 3´ to 5´ exonuclease activities (Paull and Gellert, 1998). The Mre11-dependent 3´ to 5´ end resection facilitates the removal of Ku proteins from the DNA ends and allows the formation of a long 3´ ssDNA overhang that is a substrate for HR (Reginato et al., 2017; Wang et al., 2017). Following the initial resection step by the MRX complex, the long-distance resection in the 5´ to 3´ direction is continued by Exo1 nuclease, and Dna2 nuclease together with Sgs1 helicase, which are recruited by the MRX complex (Cejka et al., 2010a; Gobbini et al., 2016; Mimitou and Symington, 2008).

The nucleolytic activity of Mre11 is stimulated by Sae2 in a CDK-dependent manner, which allows for an efficient initiation of resection (Anand et al., 2016; Cannavo and Cejka, 2014; Huertas et al., 2008). The resection is negatively regulated by Rad9 (Bonetti et al., 2015) and by the DNA damage checkpoint (reviewed in (Bonetti et al., 2018)), which counteracts hyperresection.

The absence of Mre11 nuclease activity (in nuclease-dead mutants) results in an impaired initial resection nevertheless, Exo1 and Sgs1-Dna2 execute DNA end resection with delayed kinetics. However, the deletion of individual MRX genes results in a severe resection defect, due to impaired Exo1 and Sgs1-Dna2 recruitment (Oh and Symington, 2018; Shim et al., 2010). Therefore, the deletion of any of MRX components results in a severe HR defect, which results in an extreme sensitivity to DNA damaging agents (Symington, 2016). Nonetheless, HR is not fully eliminated in the mutants lacking the MRX complex. Importantly, these mutants demonstrate decreased HR fidelity and a surge in rates of mutagenic heteroallelic recombination and other genomic re-arrangements (Bressan et al., 1999; Chung et al., 2010; Oh and Symington, 2018).

1.5.4.3 The role of the MRX complex in the MMEJ and NHEJ pathways

The nucleolytic degradation of 5´ DNA ends is an essential step in exposing microhomologies that are utilized by the MMEJ pathway (see section 1.5.3. for the detailed overview of MMEJ pathway). The MRX complex plays a central role in MMEJ not only by initiating resection, but also by providing efficient DNA end tethering (Sfeir and Symington, 2015). The *mre11* deletion mutants display a severe MMEJ defect (Lee and Sang, 2007; Ma et al., 2003; Truong et al., 2013). Importantly, in yeast, the nuclease-deficient Mre11 mutants display higher rates of MMEJ repair events compared to the *MRE11* deletion mutants (Deng et al., 2014). This is presumably because

while the DNA end resection in nuclease-dead mutants can still be carried out by Exo1 and Sgs1-Dna2, the loss of *MRE11* additionally abrogates their recruitment. In mammals, the MRX complex is essential for the MMEJ pathway (Rass et al., 2009).

The MRX complex also plays a crucial role in the repair of DSBs by the NHEJ pathway. In contrast to the HR and MMEJ pathways, the NHEJ pathway happens in the absence of DNA end resection. The MRX complex-mediated DNA end tethering is crucial for NHEJ, as abrogation of the tethering leads to DNA repair defects (Cassani et al., 2016). The Xrs2 component of the complex is directly involved in the NHEJ pathway, as its FHA domain recruits Lif1, which is crucial for the NHEJ repair complex formation (Matsuzaki et al., 2008). In mammals, Nbs1 binds to the Lif1 homologue XRCC4 (Lloyd et al., 2009), and MRX seems to play a role in the NHEJ pathway (Rass et al., 2009; Xie et al., 2009). In mammals, the precise role of the MRN complex in NHEJ is not yet understood.

1.5.4.4 The role of the MRX complex in the repair of CPT-induced lesions

The MRX complex plays an important role in the repair of CPT-induced DNA damage (for the DNA damage mechanism of CPT, see section 1.1.4.1), due to its role in HR initiation, and in the removal of DNA-protein crosslinks. Therefore, yeast mutants lacking MRX-encoding genes, as well as the nuclease-dead *mre11-H125N* allele, are extremely sensitive to even low CPT dosages (Menin et al., 2018; Oh et al., 2016). The resection function of MRX is extremely important for the initiation of the HR-mediated DNA damage repair pathway. Consequently, the resection-deficient *sae2* mutant is also hypersensitive to CPT-induced lesions, and the *MRE11* mutations that rescue resection defects in *sae2* rescue the mutant viability on CPT (Cassani et al., 2018).

The MRX complex also participates in direct removal of CPT-DNA covalent adducts, in parallel with Tdp1 and Rad1-Rad10 pathways (Liu et al., 2002; Sacho and Maizels, 2011). Due to endonucleolytic activity, Mre11 cleaves the covalent 3′-phosphotyrosyl bond between Top1 and 3'-phosphotyrosyl-DNA, and leads to the formation of 3´ phosphate DNA ends and the release of Top1 (Sacho and Maizels, 2011). Following nucleolytic cleavage, the DNA ends can be further resected and repaired.

1.5.5 RNA-templated DNA repair

Although HR usually happens between two DNA molecules, recombination events that include RNA substrates have been described (Smail et al., 2019). The RNA-templated DNA repair events were first demonstrated using oligonucleotides. Later, Storici and colleagues demonstrated that the endogenously-generated transcripts could mediate HR events (Keskin et al., 2014; Storici et al., 2007). There are two distinct modes for utilizing RNA as a donor template. In an indirect mode,

the RNA molecule undergoes reverse transcription due to the activity of Ty1 transposon-derived reverse transcriptase, resulting in the formation of cDNA, which is used as a donor sequence for the HR (Storici et al., 2007). In a direct mode, the template RNA directly base pairs with the sequences proximal to the DSB, and serves as a template for DNA synthesis, presumably by DNA Pol α and DNA Pol δ (Keskin et al., 2014; Storici et al., 2007). The RNA-templated DNA repair pathway operates *in cis*, when the RNA is transcribed from the locus at which the DSB was induced, or *in trans*, when the template is encoded elsewhere (Keskin et al., 2014). The RNA-templated DNA repair utilizes Rad52, which, in this specific repair pathway, drives an inverse strand exchange: Rad52 forms a complex with dsDNA and promotes strand exchange with homologous ssRNA or ssDNA (Mazina et al., 2017; McDevitt et al., 2018). This pathway allows for DSB repair utilizing a homologous template outside of the S and G2 phases, in which the HR pathway is active (Meers et al., 2016). Although initially described in budding yeast, RNA-templated repair is reported in rat post-mitotic neurons (Welty et al., 2018), human U2OS cells (Wei et al., 2015), and human KP6 cell lines (Onozawa et al., 2014), indicating the evolutionary conservation of the pathway.

1.5.6 Other faulty DSB repair mechanisms

Retrotransposons are repetitive mobile genetic elements that migrate through eukaryotic genomes and were implicated in the repair of DSBs in budding yeast and higher eukaryotes (Moore and Haber, 1996; Morrish et al., 2002, 2007; Teng et al., 1996). On rare occasions following the induction of a DSB at the *MAT* locus with HO endonuclease, the sequences of Ty1, a yeast retrotransposon, are inserted directly into the DSB site (Moore and Haber, 1996). This happens as follows: the mRNA of Ty1 is reverse transcribed by the Ty1-encoded reverse transcriptase (RT), which is inserted into the DSB using Ty1 integrase and NHEJ machinery (Fried et al., 2010; Yu and Gabriel, 1999). This repair pathway does not require Rad52 (Moore and Haber, 1996) and is potentially highly mutagenic.

Coïc and colleagues reported another Rad52-independent non-canonical DNA repair pathway (Coïc et al., 2008). Although it is generally accepted that Rad52 is required for efficient mitotic recombination in budding yeast, *rad52* mutants could perform mitotic recombination following UV light treatment. The authors utilized an integrated reporter system that is based on two dysfunctional *his4* alleles, which form a functional *HIS4* gene following the recombination between the split reporter alleles. The Rad52-independent recombination events depended on *RAD59*, *RAD50*, *RAD55*, and *RAD51* genes. Of note, the deletion of RAD52 leads to a roughly 100-fold decrease in the frequency of HR events; therefore, the repair events in the study were rare.

1.6 Aneuploidy as a physiological state

Aneuploidy is a condition of having a chromosome number that is not a multiple of a haploid set (Ben-David and Amon, 2020). Because practically all cellular metabolic processes and environmental responses depend on the balanced dosages of gene products, abnormalities in aneuploid karyotypes inevitably lead to disruption in cellular physiology. Aneuploidy as a condition cannot be viewed as a single genetic trait, but rather is a repertoire of altered karyotypes, and each unique karyotype affects cellular physiology in its unique way. Despite this heterogeneous nature of aneuploidy, the condition evokes systematic changes in cellular physiology that are common for all aneuploids. Importantly, studies in budding yeast demonstrated aneuploidy-induced physiological changes, which were conserved in mammalian systems, particularly in mice and humans. In this section, I will present an overview of the mechanisms of aneuploidization, the physiological consequences of aneuploidy, and the selective targeting strategies, based on studies in budding yeast and human cells.

1.6.1 Mechanisms of aneuploidization

Aneuploidy can arise due to chromosome missegregation during meiosis and mitosis, and the faulty repair of DNA damage. During meiosis, chromosomal nondisjunction produces haploid gametes that have whole chromosome aneuploidies (Gilchrist and Stelkens, 2019). This type of error underlies human whole chromosome aneuploidies, for example Down syndrome and Turner syndrome (Hassold and Hunt, 2001). Sometimes human genetic trisomies are mosaic, which means that only a fraction of cells carry the mutation. These aneuploidization events are not the result of meiotic chromosome segregation errors, as they arise following mitotic chromosome missegregation events in early embryogenesis (van Echten-Arends et al., 2011). Whole chromosome aneuploidies are routinely detected in mammalian cells, for example in hepatocytes and neurons (Knouse et al., 2014; Rehen et al., 2001, 2005). These observations imply that the basal rate of chromosome missegregation in normal mitosis and meiosis produces infrequent but detectable aneuploidization events.

The chromosomal missegregation events in mitosis occur due to incorrect attachment of the spindle microtubules to the kinetochore as a result of erroneous spindle formation, defects in kinetochore structure, altered centrosome number, and defects in sister chromatid cohesion, or failure of the spindle assembly checkpoint ((Corbett, 2017; Lampson and Grishchuk, 2017; Monda and Cheeseman, 2018), reviewed in (Chunduri and Storchová, 2019) and (Gordon et al., 2012)). In human tissues, an estimated rate of chromosomal nondisjunction events is 1 per 100 cell divisions (Cimini et al., 1999). Cancer cells often display drastically elevated levels of

chromosomal instability, which generally arise via similar mechanisms that lead to chromosomal missegregation in non-transformed cells (Gordon et al., 2012). For example, cancer cells frequently display centrosome amplification events and merotelic attachments of the spindle (which is when both chromosomes are attached to the same centrosome) (Gregan et al., 2011; Nigg, 2002). Curiously, mutations in genes involved in the spindle assembly checkpoint are rather uncommon in human malignancies (Kops et al., 2005; Sinha et al., 2019).

Cancer cells often experience replication stress, which can potentially lead to the underreplication of difficult-to-replicate genomic regions, and therefore to the loss of genetic material (Gaillard et al., 2015; Zeman and Cimprich, 2014). These difficult-to-replicate regions include common fragile sites, telomeres, and ribosomal DNA loci. When the replication fork progression through common fragile sites is impaired, ultrafine anaphase bridges are formed, which leads to genomic instability, chromothripsis, and cataegis (Liu et al., 2018; Maciejowski et al., 2015; Ozeri-Galai et al., 2011). Functional DDC signaling is important to control the replication of these difficult-to-replicate regions, yet cancer cells frequently harbor mutations in DNA damage checkpoint genes (Casper et al., 2002; Durkin et al., 2006; Eykelenboom et al., 2013). The combination of replication stress and DDC deficiency creates favorable conditions for genomic instability and potential aneuploidization.

DNA repair with BIR constitutes another source of mutagenic gross chromosomal rearrangements and segmental aneuploidies (Sakofsky and Malkova, 2017). BIR promotes half-crossovers and non-reciprocal translocations, and therefore results in fusions in donor and recipient chromosomes (Anand et al., 2014; Lydeard et al., 2007; Smith et al., 2009). BIR is associated with chromothripsis and results in a complex genomic rearrangement at the target chromosome (Kloosterman et al., 2011; Stephens et al., 2011; Zack et al., 2013). Chromoanasynthesis, which is a type of chromosomal rearrangement with copy number gains, is executed via microhomology-mediated BIR (Carvalho and Lupski, 2016; Carvalho et al., 2011). Therefore, DNA repair via BIR constitutes other another mechanism of copy number alterations, resulting in segmental aneuploidies. In budding yeast, aneuploidization can occur due to chromosome missegregation events in mitosis and meiosis, and as a consequence of genomic instability (Storchova, 2018; Syrovatkina and Tran, 2015).

1.6.2 Physiological consequences of aneuploidy

1.6.2.1 Metabolic alterations in aneuploid cells

Aneuploidy, as a condition, gives rise to a plethora of physiological alterations, which result in fitness defects and decreased proliferation capacity in budding yeast, mouse embryonic

fibroblasts, and human cell lines (Sheltzer et al., 2017; Tang et al., 2011; Torres et al., 2007). These alterations include changes in gene expression that are similar to general stress responses (Dürrbaum and Storchová, 2015; Torres et al., 2007; Zhu et al., 2018), changes in cell cycle progression (Thorburn et al., 2013), proteotoxic stress (Brennan et al., 2019; Ohashi et al., 2015; Oromendia et al., 2012), metabolic stress (Torres et al., 2007), defects in gene silencing (Mulla et al., 2017), genomic instability (Passerini et al., 2016; Storchova, 2018), hypoosmotic-like stress (Tsai et al., 2019), and many others (Figure 11) (reviewed in (Zhu et al., 2018) and (Chunduri and Storchová, 2019)).

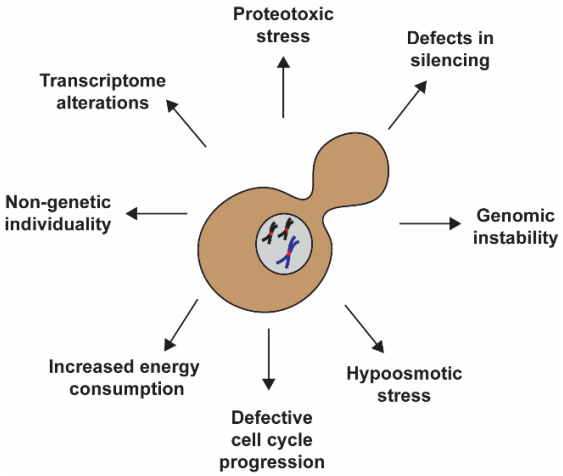

Figure 11. Effects of aneuploidy on cellular physiology. The aneuploidy condition alters cellular physiology, leading to cellular stresses and genomic instability.

Protein homeostasis is crucial for cell survival, so cells regulate their proteome on multiple levels: transcription, translation, and protein degradation. When the protein quality control systems are overwhelmed and cannot efficiently utilize misfolded, mislocalized, or otherwise defective proteins, cells suffer from potentially lethal proteotoxic stress (Guang et al., 2019). Proteotoxic stress is one of the most prominent signs of an aneuploid state, which is accompanied by the accumulation of protein aggregates in the cytoplasm and poor tolerance to conditions that challenge protein quality control systems (Brennan et al., 2019; Ohashi et al., 2015; Oromendia et al., 2012). Proteotoxic stress in aneuploids arises primarily due to the imbalances in gene dosages (Torres et al., 2007). Since the majority of protein complex components in eukaryotes are encoded on different chromosomes, this generates a stoichiometric imbalance that leads to an accumulation of aggregated proteins (Oromendia et al., 2012). These protein aggregates are enriched with peptides encoded by the exact extra chromosome present in the strain. Importantly, the nearly diploid human cell line RPE-I (which carries an extra copy of chromosome 12 or 21) formed protein aggregates that were also enriched with peptides encoded by the extra chromosome (Brennan et

al., 2019). The deficiency in Heat shock factor protein 1 (Hsf1), a key heat shock transcription factor, and in Heat shock protein 90 (Hsp90) chaperone also contribute to aneuploidy-associated proteotoxic stress in human cells (Donnelly et al., 2014).

Due to proteotoxic stress, aneuploids show an increased reliance on genes that are involved in the regulation of protein homeostasis, which was demonstrated with Ubp3 deubiquitinase (Oromendia et al., 2012). On the other hand, the mutation in deubiquitinase Ubp6 rescues growth defects in multiple disomic yeast strains, likely due to the improvement in proteasome function and increased protein degradation (Dephoure et al., 2014).

Studies in budding yeast demonstrated that aneuploidy could affect gene dosage not only by the alterations in gene copy number, but also by affecting gene silencing (Mulla et al., 2017). Yeast chromosome X disomes upregulate the transcription of silenced genes genome-wide, which contribute to protein imbalance.

Another common feature of aneuploids is a presence of gene expression signatures characteristic of hypoosmotic stress (Tsai et al., 2019). Hypoosmotic stress is a biophysical outcome of an imbalanced proteome, which manifests in the increased outer membrane pressure and impaired endocytosis. An important consequence of hypoosmotic stress is the metabolic remodeling of aneuploids due to alterations in plasma membrane transporter function and turnover, together with defects in endocytosis.

The precise coordination of metabolic pathways also depends on a balanced dosage and activity of each enzyme and regulatory proteins in the pathway. Metabolic stress is found to be a common characteristic of the aneuploid state in yeast, as the gene expression profiling revealed strong downregulation of genes involved in carbohydrate metabolism (Torres et al., 2007). However, in human cells, chromosome transfer-induced aneuploidy resulted in an increase in the energy metabolism pathway (Stingele et al., 2012). Importantly, metabolic stress in yeast manifested in an increased glucose uptake by aneuploid strains, while the accumulation of biomass was impaired (Torres et al., 2007). Similar results were reported for mouse embryonic fibroblasts, as trisomes displayed increased glucose uptake together with alterations in production of many other important metabolites (Williams et al., 2008). The data presented above clearly indicate that aneuploids have altered carbohydrate metabolism.

The metabolic alterations in aneuploid cells are accompanied by increased ROS production. Experiments in disomic yeast strains revealed an upregulation of genes involved in response to oxidative stress, which were concomitant with changes in their proteome (Dephoure et al., 2014). The increased ROS levels were also observed in aneuploid mouse embryonic fibroblasts (Li et al., 2010), and the increased ROS levels were responsible for checkpoint activation in these cells. However, the source of ROS in aneuploidy is not understood so far.

1.6.2.2 Effects of aneuploidy on cell cycle progression and DNA damage

Another prominent group of aneuploidy-associated phenotypes concerns replication, mitosis, and cell cycle progression in general. Due to the high levels of aneuploidy-associated DNA damage and genome instability together with metabolic and proteotoxic stresses, it is not surprising that aneuploids exhibit decreased proliferation capacity and abnormal cell cycle progression. The decision to enter the new cell cycle happens in the G1 phase and is known as START (reviewed in (Jorgensen and Tyers, 2004)). In a simplistic model of START, Cdc28 is activated by Cln3 cyclin. The activity of Cdc28 leads to the eviction of the G1/S transition inhibitor, Whi5, allowing the cell to enter the S phase of the cell cycle (Costanzo et al., 2004). In a parallel mechanism, expression of Cln1 and Cln2 cyclins allows passage through START in a Cln3-independent manner (Di Como et al., 1995). Disomic yeast strains displayed decreased levels of *CLN2* on a transcriptional level, which was accompanied with a delay of the cell cycle entry following pheromone-induced G1 arrest (Torres et al., 2007). On the proteome level, aneuploids displayed delayed expression of G1 cyclins, Cln1 and Cln2, and delayed nuclear eviction of Whi5, which explains the delayed passage of the mutants through START (Thorburn et al., 2013).

In aneuploid cells, the S phase is accompanied by replication stress and DNA damage. Replication stress is defined as a slowing or stalling of replication fork progression (Ovejero et al., 2020). Disomic budding yeast display an accumulation of Rad52 foci in the S phase of the cell cycle, which indicates the presence of DNA damage during replication. Moreover, aneuploids exhibited defects in DNA replication initiation and replication fork progression (Blank et al., 2015). Aneuploid human cells demonstrated slower replication kinetics accompanied with an increased sensitivity to the replication inhibitor amphidicolin, likely due to the decreased levels of replicative helicase complex MCM2-7 (Passerini et al., 2016). Highly aneuploid breast cancer and hepatocellular carcinoma tumors display disruption of the normal replication timing and signs of the replication stress (Grinberg-Rashi et al., 2010).

The high persistent levels of DNA damage and high degree of genomic instability was documented in aneuploid yeast and human cells (Blank et al., 2015; Passerini et al., 2016; Zhu et al., 2012). Disomic budding yeast displayed increased rates of chromosome missegregation events, elevated mutation rates, and defects in HDR (Sheltzer et al., 2011). Moreover, aneuploids demonstrated entry into mitosis with unrepaired DNA damage, indicating that aneuploids are predisposed to CA (Blank et al., 2015). Elevated levels of genomic instability were documented in aneuploid human cells, which displayed increased levels of DNA damage in the G1 phase of the cell cycle, as assessed by an accumulation of 53PB1 damage foci (Passerini et al., 2016). These increased DNA damage levels were accompanied by an increase in mitotic errors and *de novo*

genomic rearrangements, presumably due to the increased occurrence of lagging chromosomes (Nicholson et al., 2015). Another study on highly aneuploid human cells generated by treatment with MPS1 inhibitors demonstrated that these cells have high rates of chromosome missegregation events accompanied with high levels of DNA damage (Santaguida et al., 2017). Together, aneuploidy is accompanied with alterations in all phases of the cell cycle, including a delayed progression through START, abnormal replication kinetics, and increased entry into mitosis with unrepaired DNA damage, which leads to slower growth and increased genomic instability.

1.6.2.3 Effects of aneuploidy on the transcriptome

Aneuploidy, as a condition, has a drastic effect on the cellular transcriptome and proteome, manifesting in alterations in multiple cellular processes (Pavelka et al., 2010; Torres et al., 2007). In budding yeast, extra chromosomes are transcribed according to their copy number, creating a source of gene dosage imbalances. The effects of aneuploidy on the transcriptome and proteome seem to directly correlate with changes in the DNA copy number (Dephoure et al., 2014; Pavelka et al., 2010). In aneuploids, the majority of transcripts with altered expression are located on the extra chromosome. Importantly, the aneuploid state also induces genome-wide changes in gene expression (Gasch et al., 2016; Rancati et al., 2008). For example, human cells trisomic for chromosome 21 displayed re-wiring of the whole transcriptome (Letourneau et al., 2014; Liu et al., 2017b).

Although the literature presents conflicting data regarding whether the gene dosage compensation is operating in aneuploid yeast (Gasch et al., 2016; Torres et al., 2016), it is clear that the majority of the transcripts are expressed according to their copy numbers. In higher eukaryotes–particularly humans–the dosage compensation mechanism seems to be genomic context-dependent. For example, human sex chromosomes are subjected to the dosage compensation mechanism; therefore, the extra copies of chromosomes are silenced in triple X syndrome (47, XXX karyotype) or partially silenced in Kleinefelter syndrome (47, XXY) (Letourneau et al., 2014; Payer and Lee, 2008; Tartaglia et al., 2010). Yet, autosomal dosage compensation mechanisms seem to not be so robust, as the vast majority of aneuploidies are lethal for mouse and human development.

The analysis of transcriptome alterations in aneuploid budding yeast revealed signatures of so-called environmental stress responses and hypoosmotic-like stress (Torres et al., 2007; Tsai et al., 2019). GO term analysis has shown that the genes involved in ribosome biogenesis and nucleic acid metabolism were upregulated, while the genes involved in carbohydrate metabolism and cell cycle progression were downregulated (Torres et al., 2007). In human cells, aneuploidy

leads to the upregulation of genes involved in glycolysis, autophagy, and pathways involved in inflammatory responses, e.g. Interferon biosynthesis (Dürrbaum et al., 2014; Santaguida et al., 2017; Stingele et al., 2012). At the same time, the pathways involved in cell cycle progression and nucleic acid metabolism are downregulated in aneuploid human cells (Dürrbaum et al., 2014; Stingele et al., 2012). These results suggest that the condition of aneuploidy systematically changes the cellular transcriptome, which is one of the underlying reasons for aneuploidy-associated physiological disadvantages.

1.6.3 Aneuploidy in cancer development

Aneuploidy is classically defined as an imbalanced number of chromosomes. In humans, only three autosomal whole chromosome aneuploidies are viable, which are Down syndrome (47, XX, +21), Edwards syndrome (47, XX, +18), and Patau syndrome (47, XX, +13). The aneuploidies in sex chromosomes are better tolerated compared to the ones in autosomes (Vogel and Motulsky's Human Genetics, (Speicher et al., 2010)). The classical definition of aneuploidy was extended to include the gain and loss of chromosome arms, which frequently lead to a plethora of human genetic syndromes (Ben-David and Amon, 2020). Aneuploidy is often detected in human cancers, with roughly 90% of solid tumors being aneuploid (Taylor et al., 2018). The effect of aneuploidy on cellular physiology depends, in a paradoxical way, on the context of its occurrence: while the introduction of an extra chromosome into primary cells leads to reduced cellular fitness, transformed cancer cells seem to tolerate aneuploidy extremely well (Sheltzer et al., 2017).

Growing evidence suggests that certain types of aneuploidies may be tumorigenesis drivers, because many cancer types have the same recurring aneuploidy patterns ((Beroukhim et al., 2010; Taylor et al., 2018; Zack et al., 2013), reviewed in (Ben-David and Amon, 2020)). For example, the myelodysplastic syndrome cells that progress to acute myeloid leukaemia frequently harbor the loss of long arms of chromosomes 5 or 7, or even the entire chromosome (Greenberg et al., 1997). Even more strikingly, the loss of chromosome arm 3p in early childhood, before the tumor can even be detected, leads to clear renal cell carcinoma with more than 90 percent certainty (Mitchell et al., 2018). Besides playing a potential role in tumor initiation, aneuploidy clearly contributes to cancer progression, as later stages of the disease seem to positively correlate with the degree of aneuploidy (Ben-David and Amon, 2020). For example, the early stages of colorectal cancer have a low degree of aneuploidy, while the advanced tumors are highly aneuploid (Laubert et al., 2015).

Aneuploidy marks the transition between *in situ* to the invasive state. The gain of chromosome 3q marks the transition into the invasive state of cervical cancer (Heselmeyer et al., 1996), and the establishment of a highly aneuploid state marks the onset of esophageal adenocarcinoma (Ross-

Innes et al., 2015). The metastatic process is also associated with further karyotype evolution, in which different metastatic colonies represent sub-clones of the primary tumor ((Brastianos et al., 2015; Gao et al., 2016; Reiter et al., 2018), reviewed in (Ben-David and Amon, 2020)). Due to the strong association with disease progression, aneuploidy has a potential prognostic value for the cancer stage and the outcome for the patient, and it is frequently used to predict the treatment regimen (Ben-David and Amon, 2020). The prognostic value is tumor type-specific; although a high degree of aneuploidy is associated with a more aggressive disease and poor prognosis for the majority of cancers, a high degree of aneuploidy is a rather favorable prognostic marker for certain tumor types (Hieronymus et al., 2018; Manier et al., 2017). Together, aneuploidy seems to play an important role in tumor initiation, progression, and metastasis, which gives it a potential prognostic value for the tumor stage and the survival outcome.

1.7 Mechanisms of genotoxin resistance in human cancers

The clinical use of genotoxins for cancer treatment is overshadowed by the drug resistance problem: as soon as new chemotherapeutic or targeted molecular cancer therapies enter clinics, scientists see the rise of drug resistance mechanisms (Mullard, 2020). This resistance is achieved through multiple mechanisms, which include drug efflux, alterations in the expression of drug targets, re-activation of DNA repair pathways, inhibition of apoptosis, and many other mechanisms (reviewed in (Holohan et al., 2013) and (Bouwman and Jonkers, 2012)). The central growth regulator mTOR has been implicated in the development of cancer resistance (Butt et al., 2019; Tian et al., 2019). Tumor heterogeneity, genomic instability, and aneuploidy were also proposed to contribute to the drug resistance problem by therapy-induced selection of the resistant clones (Ben-David and Amon, 2020; Bouwman and Jonkers, 2012). Rational drug combinations are proposed to be a promising strategy in combating the resistance problem in cancer. In this section, I will present an overview of drug resistance mechanisms employed by cancer cells, focusing on the mechanisms of genotoxin resistance and DNA repair-mediated pathways in particular. I will also discuss the contribution of the mTOR pathway to resistance in cancers and the potential of combining chemotherapeutics with mTOR inhibitors clinically. Finally, I will discuss aneuploidy-induced cancer adaptability as a drug resistance source.

1.7.1 Common mechanisms of drug resistance in human cancers

In response to chemotherapies and targeted therapies, cancer cells frequently develop drug resistance. Although chemotherapy-based strategies rely on general cytotoxic effects (e.g. induction of DNA damage or replication stress) while targeted molecular targeting exploit specific tumor vulnerabilities (e.g. targeting epithelial growth factor receptor, EGFR), it is curious that the mechanisms of resistance to the aforementioned therapies are largely redundant (Holohan et al., 2013).

The coordinated action of cellular plasma membrane transporters of the ATP-binding cassette (ABC) family allows the drug's efflux, which is a commonly described mechanism that promotes the resistance to multiple chemotherapeutics (reviewed in (Chen et al., 2016)). Overcoming drug resistance by targeting the membrane transporters proved to be challenging, as there are 49 members of the ABC family transmembrane transporters and their functions are redundant. For example, targeting the MDR1 transporter that confers chemoresistance in lung and breast cancers with the MDR1 inhibitor, tariquidar, was inefficient in clinical trials, likely because of the functional redundancy of the ABC family transmembrane transporters ((Nooter et al., 1997; Pusztai et al., 2005; Zalcberg et al., 2000), reviewed in (Holohan et al., 2013)).

Many chemotherapeutics require drug activation by metabolic enzymes. For example, the conversion of capecitabine into the antimetabolite, 5-fluorouracil, requires thymidine phosphorylase. The expression of thymidine phosphorylase is silenced in response to capecitabine treatment, which confers drug resistance (Kosuri et al., 2010; Malet-Martino and Martino, 2002).

Alterations in drug target expression levels have been demonstrated to constitute another mechanism of drug resistance. In response to Top1 inhibitors, e.g. irinotecan, cancer cells decrease Top1 expression levels or acquire mutations in the *TOP1* gene, thereby becoming resistant (Tsurutani et al., 2002). The increased drug target expression can also confer the resistance, as it was shown for the androgen receptor and its inhibitor, bicalutamide (Palmberg et al., 1997).

Ultimately, both DNA damage-induced chemotherapies and targeted therapies intend for the drug-induced damage to lead to cell death by apoptosis. The deregulation of apoptosis is one of the hallmarks of cancer, which promotes cancer cell resistance to therapies by the simple evasion of cell death signals (Hanahan and Weinberg, 2011). Cancer cells rely on the pro-survival signals from anti-apoptotic proteins, which makes them therapeutic targets. The members of the BCL-2 family of anti-apoptotic proteins were shown to promote drug resistance following chemotherapy; yet, cancer cells become resistant to the pharmacological inhibitors of BCL-2 proteins ((Konopleva et al., 2006), reviewed in (Holohan et al., 2013)). The combination of therapies that combine targeting anti-apoptotic proteins together with chemotherapeutics are very promising nonetheless. Cancer cells also activate pro-survival signaling pathways that drive drug resistance, which include Ras signaling, Wnt and NOTCH signaling, Akt/Pi3K signaling, TGF-β signaling, and many others (reviewed in (Panda and Biswal, 2019)). These changes in cell signaling pathways modulate the tumor's microenvironment and promote the secretion of growth factors, which sustain cancer cell growth even during targeted therapies (Holohan et al., 2013; Panda and Biswal, 2019). The secretion of extracellular vesicles also substantially contributes to the formation of the resistance to chemotherapy (reviewed in (Namee and O'Driscoll, 2018)). Finally, in response to chemotherapeutics, cancer cells alter their DDR pathways and often restore DNA repair, which will be discussed in the section below. The problem of drug resistance could potentially be solved by the rational combinations of the therapies that simultaneously target different pathways in the cell, thereby decreasing the likelihood that resistant mutations could be selected (Holohan et al., 2013).

1.7.2 Mechanisms of alterations in DNA repair that lead to genotoxin resistance in BRCA1 and BRCA2 deficient tumors

DNA damaging agents, particularly those that induce DSBs and intra- and interstrand crosslinks, are very efficient in targeting tumors that have DNA repair deficiencies, especially in HR or MMR pathways. Therefore, the way tumors regulate their DNA repair pathways is a predictor of the efficiency of genotoxin-based therapies. The deficiency in HR, for example, is a double-edged sword: these tumors are very sensitive to DSB-inducing genotoxins, yet they have increased rates of genomic instability that allows selection of the therapy-resistant clones (reviewed in (Bouwman and Jonkers, 2012)).

The resistance to genotoxin therapy in HR-deficient tumors could either be intrinsic or acquired by the selection of the resistance-inducing mutations. Certain types of human ovarian tumors demonstrate intrinsic drug resistance to cisplatin because they lack expression of the copper transporter CTR1 that is important for drug uptake (Ishida et al., 2010). Yet, the majority of drug resistance in cases is acquired during the course of chemotherapy, leading to relapse of the disease in patients (Bouwman and Jonkers, 2012).

The restoration of DNA repair due to the re-activation of the HR pathway could be caused by genetic reversions. The breast cancer 2 (BRCA2) protein binds Rad51 and promotes HR pathway-mediated DSB repair (Moynahan et al., 2001). BRCA2-deficient ovarian carcinomas are routinely treated with cisplatin, yet the cancer cells develop cisplatin resistance following the repeated exposures. The resistance is mediated by the secondary mutations in the BRCA2 gene, which restore wild-type BRCA2 and, therefore, make cancer cells HR-proficient. These mutations were observed in ovarian cancer and pancreatic cancer cell lines, as well as in primary tumors (Sakai et al., 2008). The restoration-of-function BRCA2 mutations in the poly (ADP-ribose) polymerase (PARP) inhibitor-resistant clones of pancreatic cancers and BRCA2 mutant cell lines were reported in a different study (Edwards et al., 2008). The amplification of the mutant BRCA2 allele, which leads to increased expression of the truncated hypomorphic BRCA2 isoform, also leads to the restoration of HR and genotoxin resistance in a pancreatic cancer cell line (Park et al., 2020).

Mutations in BRCA1 also result in HR pathway defects, and the administration of PARP inhibitors is a common therapeutic strategy for BRCA1-defective tumors (Lee et al., 2014; Roy et al., 2012). The restoration of the HR pathway can happen in a BRCA1-independent manner. For example, the loss of 53BP1 restores HR-mediated DNA repair in BRCA1-defective cells by restoration of the resection that depends on ATM kinase activity (Bunting et al., 2010; Jaspers et al., 2013). The loss of RIF1, which is downstream of 53BP1, also restores DNA end resection in BRCA1-defective cells (Escribano-Díaz et al., 2013). The depletion of the translesion synthesis polymerase ξ

subunit, REV7, restores HR-mediated DNA repair due to the restoration of DNA end resection: REV7 acts as an inhibitor of the resection downstream of 53BP1 (Xu et al., 2015). The recently identified Shieldin complex (comprising REV7 and the RINN1, RINN2, and RINN3 proteins) acts downstream of 53BP1 and the RIF1 proteins, and its loss confers resistance in BRCA1-defective cells (Gupta et al., 2018). The telomere end protection CST complex (which consists of CTC1, STN1, and TEN1) was shown to act as an antagonist of DNA end resection; the loss of any one of the CST complex members confers PARP inhibitor resistance in BRCA1-defective cells via the restoration of DSB resection, and thus the HR pathway (Barazas et al., 2018). Together, these studies demonstrate that the restoration of resection due to the loss of DSB resection antagonists promotes the resistance to PARP inhibitors in BRCA1-mutated cancers.

The resistance to PARP inhibitors in BRCA-deficient tumors could be acquired without the restoration of HR repair. The mutations in PARP1, both inside and outside of the DNA-binding zinc finger domains, lead to reduced trapping of PARP1 on DNA during treatment with PARP inhibitors, and, therefore, to chemoresistance (Pettitt et al., 2018). The loss of the PAR glycohydrolase, PARG, confers resistance to PARP inhibitors in BRCA2-deficient breast tumors (Gogola et al., 2018). Mechanistically, the downregulation of PARG rescues parylation even upon the treatment with PARP inhibitors.

Because BRCA1 and BRCA2 proteins are implicated in replication fork protection (Schlacher et al., 2012), chemoresistance could be acquired via the alternative mechanisms of replication fork protection. For example, the loss of the MLL3/4 complex protein, PTIP, leads to the deficient recruitment of the nuclease Mre11 that degrades stalled replication forks. Therefore, the loss of PTIP stabilizes replication forks, which leads to chemoresistance in BRCA1- and BRCA2-deficient cells (Chaudhuri et al., 2016). The protein EZH2 is a part of the polycomb repressor complex, which deposits H3K27me at replication forks, thereby repressing transcriptional activity (Morey and Helin, 2010). The loss of EZH2 leads to replication fork protection due to the defective recruitment of the resolvase MUS81, which cleaves the stalled forks, thereby conferring chemoresistance (Rondinelli et al., 2017).

To summarize, HR-deficient tumors acquire chemoresistance due to mechanisms that allow alterations in drug target regulation, HR restoration, or improved replication fork protection.

1.8 Scope of the thesis

Checkpoint adaptation, which is a cell division in the presence of unrepaired DNA damage, was described by the Zakian lab in 1993 (Sandell and Zakian, 1993). Although discovered in budding yeast, adaptation was shown to be conserved in higher eukaryotes (Syljuåsen, 2007; Yoo et al., 2004). Checkpoint adaptation happens when the DNA damage is irreparable by nature, either due to the genomic context of the damage or due to the defects in cellular DNA repair pathways. It has long been appreciated that adaptation results in genomic instability (Galgoczy and Toczyski, 2001). Genomic instability can result in aneuploidy, a condition that invokes physiological alterations and cellular stresses, yet allows increased adaptability to changing environments (reviewed in (Chen et al., 2015; Chunduri and Storchová, 2019; Kaya et al., 2020)).

Human cancers frequently harbor mutations in the BRCA1 and BRCA2 DNA repair genes, which result in homologous recombination defects, and display genomic instability and aneuploidy (Han et al., 2017; Moynahan et al., 2001; Venkitaraman, 2019). At the same time, repair-defective tumors acquire resistance to genotoxins, which represents a major challenge in cancer treatment (Mullard, 2020). I wanted to model a scenario in which homologous recombination-defective cells develop resistance following genotoxin treatment. This allows me to dissect the molecular mechanisms that contribute to the resistance development and understand how to target the resistant cells. Therefore, I used diploid budding yeast that are homozygous for the *RAD52* gene knock-out, and have defects in homologous recombination similar to BRCA2-defective tumors. Using the *rad52* model, I show that checkpoint adaptation precedes the formation of genotoxin-resistant repair-defective colonies during genotoxic treatment with X-rays or Camptothecin. The resistant colonies undergo dramatic chromosome loss events and become aneuploid. I demonstrate that repair-defective aneuploids, which arise following adaptation to genotoxins, suffer from aneuploidy-associated phenotypes (Torres et al., 2007) and could be targeted pharmacologically. I have also analysed the contribution of different DNA repair proteins and pathways to the formation of genotoxin resistance in *rad52* mutants. I find that neither non-homologous end joining, nor restoration of homologous recombination confers chemoresistance in *rad52* mutants. Instead, I show that the Mre11-Rad50-Xrs2 complex confers the resistance of *rad52* mutants to Camptothecin. This proof-of-concept study provides a link between checkpoint adaptation, aneuploidization, and chemoresistance. Moreover, the study solidifies the rationale to target drug-resistant homologous recombination-defective cells with aneuploidy-selective drugs. Finally, the study demonstrates the role of the Mre11-Rad50-Xrs2 complex in the formation of Camptothecin resistance, which should be investigated further.

2. Results

2.1 Checkpoint adaptation promotes re-growth in repair-defective *rad52* strains following genotoxic treatment

In order to better understand the consequences of checkpoint adaptation (CA) in repair-defective cells, I used homozygous diploid *Saccharomyces cerevisiae* strains that lack the key HR gene *RAD52*. These strains are unable to repair DSBs with any of the homology-directed repair (HDR) pathways that are preferentially used for DSBs repair in budding yeast. This renders HR deficient cells prone to undergo CA (Galgoczy and Toczyski, 2001). I have used two different ways to induce double-strand breaks (DSBs) in *rad52* cells (all strains in this thesis are homozygous diploid unless indicated otherwise). First, I irradiated cells with 45 Gy of X-rays, which induces DSBs, intra- and interstrand crosslinks, and single strand breaks. I have also induced DSBs by treating cells with Camptothecin (CPT), which traps the Topoisomerase 1 (Top1) cleavage complex (Top1cc) on the DNA (Hsiang et al., 1989). Genetic experiments using an adaptation-defective *cdc5-ad* allele of Polo-like kinase *CDC5* and the deletion of a non-catalytic subunit of Casein kinase II *ckb2* (Toczyski et al., 1997) were used to understand the role of adaptation in the survival of repair-defective *rad52* strains upon treatment with CPT and X-rays. These results were further enforced by using adaptation-defective deletion of *SAE2* endonuclease (Clerici et al., 2006). Some of the initial experiments with *rad52 cdc5-ad* strains were performed by Dr. Julia Klermund, and are part of a manuscript (https://doi.org/10.1101/464685).

2.1.1 Preventing checkpoint adaptation using *cdc5-ad* allele decreases the occurrence of X-ray- and CPT-resistant *rad52* colonies

We set out to investigate whether the adaptation to DDC promotes colony formation in repair-defective *rad52* cells following 45 Gy X-ray irradiation or treatment with 2 μM CPT. We have observed that following 45 Gy irradiation, colony formation in repair-defective *rad52* cells was strongly compromised after 2 days of incubation at 30°C (data not shown), however after 4 days of incubation the resistant colonies started to arise (Figure 12a). The colonies were heterogeneous in size and had an increased uptake of the vital dye, Phloxine B (pink coloring), indicating a potential decrease in their metabolic activity (loss of viability) (Minois et al., 2005). Preventing CA using an adaptation-defective *cdc5-ad* allele drastically and significantly reduced the amount of colonies formed after X-ray irradiation, and quantification of the cell survival rate by dividing the numbers of colonies on drug plates to “no drug” control showed the reduction from roughly 20% survival in *rad52* mutants to 4% survival in *rad52 cdc5-ad* mutants. These results indicate that CA

is required for the delayed colony formation following X-ray treatment (Figure 12b). We have observed similar results when I plated *rad52* cells onto 2 µM CPT containing plates (Figure 12c). The formation of CPT-resistant *rad52* colonies occurred 8 days following CPT treatment. Importantly, in the presence of adaptation-defective *cdc5-ad* allele, the survival of *rad52* cells on CPT was reduced from roughly 80% to roughly 30%. We did not observe decreased colony formation in repair-proficient *cdc5-ad* cells neither after X-ray irradiation nor upon CPT treatment, suggesting that the allele does not compromise cellular viability *per se*. Together, these results indicate that preventing CA in *rad52* cells upon genotoxic treatment greatly reduced the formation rates of resistant colonies.

2.1.2 Preventing adaptation using the deletion of Casein kinase subunit *CKB2* decreases the formation of X-ray- and CPT-resistant *rad52* colonies

In a screen for CA defective mutants, Toczyski and colleagues have also identified mutants in Casein kinase II as the ones with a strong adaptation defect (Toczyski et al., 1997). I wanted to further verify that CA is required for delayed colony formation after the X-ray or CPT treatment in *rad52* mutants. Therefore, I used a deletion in a non-catalytic subunit of Casein kinase II *CKB2*. Similar to *cdc5-ad* mutants, adaptation-defective *rad52 ckb2* mutants displayed a significant reduction in colony formation after X-ray irradiation (Figure 12d) and on plates containing 2 µM CPT (Figure 12e). The deletion of *CKB2* did not compromise the viability of repair-proficient cells upon the DNA damage, indicating that the reduced colony formation was adaptation-specific. The reduction in numbers of resistant colonies was more prominent in *cdc5-ad* mutants than in *ckb2* mutants, which is consistent with a lower penetrance of the *ckb2* allele in respect to a defective adaptation (Toczyski et al., 1997). Together, these results indicate that preventing CA by deleting *CKB2* decreases the re-growth of repair-defective strains following genotoxic treatment.

2.1.3 Adaptation defective *rad52* mutants lacking *SAE2* are sensitized to X-Rays and CPT treatment

The initial processing step for the repair of a DSB involves the recruitment of MRX complex, which, besides the resection of DNA ends, has an important function in the initiation of DDC signaling by recruiting Tel1 (Nakada et al., 2003) and regulating Mec1 activation (Nakada et al., 2004). At DSBs, the MRX complex also recruits the Sae2 nuclease, which in turn negatively regulates both Mec1- and Tel1-dependent checkpoint responses. Therefore, *SAE2* deletion mutants are defective in the attenuation of DDC, which results in a CA defect (Clerici et al., 2006). To additionally validate my findings regarding the role of CA in the re-growth of repair-defective *rad52*

cells upon the genotoxic stress conditions, I tested whether *rad52 sae2* double mutants will be sensitized to genotoxic treatment. Indeed, I recovered significantly fewer numbers of *rad52 sae2* colonies compared to *rad52* colonies following treatment with X-rays (Figure 12f) and 2 µM CPT (Figure 12g). These results corroborate that CA precedes the colony formation when repair-deficient cells are treated with genotoxins.

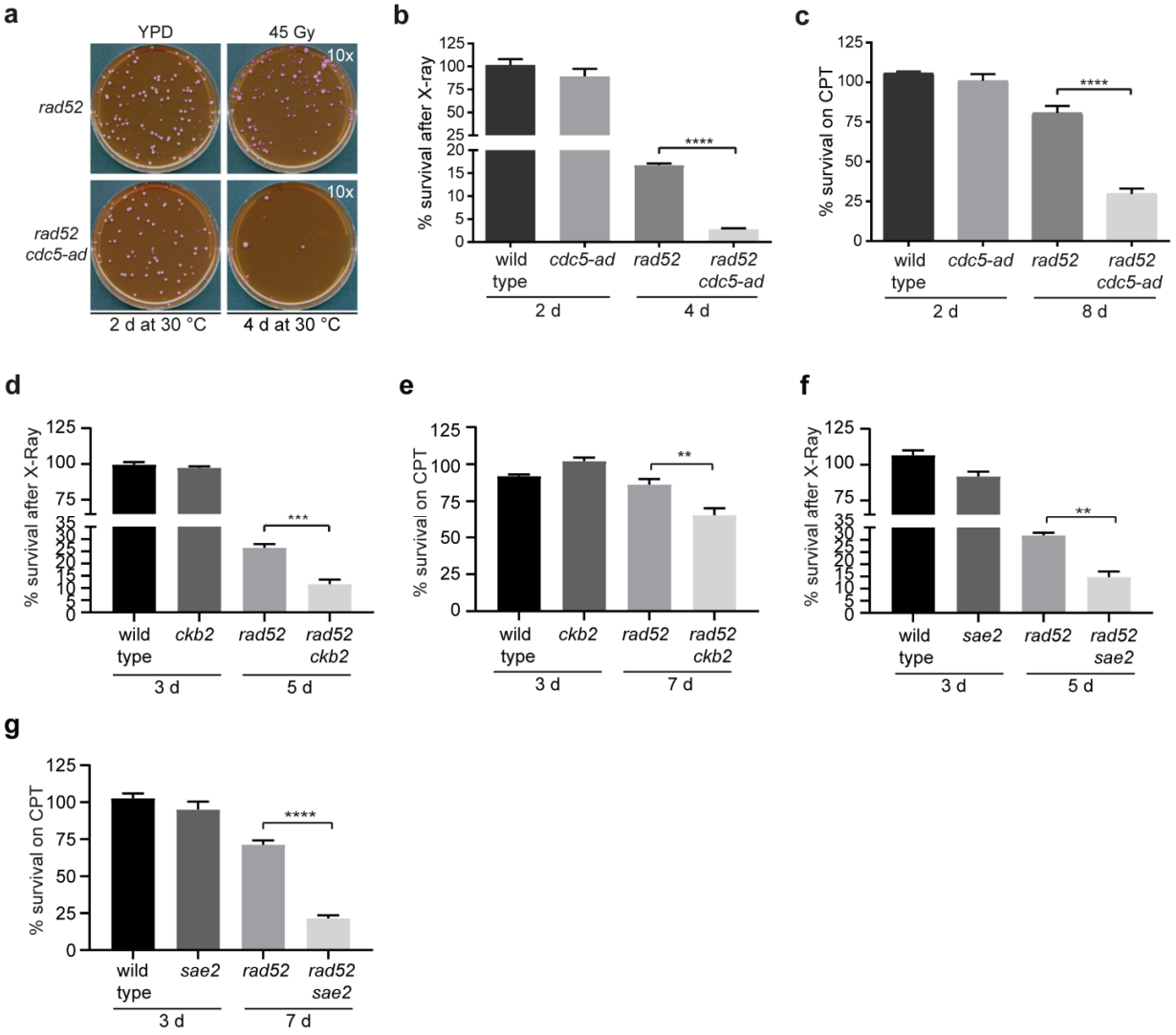

Figure 12. Adaptation to the DDC promotes re-growth following genotoxic treatment. (a) Representative images of a plating assay. Indicated homozygous diploid strains were plated onto YPD plates, untreated or irradiated with 45 Gy of X-Rays, and incubated at 30°C for the indicated times. Phloxine B (8 µg/mL) was added to the agar plates to estimate the metabolic activity of yeast colonies. **(b)** Quantification of the plating assay. Cells were plated onto YPD plates containing DMSO (control) or treated with 45 Gy of X-rays. All visible colonies were counted, and the number of colonies on drug plates were divided by the number of colonies on control plates. Data are represented as mean values and SEM of three independent experiments. For statistical

analysis ANOVA test with Tukey's post-hoc test was applied (****p≤0.0001). **(c)** Quantification of the plating assay in response to 2 μM CPT was performed similarly to (b). **(d)** to **(g)** Quantification of the plating assay in response to X-ray (d) or CPT (e) treatment was performed similarly to (b). (***p≤0.001, **p≤0.01). **Panels (a), (b), and (c) were performed by Dr. Julia Klermund.**

2.2 Repair-defective cells acquire a growth advantage following a repeated exposure to genotoxins

Treatment with genotoxic agents might result in an acquisition of resistance towards the genotoxic agent used. For example, in humans, HR defective BRCA2-deficient tumors strongly rely on PARP1-mediated parylation in order to repair their DSBs; therefore, inhibitors of PARP1 are a common therapy for these tumors (Lord and Ashworth, 2017). Multiple reports in the literature demonstrate that HR defective tumors are able to acquire resistance to PARP inhibitors, either by restoring homology-directed repair or by stabilizing their replication forks (Chaudhuri et al., 2016; Xu et al., 2015). Because I induce DSBs in a repair-deficient scenario in the homozygous diploid *rad52* yeast model, we wondered whether *rad52* cells eventually acquire resistance to further genotoxic treatment, similarly to the human repair-defective BRCA2-deficient cancers.

In order to understand whether repair-deficient *rad52* cells eventually acquire resistance to genotoxic agents, we first treated *rad52* cells with either 45 Gy of X-rays or 2 μM CPT. When the adapted cells formed colonies after the treatment, we re-spotted them in 1:10 serial dilutions onto the drug-containing plates in order to expose them to a second genotoxic challenge (Figure 13a). The X-ray adapted cells were exposed to 45 Gy of X-rays, a radiomimetic drug bleomycin (Bleo) (2.2 U/L), or 2 μM CPT (Figure 13b). As can be appreciated, X-ray adapted *rad52* mutants displayed significant growth advantage after the exposure to 45 Gy of X-rays, or 2.2 U/L Bleo compared to the naïve *rad52* cells (compare lane 5 to lanes 7-10). Interestingly, we did not observe any survival advantage of X-ray adapted cells on 2 μM CPT, which might be related to the different mechanisms of genotoxicity induction between X-rays and CPT. The rare adapted *rad52 cdc5-ad* cells also gained a certain degree of growth advantage upon the repeated genotoxic exposures compared to the naïve *rad52 cdc5-ad* cells (compare lane 6 to lanes 11 and 12). These results indicate that once adapted to X-rays, the repair-defective cells acquire resistance to further exposures to similar genotoxic agents.

We have additionally examined whether the *rad52* cells adapted to CPT also become resistant to further genotoxic treatments (Figure 13c). One can appreciate that CPT adapted *rad52* acquire strong growth advantage when exposed to 2 μM CPT, 2.2 U/L Bleo, or irradiated with 65 J/m^2 of UV light (compare lane 5 to lanes 7-9). Similar to X-ray adapted *rad52 cdc5-ad* mutants, rare CPT adapted *rad52 cdc5-ad* cells showed remarkable resistance to further genotoxic treatments (compare lane 6 to lanes 10 and 11). Together, these data demonstrate that adapted repair-

deficient *rad52* cells develop resistance to further treatment with genotoxins. Experiments in Figure 13b and 13c were performed by Dr. Julia Klermund, and are a part of a submitted manuscript (https://doi.org/10.1101/464685).

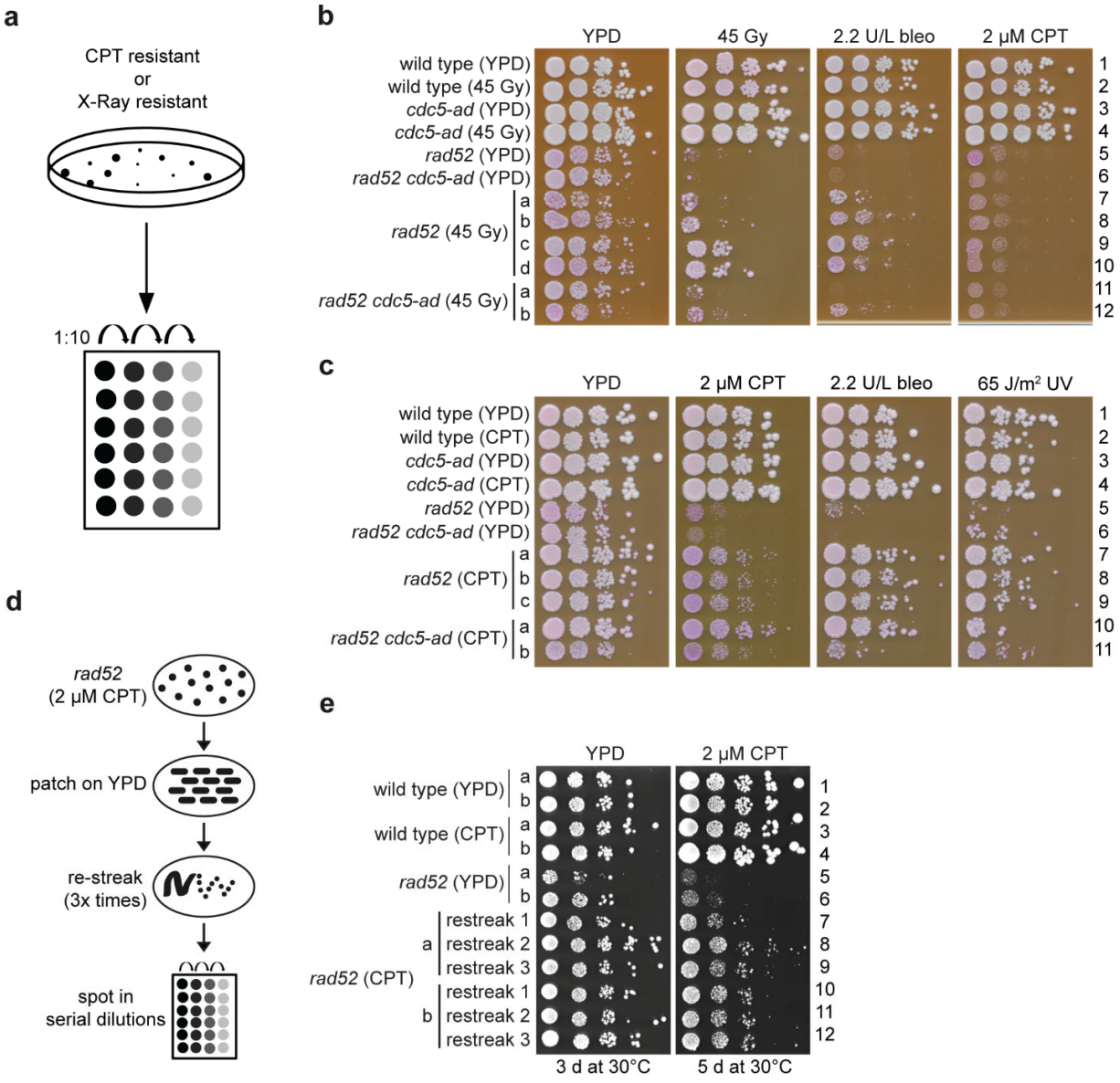

Figure 13. Repair-defective cells acquire growth advantage following repeated exposure to different genotoxins. (a) Scheme of the experimental set-up. Here, *rad52* and *rad52 cdc5-ad* strains were plated onto 2 µM CPT for 8 days, or irradiated with 45 Gy of X-rays and grown for 4 days at 30°C. The colonies that formed on the CPT-containing plates were patched onto YPD plates first. Strains were inoculated in YPD, grown overnight, and spotted in 1:10 serial dilutions. **(b)** Indicated strains were grown overnight in liquid YPD media, and spotted in 1:10 serial dilutions onto YPD plates (control), or onto plates containing 2.2 U/L Bleo, 2 µM CPT, or irradiated with 45 Gy of X-rays. All plates contained 8 µg/mL of Phloxine B. Colony formation was assessed after 3

days at 30°C. Letters indicate individual colonies derived from drug plates. **(c)** Indicated strains were grown overnight in liquid YPD media, and spotted in 1:10 serial dilutions onto YPD plates (control), or onto plates containing 2 µM CPT, 2.2 U/L Bleo, or irradiated with 65 J/m^2 of UV light. All plates contained 8 µg/mL of Phloxine B. Letters indicate individual colonies derived from drug plates. **(d)** Scheme of the experimental set-up. Following 8 days of incubation, *rad52* strains derived from plates containing 2 µM CPT were patched onto YPD plates to recover and subsequently re-streaked three times. Colonies from the different re-streaks were grown overnight, and spotted in 1:10 serial dilutions. **(e)** Indicated strains were grown overnight in liquid YPD media, and spotted in 1:10 serial dilutions onto YPD plates (control), or plates containing 2 µM CPT. Letters indicate individual colonies. **Panels (b) and (c) were performed by Dr. Julia Klermund.**

Short-term evolutionary experiments in yeast demonstrated that different stress conditions can induce readily reversible adaptation responses, which are not maintained when the initial stress source is ceased (Chen et al., 2012a; Yona et al., 2012). I wanted to understand whether the prominent resistance phenotype of CPT adapted *rad52* cells is maintained in the absence of CPT-induced genotoxic challenge. Therefore, I have subsequently passaged CPT adapted *rad52* cells onto YPD plates (Figure 13d). I then spotted cells that were passaged onto YPD plates for three consecutive re-streaks onto CPT-containing plates (Figure 13e). CPT adapted *rad52* cells displayed an evident resistance phenotype compared to the naïve *rad52* cells (Figure 13e, compare lanes 5 and 6 to lanes 7 and 10), which was maintained after three independent re-streaks, corresponding to approximately 75 population doublings. Together, this data indicates that repair-defective *rad52* cells acquire resistance following genotoxic treatments. The prominent CPT resistant phenotype is maintained even following the withdrawal from the genotoxic challenge for approximately 75 generations. The speculation regarding the source of the genotoxin resistance phenotype in *rad52* cells will be presented later in the discussion section.

2.3 Repair-defective *rad52* cells experience drastic chromosome loss events following adaptation to genotoxin treatment

The resistance towards genotoxins and other stress agents and conditions is frequently associated with the acquisition of genomic re-arrangements, as well as whole chromosome gains and losses, ploidy changes, segmental aneuploidies, and gene amplifications and deletions (Dunham et al., 2002; Rancati et al., 2008; Selmecki et al., 2015; Yang et al., 2019). At the same time, the loss of the *rad52* gene increases the frequency of chromosome loss events, which is further exacerbated by treatment with X-rays (Mortimer et al., 1981). This prompted me to investigate the karyotype changes that occur in adapted *rad52* cells following X-Ray or CPT exposures.

2.3.1 Exposure of *rad52* cells to 45 Gy of X-Rays or CPT induces drastic changes in ploidy

In order to check whether *rad52* cells lose chromosomes following the irradiation with 45 Gy of X-rays or treatment with 2 µM CPT, I analyzed the DNA content of naïve and adapted mutants using a flow cytometry approach. The DNA content analysis of *rad52* mutants adapted to X-rays revealed extensive chromosome loss events in more than 50 clones tested (Figure 14a and data not shown). I recovered adapted mutants with a nearly diploid DNA content, an intermediate ploidy state between 2C and 1C, and a nearly haploid chromosome set. This mixture of ploidy states might be due to the stochastic nature of the treatment with X-rays, as different cells might obtain different numbers of DSBs in random genomic locations. I have observed even more pronounced chromosome loss events in *rad52* mutants adapted to 2 µM CPT in more than 50 clones tested (Figure 14b and data not shown). All the CPT resistant clones tested were nearly haploid, which likely reflects a high DNA damage load and a rather homogeneous distribution of DSBs (as Top1 acts genome-wide) upon the concentrations of the drug I used. Although adaptation-defective *rad52 cdc5-ad* cells form genotoxin-resistant colonies with a reduced frequency (Figure 12 a-c), the rare adapted clones still display chromosome loss patterns similar to adapted *rad52* mutants (Figure 14b). To ensure that changes in the DNA content I observe using flow cytometry approach are not due to the loss of mitochondrial DNA, I generated *rho- rad52* strains depleted of their mitochondrial DNA. Afterwards, I subjected them to treatment: either with 45 Gy of X-Rays, or 2 µM CPT. Although I observed a lesser amount of DNA content in naïve *rho- rad52* strains compared to *rad52* mutants (Figure 14c), *rho-* strains still displayed additional chromosome loss events. These results suggest that the loss of mitochondrial DNA cannot account for the drastic changes in DNA content that adapted cells experience. Together, this indicates that repair-defective *rad52* mutants experience drastic loss of their DNA content following genotoxic challenge.

2.3.2 Whole genome sequencing reveals that adapted *rad52* cells experience whole chromosome losses

My flow cytometry results indicate that *rad52* mutants experience loss of genomic material in response to genotoxic challenge. Yet, the flow cytometry method does not provide me with understanding of which types of genomic rearrangements are characteristic of the adapted *rad52* cells. In order to elucidate whether (i) adapted cells undergo gross chromosomal re-arrangements and (ii) whether certain types of genomic rearrangements are systematic, we have employed the whole genome sequencing approach. The whole genome sequencing experiment was performed by Dr. Katharina Bender, and data analysis was performed by Dr. Anke Busch. The data are now

part of a manuscript (https://doi.org/10.1101/464685). Briefly, wild type and *rad52* strains were either plated onto YPD agar (YPD), irradiated with 45 Gy of X-rays, or plated onto YPD plates containing 2 μM CPT. Subsequently, the indicated strains were grown to as exponential cultures in liquid YPD media at 30 °C. We extracted genomic DNA (gDNA) and performed whole-genome sequencing (Figure 14c). We did not observe chromosome loss events or other genomic rearrangements in repair-proficient wild type cells even following genotoxic treatment. The X-ray adapted *rad52* mutants displayed whole chromosome losses resulting in a mixture of ploidies, from a nearly diploid karyotype that have only lost chromosome I (clone c) to a nearly haploid karyotype that have retained chromosomes III and XI (clone a). The *rad52* mutants that adapted to 2 μM CPT had lost half of their chromosomes (chromosome loss events are marked in red), and preferentially retained chromosome III. We did not observe gross genomic rearrangements other than whole chromosome loss, e.g. translocations, insertions, or deletions. Together, these results indicate that repair-defective *rad52* mutants undergo extensive whole chromosome loss events following treatment with genotoxins. Treatment of *rad52* cells with X-rays yields a spectrum from nearly diploid to nearly haploid karyotypes, while treatment with 2 μM CPT results in an almost haploid karyotype with an extra chromosome III.

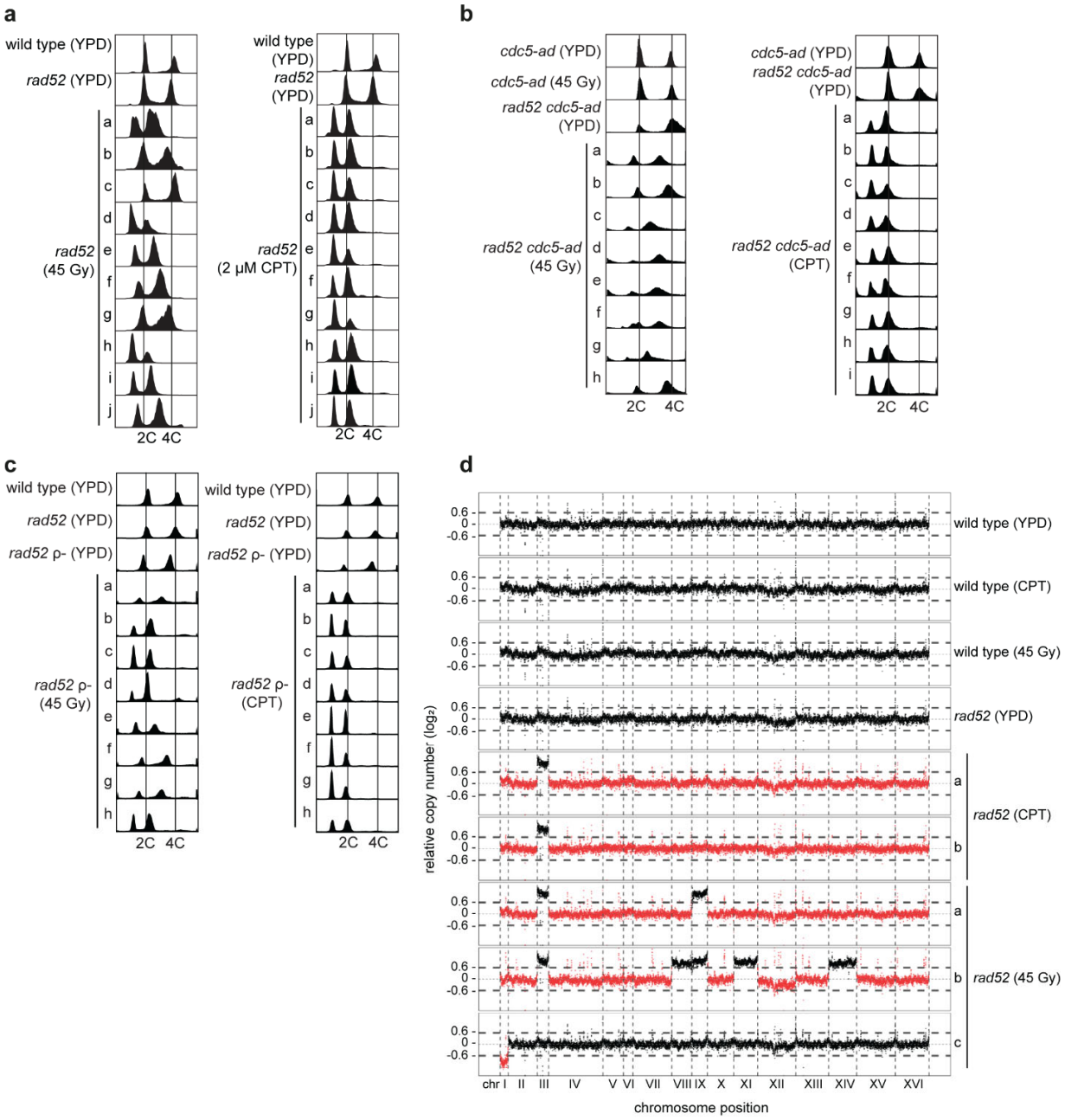

Figure 14. Exposure of repair-defective *rad52* cells to X-Rays and CPT induces extensive chromosome loss. (a) DNA content of the indicated yeast strains was assessed using flow cytometry. Briefly, after *rad52* colonies were formed on control YPD plates, 2 μM CPT plates, or plates exposed to 45 Gy of X-rays, single colonies were grown in liquid YPD media overnight and analyzed. Letters indicate single colonies derived from genotoxin-treated plates. **(b)** DNA content of genotoxin-treated adaptation-defective *rad52 cdc5-ad* mutants was assessed using flow cytometry. Letters indicate single colonies derived from genotoxin-treated plates. **(c)** DNA content of mitochondrial DNA-deficient *rho- rad52* strains that were treated either with 45 Gy of X-Rays or 2 μM CPT. Letters indicate single colonies derived from genotoxin-treated plates. **(d)** The representative segmentation plot depicts relative chromosome copy number in indicated strains.

The segmentation plot depicts the $\log_2$ ratio of binned reads (reads per million (RPM), y-axis) for the respective chromosome position (x-axis) normalized to the sample median number of reads per bin (RPM). Dashed horizontal lines indicate a threshold of 0.6 or -0.6, respectively, to allow the identification of chromosome loss events, which are indicated in red. Letters indicate single colonies derived from genotoxin-treated plates. **DNA sequencing for the panel (c) was performed by Dr. Katharina Bender, and data analysis was performed by Dr. Anke Busch.**

2.4 Acute exposure to high CPT dosages results in heterogeneous karyotypes in *rad52* mutants

I wondered whether the difference in karyotypes acquired by *rad52* mutants adapted to 45 Gy of X-rays or 2 µM CPT arise due to the different duration of the treatment: while irradiation with X-rays is acute, the treatment with 2 µM CPT is chronic and lasts for eight days. I also wondered whether preventing adaptation upon acute treatment with CPT will allow to decrease the rates of genotoxin resistance. In order to address these questions, I have treated exponential cultures of *rad52* or *rad52 cdc5-ad* mutants with 20 µM CPT for 4 hours and allowed the cells to recover for two to six days and form colonies on YPD agar plates (Figure 15a).

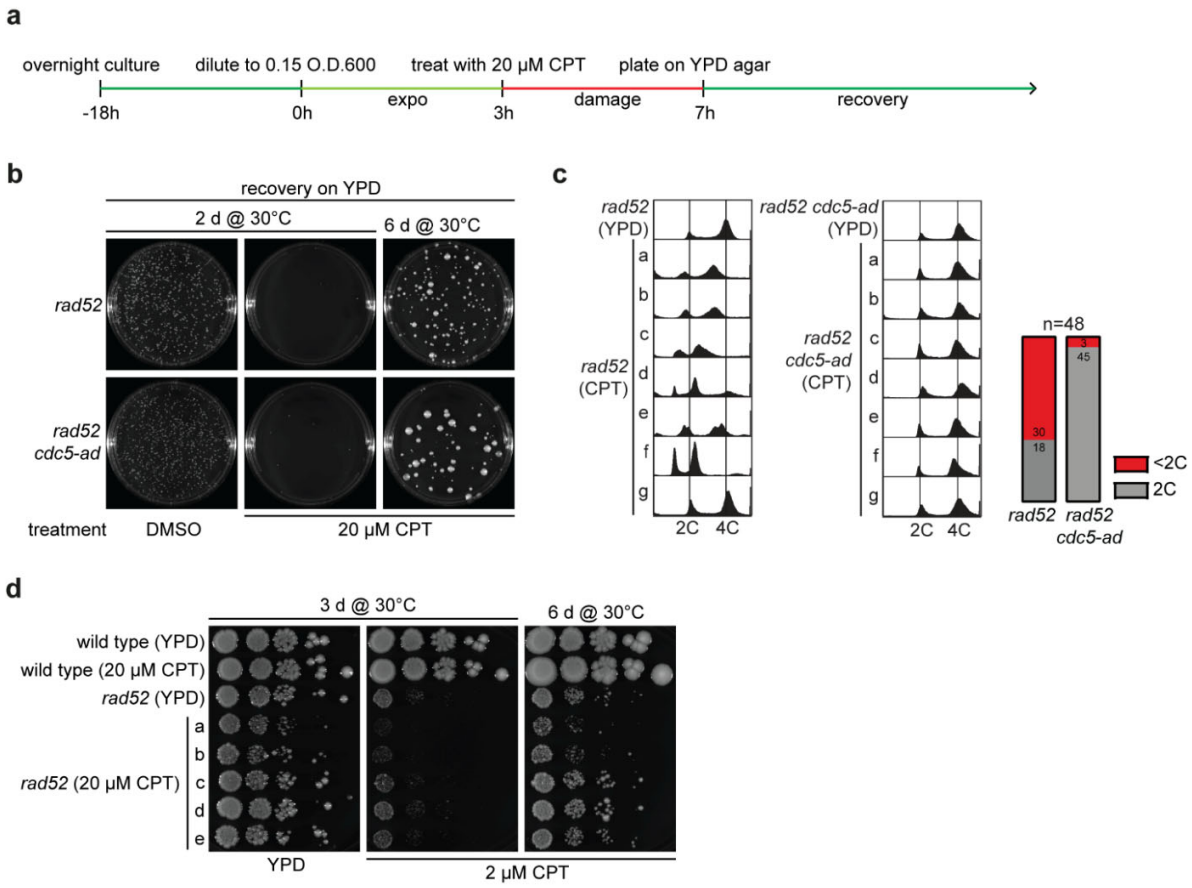

Figure 15. Acute exposure of repair-defective *rad52* cells to CPT leads to extensive chromosome loss, but does not facilitate growth advantage in adapted cells upon repeated exposure. *Figure legend, see next page.*

Figure 15. Acute exposure of repair-defective *rad52* cells to CPT leads to extensive chromosome loss, but does not facilitate growth advantage in adapted cells upon repeated exposure. (a) Scheme of the experimental set-up. Overnight cultures were grown in YPD at 30°C and diluted in the morning to 0.15 OD600nm. Cultures were grown for 3 h to reach the exponential phase, and were either mock-treated (DMSO) or treated with 20 μM CPT for 4 h. Approximately 3000 cells per plate were plated on YPD agar and grown at 30°C for 2 to 6 days to recover all the possible colonies. **(b)** Representative images of plates with indicated strains that were acutely treated with 20 μM CPT as described in (a). **(c)** DNA content of single colonies from (b) was analyzed using flow cytometry. Letters indicate single colonies. Accompanying histogram summarized the analysis of DNA content from 48 independent colonies that were generated during 4 independent experiments. **(d)** Indicated strains from (b) were grown in liquid YPD media overnight at 30°C and spotted in serial dilutions onto YPD plates or CPT-containing plates. Letters indicate single colonies.

The acute treatment with 20 μM CPT suppressed colony formation in the repair-defective cells 2 days after the treatment, while the repair-proficient cells were not affected (Figure 15b, and data not shown). In *rad52* mutants, heterogeneously sized colonies started to appear after six days of incubation at 30°C. When a similar number of cells was plated, I recovered fewer colonies of adaptation-defective *rad52 cdc5-ad* mutants compared to adaptation-proficient *rad52* mutants, indicating that CA contributed to the re-growth of *rad52* cells after the acute CPT treatment. DNA content analysis revealed that acute treatment with 20 μM CPT induced extensive chromosome loss events in *rad52* mutants (30 out of 48 clones tested), yielding heterogeneous karyotypes similarly to X-ray treatment (Figure 15c). Interestingly, the frequency of chromosome loss following the acute CPT treatment in adaptation-defective *rad52 cdc5-ad* mutants was drastically lower, with only 3 out of 48 clones showing detectable chromosome loss events. This indicates that CA precedes chromosome loss following the acute treatment with a high CPT dosage.

Finally, I tested whether the acute CPT treatment also leads to the formation of genotoxin resistance, similarly to chronic CPT exposure. I spotted *rad52* mutants recovered after the acute CPT treatment onto control plates (YPD) or plates containing 2 μM CPT (Figure 15d). In contrast to chronic CPT exposure, that resulted in the formation of CPT resistant *rad52* colonies (Figure 13c), the acute CPT treatment did not lead to genotoxin resistance, suggesting that the resistance may be related to the nearly haploid state and not the chromosome loss events, *per se*. A few nearly haploid *rad52* mutants that were recovered following the acute treatment with 20 μM CPT also displayed resistance to CPT (data not shown), supporting the notion that nearly-haploid state facilitates CPT resistance. In summary, these data indicate that acute treatment of *rad52* cells with a high CPT dosage

results in heterogeneous chromosome loss patterns similarly to X-ray irradiation and does not lead to resistance to further CPT exposure.

2.5 The resistance to CPT in adapted *rad52* cells is facilitated by a nearly-haploid karyotype

We have observed that following CPT treatment repair-defective *rad52* cells have become nearly haploid but retained an extra chromosome III (Figure 14c). Whole chromosome aneuploidies were reported to facilitate resistance to the antifungal drug caspofungin in *Candida albicans* or resistance to hydroxyurea treatment in *S. cerevisiae* (Yang et al., 2019). Evolutionary experiments in different stress conditions showed that chromosome gains provided adaptive means for stress tolerance (Chen et al., 2012a, 2012b; Rancati et al., 2008). Moreover, whole chromosome aneuploidies were reported to facilitate resistance to unrelated stress conditions and drugs (Yang et al., 2019), which we observed in CPT resistant *rad52* mutants (Figure 12c). I therefore wondered whether this nearly haploid karyotype is intrinsically resistant to CPT treatment, and whether the presence of an extra copy of chromosome III provides a selective advantage upon genotoxic challenge. In order to address these questions, I compared the growth of haploid *rad52* strains derived from CPT-containing plates on 2 µM CPT to the strains that had similar karyotype, but were generated by a sporulation of triploid strain and were not previously treated with genotoxins (Mulla et al., 2017; Pavelka et al., 2010) (Figure 16a).

I have knocked-out *rad52* in a strain disomic for chromosome III or chromosomes III + XII, and confirmed that positive transformants retained an extra copy of chromosome III by qPCR (Figure 16b). All the chromosomes III + XII disomes tested had rapidly lost their extra copy of chromosome XII after the transformation, and I was therefore only able to recover chromosome III disomes. The *rad52* mutants disomic for chromosome III grew similarly to the *rad52* haploids on the CPT-containing plates, indicating that aneuploidy did not provide an advantage and is likely not responsible for the genotoxin resistance (compare lanes 3 to lanes 8 and 10). Rather, the nearly haploid karyotype itself facilitated the growth of *rad52* mutants in the presence of CPT (lanes 3 to 6, 8, and 10). Mating locus heterozygosity in *S. cerevisia*e influences the DNA repair pathway choice by the suppression of the NHEJ pathway in diploid yeast due to the downregulation of Nej1 levels (Frank-Vaillant and Marcand, 2001). Interestingly, the effects of chromosome III disomy were independent of the mating cassette present, indicating that NHEJ might be dispensable for the CPT resistance (compare lanes 8 and 10). Together, these data indicate that the nearly haploid state, but not the presence of extra chromosome III, facilitates the resistance of *rad52* mutants to CPT.

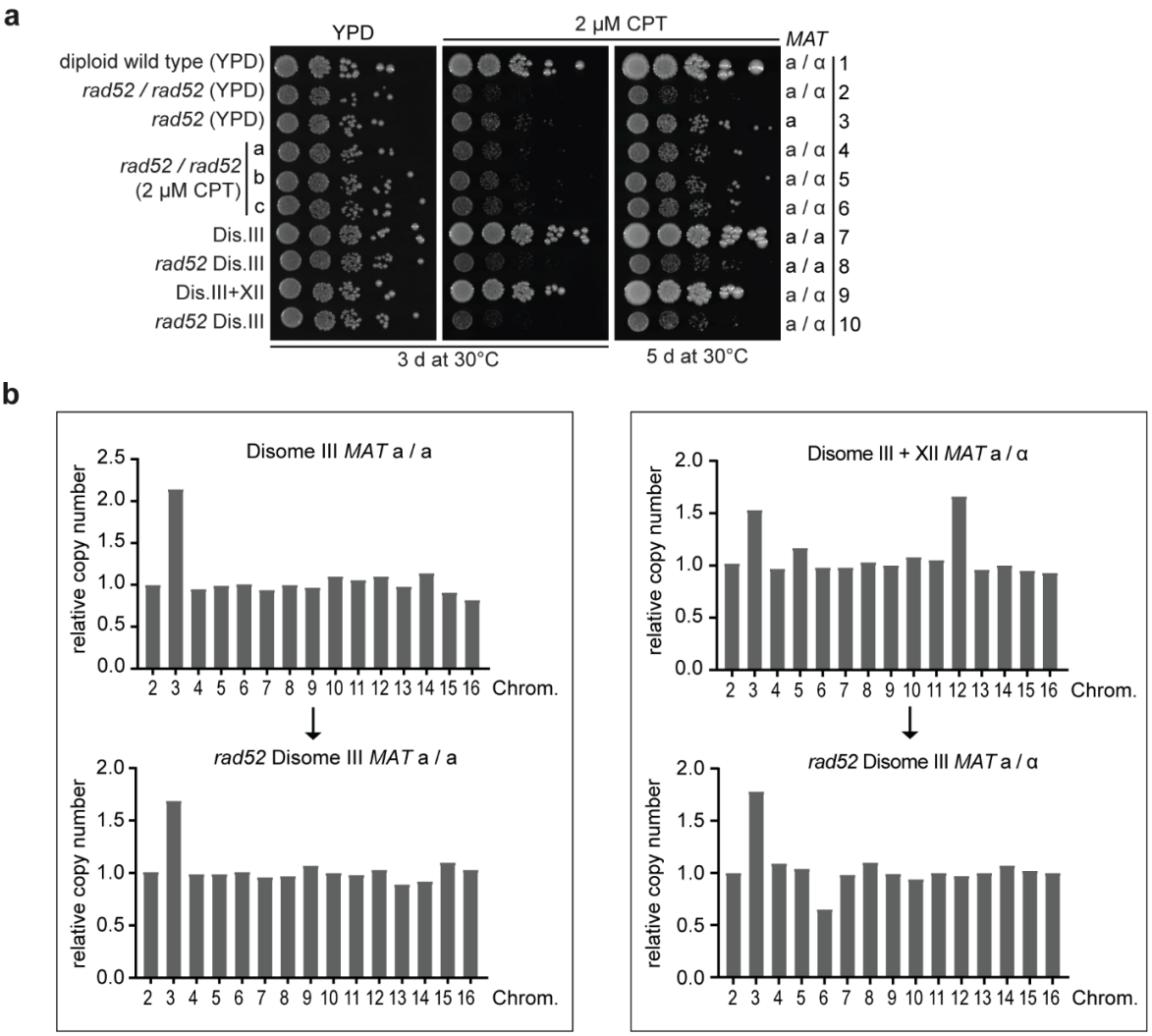

Figure 16. Nearly-haploid karyotype facilitates the resistance of repair-defective *rad52* cells to CPT. (a) Yeast strains of the indicated genotypes were grown in liquid YPD media at 30°C, and spotted in serial dilutions onto YPD plates, or plates containing 2 µM CPT. Colony formation was monitored after 3 and 5 days at 30°C. Letters indicate single colonies. **(b)** Relative chromosome copy number of disomic strains (from a) before and after *RAD52* knock-out. Briefly, the indicated strains were grown in liquid YPD media to the exponential cultures. Following the gDNA extraction, qPCR-based quantification of chromosome copy number was performed. The normalization procedure is described in the materials and methods section.

2.6 Extra copy of chromosome III is lost during the progressive passaging of *rad52* mutants

Although I have excluded the importance of chromosome III disomy for the CPT resistance (Figure 16a), I tried to understand the reason as to why it is frequently retained in adapted *rad52* colonies. I hypothesized that the process of chromosome loss upon CPT treatment may be gradual and produces a variety of aneuploid karyotypes. Certain aneuploid karyotypes are lethal in yeast: for example, disomes for chromosome 6 are inviable due to the presence of an extra copy of the β-

tubulin encoding *TUB2* gene (Torres et al., 2007). Hence, the mating locus in yeast is located on chromosome III, so retaining the chromosome appears to be advantageous to prevent potentially lethal mating events between aneuploids with imbalanced chromosome numbers. When the mutants reach the nearly-haploid state after progressive chromosome loss, it is no longer an advantage to maintain an extra copy of chromosome III over many generations. To set out experiments that will help examine the aforementioned hypothesis, I first aimed to confirm chromosome III disomy in a larger number of CPT resistant *rad52* strains. Second, I set out to monitor the dynamics of chromosome III loss in unchallenged conditions.

I first aimed to confirm that the vast majority of CPT resistant *rad52* that I initially recover retain an extra copy of chromosome III. I reasoned that when an extra copy of chromosome III is maintained, CPT resistant mutants should be heterozygous for the mating type cassette (can be *MAT* a or *MAT* α) present. Mating locus heterozygosity can be experimentally confirmed by PCR (Huxley et al., 1990). The PCR with the *MAT* a template DNA generates a 544 bp product, and the PCR with *MAT* α template DNA generates a 404 bp product. The PCR on DNA from diploid *MAT* a / α cells generates both products. My analysis demonstrated that amongst 38 examined CPT resistant *rad52* clones, 38 were heterozygous for the mating locus (Figure 17a and data not shown). This indicates that the vast majority of CPT resistant *rad52* that I initially recover from CPT plates indeed retain an extra copy of chromosome III.

Next, I analyzed whether an extra copy of chromosome III is lost if CPT adapted *rad52* cells are grown in unchallenged conditions. I have isolated single CPT resistant *rad52* colonies and tested whether they retain extra chromosome III by their ability to mate with mating tester strains (Figure 17b). Mating with a mating tester strain will result in complementation of their auxotrophic markers - and allow the resulting diploids to grow on a minimal SD media. I observed that CPT resistant *rad52* mutants frequently lose a random extra copy of chromosome III (Figure 17c), which supports my initial hypothesis.

Together, my data indicate that although CPT resistant *rad52* cells initially retain an extra copy of chromosome III – presumably to prevent potentially deleterious mating events between aneuploids – they lose it during progressive passaging in unchallenged conditions. Hence there is no specificity for chromosome III retention, rather its increased disomy is specifically a result of growth conditions where selective growth advantages can be selected for.

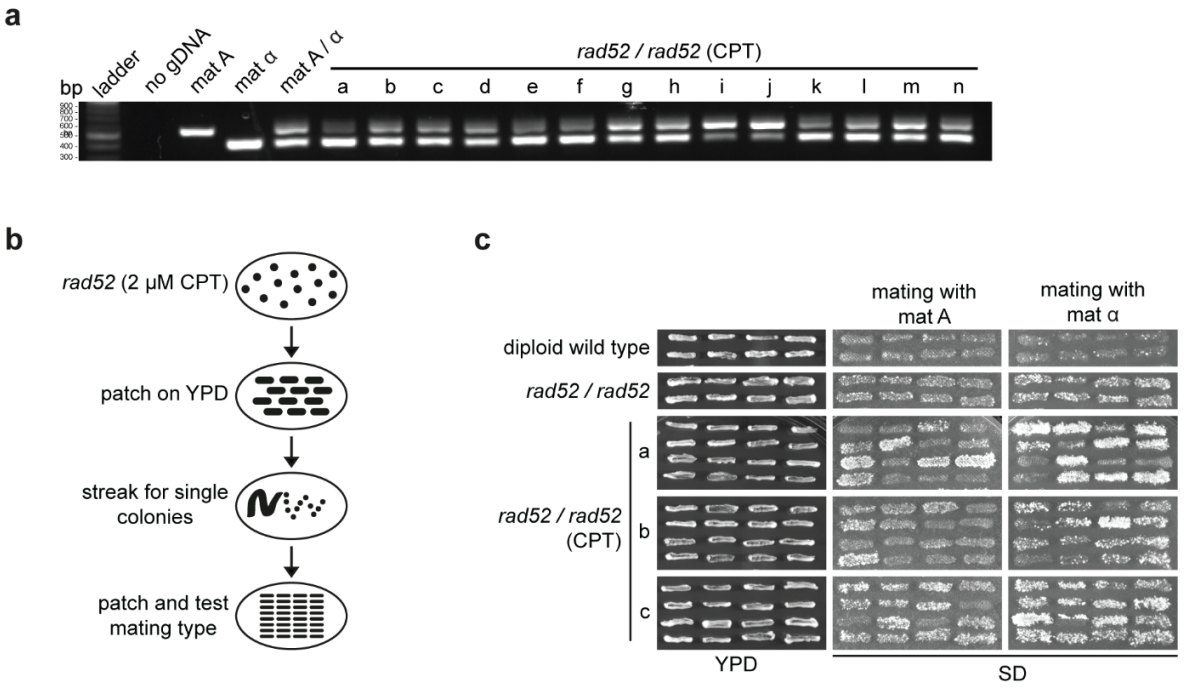

Figure 17. CPT resistant *rad52* cells do not maintain an extra chromosome III during progressive passaging. (a) Characterization of mating locus heterozygosity in homozygous diploid *rad52* strains treated with 2 µM CPT. Overnight culture in YPD at 30°C was followed by the gDNA extraction and the PCR-based amplification of the mating locus cassettes. PCR products were separated on 1% agarose gel containing SYBR® Safe DNA stain. Letters indicate individual colonies derived from CPT-containing plates. bp - base pairs. **(b)** Scheme of the experimental set-up. Ten independent single colonies derived from plates containing 2 µM CPT were first patched onto YPD agar and afterwards re-streaked for single colonies. At least 100 CPT-derived single colonies were patched and tested for their mating type. The strains were mated with *MAT* A and *MAT* α mating tester strains and the resulting diploids were selected based on their ability to grow on minimal SD media. **(c)** Characterization of chromosome III loss frequency by the estimation of the occurrence of mating to the *MAT* A and *MAT* α mating tester strains. Experiment was performed as described in (a). Representative images of minimal SD plates are shown. Letters indicate individual colonies derived from CPT-containing plates.

2.7 Adapted *rad52* undergo gradual chromosome loss to acquire balanced haploid karyotype

It was formerly demonstrated that induction of a single DSB that causes telomere attrition on the non-essential chromosome in repair-defective *rad52* cells leads to a propagation of the damaged chromosome for up to ten generations, until the damaged chromosome is lost due to resection (Sandell and Zakian, 1993). The chromosome loss in diploid strains will produce aneuploid karyotypes, which, in turn, are also unstable. The frequent chromosome loss and genomic instability in aneuploid cells was reported from yeast to humans (Passerini et al., 2016; Ravichandran et al., 2018). I therefore wondered if the *rad52* cells resistant to 45 Gy of X-rays

undergo progressive chromosome loss events, and if there is a stable karyotype that they acquire after the progressive passaging. In order to address these questions, I passaged strains in liquid media for ten days and monitored their DNA content using flow cytometry (Figure 18a). The repair-proficient wild type cells maintained stable ploidy over the course of the experiment, while the repair-deficient *rad52* strains maintained stable ploidy in the absence of DNA damage. This indicates that chromosome loss is induced majorly when DNA damage is not properly repaired. All of the fifteen X-ray resistant *rad52* clones analyzed showed progressive chromosome loss resulting in a nearly-haploid DNA content within the first three to four days of passaging. This DNA content was stably maintained over the course of the experiment (Figure 18b). In line with previously published observations (Sandell and Zakian, 1993), these results demonstrate that following DNA damage *rad52* cells lose chromosomes in a gradual manner until they achieve a stable haploid karyotype.

Ploidy in yeast was reported to be an important determinant of their adaptability to specific environmental conditions: for example, a tetraploid state promotes resistance to fungicides (Selmecki et al., 2015; Storchova, 2014). I wondered whether *rad52* cells that experienced drastic chromosome loss events upon treatment with CPT or X-rays will eventually re-diploidize during progressive passaging to restore their initial ploidy. Yet, both CPT resistant *rad52* and X-ray resistant *rad52* clones maintained a stable nearly-haploid karyotype over the course of the experiment (Figure 18b). Together, these data indicate that following DNA damage, repair-defective *rad52* cells experience progressive chromosome loss until they reach a nearly-haploid state, which they stably maintain over many generations.

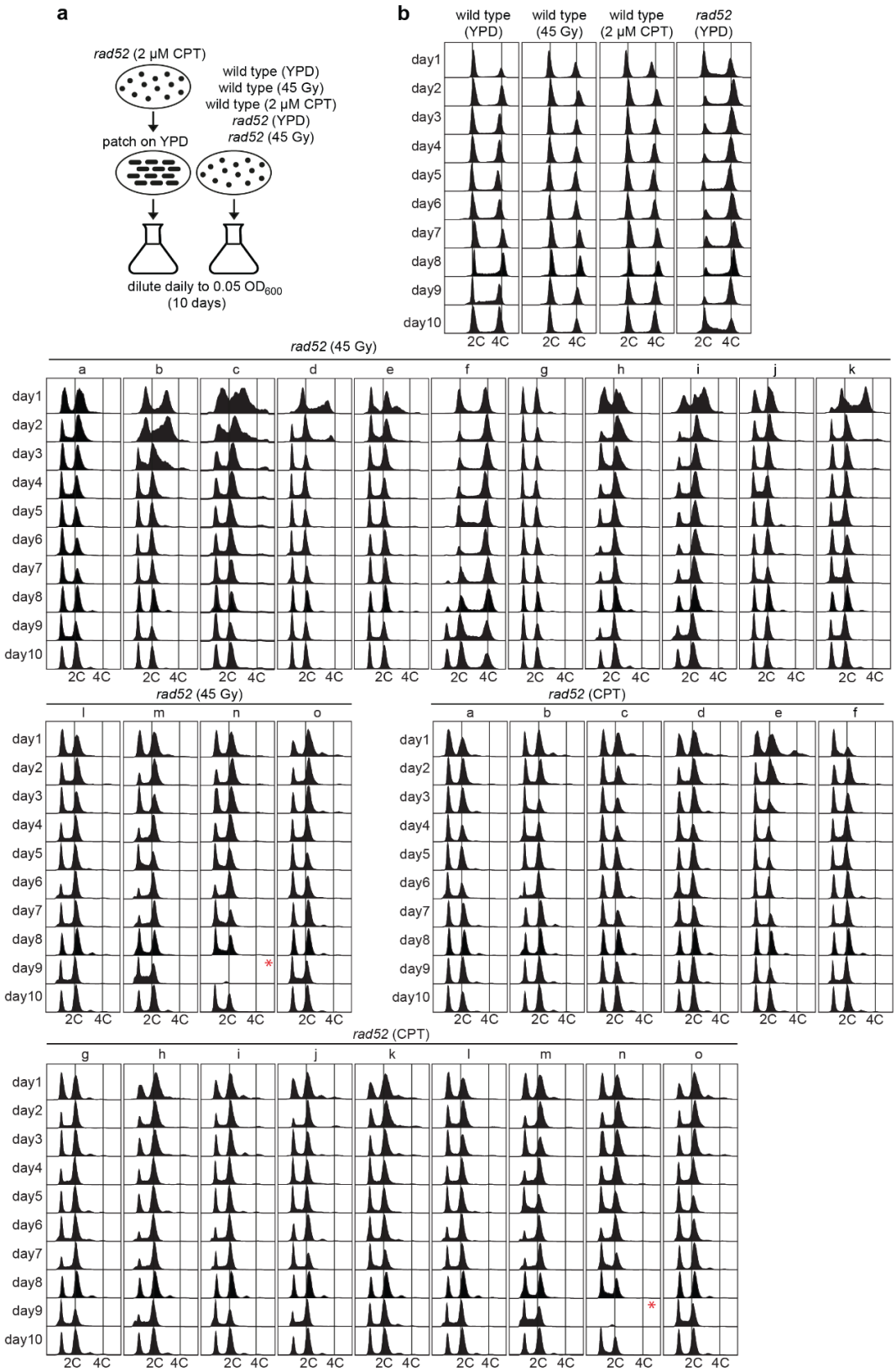

Figure 18. Highly aneuploid adapted *rad52* cells undergo gradual chromosome loss and acquire a balanced haploid karyotype *Figure legend, see next page.*

Figure 18. Highly aneuploid adapted *rad52* cells undergo gradual chromosome loss and acquire a balanced haploid karyotype. (a) Scheme of the experimental set-up. Single colonies of *rad52* strains derived from CPT-containing plates were first patched onto YPD agar and then inoculated into liquid YPD media overnight at 30°C. Single colonies of wild type or *rad52* strains derived from control YPD plates, 2μM CPT containing plates, or plates irradiated with 45 Gy of X-rays, were inoculated directly from the plates. Cultures were diluted daily to 0.05 OD600nm in 5 mL YPD for 10 days. Flow cytometry samples were collected daily before the cultures dilution. **(b)** Analysis of chromosome loss dynamics in *rad52* strains after 2 μM CPT or 45 Gy X-ray exposure. Experiment was performed as described in (a). 2C - diploid DNA content, 4C- tetraploid DNA content. Representative plots are shown. Asterisk indicates missing samples.

2.8 Adapted *rad52* mutants become aneuploid and suffer from aneuploidy-associated proteotoxic stress

Aneuploidy is the condition of having an abnormal number of chromosomes that is not a multiple of a haploid set. My results demonstrate that repair-defective *rad52* cells undergo extensive chromosome loss following treatment with both X-rays, and CPT (Figure 14a), meaning that adapted cells become aneuploid. To my knowledge, aneuploidy-associated phenotypes have so far been studied in yeast strains created in a very controlled manner: either by sporulation of a triploid strain (Pavelka et al., 2010), chromosome transfer strategy (Torres et al., 2007), or by acute induction of chromosomes mis-segregation upon cell division (Beach et al., 2017). Yet, adapted cells become aneuploid as a result of the dramatic genotoxin treatment, which might yield a different spectra of alterations in cellular physiology. Moreover, aneuploid cells used in this study are also HDR defective. This budding yeast system could be seen as a parallel to human tumors, which frequently become aneuploid (Ben-David and Amon, 2020), and are often deficient in HDR pathways (Ledermann et al., 2016). Understanding physiological disadvantages of repair-defective adapted cells provides me with a strategy for how to target their growth post-adaptation. Therefore, I set out to scrutinize physiological alterations in adapted repair-defective aneuploid *rad52* cells, based on the published observations about the aneuploidy-associated phenotypes (Chen et al., 2015; Oromendia et al., 2012; Torres et al., 2007). This allowed me to develop a strategy for how to pharmacologically target repair-defective *rad52* cells post-adaptation.

2.8.1 X-ray resistant *rad52* mutants suffer from proteotoxic stress

In budding yeast, chromosomes are transcribed according to their copy number (Dephoure et al., 2014; Torres et al., 2016); therefore, imbalances in gene copy numbers potentially translate into imbalances in protein complex stoichiometry. This renders aneuploid cells predisposable to the formation of protein aggregates, especially upon the conditions that exaggregate a load onto cellular protein quality control systems (Oromendia et al., 2012). The resulting proteotoxic stress potentially threatens cellular survival in suboptimal conditions, which was demonstrated for

multiple disomic yeast strains (Oromendia et al., 2012). I aimed to assess whether the adapted *rad52* cells have hallmarks of proteotoxic stress similar to the disomic yeast strains.

Elevated temperatures induce increased load on protein quality control systems (Richter et al., 2010), and stressed aneuploid cells can have reduced capacity to adapt their physiology to the challenge (Oromendia et al., 2012). Upon the standard growth conditions, the Hsp104 disaggregase is diffusely localized within the cytoplasm of the cell; however, upon proteotoxic stress induction the disaggregase co-localizes with cytoplasmic protein aggregates (Mogk et al., 2015). As the formation of protein aggregates is indicative of proteotoxic stress, monitoring the formation of disaggregase foci allows me to assess whether the cell suffers from proteotoxic stress. I have monitored the formation and resolution of GFP-Hsp104 foci upon heat stress conditions in X-ray adapted *rad52* cells using high-throughput fluorescence microscopy (Figure 19a). When shifted to 37°C, non-aneuploid wild type and naïve *rad52* cells form Hsp104-GFP foci after 1 hour at elevated temperatures, which are resolved after 3 h (Figure 19b, c). The resolution of Hsp104-GFP foci indicates that cells have adapted their cellular physiology to higher temperatures. Of note, repair-defective *rad52* cells showed slower kinetics of the Hsp104-GFP foci resolution, which might indicate that the deletion of *rad52* already induces a mild degree of proteotoxic stress. In contrast to euploid controls, aneuploid X-ray resistant *rad52* cells fail to resolve Hsp104-GFP foci after 3 h at 37 °C, indicating that aneuploid cells have a decreased capacity to adapt their physiology to the heat conditions. The decreased capacity to resolve Hsp104-GFP foci correlates with the inability of adapted *rad52* cells to survive and form colonies at the elevated temperatures (Figure 19c, d). The two X-ray resistant *rad52* clones that were able to survive at the elevated temperatures displayed a nearly diploid DNA content and an adequate dynamics of the Hsp104-GFP foci resolution (Figures 19d and 8e, clones A and F). Together, these results indicate that highly aneuploid *rad52* mutants suffer from proteotoxic stress, and are therefore unable to adapt and grow in the condition of elevated temperatures.

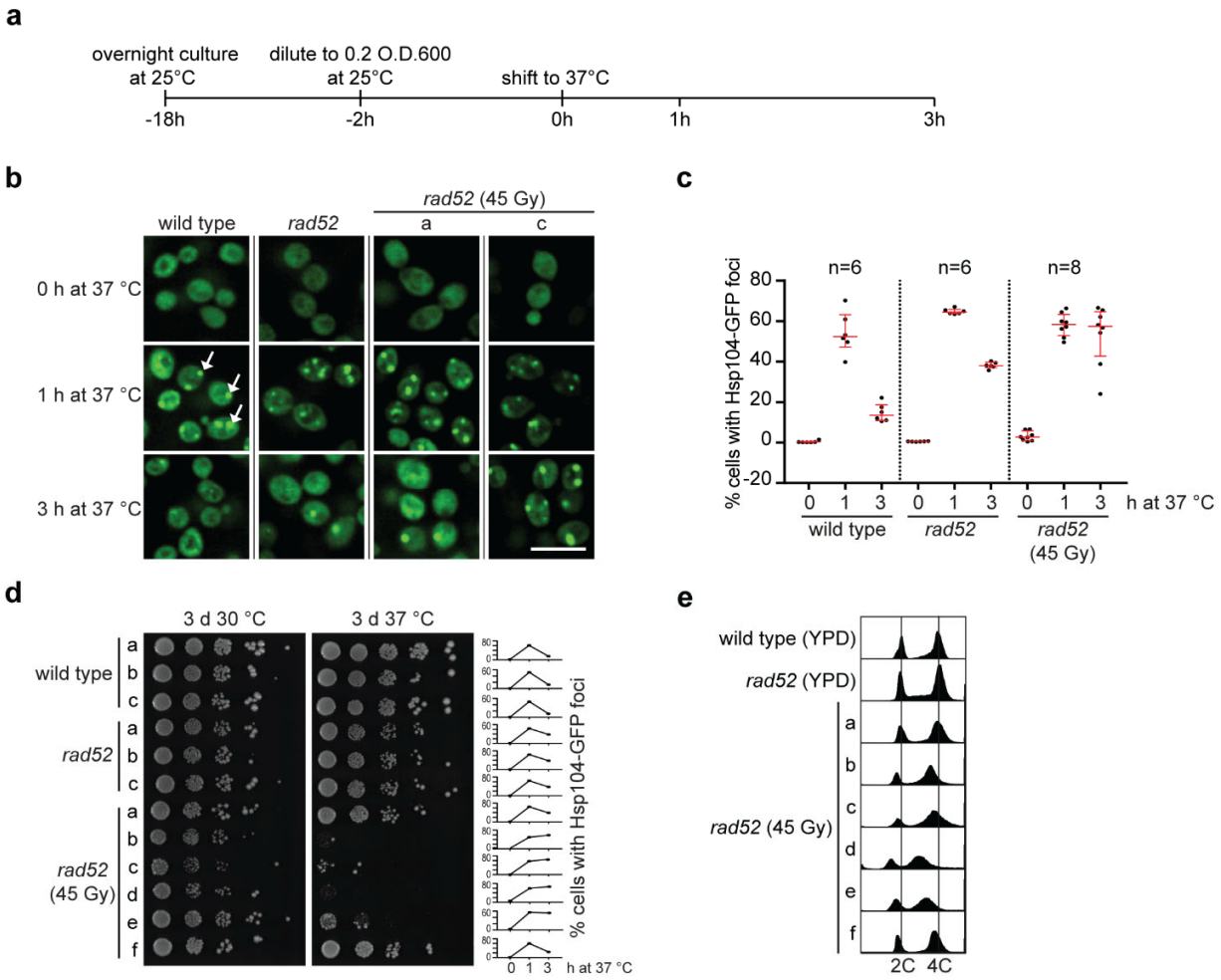

Figure 19. Highly aneuploid X-ray adapted *rad52* cells experience proteotoxic stress.
(a) Scheme of the experimental set-up. Control strains and 45 Gy resistant *rad52* colonies were grown overnight at 25 °C, in the morning diluted to 0.2 OD600nm and grown to exponential cultures. Afterwards, cultures were exposed to 37 °C heat for 3 h. I collected samples for fluorescence microscopy at 0h, 1h, and 3h at 37 °C in order to monitor Hsp104-GFP foci formation and resolution. **(b)** Representative microscopic images of indicated strains upon the heat challenge. All strains expressed endogenous Hsp104 fused with GFP. Arrows indicate Hsp104-GFP foci. For more details on automated foci analysis see methods section. Scale bar, 10 µM. **(c)** Quantification of Hsp104-GFP foci formation upon heat challenge in strains from (b) monitored using fluorescent microscopy. At least 3000 cells (each point on the histogram) per biological replicate were imaged. Error bars indicate median with interquartile range. **(d)** Strains of the indicated genotypes grown overnight at 25°C were spotted in 1:10 serial dilutions on YPD plates. The right panel indicates the percentage of Hsp104-GFP foci upon shift to 37 °C, summarized in (c). **(e)** DNA content of the indicated yeast strains corresponding to panel (d) was assessed by flow cytometry. Letters indicate independent colonies, which are the same clones in panels (b) to (e).

2.8.2 Nearly haploid CPT resistant *rad52* mutants do not suffer from proteotoxic stress

Although it is clearly established that aneuploidy causes proteotoxic stress in yeast that harbor even one extra chromosome (Oromendia et al., 2012; Santaguida et al., 2015), studies on disomes that carry an extra copy of chromosome III have not been done to my knowledge. Intriguingly, laboratory evolution experiments showed that the gain of an extra copy of chromosome III was an adaptive mechanism that allowed heat tolerance in budding yeast (Yona et al., 2012). Therefore, I set out to investigate whether the CPT adapted *rad52* mutants suffer from proteotoxic stress. Similarly to the experiments with the X-ray adapted *rad52* cells (Figure 19), I have monitored the formation and the resolution of Hsp104-GFP foci upon the heat stress conditions using high-throughput fluorescence microscopy (Figure 20a). CPT adapted *rad52* cells were able to form Hsp104-GFP foci after 1 h at 37 °C and resolve them after 3 h at 37 °C, similarly to euploid *rad52* parental strains (Figure 20b, and c). This correlated with the ability of CPT resistant *rad52* cells to form viable colonies at the elevated temperature (Figure 20d). The only temperature-sensitive CPT resistant clone (Figure 20d, clone e) still displayed an adequate dynamics of Hsp104-GFP foci formation and resolution. The loss of viability at the elevated temperatures could be explained by the formation of a temperature-sensitive mutation in an essential gene (or multiple ones) (Pringle, 1975) during the highly mutagenic genotoxic treatment. Using flow cytometry, I confirmed that all the CPT resistant *rad52* strains used in this experiment were nearly haploid (Figure 20e). Together, nearly haploid CPT resistant *rad52* cells do not display signs of proteotoxic stress and can form colonies at elevated temperatures.

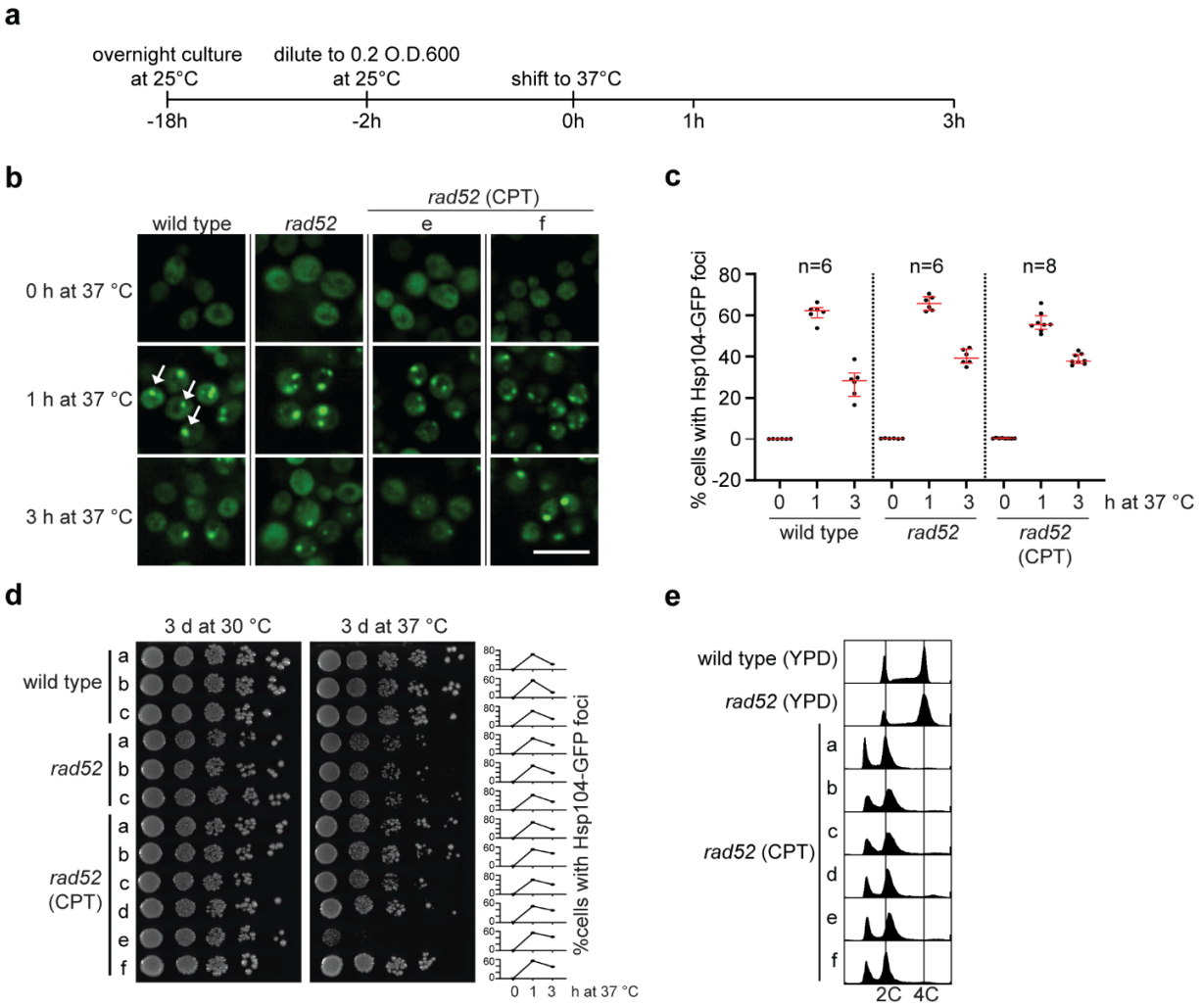

Figure 20. Nearly haploid CPT adapted *rad52* cells do not suffer from proteotoxic stress. **(a)** Scheme of the experimental set-up. Control strains and CPT resistant *rad52* colonies were grown overnight at 25 °C, in the morning diluted to 0.2 OD600nm, and grown to exponential cultures. Afterwards, the cultures were exposed to 37 °C heat for 3 h. I collected samples for fluorescence microscopy at 0h, 1h, and 3h at 37 °C in order to monitor Hsp104-GFP foci formation and resolution. **(b)** Representative microscopic images of indicated strains upon a heat challenge. All strains expressed endogenous Hsp104 fused with GFP. Arrows indicate Hsp104-GFP foci. For more details on automated foci analysis see methods section. Scale bar, 10 µM. **(c)** Quantification of Hsp104-GFP foci formation upon a heat challenge in strains from (b) monitored using fluorescent microscopy. At least 3000 cells (each point on the histogram) per biological replicate were imaged. Error bars indicate median with interquartile range. **(d)** Strains of the indicated genotypes grown overnight at 25°C were spotted in 1:10 serial dilutions on YPD plates. The right panel indicates the percentage of Hsp104-GFP foci upon shift to 37 °C, summarized in (c). **(e)** DNA content of the indicated yeast strains corresponding to panel (d) was assessed by flow cytometry. Letters indicate independent colonies, which are the same clones in panels (b) to (e).

2.8.3 X-ray resistant *rad52* mutants are sensitive to inhibitors that interfere with protein quality control system

My results demonstrate that highly aneuploid *rad52* cells adapted to X-rays suffer from proteotoxic stress (Figure 19), which opens up a possibility to target repair-defective *rad52* cells after adaptation, thereby diminishing the resistance. Studies in disomic yeast strains demonstrated that chemical compounds that target the protein quality control machinery of aneuploids effectively inhibit their growth (Torres et al., 2007, 2010).

The 26S proteasome is an integral part of the protein quality control of the cell, which is important for the degradation of a large fraction of peptides in the cell (Schubert et al., 2000). Aneuploid strains have shown to have an increased dependency on the 26S proteasome function and a high sensitivity to a specific proteasome inhibitor: MG132 (Torres et al., 2007, 2010). Therefore, the inhibition of 28S proteasome using MG132 provides pharmacological means to target highly aneuploid X-ray adapted *rad52* cells. In order to test whether X-ray adapted *rad52* cells are sensitive to the proteasome inhibition, I performed a growth curve assay in the presence of low dosages of MG132. As the function of proteasome is essential for cellular growth and survival, I used low (5 to 10 μM) dosages of the inhibitor, to achieve only partial inhibition of proteasome function. In order to allow the uptake of the inhibitor, I performed my experiments in a strain background that lacks the multidrug resistance conferring transporter *PDR5* (Balzi et al., 1994). The growth curve experiment revealed that a partial proteasome inhibition with MG132 invokes small but consistent changes in the population doubling time in euploid wild type and *rad52* control strains (Figure 21a). Higher MG132 sensitivity of euploid *rad52* cells compared to wild type cells is consistent with the idea that *rad52* deletion strains have low levels of proteotoxic stress, as assessed by the dynamics of Hsp104-GFP foci resolution (Figure 19c). Strikingly, highly aneuploid X-ray adapted *rad52* mutants displayed high sensitivity to the proteasome inhibition. Although the doubling time of aneuploid X-ray adapted *rad52* strains was already elevated in unchallenged conditions, the magnitude of changes in their doubling time upon MG132 treatment had exceeded that of the euploid parental *rad52* strain (Figure 21a). Using flow cytometry, I confirmed that X-ray adapted mutants used in my assay were highly aneuploid (Figure 21b). These results indicate that although the repair-defective *rad52* cells already suffer from proteotoxic stress to a minor degree, highly aneuploid adapted *rad52* mutants suffer from strongly pronounced proteotoxic stress, which renders them extremely sensitive to the inhibition of proteasome.

Chaperones constitute another essential component of the cellular protein control system, as they provide the vital functions of protein folding, assembly, and trafficking (Young et al., 2004). Amongst them, Hsp90 is one of the most abundant chaperones that supports a plethora of

essential cellular processes in unperturbed conditions, as well as under proteotoxic stress (McClellan et al., 2007). Due to the increased generation of misfolded proteins and protein aggregates, aneuploid yeast strains demonstrated an increased reliance on Hsp90 function and a high sensitivity to Hsp90 inhibitors, Geldanamycin and Radicicol (Oromendia et al., 2012; Torres et al., 2007). I therefore tested whether aneuploid X-ray adapted *rad52* mutants are sensitive to a partial inhibition of Hsp90 (Figure 21c). All strains used in the experiment were in *pdr5* background, to allow for the uptake of the drug. Of note, as Hsp90 is an essential protein, I did not use a Radicicol dosage that fully inhibits Hsp90. Upon the Radicicol treatment, I observed a moderate increase in the population doubling time for both euploid control strains, and aneuploid X-ray resistant *rad52* mutants. I confirmed that X-ray adapted mutants used in my assay were highly aneuploid (Figure 21d), excluding that the moderate sensitivity to Hsp104 inhibition was due to a low degree of aneuploidy in randomly selected X-ray resistant mutants. The result of the growth curve assay indicates the moderate sensitivity of adapted aneuploid *rad52* strains to Hsp104 inhibition with Radicicol.

Together, these results indicate that X-ray adapted *rad52* strains are highly sensitive to the 26S proteasome inhibitor MG132 and moderately sensitive to the Hsp90 inhibitor Radicicol, providing a pharmacological means to target X-ray resistant cells post-adaptation.

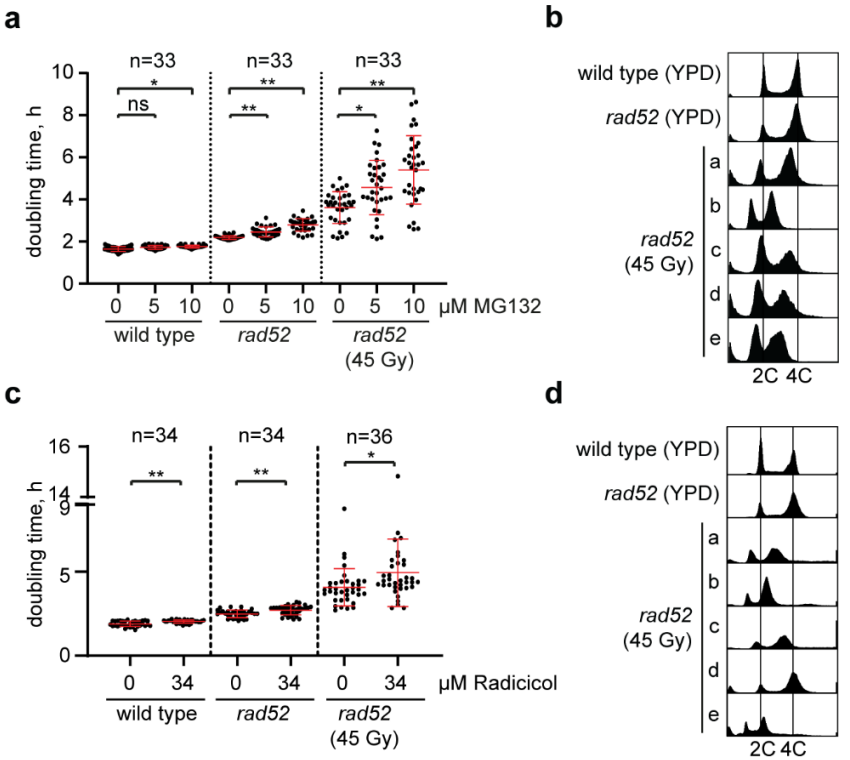

Figure 21. Highly aneuploid X-ray adapted *rad52* mutants are highly sensitive to the inhibition of 26S proteasome and Hsp90. *Figure legend, see next page.*

Figure 21. Highly aneuploid X-ray adapted *rad52* mutants are highly sensitive to the inhibition of 26S proteasome and Hsp90. (a) Population doubling times of control euploid strains and X-ray resistant *rad52* mutants (all in *pdr5* background to facilitate MG132 uptake) was determined in a growth curve assay at 30 °C in YPD media containing DMSO (as a control) or the indicated concentrations of MG132. Data are represented as a scatter plot with indicated mean and SD. Thirty-three independent colonies derived from two biological replicates were analysed. Statistical analysis was performed using the Scheirer-Ray-Hare test followed by pairwise Bonferroni-corrected Mann-Whitney-U-tests (* is $p \leq 0.05$ and ** is $p \leq 0.001$). **(b)** Representative DNA content flow cytometry profiles of euploid and X-ray adapted aneuploid mutants corresponding to panel (a). Letters indicate independent colonies analysed. **(c)** Population doubling times of control euploid strains and X-ray resistant *rad52* mutants (all in pdr5 background) was determined in a growth curve assay in YPD media containing DMSO (as a control) or 34 µM of Hsp90 inhibitor Radicicol at 30 °C. Data are represented as a scatter plot with indicated mean and SD. Thirty-four independent colonies of euploid control strains, and thirty six X-ray resistant *rad52* colonies derived from two biological replicates were analysed. Statistical analysis was performed using the Scheirer-Ray-Hare test followed by pairwise Bonferroni-corrected Mann-Whitney-U-tests (* is $p \leq 0.05$). **(d)** Representative DNA content flow cytometry profiles of euploid and X-ray adapted aneuploid mutants corresponding to panel (c). Letters indicate independent colonies analysed. **Statistical analysis was performed by Dr. Anke Busch.**

2.8.4 CPT resistant *rad52* mutants are slightly sensitive to proteasome inhibition

My results indicate that highly aneuploid X-ray resistant *rad52* mutants suffer from proteotoxic stress (Figure 19) and therefore display high sensitivity to proteasome inhibitors (Figure 21). Although I only observed minor signs of proteotoxic stress in CPT resistant *rad52* strains that were comparable to the parental diploid *rad52* strain (Figure 20), I was not able to predict whether an extra challenge on the protein quality control system in CPT resistant disomes would overwhelm their cellular capacity to respond to it. This prompted me to investigate whether CPT resistant *rad52* strains, that are aneuploid for chromosome III, display growth disadvantages upon a partial inhibition of the 26S proteasome with MG123 (Figure 22a). Because CPT resistant *rad52* strains are nearly-haploid, I included haploid control strains in my analysis. This allowed me to ensure that the dosage of genes that encode proteasome subunits will not underlie the changes that I observe during the treatment with similar inhibitor dosages. All strains used in the experiment were in the *pdr5* background. Growth curve analysis revealed that a partial proteasome inhibition with MG132 consistently increased the population doubling time in haploid and diploid control strains, as well as in CPT resistant *rad52* strains. However, in contrast to X-ray adapted aneuploid strains (Figure 21a), the magnitude of the growth delay in CPT resistant *rad52* was comparable to the diploid *rad52* strain. This result was in line with the low levels of proteotoxic stress in CPT resistant *rad52* mutants (Figure 20). I analysed the DNA content of examined strains to ensure that the randomly selected CPT resistant *rad52* mutants were haploid (Figure 22b). Together, nearly haploid CPT resistant *rad52* strains do not display prominent sensitivity to the proteasome inhibitor MG132.

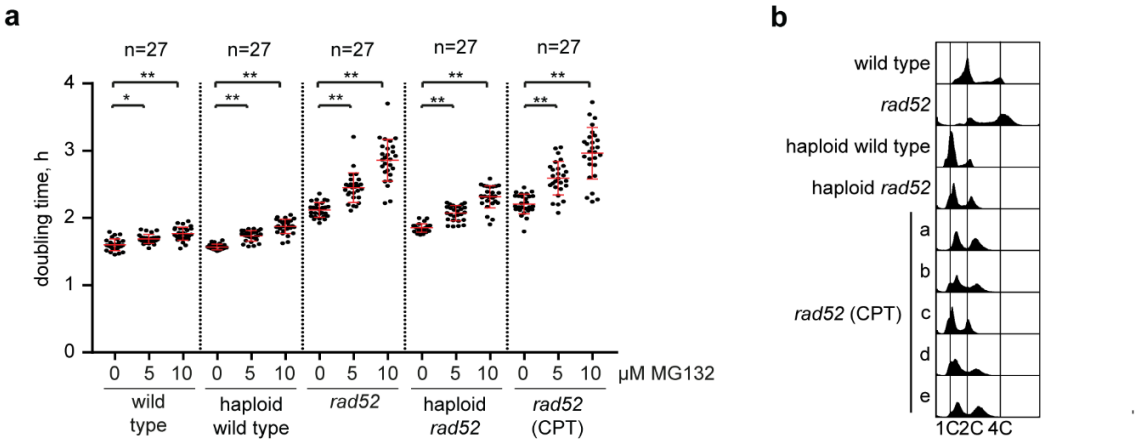

Figure 22. Nearly haploid CPT resistant *rad52* mutants are not sensitive to proteasome inhibition. (a) Population doubling times of control euploid strains and CPT resistant *rad52* mutants (all in *pdr5* background to facilitate MG132 uptake) was determined in a growth curve assay at 30 °C in YPD media containing DMSO (as a control) or the indicated concentrations of MG132. Data are represented as a scatter plot with indicated mean and SD. Twenty-seven independent colonies derived from two biological replicates were analysed. Statistical analysis was performed using the Scheirer-Ray-Hare test followed by pairwise Bonferroni-corrected Mann-Whitney-U-tests (* is $p \leq 0.05$ and ** is $p \leq 0.001$). **(b)** Representative DNA content flow cytometry profiles of euploid and CPT adapted aneuploid *rad52* mutants corresponding to panel (a). Letters indicate independent colonies analysed. **Statistical analysis was performed by Dr. Anke Busch.**

2.9 Adapted *rad52* mutants have decreased TORC1 activity

Aneuploidy as a condition comes with high cellular fitness costs, which are proportional to the degree of aneuploidy. Besides proteotoxic stress, the aneuploidy condition alters many other aspects of cellular metabolism, such as energy consumption, gene silencing, osmotic pressure in the cytoplasm, and many others (Mulla et al., 2017; Torres et al., 2007; Tsai et al., 2019). Aneuploids display highly altered energy metabolism, and increased glucose consumption by aneuploids does not result in proportionally high biomass accumulation (Torres et al., 2007). This physiological flaw opens the possibility for targeting aneuploid cells with low energy mimetics. Studies in disomic yeast strains demonstrated their sensitivity to the TORC1 inhibitor rapamycin (Torres et al., 2007), while studies in triploid mouse embryonic fibroblasts and aneuploid human cancer cell lines, showed their high sensitivity to the low-energy state mimetic AICAR (Tang et al., 2011). Therefore, I set out to investigate whether aneuploid *rad52* mutants can also be targeted post-adaptation with the starvation mimicking drug, rapamycin.

2.9.1 X-ray resistant *rad52* mutants have decreased TORC1 activity and are sensitive to rapamycin

The target of rapamycin complex (TORC1) is an essential regulator of cellular growth and proliferation in response to nutrient availability (Loewith and Hall, 2011). An antifungal metabolite rapamycin, in complex with the FKBP12 adaptor protein, binds to TORC1 complex, and inhibits its activity (Heitman et al., 1991). Treatment with rapamycin mimics the conditions of nutrient starvation, and results in a cessation of cellular growth and proliferation. As aneuploid cells were reported to have an altered nutrient metabolism and an elevated energy demand (Torres et al., 2007), I wanted to understand whether highly aneuploid adapted cells have an increased sensitivity to rapamycin.

I monitored population doubling times of euploid control strains, as well as highly aneuploid X-ray resistant *rad52* mutants in the presence of low dosages of rapamycin (Figure 23a). Treatment with rapamycin evoked small but consistent changes in the population doubling time in the control strains. Importantly, treatment with rapamycin resulted in a drastic increase in the population doubling time in X-ray resistant *rad52* mutants. The magnitude of delay in growth rates in aneuploid X-ray resistant *rad52* mutants exceeded the one of the parental euploid *rad52* mutants. Using flow cytometry, I confirmed that X-ray resistant mutants used for the growth curve were indeed highly aneuploid (Figure 23b). These results indicate that X-ray adapted *rad52* mutants can potentially be targeted with rapamycin treatment.

High sensitivity to rapamycin in aneuploid cells may arise due to the altered activity of TORC1 complex. On one hand, as the activity of TORC1 is downregulated in response to practically all types of cellular stresses (Loewith and Hall, 2011), stress-burdened aneuploids may have decreased kinase activity of TORC1. On the other hand, high glucose consumption by aneuploids (Torres et al., 2007) might be a consequence of a compensatory upregulation in metabolic pathways reflected in elevated TORC1 activity. In order to better understand the physiological basis of the increased sensitivity of X-ray adapted aneuploids to rapamycin, I set out to investigate TORC1 status in adapted cells. To monitor the activity of TORC1, I assessed the phosphorylation status of TORC1 *bona fide* target Sch9 (Urban et al., 2007) using an antibody that specifically recognizes multiple phosphorylation sites on the C-terminus of Sch9 (Figure 23c). Treatment of a wild type strain with 50 nM rapamycin (Rapa) served as a negative control, while treatment with 25 µg/mL cycloheximide (CHX) served as a positive control. I observed that even the euploid *rad52* strain already had decreased levels of pSch9, indicating attenuated TORC1 activity (Figure 23a). This result is in line with the slower growth of *rad52* mutants (compared to wild types), even in unchallenged conditions. Highly aneuploid X-ray resistant *rad52* mutants displayed even further

downregulated pSch9 levels, which is indicative of very low TORC1 activity. These results suggest that high sensitivity of aneuploid X-ray resistant *rad52* mutants to rapamycin arises from very low basal levels of TORC activity in these cells. Of note, the total expression of the Sch9 protein also varied in aneuploid strains, making precise quantification of the pSch9/Sch9 ratio misleading. In summary, X-ray resistant *rad52* mutants have decreased levels of TORC1 activity.

TORC1 regulates multiple aspects of cellular growth in response to environmental conditions via a plethora of its downstream targets (Loewith and Hall, 2011). I wanted to ensure that TORC1 activity in X-ray resistant *rad52* mutants is downregulated in general, and not only towards the Sch9 target. Downregulation of TORC1 activity in response to starvation induces autophagy (Yorimitsu et al., 2007); therefore, assessing autophagy levels in X-ray resistant *rad52* mutants can serve as an additional read-out for TORC1 activity. I monitored autophagy induction in aneuploid X-ray resistant *rad52* mutants using a previously published GFP-Atg8 autophagy reporter (Klermund et al., 2014) (Figure 23d). The GFP-Atg8 fusion protein is usually associated with an autophagosome. When autophagy is activated, the fusion of an autophagosome and a lysosome results in the cleavage of the construct, and a subsequent accumulation of free GFP in the lysosomal lumen (Klionsky, 2011). I used a treatment with 50 nM rapamycin (Rapa) as a positive control for the autophagy induction and an autophagy-deficient *rad52 atg1* strain as a negative control. My results show that no detectable activation of autophagy is observed in exponential wild type cultures (Figure 23d). I observed a slight activation of autophagy in the euploid parental *rad52* strain and even more pronounced activation of autophagy in X-ray resistant *rad52* mutants. These results enforce the observation that X-ray adapted *rad52* mutants have decreased TORC1 activity.

Together, highly aneuploid X-ray resistant *rad52* mutants have decreased activity of TORC1, which renders them sensitive to rapamycin. These findings provide an additional strategy for targeting resistant cells post-adaptation.

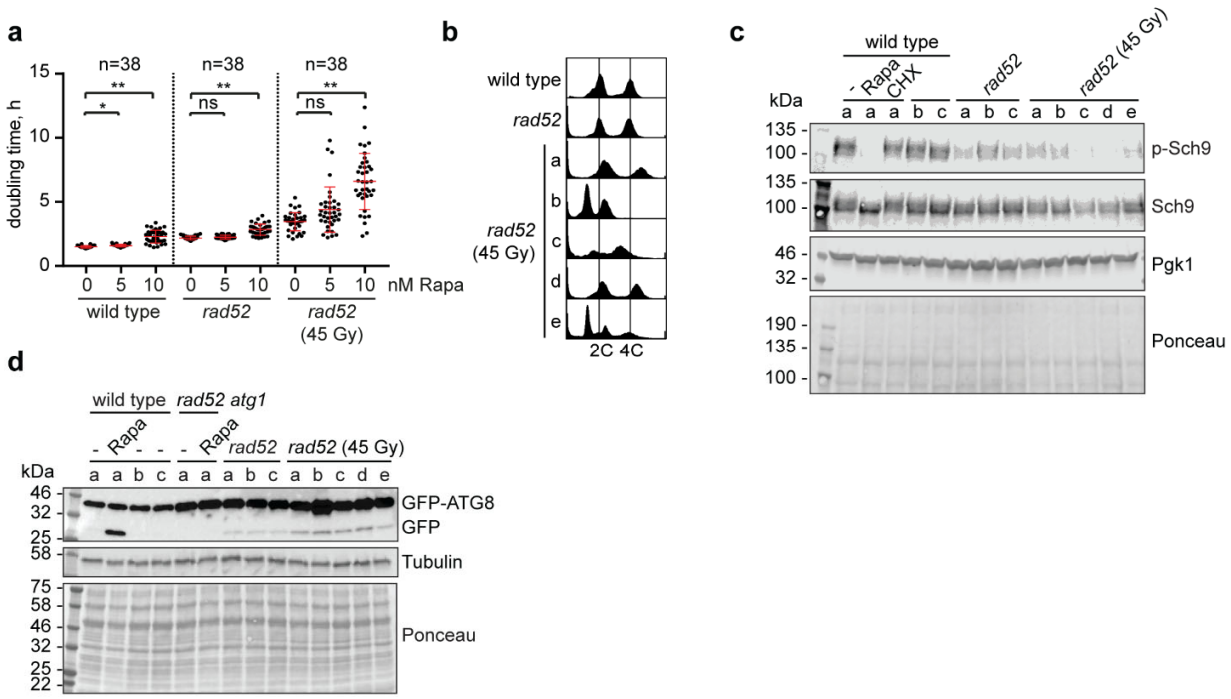

Figure 23. X-ray resistant *rad52* mutants have decreased TORC1 activity and are sensitive to rapamycin. (a) Population doubling times of the indicated strains in YPD media at 30 °C containing DMSO (control) or the indicated concentrations of rapamycin. Thirty eight independent colonies derived from three biological replicates were analysed. Data are represented as a scatter plot indicating mean values and SD. Statistical analysis was performed using the Scheirer-Ray-Hare test followed by pairwise Bonferroni-corrected Mann-Whitney-U-tests (* is $p \leq 0.05$ and ** is $p \leq 0.001$). **(b)** Representative DNA content flow cytometry profiles of yeast strains corresponding to (a). Letters indicate independent colonies analysed. **(c)** Indicated euploid control strains and X-ray resistant *rad52* colonies were grown to exponential cultures in YPD at 30°C and collected at 0.6 OD600nm. Control cultures were either mock-treated, or treated for 15 min with either 50 nM rapamycin (Rapa) or 25 µg/mL cycloheximide (CHX). Whole protein lysates were separated by SDS-PAGE and membranes were probed with the indicated antibodies. Letters indicate independent freshly derived colonies. **(d)** Strains expressing plasmid-encoded GFP-Atg8 were grown to exponential cultures in selective media at 30°C and monitored for autophagy induction. Treatment with 50 nM rapamycin (Rapa) for 1 h served as a positive control. Whole protein lysates were separated by SDS-PAGE and membranes were probed with indicated antibodies. Letters indicate independent freshly derived colonies. **Statistical analysis was performed by Dr. Anke Busch.**

2.9.2 X-ray resistant *rad52* mutants have decreased TORC1 activity and are sensitive to Rapamycin

Studies in aneuploid yeast strains demonstrated that the presence of even one extra chromosome is sufficient to render the mutant to be sensitive to rapamycin (Torres et al., 2007). However, the extent of sensitivity to the drug varied depending on which chromosome was present as the extra copy. The sensitivity of strains disomic on chromosome III was not assessed in the study.

Therefore, I set out to investigate whether nearly-haploid CPT resistant *rad52* mutants can be targeted with the TORC1 inhibitor rapamycin.

I monitored the population doubling time of euploid wild type and *rad52* strains, as well as nearly-haploid CPT resistant *rad52* mutants in the presence of 10 nM rapamycin (Figure 24a). I have observed that rapamycin addition evoked small, but statistically significant changes in all strains used in my experiments. I did not observe greater sensitivity of nearly haploid CPT resistant *rad52* strains compared to the diploid wild type control. I ensured that the randomly selected CPT resistant *rad52* mutants were indeed nearly haploid using flow cytometry (Figure 24b). Next, I examined the activity of TORC1 towards its downstream target Sch9 in the experiment similar to the one described in Figure 23b. I observed that CPT resistant *rad52* mutants have Sch9 phosphorylation levels comparable to the ones of the diploid *rad52* mutants. This result explains why the CPT resistant *rad52* mutants are not preferentially sensitive to rapamycin (Figure 24a). In line with these results, I observed that CPT resistant *rad52* mutants display autophagy levels similar to the ones of the parental *rad52* strain (Figure 24d). For a detailed description of the GFP-Atg8 reporter and the experiment, see section 2.9.1. Together, these results indicate that nearly-haploid CPT resistant *rad52* mutants have TORC1 activity similar to that of euploid *rad52* strains, and do not display elevated sensitivity to rapamycin.

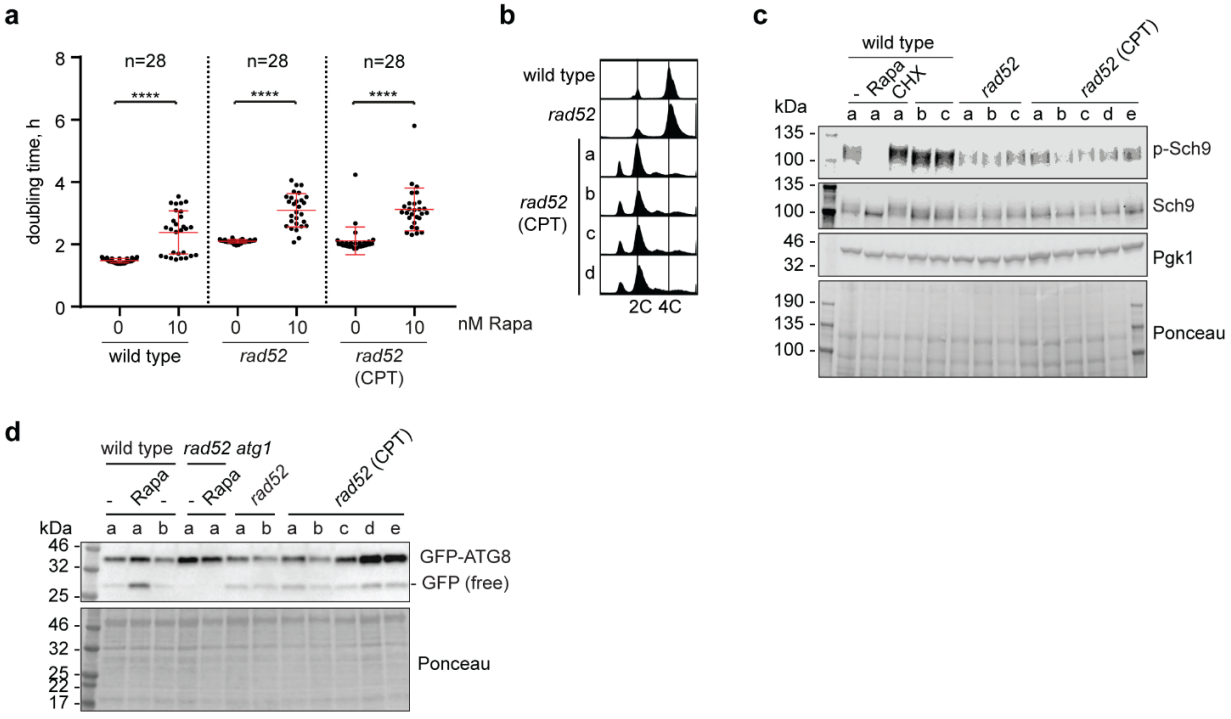

Figure 24. CPT resistant *rad52* mutants do not display low TORC1 activity or enhanced sensitivity to rapamycin. *Figure legend, see next page.*

Figure 24. CPT resistant *rad52* mutants do not display low TORC1 activity or enhanced sensitivity to rapamycin. (a) Population doubling times of indicated euploid control strains and CPT-resistant *rad52* mutants in YPD media containing DMSO or the indicated concentrations of rapamycin at 30 °C. Twenty eight independent freshly derived colonies from three biological replicates were analysed. Statistical analysis was performed using the Scheirer-Ray-Hare test followed by pairwise Bonferroni-corrected Mann-Whitney-U-tests (**** is $p \leq 0.00001$). **(b)** Representative DNA content flow cytometry profiles of yeast strains corresponding to (a). Letters indicate independent colonies analysed. **(c)** Indicated euploid strains and CPT resistant *rad52* colonies were grown to exponential cultures in YPD at 30 °C and collected at 0.6 OD600nm. Cultures were either mock-treated or treated for 15 min with either 50 nM rapamycin (Rapa) or 25 µg/mL cycloheximide (CHX). Whole protein lysates were separated by SDS-PAGE and membranes were probed with the indicated antibodies. Letters indicate independent freshly derived colonies. **(d)** Strains expressing plasmid-encoded GFP-Atg8 were grown to exponential cultures in selective media at 30°C. Treatment with 100 nM rapamycin for 1 h served as a positive control. Whole protein lysates were separated by SDS-PAGE and membranes were probed with an anti-GFP antibody. Letters indicate independent freshly derived colonies. **Statistical analysis was performed by Dr. Anke Busch.**

2.10 The *rad52* mutants display elevated levels of Cdc5

An elevated expression levels of the human polo-like kinase PLK1 was linked to a cancer resistance towards genotoxic treatment with doxorubicin, gemcitabine, and many other therapeutic agents with a variety of action modes (Gutteridge et al., 2016; Saatci et al., 2018; Zuco et al., 2015). The yeast homolog $Cdc5^{PLK1}$ has not yet been linked to a drug resistance, to my knowledge. However, Cdc5 is a key regulator of adaptation to the DDC (Serrano and D'Amours, 2016; Toczyski et al., 1997; Vidanes et al., 2010). Because my results indicate that CA precedes the formation of resistant repair-defective colonies under the conditions of genotoxin challenge (Figure 12), I wanted to investigate whether the levels of Cdc5 are altered in adapted cells.

In order to answer this question, I analyzed Cdc5 protein levels in the exponentially growing cultures of wild type and *rad52* strains, as well as in X-ray resistant *rad52* mutants using western blotting with an antibody that specifically recognizes endogenous Cdc5 (Figure 25a). I used a GFP-tagged version of Cdc5 to confirm the specificity of the antibody. I have quantified the intensity of the Cdc5 signal over the total activated gel signal from two independent experiments (Figure 25b). My results demonstrate that the deletion of *rad52* results in an approximate 2-fold increase in Cdc5 levels. However, adapted cells do not display further elevation in Cdc5p levels, indicating that the resistance phenotype of X-ray adapted cells is unlikely to be explained by the Cdc5 levels.

I also analyzed whether Cdc5 levels are elevated in CPT resistant *rad52* mutants (Figure 25c). The quantification of the relative Cdc5 signal (Figure 25d) again demonstrated that CPT resistant *rad52* mutants have Cdc5 levels similar to the parental naïve *rad52* strain. Together, *rad52*

mutants have elevated levels of Cdc5, which are not further increased in X-ray and CPT adapted *rad52* mutants.

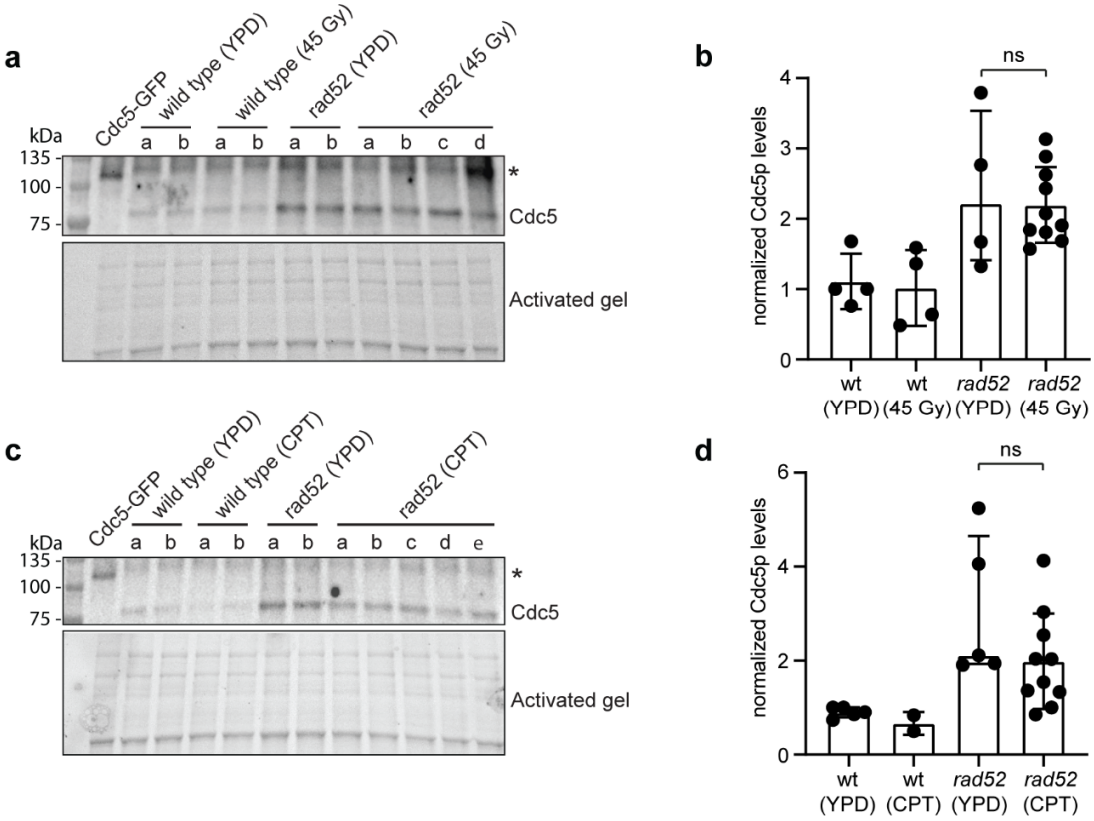

Figure 25. The *rad52* mutants have elevated Cdc5 levels.
(a) Strains derived from either control plates (YPD) or plates irradiated with 45 Gy of X-rays were grown to exponential cultures in YPD at 30 °C. Whole protein lysates were separated by SDS-PAGE and membranes were probed with anti-Cdc5 antibody. Letters indicate independent freshly derived colonies. Asterisk (*) indicates an unspecific band. **(b)** Relative quantification of Cdc5 levels combined from two independent experiments. For normalization procedure details, see materials and methods section. Four colonies of wild type strains derived either from YPD plates or plates irradiated with 45 Gy of X-rays, and of *rad52* strain derived from YPD plates were analysed. For *rad52* strain irradiated with 45 Gy of X-rays, ten colonies were analysed. Error bars indicate median with interquartile range. Statistical analysis was performed using ANOVA with Tukey's post-hoc test. ns, not significant. **(c)** Strains derived from either control plates (YPD) or plates containing 2 µM CPT were grown to exponential cultures in YPD at 30 °C. Whole protein lysates were separated by SDS-PAGE and membranes were probed with the indicated antibodies. Letters indicate independent freshly derived colonies. Asterisk (*) indicates an unspecific band. **(d)** Relative quantification of Cdc5p levels from two independent experiments was performed similarly to panel (c). Four colonies of wild type strains from YPD plates, two colonies of wild type from 2 µM CPT, five colonies of *rad52* strain from YPD plates, and ten colonies of *rad52* strain derived from plates containing 2 µM CPT were analysed. ns, not significant.

2.11 Mitotic recombination proteins Rad51, Rad59, and Rad55 do not contribute to resistance formation in *rad52* mutants

The two major HR pathways in yeast require either Rad51, Rad55, and Rad57 proteins, or Rad59, and the MRX complex. Although the Rad52 recombinase is essential for all the HDR pathways, the deletion of *RAD52* does not fully eliminate gene conversion events in the yeast cell (Coïc et al., 2008). Moreover, following UV irradiation, the frequency of gene conversion events in *rad52* mutants increased in a *RAD51*, *RAD55*, *RAD59*, and *RAD50* dependent manner (Coïc et al., 2008). Despite the very low rates of recombinant formation in the study, I nonetheless wondered whether the resistance of *rad52* mutants to the treatment with genotoxins is supported by HR proteins Rad59, Rad51, and Rad55.

I therefore combined the knock-out of *rad52* with the knock-out of either *RAD59*, *RAD51*, or *RAD55* (Figure 26). Although the NHEJ pathway is suppressed in diploid yeast cells through the cell cycle in a transcription-dependent manner by Nej1 (Frank-Vaillant and Marcand, 2001; Valencia et al., 2001), I have deleted a key NHEJ gene *DNL4* to ensure that the pathway is not restored under the genotoxin treatment conditions. This allowed me to specifically evaluate the contribution of *RAD59*, *RAD51*, and *RAD55* genes to the survival of *rad52* mutants. My results indicate that the deletion of *RAD59* did not affect the survival of *rad52* mutants in response to either 45 Gy of X-rays of 2 µM CPT (Figure 26a, and b). The *rad51 rad52* double mutants also displayed survival rates similar to ones of *rad52* alone both after 45 Gy of X-rays or on plates containing 2 µM CPT (Figure 26c, and d). Finally, I also did not observe any additive DNA damage sensitivity effects in *rad52 rad55* mutants (Figure 26e, and f). Together, these results indicate that the HDR proteins Rad59, Rad51, and Rad55 are not involved in the survival of *rad52* cells in response to genotoxic treatment. These results exclude that the restoration of HDR in an alternative manner supports the resistance of *rad52* cells towards genotoxins.

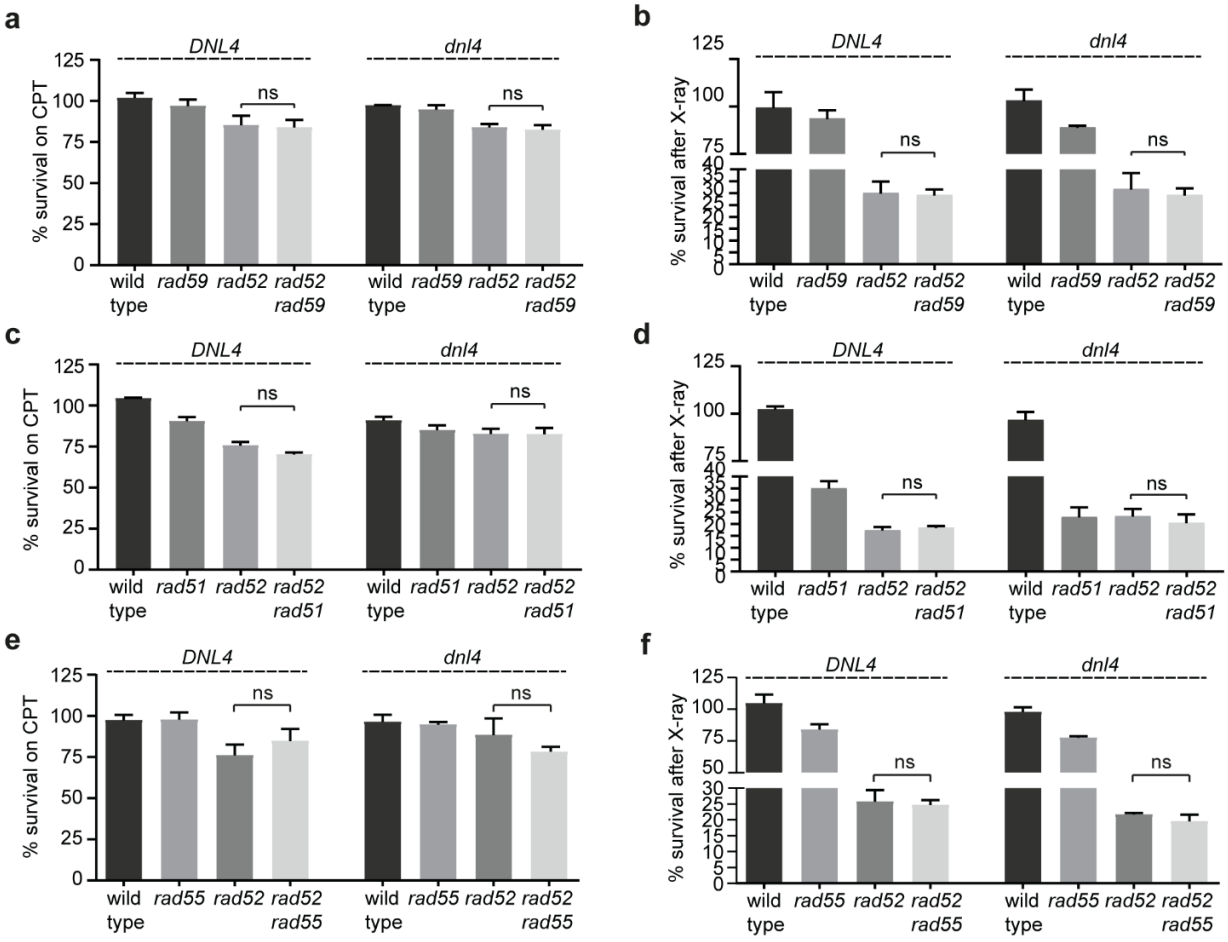

Figure 26. HDR proteins Rad59, Rad51, and Rad55 are not involved in the formation of resistant colonies following X-ray and CPT treatment in *rad52* mutants. (a-f) Quantification of cell survival in response to 45 Gy of X-rays or 2 μM CPT. All visible colonies were counted and the number of colonies on drug plates was divided by the number of colonies on control plates. Data are represented as mean values with the SEM of 3 independent experiments. For statistical analysis, ANOVA test with Tukey's post-hoc test was applied. ns, not significant.

2.12 The MRX complex supports the viability of *rad52* mutants upon DNA damage

Microhomology-mediated end joining (MMEJ) is a faulty backup DNA repair pathway that operates independently of *rad52*-mediated HDR pathways, or Ku proteins essential for the NHEJ pathway (Ma et al., 2003). MMEJ involves the alignment of DSB-proximal microhomologies, and subsequent re-joining of DNA ends (see section 1.5.3 for the detailed overview of the pathway) (Sfeir and Symington, 2015). Studies using intra- and interchromosomal reporter systems have identified the MRX (Mre11-Rad50-Xrs2) complex as a key player in the MMEJ pathway (Lee and Sang, 2007; Ma et al., 2003; Meyer et al., 2015). The other key components of MMEJ pathway are the DNA polymerase δ subunit Pol32, the Polymerase λ (Pol4), as well as the DNA endonuclease Rad1 (Ma et al., 2003; Meyer et al., 2015). This backup repair pathway was shown to operate in HR-deficient *rad52* mutants of NHEJ-deficient Ku mutants (Lee et al., 2019; Meyer et al., 2015), suggesting that MMEJ might be responsible for the survival of and the formation of resistance in *rad52* mutants subjected to X-rays and CPT treatment. I set out a series of experiments to dissect the role of the MMEJ pathway in the survival of *rad52* mutants upon genotoxic treatment pre- and post-adaptation.

2.12.1 The MRX complex is essential for the viability of *rad52* mutants on CPT

The MRX complex plays a central role in the DSB repair, and executes multiple functions that include the tethering of DNA ends, the resection of the DNA ends in the 3' to 5' direction, the activation of the checkpoints signaling, and the recruitment of other repair proteins that also facilitate the DSBs repair (Bonetti et al., 2018; Oh and Symington, 2018). Due to the function of the MRX complex, it was majorly studied in the NHEJ or HDR pathways, however the complex also plays crucial role in MMEJ (see section 1.5.4.3 for the detailed overview of the MRX role in MMEJ, and section 1.5.4.4 for the overview of the MRX role in the repair of CPT-induced damage) (Ma et al., 2003; Meyer et al., 2015). I therefore have set out to investigate whether the function of the MRX complex is important for the survival of *rad52* mutants following DNA damage.
I have first created a mutant that combines the deletion of *RAD52* with the deletion of *MRE11*, a nuclease subunit of the MRX complex. I also deleted *DNL4* to ensure that the NHEJ restoration is not responsible for the re-growth of *rad52* mutants following genotoxic challenge. I have subjected *rad52 mre11* double mutants to a treatment with either 45 Gy of X-rays or 2 μM CPT (Figure 27a). Strikingly, I have observed that the *rad52 mre1*1 double mutants are extremely sensitive to 2 μM CPT, while the *rad52* mutant alone and the *mre11* mutant alone were still able to form adapted colonies (Figure 27b). The double mutant colonies that still formed were barely visible with a naked eye. I have also observed a small, but not significant, decrease in the numbers of *rad52 mre11*

colonies formed after the treatment with 45 Gy of X-rays (Figure 27c). Importantly, these X-ray resistant colonies were visually smaller (Figure 27a), indicating that *rad52 mre11* mutant is also slightly sensitized to the X-ray treatment. Together, the loss of MRE11 in *rad52* mutants renders them extremely sensitive to CPT and slightly sensitizes them to X-rays.

I wanted to confirm that the function of the whole MRX complex is critical for the survival of *rad52* mutants in response to genotoxic stress, especially following CPT treatment. Therefore, I have created a *rad52* mutant that lacks another MRX component, *RAD50.* I have subjected *rad52 rad50* double mutants to a treatment of either 45 Gy of X-rays or 2 μM CPT (Figure 27d). Similar to the *rad52 mre11* double mutants, the sensitivity of *rad52 rad50* mutants to CPT greatly exceeds the sensitivity of either *rad52* or *rad50* mutants alone (Figure 27e). I have also observed that the *RAD50* knock-out resulted in a slight decrease in the numbers of *rad52* mutants recovered after the X-ray treatment (Figure 27f), and the re-grown *rad52 rad50* colonies were smaller compared to *rad52* or *rad50* colonies alone (Figure 27d). These results indicate that the MRX complex sustains viability of the HR-defective *rad52* mutants following CPT treatment.

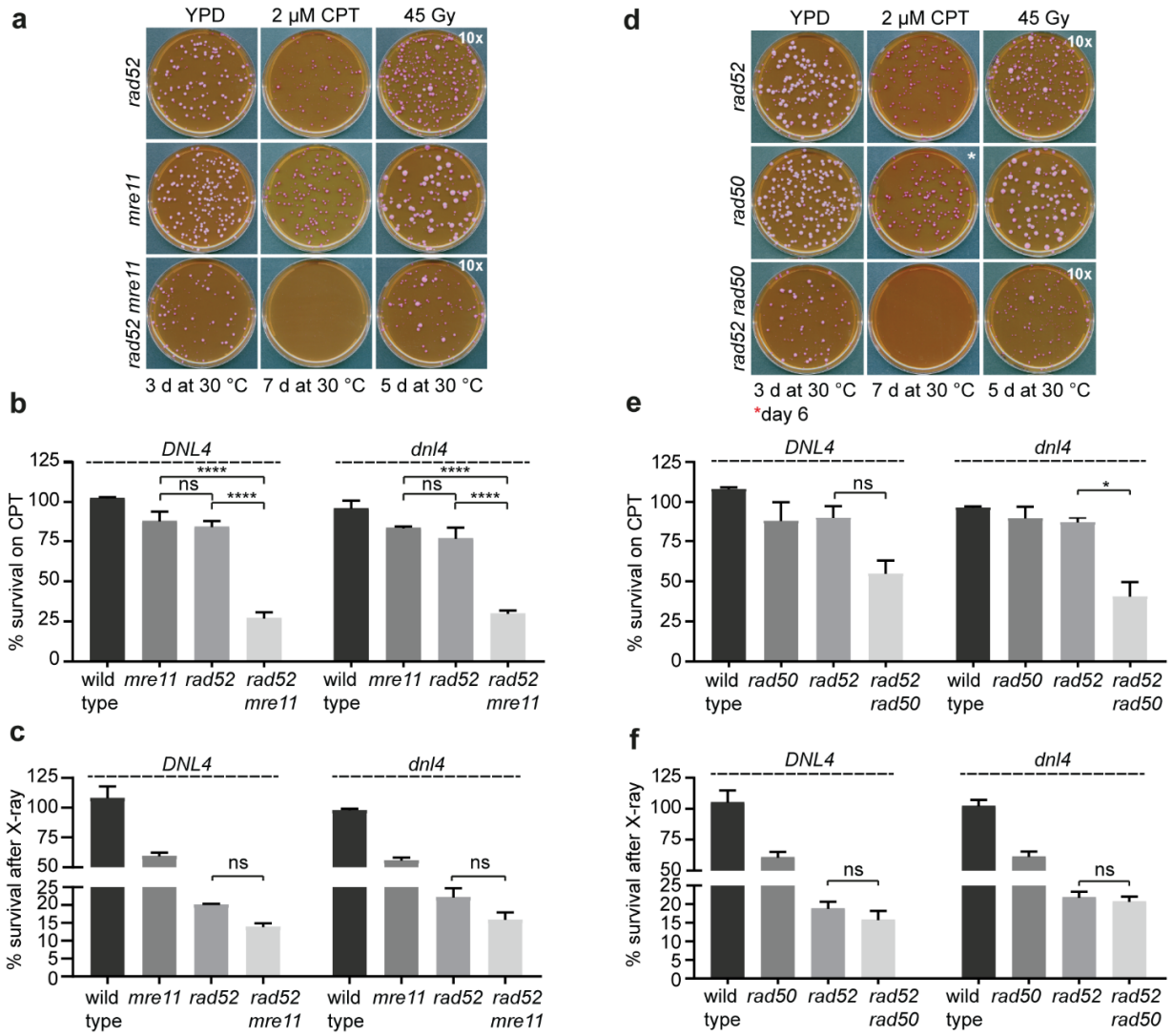

Figure 27. MRX complex promotes survival of *rad52* mutants on CPT.
(a) Representative images of a plating assay. Strains with indicated genotypes were plated onto YPD or plates containing 2 µM CPT (all containing 8 µg/mL Phloxine B) and incubated at 30°C for the indicated times. Of note, the cell number plated on X-ray treated plates was ten-times higher compared to control plates. **(b, c)** Quantification of cell survival in the presence of 2 µM CPT or after exposure to 45 Gy of X-rays after normalization to control YPD plates. All data are represented as mean values and the error bars indicate the SEM of 3 independent experiments. For statistical analysis ANOVA test with Tukey's post-hoc test was applied. (****p≤0.0001). ns, not significant. **(d)** Representative images of a plating assay similar to (a). The cell number plated on X-ray treated plates was ten-times higher compared to control plates. Asterisk (*) indicates that the plate image was taken after six days. **(e, f)** Quantification of cell survival in the presence of 2 µM CPT or after exposure to 45 Gy of X-rays was performed similarly to panels (b, c). (*p≤0.05). ns, not significant.

2.12.2 The MRX complex is essential for the survival of *rad52* mutants on CPT post-adaptation

Our previous results demonstrated that the repair-defective *rad52* mutants gain an evident genotoxin resistance following the initial treatment with 2 µM CPT (Figure 13c). At the same time, the MRX complex plays a critical role in the re-growth of *rad52* mutants on 2 µM CPT (Figure 27b). I therefore wondered whether the *rad52* mutants that gained resistance following the initial CPT treatment still rely on the MRX complex to repair their DNA. Because it is nearly impossible to obtain viable *rad52 mre11* mutants after the treatment with 2 µM CPT, I generated an auxin-inducible degron of Mre11 (Morawska and Ulrich, 2013). Briefly, I fused the 3' end of the *MRE11* gene with a sequence that contains an auxin-inducible degron (AID*) and a 9MYC tag (Figure 28a).

In order to generate CPT resistant *rad52* Mre11-AID* mutants, I plated them onto 2 µM CPT in the absence of IAA (auxin) for seven days, and afterwards patched them on YPD plates to recover viable cells. Subsequently, I subjected CPT resistant *rad52* Mre11-AID* mutants to a second round of CPT treatment, either in the presence or absence of IAA (Figure 28b). The depletion of Mre11 with IAA without the induction of DNA damage did not affect the growth of naïve and CPT resistant *rad52* mutants. In the presence of 2 µM CPT, the strains derived from CPT containing plates demonstrated strong growth advantage compared to the naïve parental strains (compare *rad52* [YPD] to *rad52* [CPT]; compare *rad52* Mre11-AID* [YPD] to *rad52* Mre11-AID* [CPT]). However, when Mre11 was depleted with IAA during the CPT treatment, the CPT derived *rad52* Mre11-AID* re-gained their sensitivity to the genotoxic treatment (compare *rad52* [CPT] to *rad52* Mre11-AID* [CPT] on the plate containing 1 mM IAA and 2 µM CPT). I have ensured that the resistant *rad52* Mre11-AID mutants efficiently degrade Mre11 following the IAA addition using western blotting (Figure 28C).

Given a different growth capacity of the naïve and resistant *rad52* Mre11-AID* mutants in the unperturbed conditions (Figure 28b, YPD plate), I wanted to evaluate these results using a more quantitative approach. I therefore generated CPT resistant *rad52* Mre11-AID* mutants as described above and compared their colony formation capacity with the naïve *rad52* Mre11-AID mutants in a colony formation assay (Figure 28d). I have also evaluated the growth of naïve and CPT treated Mre11-AID* mutants, and *rad52* mutants as a control. My results indicate, that the CPT resistant *rad52* mutants rely on the MRX complex for growth on CPT to a similar extent as the naïve *rad52* strains (compare naïve and CPT resistant *rad52* Mre11-AID mutants plus IAA). Together, these results indicate that the MRX complex is essential for the viability of the CPT resistant *rad52* mutants on CPT post-adaptation.

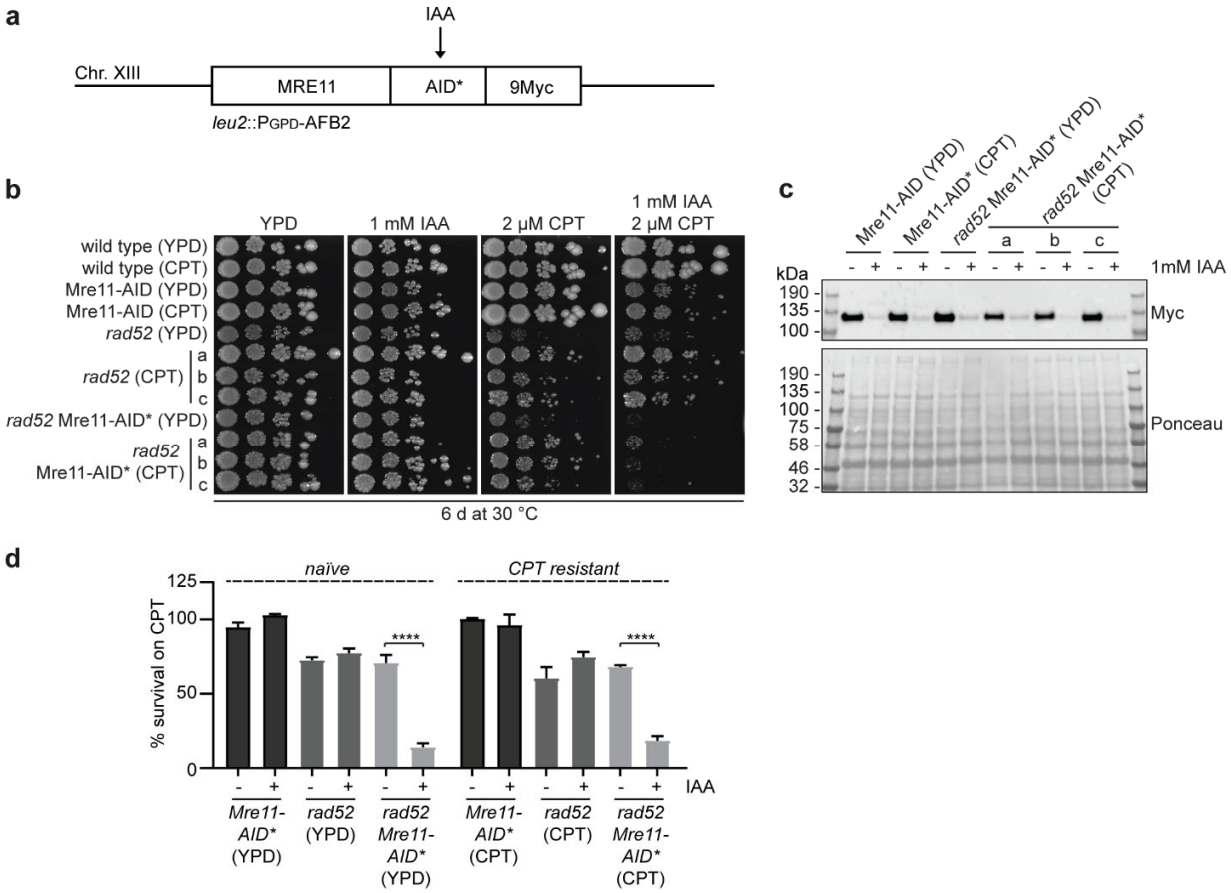

Figure 28. MRX complex supports the growth of CPT adapted *rad52* cells.
(a) Schematic of the endogenous tag of *MRE11* with an auxin-inducible degron. The AID* sequence and a 9MYC epitope tag were fused to the 3' end of the MRE11 gene. The strain expressed the Arabidopsis thaliana F-box protein (AFB2) from the GPD promoter. Treatment with IAA (auxin) induced the recognition of Mre11-AID* protein by AFB2 and its subsequent degradation via the 26S proteasome. **(b)** Strains of the indicated genotype were spotted in 1:10 serial dilutions onto YPD plates (control), plates containing 1 mM IAA, plates containing 2 µM CPT, and plates containing 2 µM CPT combined with 1 mM IAA. Images were taken following six days of incubation at 30°C. Letters indicate freshly derived independent clones. **(c)** Strains derived from either control plates (YPD) or plates containing 2 µM CPT were grown to the exponential phase and then either mock-treated or treated with 1 mM IAA for 2 h. All strains stably expressed GDP-AFB2 to facilitate auxin-mediated protein degradation. Whole protein lysates were separated by SDS-PAGE and membranes were probed with an anti-MYC tag antibody. **(d)** Quantification of cell survival in the presence of 2 µM CPT upon Mre11 depletion. Strains that harbor an auxin-inducible degron of Mre11 were plated onto control plates (YPD) or plates containing 2 µM CPT. Afterwards, strains were repeatedly plated onto either YPD plates (control), plates containing 2 µM CPT, plates containing 1 mM IAA, or plates containing 2 µM CPT and 1 mM IAA. The survival in the presence of 2 µM CPT was normalized to plates containing 1 mM IAA. Data are represented as mean values and the error bars indicate the SEM of three independent experiments, in which three biological replicates were analysed for strains derived from YPD plates, and four biological replicates for *rad52* strains derived from CPT plates. Statistical analysis was performed using two-way ANOVA with Tukey's post-hoc test (**** is $p \leq 0.0001$).

2.12.3 The nuclease, the checkpoint activation, and the NHEJ-promoting functions of the MRX complex are dispensable for the survival of *rad52* mutants on CPT

The MRX complex has multiple functions in the repair of DSBs, with the pivotal function in the initiation of DNA ends resection via the Mre11 nuclease activity, the activation of DDC signaling via the recruitment of Tel1, and the recruitment of other repair proteins that also facilitate DSB repair via both the NHEJ and HR pathways (Bonetti et al., 2018; Oh and Symington, 2018). Although the diploid *rad52* yeast lacks the HDR pathway and has the NHEJ pathway transcriptionally suppressed (Frank-Vaillant and Marcand, 2001; Valencia et al., 2001), the MRX complex still plays a crucial role in the *rad52* survival following CPT-induced DNA damage (Figure 27b). I therefore created a series of experiments in order to determine which exact function of the MRX complex is important for CPT resistance in *rad52* mutants.

Either the adaptation defect in *rad52 mre11* mutants, or its checkpoint deficiency can potentially lead to a drastic reduction of the viability following CPT treatment. Upon DSB induction, the MRX complex is responsible for the recruitment and activation of the checkpoint kinase Tel1 (Cassani et al., 2019). The hyperactivation of Tel1 is sufficient to trigger the CA defect in response to DNA damage (Baldo et al., 2008). I therefore wondered whether the sensitivity of *rad52 mre11* double mutants towards CPT arises from the lack of Tel1 activation. In order to address this question, I have created the *tel1 rad52* double mutant, and spotted the mutant in 1:10 serial dilutions onto the plates containing 2 µM CPT (Figure 29a). The sensitivity of *rad52 mre11* double mutants to CPT exceeds the sensitivity of *rad52 tel1* double mutants. This result indicates that the deletion of *MRE11* does not sensitize *rad52* mutants to CPT due to the defective Tel1 activation.

On one hand, the MRX complex is also involved in the Mec1-mediated DDC activation via the generation of ssDNA upon DSB induction (Clerici et al., 2014; Gobbini et al., 2016). Therefore, the inactivation of the MRX complex could potentially impair the other checkpoint signaling branch. On the other hand, although the involvement of the MRX complex in the CA process was ruled out for the HO endonuclease-induced DSB (Lee et al., 1998), the role of MRX in the adaptation to CPT-induced DNA damage has not yet been assessed. Therefore, the MRX inactivation could potentially render cells CA-defective in response to CPT-induced DNA damage. To rule out that the checkpoint function of the MRX complex is responsible for the sensitization of the *rad52* mutants to CPT, I decided to employ the checkpoint-defective allele (*rad53-11*) of a key downstream checkpoint kinase, Rad53 (Weinert et al., 1994). This allele has a point G653E mutation in its forkhead associated (FHA) domain, which fully abolishes the protein function in the DDC. If the deletion of *MRE11* sensitizes *rad52* cells to CPT because of the checkpoint deficiency, the loss of DDC in *rad52 rad53-11* mutants should phenocopy the *rad52 mre11* growth defect on

CPT containing plates. Alternatively, if the deletion of *MRE11* sensitized *rad52* cells to CPT due to the adaptation defects similar to the *cdc5-ad* allele or the *SAE2* deletion (Figure 12c and 12g), the alleviation of the DDC in *rad52 mre11 rad53-11* triple mutants should restore the viability of the mutant on CPT-containing plates. I created *rad52 mre11 rad53-11* mutants, and spotted them in serial 1:10 dilutions either onto YPD plates, or plates containing 2 μM CPT (Figure 29b). The alleviation of DDC in *rad52 rad53-11* mutants did not result in the sensitization of the mutant to CPT, indicating that the potential checkpoint deficiency does not render the mutant extremely CPT-sensitive. Additionally, the ablation of the checkpoint in *rad52 mre11 rad53-11* mutants did not rescue the growth of the mutant on CPT-containing plates, indicating that *MRE11* is not involved in the CA to CPT-induced DNA damage. These results indicate that the checkpoint-mediating function of the MRX complex is dispensable for the survival of *rad52* mutants upon CPT treatment.

The nuclease function of Mre11 is important for the generation of ssDNA and the subsequent repair of the DSB via the HDR pathway. In human cells, the nuclease activity of the MRX complex is also important for the MMEJ repair of the DSBs (for the detailed overview, see section 1.5.4.3) (Lee-Theilen et al., 2011; Truong et al., 2013). I therefore set out to test whether the nuclease function of Mre11 is required for the survival of *rad52* mutants on CPT plates using a separation of function mutants. The *mre11-D56N* and *mre1111-H125N* alleles of *MRE11* carry a mutation in their Phosphodiesterase motifs II and III, respectively (Krogh et al., 2005), and are nuclease-deficient. I have reconstituted the *rad52 mre11* double mutants either with wild-type *MRE11*, or with the *mre11-D56N* and *mre11-H125N* alleles encoded on plasmid and assessed their ability to form colonies on CPT-containing plates (Figure 29c). Of note, I used a lower CPT concentration (0.5 μM), because the drug had a stronger effect on SD-Leu plates compared to the YPD plates. The *MRE11*, *mre11-D56N*, and *mre11-H125N* alleles have rescued the sensitivity of *mre11* cells to CPT, indicating that the plasmid-encoded alleles are expressed and that they encode for a functional mutant protein. I observed that the nuclease dead *mre11-D56N*, and *mre11-H125N* alleles were able to sustain the growth of *rad52* mutants on CPT, suggesting that the resection function of Mre11 is dispensable for the MRX-mediated survival of *rad52* mutants on CPT-containing plates.

The Xrs2 protein plays a critical role in promoting the NHEJ repair pathway by interacting with Lif1p (Matsuzaki et al., 2008). Two point mutations in the FHA domain of the *XRS2* gene, *xrs2-S47A, H50A*, leads to a strong defect in NHEJ repair pathway (Matsuzaki et al., 2008). I wanted to assess whether the end joining function of Xrs2 function within the MRX complex is important for the survival of *rad52* mutants on CPT plates. I therefore have reconstituted *rad52 xrs2* mutants

with the plasmid-borne *XRS2*, or *xrs2-S47A, H50A* alleles, and assessed whether the mutants can re-grow on CPT-containing plates (Figure 29d).

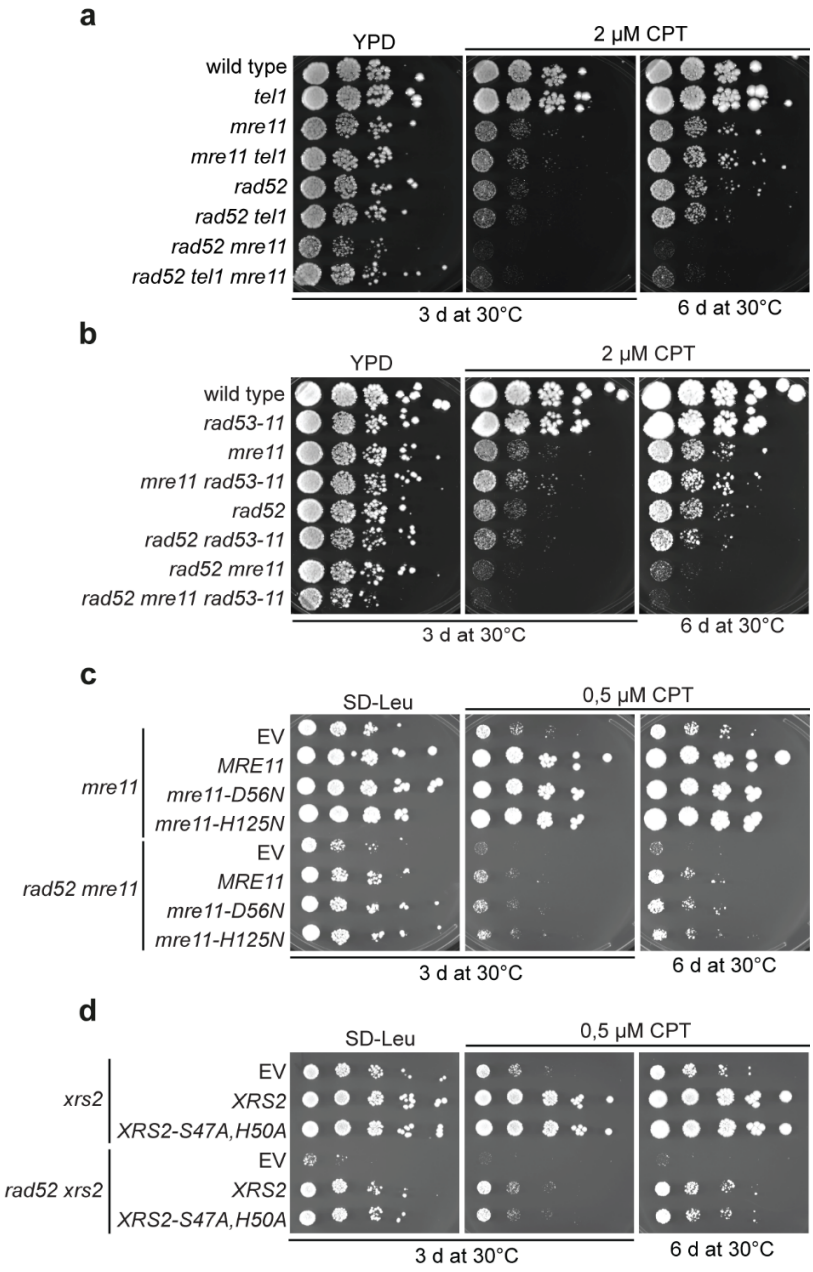

Figure 29. Understanding a specific MRX function that supports *rad52* mutant survival on CPT. (a, b) Strains of indicated genotypes were spotted in 1:10 serial dilutions onto YPD plates or plates containing 2 µM CPT and grown at 30°C for three to six days. **(c, d)** Strains of indicated genotypes were transformed either with an empty vector (EV), or with indicated plasmid-encoded alleles, and then spotted in 1:10 serial dilutions onto either selective SD-Leu media, or plates containing 0.5 µM CPT, and grown at 30°C for three to six days.

I observed that both the wild-type *XRS2* and the mutant *xrs2-S47A, H50A* allele have rescued the sensitivity of the *xrs2* mutant to CPT, indicating that the plasmid-borne constructs are expressed and functional. The *xrs2-S47A, H50A* allele rescued the growth of *rad52 xrs2* double mutant similarly to wild type *XRS2*, indicating that the NHEJ function of *XRS2* is dispensable for the re-growth of *rad52* cells on CPT plates. Of note, *rad52 xrs2* double mutants displayed a strong growth defect that exceeded that of *rad52 mre11* mutants, potentially due to an elevated rates of plasmid loss.

Together, the checkpoint activation, the nuclease activity, and the NHEJ-promoting functions of MRX complex are dispensable for the formation of the CPT resistance in *rad52* mutants.

2.13 The role of MMEJ factors Pol4 and Rad1 in the survival of *rad52* mutants upon DNA damage

Besides the MRX complex, the MMEJ pathway requires other factors that include DNA polymerase δ subunit Pol32, the Polymerase λ (Pol4), as well as the DNA endonuclease Rad1 (Ma et al., 2003; Meyer et al., 2015). The deletion of the polymerase δ subunit *POL32* almost fully abolishes MMEJ repair events in the cells (Meyer et al., 2015). Unfortunately, the deletion of *RAD52* is synthetically lethal with deletion of *POL32*, which has prevented me from performing the experiment in which the survival of *rad52 pol32* double mutants is assessed in response to CPT treatment. I therefore looked at the other factors that contribute to the MMEJ repair pathway. The yeast Rad1 and Rad10 proteins form a stable complex that has an endonuclease function on flap substrates (Tomkinson et al., 1994). The Rad1-Rad10 complex was demonstrated to participate in the MMEJ pathway. The deletion of *RAD1* decreases the MMEJ efficiency on different reporter systems used in the studies, yet does not fully abolish the pathway (Ma et al., 2003; Meyer et al., 2015). I wanted to understand whether the deletion of MMEJ pathway players will sensitize the repair-defective *rad52* cells to CPT and X-rays. In order to address this question, I have created the *rad52 rad1* double mutants, and subjected the mutant to treatment with 2 μM CPT (Figure 30a) or 45 Gy of X-rays (Figure 30b). I have deleted *DNL4* ligase that is essential for the NHEJ pathway, in order to ensure that the restoration of NHEJ will not be responsible for the formation of genotoxin resistant *rad52* colonies. I have observed a small, but not significant, decrease in the survival of *rad52 rad1* double mutants in a *dnl4* background on 2 μM CPT (Figure 30a, compare the last two bars) and in response to 45 Gy of X-rays (Figure 30b, compare the last two bars). These results indicate that the endonuclease Rad1 is not essential for the survival of *rad52* mutants following genotoxic treatment.

I next set out to investigate whether the MMEJ-involved yeast Polymerase λ (Pol4) (Meyer et al., 2015) contributes to the survival of *rad52* mutants following genotoxin treatment. I therefore created *rad52 pol4* double mutants in a *dnl4* background, and assessed the viability of the mutants following the treatment with 2 µM CPT (Figure 30c) or 45 Gy of X-rays (Figure 30d). I did not observe any effect on the survival of *rad52* mutants when *POL4* gene was deleted, indicating that the MMEJ-involved polymerase Pol4 is dispensable for the survival of *rad52* mutants on 2 µM CPT or following the treatment 45 Gy of X-rays. Together, these results indicate that the deletions of MMEJ pathway components *RAD1* and *POL4* do not significantly sensitize *rad52* mutants to genotoxin treatment.

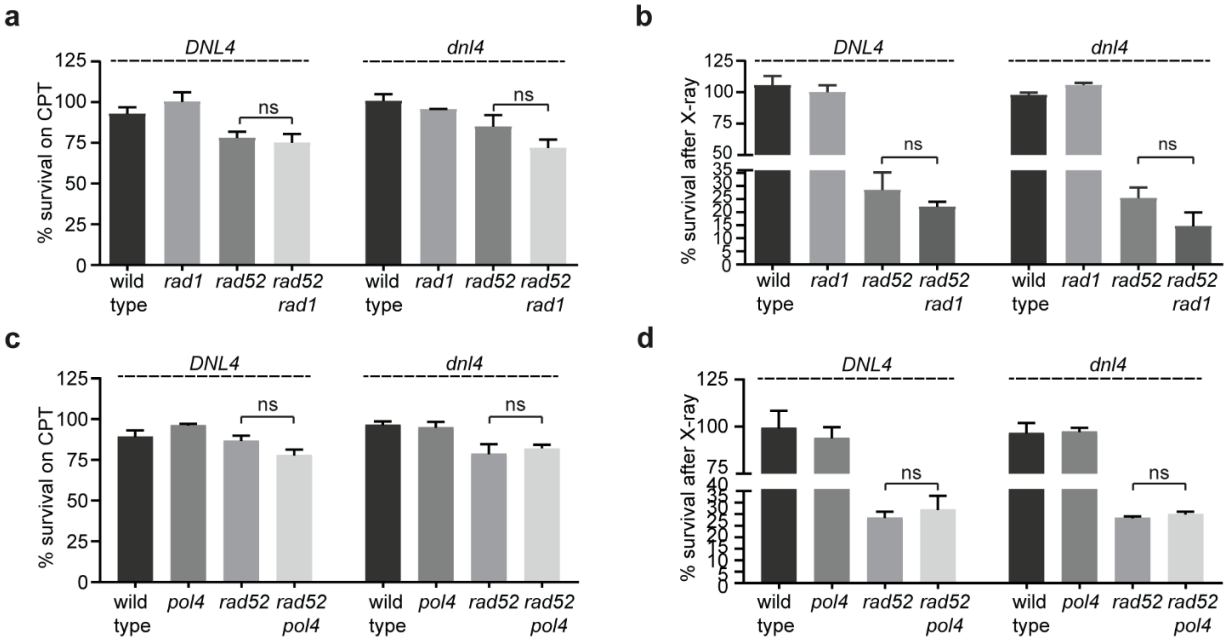

Figure 30. Contribution of the MMEJ factors Rad1 and Pol4 to the survival of *rad52* mutants following X-ray or CPT treatment. (a-d) Quantification of cell survival in the presence of 2 µM CPT or after exposure to 45 Gy of X-rays after normalization to control YPD plates. All data are represented as mean values and the error bars indicate the SEM of three independent experiments. For statistical analysis, ANOVA test with Tukey's post-hoc test was applied. (****p≤0.0001). ns, not significant.

2.14 CPT resistant *rad52* mutants do not display elevated levels of interchromosomal MMEJ events

My genetic data indicate that the depletion of Mre11, which plays a key role in the MMEJ pathway, sensitizes the repair-defective *rad52* mutants to CPT (Figure 27a-c), which potentially implies that the *rad52* mutants rely on the MMEJ pathway to survive genotoxin treatment. Yet, the knock-out of the other MMEJ players *POL4* and *RAD1* did not result in the sensitization of *rad52* to the genotoxins (Figure 30a-d). I therefore performed an experiment using a published

interchromosomal MMEJ reporter (Meyer et al., 2015) in order to determine whether the CPT resistant *rad52* mutants utilize the MMEJ pathway and whether the pathway is upregulated in those mutants.

I have utilized the homozygous diploid *rad52* mutant in a W303 background that contains the integrated MMEJ reporter (Meyer et al., 2015). The interchromosomal MMEJ reporter consists of the split on two different chromosomes *HIS3* gene, the split parts of which share 20 bp microhomology between each other (Figure 31a). The DSBs are induced with the HO endonuclease that recognizes 117 bp of the sequence proximal to the reporter. The repair event that utilizes microhomologies in the split reporter will lead to the reconstitution of the HIS3 gene, which allows for the selection of positive recombinants based on an auxotrophic marker.

I have plated *rad52* mutants with the MMEJ reporter onto plates containing 0.8 μM CPT, and following the formation of resistant colonies, I have selected the ones that contained the intact MMEJ reporter sequences (see materials and methods, section 4.2.3 for the detailed procedure) (Figure 31b). I have used a lower CPT dosage because of the different sensitivity of yeast in a W303 background to CPT compared to the standard S288C background. Using flow cytometry, I have ensured that the *rad52* colonies underwent dramatic chromosome loss events following CPT treatment (Figure 31c). The vast majority of strains that I recovered from the CPT-containing plates were close to reaching the nearly-haploid state. However, some mutants still displayed an intermediate ploidy state, presumably due to the lower CPT dosage I used for their generation. I proceeded to perform interchromosomal MMEJ reporter assays with the selected nearly-haploid CPT resistant mutants, according to the published procedure (Meyer et al., 2015), with minor modifications (Figure 31d). I have calculated the MMEJ rates by dividing the numbers of *HIS3*+ recombinants by the total number of viable colonies. My data show that the CPT resistant *rad52* mutants indeed use the MMEJ pathway to repair the DSBs. However, I only observed the upregulation of the MMEJ events in a few individual CPT resistant clones, while the median efficiency of repair did not differ from the naïve parental strain.

Together, the vast majority of the CPT resistant *rad52* mutants do not display elevated interchromosomal MMEJ levels. This result indicates that the CPT resistant phenotype in adapted *rad52* mutants is unlikely to be explained with the upregulation of the MMEJ pathway.

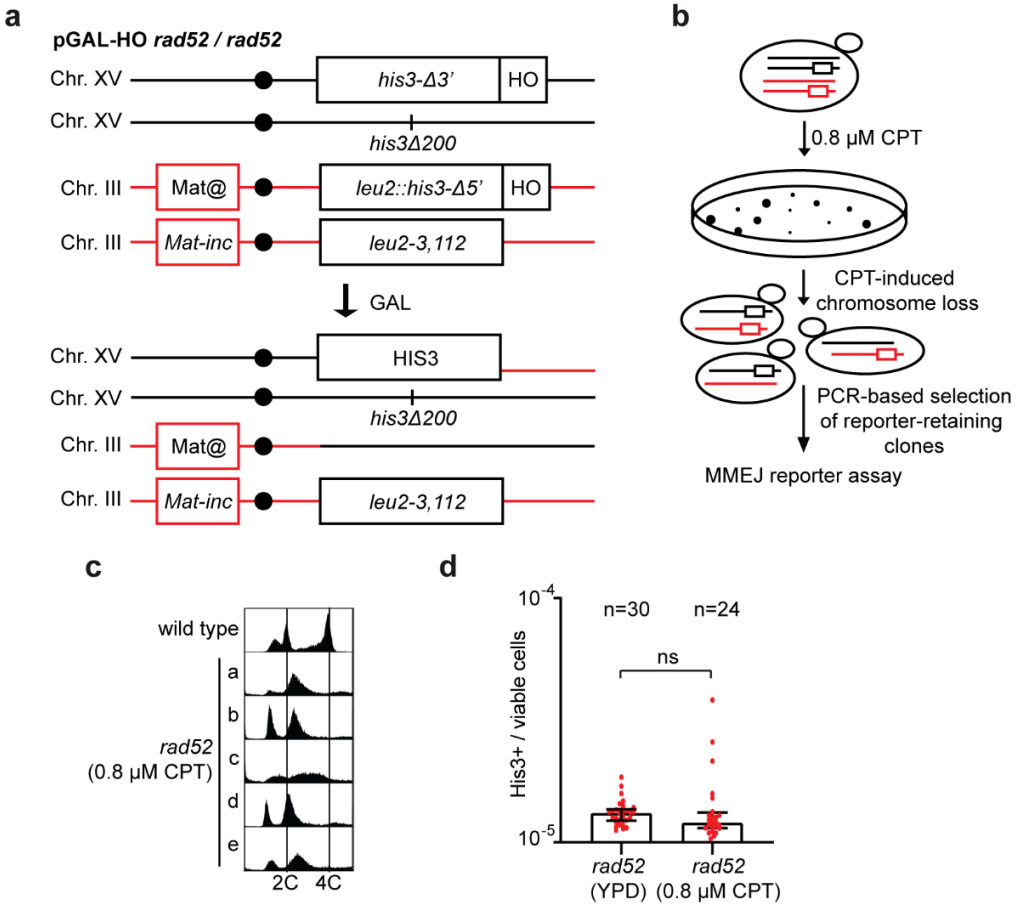

Figure 31. Evaluation of the frequency of interchromosomal MMEJ events in naïve and CPT resistant *rad52* mutants. (a) Schematic of the interchromosomal MMEJ reporter. The diploid yeast strain with a homozygous *rad52* / *rad52* mutation has the galactose-inducible HO endonuclease integrated at the *TRP1* locus. The MMEJ reporter is composed of the *HIS3* gene split between chromosome XV and chromosome III. The split sequences of the *HIS3* gene share 20 bp microhomology and are fused to the 117 bp of the HO cut site. The homologous chromosome XV contains the *his3Δ200* allele, which is a complete deletion of the *HIS3* gene. Upon galactose induction, two simultaneous DSBs are introduced at the HO cut sites that are adjacent to the reporter sequences. The recombination between the MMEJ reporter substrates generates a translocation between chromosome XV and chromosome III, and restores the *HIS3* gene. Of note, the strain contains an HO-incleavable sequence at the mating loci, preventing the generation of two irreparable DSBs. **(b)** Schematic of the generation of the CPT resistant *rad52* mutants that harbor the interchromosomal MMEJ reporter. Due to the extensive chromosome loss events following CPT treatment of *rad52* mutants (Figure 14a), I expect that the MMEJ reporter strain will lose the random copy of chromosome XV and potentially also chromosome III that contain the MMEJ reporter, as well as a random copy of chromosome VII that contains the pGAL-HO gene (all the chromosomes are heterozygous for the reporter sequences). Therefore, after the *rad52* / *rad52* strain was plated on CPT containing plates, the CPT resistant mutants were streaked for single colonies on YPD plates. These single colonies were genotyped by PCR, in order to ensure that the clone carries the MMEJ reporter sequences. **(c)** DNA content of the CPT resistant *rad52* mutants that carry MMEJ reporter sequences was assessed using flow cytometry. **(d)** Quantification of interchromosomal MMEJ frequency by normalization of cell survival on SD-His to control YPD plates. Strains derived from either control plates (YPD) or plates containing 0.8

μM CPT were grown overnight in YP-Raff. The HO expression was induced by a switch to galactose-containing medium for four h and then cells were plated onto SD-His or YPD plates. Data are represented as median values and the error bars indicate interquartile range. Statistical analysis was performed using Student's t-test. ns, not significant.

3 Discussion

3.1 Checkpoint adaptation precedes the formation of genotoxin resistant *rad52* mutants

3.1.1 Why do cells undergo checkpoint adaptation?

Adaptation to the DDC is accompanied with genomic instability and the loss of viability, as was shown in cells that harbor unprotected or eroded telomeres (Coutelier et al., 2018; Klermund et al., 2014). Preventing CA either genetically, or by inhibition of TORC1 with rapamycin, improved the viability following the prolonged checkpoint arrest (Klermund et al., 2014). I have also observed that repair-defective *rad52* mutants adapt to the DDC when treated with genotoxins (Figure 12). Why would cells undergo adaptation? One possibility is that if the DSB cannot be repaired in the G2/M phase of cell cycle by the HR pathway, it can be repaired in the subsequent cell cycle phase by an alternative available pathway. Another possibility is that following adaptation, the damaged chromosome will be lost, and the diploid or polyploid cell will resume proliferation with the other chromosome copy available. In other words, CA allows to escape the permanent cell cycle arrest in expense of huge genomic instability and high cell death rates that come after the adaptation. Adaptation can also create a substrate for the evolutionary selection: high genomic instability potentially creates new karyotypes that might be better adapted to their new environment. Adaptation to checkpoints is not restricted to the DDC, as cells adapt to the so-called decatenation checkpoint, to the spindle assembly checkpoint, to the G1 checkpoint arrest during hyperosmotic stress etc. (Arroyo et al., 2020; Migdal et al., 2008; Vernieri et al., 2013). This potentially suggests that adaptation, and adaptation to the DDC in particular, is an intrinsic property of organisms that allowed cells to survive and potentially evolve in challenging environmental conditions. In multicellular eukaryotes, there are additional systems to ensure that cells with DNA damage and genomic instability do not propagate: the apoptosis signaling cascade, the p53-mediated G1 checkpoint, the immune system that recognizes stressed cells, and many more. Yet, given that CA was described in human cells, it is tempting to speculate that adaptation contributes to cancer development and progression. The latter, however, remains to be experimentally demonstrated.

3.1.2 Adaptation allows the re-growth of *rad52* cells following genotoxic treatment

Repair-defective *rad52* mutants can re-grow following genotoxic treatment with X-rays or CPT, although the re-growth required an extended period of time (Figure 12a). Because these cells lack both the HR and NHEJ pathways to effectively repair DSBs, I wondered whether CA is required for colony formation. Using a genetic approach, I found that prevention of adaptation with the *cdc5-ad* allele, *ckb2* deletion, or *SAE2* deletion significantly reduced colony formation following

genotoxin exposure (Figure 12b-f). Importantly, preventing adaptation in repair-proficient cells did not affect their viability, because these cells repaired their DNA before the adaptation occurred. The aforementioned alleles affect adaptation in three different ways: while the *cdc5-ad* allele presumably alters the substrate specificity of the major adaptation driver Cdc5, the *CKB2* deletion prevents Rad53 dephosphorylation by Ptc2, and the *SAE2* deletion prevents adaptation majorly due to the increased MRX-mediated hyperactivation of the Tel1 checkpoint kinase (Clerici et al., 2006; Guillemain et al., 2007; Rawal et al., 2016). These mutations prevented CA in other systems: the adaptation defect of *cdc5-ad* allele was shown in cells that suffer irreparable DSB at the mating locus, and in *cdc13-1* mutants that suffer DNA damage induced by deprotected telomeres (Klermund et al., 2014; Toczyski et al., 1997). The *CKB2* and *SAE2* deletions prevent adaptation in response to irreparable DSB at the mating locus (Clerici et al., 2006; Guillemain et al., 2007). This genetic approach confirmed that adaptation precedes colony formation in *rad52* mutants that were exposed to genotoxins. While the adaptation in *rad52* mutants in response to X-rays was demonstrated before (Galgoczy and Toczyski, 2001), this work shows that the adaptation precedes the colony formation for a different type of genotoxin, CPT.

While I measured only 20% survival after X-ray, 80% CPT-treated cells remained viable (Figure 12). It is unlikely that the CPT dosages that were used invoked less DNA damage compared to the X-rays treatment, because the colonies were formed only after eight days of CPT exposure. These results might be explained by the observation that CPT is a “checkpoint blind” genotoxin that does not induce intra-S phase DDC (Redon et al., 2003). Because I used a very low CPT dosage (2 µM), the damage load might have not been sufficient to induce arrest during the first cell division, therefore the adaptation occurred once the micro colony was already formed (*rad52* cells arrested at four-cell micro colony stage on CPT-containing plates – PhD thesis of Dr. Katharina Bender). Initial checkpoint arrest at the micro colony stage increases a statistical probability of adaptation and cell survival within the micro colony (compared to a checkpoint arrested single cell). The *cdc5-ad* allele sensitized *rad52* mutants more strongly compared to the *ckb2* deletion (Figure 12b-e). This was observed before by Toczyski and colleagues (Toczyski et al., 1997) and is explained by the different penetrance of the alleles.

Although I used a repair-defective yeast model to induce adaptation, the process is conserved in higher eukaryotes. CA in response to genotoxins was described in human osteosarcoma cancer cell line following the treatment with X-rays (Syljuåsen et al., 2006). Human HT-29 adenocarcinoma cells demonstrated an entry into mitosis with DNA damage following cisplatin treatment (Swift and Golsteyn, 2016). It is tempting to speculate that the repair-defective BRCA2-deficient cells can enter mitosis with unrepaired DNA damage. While the majority of yeast cells experience the loss of viability following adaptation, the fraction of cells remain viable. Mammalian

cells also experience the loss of viability following adaptation (Swift and Golsteyn, 2016). To my knowledge, it was not addressed experimentally whether a fraction of adapted cells could still remain viable in human cells. Treatment with DDC inhibitors induced a forced entry into mitosis with DNA damage, which sensitized BRCA2-deficient cells to PARPi olaparib (Schoonen et al., 2019). Nevertheless, the repair-defective BRCA2-deficient mutants undergo the selection of genotoxin- and PARPi- resistant clones, suggesting that a fraction of cells might remain viable following the genotoxin treatment. Whether the repair-defective cells undergo adaptation in response to endogenously-induced DNA damage was not addressed yet neither in yeast nor mammals.

3.2 Genotoxin resistant *rad52* mutants undergo aneuploidization

Galgoczy and colleagues have demonstrated that diploid *rad52* mutants experience genomic instability following adaptation to X-rays, indicating that adaptation leads to genome instability (Galgoczy and Toczyski, 2001). Using identical system, we observed that the repair-defective *rad52* mutants treated with X-rays acquire evident resistance to X-rays and radiomimetic drug bleomycin, which is accompanied by drastic chromosome loss events (Figures 2b and 3a). The CPT-treated *rad52* mutants have acquired resistance not only to CPT, but also to X-rays and UV light, which was accompanied by the loss of nearly half of genomic content in these cells (Figures 13c and 14a). Although correlative, these results strongly imply that the aneuploid karyotype may facilitate the acquisition of genotoxin resistance. These findings resemble clinical observations that tumor cells treated with X-rays or the Top1 inhibitor irinotecan eventually acquire resistance ((Zhang et al., 2018), reviewed in (Kim et al., 2015)). It is likely that following DNA damage, adaptation is an upstream event that precedes aneuploidization in budding yeast. Adaptation can promote aneuploidization in different ways (Figure 32). First, the unrepaired DSB could lead to a loss of a chromosome arm, because during the cell division the spindle is attached to the centromere. Alternatively, following adaptation, the G1-operating NHEJ pathway could incorrectly re-join different damaged chromosomes. Adaptation was shown to induce highly mutagenic DNA repair via BIR, which potentially leads to large deletions or duplications, resulting in segmental aneuploidy (Galgoczy and Toczyski, 2001). Finally, in the absence of DNA repair, the damaged chromosome could be lost due to continuous DSB resection (Sandell and Zakian, 1993). Curiously, when the initial checkpoint arrest is overridden by adaptation, cells do not display checkpoint arrest during the second cell division cycle, despite the DSB persistence. The damaged chromosome is therefore lost following approximately 10 cell divisions (Sandell and Zakian, 1993). In line with this observation, X-ray resistant *rad52* mutants displayed continuous loss of genetic material, which plateaued on nearly haploid DNA content (Figure 18). While

adaptation allows survival in response to irreparable DNA damage, it is unlikely that adaptation triggers genotoxin resistance directly. Rather, the adaptation-preceded genome instability allows the selection of aneuploid karyotypes that facilitate genotoxin resistance.

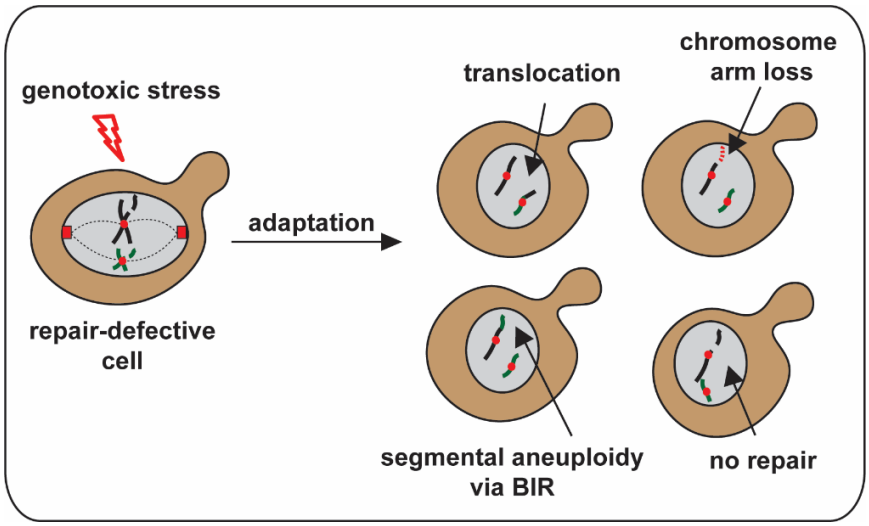

Figure 32. Potential mechanisms how CA promotes aneuploidization. Adaptation can promote aneuploidization due to the generation of chromosomal translocations by NHEJ pathway in subsequent G1 phase. Additionally, the damaged chromosome arm might be lost in mitosis due to the lack of the kinetochore attachment. Adaptation promotes faulty DNA repair by BIR, which could result in deletions or segmental aneuploidy. Finally, in the absence of any repair events, the damaged chromosome might persist until it is degraded by nucleases. Red box indicates kinetochore.

3.2.1 Repair-defective *rad52* mutants acquire different aneuploid karyotypes in response to different genotoxins

The DNA sequencing results demonstrated that the *rad52* mutants indeed undergo multiple chromosome losses following the X-rays treatment, while following CPT exposure they acquire nearly haploid karyotype that retains an extra copy of chromosome III (Figure 14d). These results clearly demonstrate that the two genotoxins induce different patterns of aneuploidization. The underlying reason is the difference in exposure time to a genotoxin: while the X-rays treatment is acute, the CPT treatment lasts for seven to eight days. In line with this argument, an acute treatment with high CPT dosage induces chromosome loss that yields a mixture of different ploidies (Figure 15). While the X-rays-treated cells that displayed mixed ploidies were only resistant to a similar by nature treatments, the nearly haploid CPT-treated clones displayed the resistance to a broader spectrum of unrelated genotoxins (Figure 13). These results raise the

possibility that a specific karyotype facilitates the resistance to a specific genotoxin. How would these specific karyotypes evoke the resistance?

The X-ray treated *rad52* mutants undergo chromosome loss events that result in a broad spectrum of aneuploids. While nearly haploid or nearly diploid clones are more resistant to genotoxic treatment, the clones of intermediate ploidy actually display severe growth disadvantages (Figure 13b, and personal communication with Dr. Katharina Bender). The diverse karyotypes originated from the initial X-rays treatment create a substrate for the selection of potentially genotoxin resistant clones. The karyotype imbalances, however, translate into physiological disadvantages, which likely cause the growth defect in *rad52* mutants and mask the resistance. In human cancers, high karyotype heterogeneity within a tumor strongly associates with tumor growth and drug resistance ((Andor et al., 2016), reviewed in (Sansregret and Swanton, 2017)). Yet, the degree of aneuploidy is not linearly correlated with the drug resistance, as highly complex karyotypes seem to be more vulnerable to chemotherapeutics (Andor et al., 2016; Ben-David and Amon, 2020; Jamal-Hanjani et al., 2015).

The CPT treated *rad52* mutants display a nearly haploid karyotype that have an additional copy of chromosome III (Figure 14d). This rises two possibilities as how the resistance is achieved: first, the presence of an extra copy of chromosome III confers resistance to CPT; second, the nearly haploid state itself confers the resistance. The naïve *rad52* chromosome III disomes were intrinsically resistant to CPT, but so were the haploid *rad52* strains (Figure 16a). The budding yeast chromosome III harbors the *MAT* locus, which influences the DNA repair by suppressing the HR defect in deletions of *RAD55* or *RAD57*, an ATPase-defective Rad51 mutation, and a C-terminal truncation of Rad52, but not in complete *RAD52* deletion (Valencia-Burton et al., 2006). On the other hand, the mating locus heterozygosity suppresses NHEJ pathway, which does not provide any apparent DNA repair benefit in *rad52* mutants (Frank-Vaillant and Marcand, 2001). I did not observe the difference in CPT resistance in *rad52* chromosome III disomes with different *MAT* cassettes present (Figure 16a), which suggests that in this case the *MAT* locus is unlikely to confer the CPT resistance in haploid *rad52* mutants. Because the naïve haploid *rad52* mutants displayed similar to CPT adapted *rad52* mutants on CPT, the nearly haploid state of genome likely confers the CPT resistance. The ploidy changes that allow adaptation are not uncommon in yeast. Tetraploidization was shown to allow adaptation to poor carbon sources (Selmecki et al., 2015). Ploidy changes were shown to drive resistance in human pathogens, *Cryptococcus meningitis* and *Candida albicans* (Stone et al., 2019; Yang et al., 2019). How exactly the haploid state confers CPT resistance remains unclear.

In *rad52* mutants, an extra copy of chromosome III does not contribute to the genotoxin resistance *per se*, yet it was preferentially retained in both CPT-resistant and X-ray resistant mutants (Figure

14d). There are two possible explanations for this phenomenon, which are non-exclusive. First, as chromosome III contains the *MAT* locus, retaining an extra copy of the chromosome would prevent potentially deleterious mating events during the chromosome loss on CPT-containing plates. This explanation is supported by the observation that the chromosome III is lost during the progressive passaging in unchallenged conditions (Figure 17). Second, an acquisition of an extra chromosome III allows tolerance to the elevated temperatures, a known proteotoxic stress-causing conditions (Yona et al., 2012). Aneuploidy is a known cause of proteotoxic stress (Oromendia et al., 2012). Therefore, following the chromosome loss events *rad52* mutants, an extra copy of chromosome III would allow to compensate the proteotoxic stress associated with the aneuploid state.

Importantly, aneuploidization in response to a certain type of stress still imposes cellular fitness costs; therefore, it represents only a transient state, which is further balanced by point mutations (Yona et al., 2012). The progressive passaging of both X-rays- and CPT-treated aneuploid *rad52* mutants demonstrated gradual chromosome loss that resulted in haploidization (Figure 18). These results suggest that due to the high physiological cost of aneuploidy, cells proceed with chromosome loss until they acquire the next stable karyotype.

3.2.2 How does aneuploidization enable genotoxin resistance?

Aneuploidization seems to be a rather common mechanism in response to a plethora of stresses, implying that aneuploidy allows growth advantage in response to particular adverse conditions (Chen et al., 2015; Gilchrist and Stelkens, 2019). In simple eukaryote *S. cerevisiae*, acquisition of an extra copy of chromosome V is required for growth in high pH conditions (Yona et al., 2012). Aneuploidization also happens in response to an impairment in cellular pathways. For example, continued inhibition of the Hsp90 chaperone leads to an emergence of resistant aneuploids with a gain of chromosome XV (Chen et al., 2012a). Upon knock-out of the only myosin II-encoding gene, *MYO1*, yeast cells undergo rapid adaptation via polyploidization and complex aneuploidization (Rancati et al., 2008). Aneuploidization as an adaptive means was also reported upon the induction of endoplasmic reticulum stress, telomerase insufficiency, high ethanol conditions, and many others (Beaupere et al., 2018; Millet and Makovets, 2016; Voordeckers et al., 2015). Similar observations were also made for different wild yeast isolates and a pathogenic fungus *C. albicans* (Hose et al., 2020; Yang et al., 2019). These examples strongly suggest that aneuploidy is an adaptive means that allows cells to tolerate otherwise lethal conditions (reviewed in (Tsai and Nelliat, 2019)). It is therefore conceivable that aneuploidization following CA is not only a consequence of DNA repair deficiency in *rad52* mutants. Rather, although genotoxic

treatment induces chromosome loss events, the consequential karyotype heterogeneity allows the selection of genotoxin-re-resistant clones.

Aneuploidization allows the change in expression of some condition-relevant genes that are amplified via chromosome gains. Alternatively, chromosome loss events could also confer chemoresistance by the exposure of recessive mutations. In budding yeast, in response to endoplasmic reticulum stress, cells acquire an extra chromosome II, which confers resistance by the increased expression of *ALG7* and *PRE7* genes (Beaupere et al., 2018). Aneuploidization could also confer resistance by re-wiring the whole cellular proteome and transcriptome, independently of the few dosage-sensitive genes that are present in altered copy (Dürrbaum and Storchová, 2016). Finally, because aneuploidization induces genome instability, it can facilitate the selection of multiple parallel resistance mechanisms through clonal evolution (Chen et al., 2015). I think that some of those mechanisms could facilitate genotoxin resistance in *rad52* mutants. For example, re-wiring the regulation of cellular proteome might allow to unleash the activity of faulty DNA repair pathways, conferring chemoresistance. Aneuploidization could also upregulate the expression of genes required for the removal of CPT-induced Top1-cc from the DNA. I did not test these assumptions experimentally.

Aneuploidization as an adaptation to the change in environment was also reported in mammalian systems. For example, trisomy on chromosome 8 or trisomy on chromosome 11 occur sporadically but frequently, and they confer strong growth advantages in mouse embryonic stem cells grown in standard cell culture conditions (Ben-David and Benvenisty, 2012). Experiments with the diploid colorectal cancer cell line, DLD, which carried either an additional chromosome 7 or chromosome 13, demonstrated that aneuploidization provided a selective advantage upon serum deprivation or upon treatment with the chemotherapeutic drug, 5-fluorouracil (Rutledge et al., 2016). Even more strikingly, patient-derived cell lines, xenografts, and organoids rapidly undergo whole chromosome gains and losses in order to adapt their karyotype to the new environment. The resulting karyotypes differed from the ones that occurred naturally during the tumor's development in patients ((Ben-David et al., 2017, 2018; Bolhaqueiro et al., 2019), reviewed in (Ben-David and Amon, 2020)). Whole chromosome gains and losses in response to altered gene expression also occur in mammalian cells. In a mouse model of breast cancer, overexpression of the *MYC* oncogene is accompanied by the gain of an extra chromosome 15 (Ben-David et al., 2016).

In general, aneuploidy is associated with increased chromosomal instability, which creates diverse variants for karyotype evolution upon selective pressure (Sansregret and Swanton, 2017). This might be one of the underlying reasons why highly aneuploid tumors with high genomic instability display multidrug resistance and lesser sensitivity to genotoxic agents (Islam et al., 2018; Lee et al., 2011; Li et al., 2018). Importantly, high karyotype heterogeneity within a tumor is strongly

associated with tumor growth and drug resistance ((Andor et al., 2016), reviewed in (Sansregret and Swanton, 2017)). Together, aneuploidy and karyotype heterogeneity are associated with the adaptation to environmental and other types of stresses.

3.3 Genotoxin resistant *rad52* mutants suffer from aneuploidy-associated proteotoxic stress

The repair-defective *rad52* mutants acquire genotoxin resistance via aneuploidization, which imposes severe cellular fitness defects on cellular physiology (summarized in section 1.6). The aneuploidy-associated phenotypes have a therapeutic potential, although until now they have been infrequently used in cancer treatment (reviewed in (Ben-David and Amon, 2020)). Because aneuploidy evokes systematic changes in cellular physiology, targeting aneuploid state has an advantage that it could be efficient in practically any aneuploid tumors. Given that up to 90% of solid tumors are aneuploid, targeting aneuploidy-associated phenotypes has a potential to have a broad application (Ben-David and Amon, 2020; Guang et al., 2019). Aneuploidy-associated phenotypes seem to be conserved from yeast to humans, which makes budding yeast a great model to study aneuploidy-associated cellular alterations (Ben-David and Amon, 2020).

To date, aneuploidy-associated phenotypes were studied in yeast strains created in a very controlled manner: either by sporulation of a triploid strain (Pavelka et al., 2010), chromosome transfer strategy (Torres et al., 2007), or by acute induction of chromosomes mis-segregation upon cell division (Beach et al., 2017). The aneuploidy-associated phenotypes were not studied in cells that have mutations in DNA repair genes. Moreover, the vast majority of studies have omitted chromosome III disomes, due to the altered mating bechaviour of these cells (Beach et al., 2017; Oromendia et al., 2012; Torres et al., 2007). Following CA, the repair-defective *rad52* mutants become aneuploid due to genotoxin treatment that evokes chromome loss, but also potentially many mutations that alter cellular physiology. Therefore, I have set out to investigate whether the adapted *rad52* cells suffer from aneuploidy-associated phenotypes (Figures 19 and 20). For this, I used a previously published system, in which following the heat induction the formation and the resolution of Hsp104-GFP disaggregase foci is monitored using fluorescence microscopy (Oromendia et al., 2012). I was able to confirm that the X-rays adapted aneuploid cells suffer from proteotoxic stress, a hallmark of aneuploidy (Brennan et al., 2019; Oromendia et al., 2012). The degree of aneuploidy-associated defects was reported to correlate with the number of extra chromosomes present (Beach et al., 2017). I was able to recapitulate this result, as the X-ray resistant *rad52* cells displaying intermediate ploidy displayed the highest degree of proteotoxic stress (Figure 19). Interestingly, I did not observe signs of proteotoxic stress in nearly-haploid CPT

resistant *rad52* mutants (Figure 9). These cells harbour only an extra copy of chromosome III, which is the second smallest yeast chromosome that only harbors 184 open reading frames. Additionally, an extra copy of chromosome III was shown to confer heat resistance in evolutional experiments, which suggests that this specific aneuploidy rather helps to tolerate proteotoxic stress than to induce it (Yona et al., 2012).

I have observed that the naïve diploid *rad52* cells already display signs of mild proteotoxic stress compared to wild type cells, which manifests in slightly impaired growth at elevated temperatures, and defective protein aggregates resolution (Figure 19). The RNA-seq experiments showed signs of environmental stress response in *rad52* diploids (PhD thesis of Dr. Katharina Bender). The frequent chromosome loss events in *rad52* mutants were appreciated long ago (Mortimer et al., 1981). These results might suggest that the relatively frequent chromosome loss events in diploid *rad52* mutants are sufficient to trigger mild proteotoxic stress. Curiously, the BRCA2-deficient non-malignant breast tissues also display elevated levels of aneuploidy (Karaayvaz-Yildirim et al., 2020). The ploidy-associated aberrations are greatly exacerbated and freequently occur in BRCA2-deficient and otherwise HR deficient tumors with genomic instability (Deans et al., 2003; Jonsdottir et al., 2012). Therefore, it seems that the repair-defective cells display mild aneuploidy-associated phenotypes even before genotoxin treatment-induced aneuploidization. One can speculate that because the mutations in DNA repair genes, such as BRCA2, induce slight degrees of aneuploidy in non-malignant tissues, the aneuploidy-targeting anti-cancer strategies should account for elevated sensitivity of non-malignant repair-defective cells.

3.3.1 Adapted cells can be targeted pharmacologically by the proteasome inhibition

The strategy of targeting aneuploid cancer cells based on the aneuploidy-associated phenotypes represents an attractive therapeutic plan, although they are infrequently implemented clinically so far (Ben-David and Amon, 2020; Guang et al., 2019). The proof-of-concept studies in budding yeast demonstrated that aneuploidy-associated cellular defects could be targeted pharmacologically. For example, due to proteotoxic stress, aneuploid budding yeast demonstrated high sensitivity to the inhibition of the proteasome with MG132, inhibition of the Hsp90 with geldanamycin, and inhibition of protein translation with cycloheximide (Torres et al., 2007). In line with these observations, I have confirmed that the *rad52* mutants adapted to X-rays are preferentially sensitive to proteasome inhibition with low dosages of MG132 (Figure 21a). I have observed that naïve diploid *rad52* mutants have elevated MG132 sensitivity compared to diploid wild-type cells, which is in line with the notion that repair-defective *rad52* mutants experience mild proteotoxic stress. Because the MG132 sensitivity of X-ray adapted *rad52* mutants highly

exceeded the one of parental diploid strain, these results suggest that proteasome inhibition can selectively target repair-defective aneuploid cells. The MG132 sensitivity of CPT adapted *rad52* mutants, which are nearly haploid, did not exceed the one of diploid *rad52* mutants (Figure 22). These results are in line with the aforementioned observation that the severity of aneuploidy-associated defects correlates with the degree of aneuploidy (Beach et al., 2017). Curiously, although literature reports high sensitivity of aneuploid yeast cells to Hsp90 inhibitors (Torres et al., 2007), I observed only modest effect of the Hsp90 inhibitor radicicol on the X-ray adapted *rad52* mutants compared to the diploid *rad52* mutants (Figure 21c). These results could partially be explained by high sensitivity of diploid *rad52* mutants to Hsp90 inhibition, especially with higher dosages of radicicol (data not shown). I think that targeting Hsp90 is an efficient strategy in other than *rad52* genetic backgroungs.

The proof-of-principle study in mammalian cell lines demonstrated that due to proteotoxic stress, mammalian cells (both primary mouse embryonic fibroblasts and human aneuploid cancer cells) are sensitive to protein folding inhibitor 17-AAG and autophagy inhibitor chloroquine (Tang et al., 2011). Given that the vast majority of human solid cancers are highly aneuploid (discussed in section 1.6.3), these studies provide a strategy to target aneuploid cells based on general flaws in their physiology. Therapies to target proteotoxic stress as an aneuploidy-associated phenotype are developed for multirole myeloma and triple negative breast cancer tumors either are used in clinics, or are at the stage of clinical trials (Guang et al., 2019). Multiple myeloma is a plasma cell type malignancy, which is frequently highly aneuploid (Manier et al., 2017). These cells have high synthesis rates of immunoglobulins, and therefore experience an accumulation of defective aberrant peptides that drive strong proteotoxic stress unless removed by a proteasome (Meister et al., 2007). Treatment of multiple myeloma now includes different FDA approved proteasome inhibitors. The novel inhibitors of proteasome, aggregasome pathway, Hsp90, autophagy, and unfolded protein response modulators are now utilized in pre-clinical studies and clinical trials (reviewed in (Guang et al., 2019)). Triple negative breast cancer is an aggressive intrinsically chemoresistant cancer that have high degree of karyotype complexity accompanied by genomic instability (Kim et al., 2018). Although studies with proteasome inhibitors demonstrated that they are less efficient in triple negative breast cancer (Weyburne et al., 2017), they seem to have a clinical potential in combination with other chemotherapeutics ((Deshmukh et al., 2017; Hernández-Vargas et al., 2007), reviewed in (Guang et al., 2019)). The novel proteasome targeting anti-cancer drugs that are being in pre-clinical development, as well as in first phases of clinical trials, include ubiquitin-conjugating enzymes, the inhibitors of the 20S proteasome catalytic core particle and the 19S proteasome regulatory particles (reviewed in (Zhang et al., 2020)). Although so far aneuploidy-associated phenotypes are targeted in very limited number of cases,

it is feasible to extend this strategy on other types of tumors. Therefore, it is crucial to understand the peculiarities of aneuploidy-induced disadvantages in different types of cells. Because the degree of aneuploidy seems to directly correlate with the degree of proteotoxic stress, targeting highly aneuploid cancers with proteasome inhibitors is a very promising strategy to overcome genotoxin resistance.

Malignant cells, besides experiencing proteotoxic stress, display strong upregulation of the heat shock response pathway (Donnelly and Storchová, 2015). Heat shock proteins in general, and Hsp90 in particular, play essential role in tumorigenesis by forming high molecular weight complexes that facilitate cell survival (Rodina et al., 2016). Hsp90 chaperone has a plethora of client proteins that are implicated in tumorigenesis, including Akt, p53, and Telomerase (reviewed in (Sidera and Patsavoudi, 2013)). The function of Hsp90 chaperone is impaired in aneuploid human cells, which renders these cells extremely sensitive to the Hsp90 inhibition (Donnelly et al., 2014). The natural Hsp90 inhibitors, geldanamycin and Radicicol, are not used in clinics due to their poor pharmacological properties. Yet, their multiple derivatives, and other chemically different Hsp90 inhibitors are actively developed (reviewed in (Sidera and Patsavoudi, 2013)). Several studies indicate high therapeutic potential of Hsp90 inhibition in aneuploid malignancies. For example, targeting HSF1, an upstream regulator of Hsp90, with triptolide, induced apoptosis in highly aneuploid chronic lymphocytic leukemia cells (Ganguly et al., 2015). Moreover, combination of radiotherapy with Hsp90 inhibition was shown to overcome resistance in pancreatic cancers, and in HCT cell line (Nagaraju et al., 2019; Spiegelberg et al., 2020). My results suggest that highly aneuploid genotoxin resistant cells, which arise when the repair-defective cells are treated with genotoxins, could be targeted with Hsp90 inhibitors. In my yeast model, the efficacy of Hsp90 inhibition correlated with the degree of aneuploidy.

3.3.2 Adapted cells could be targeted pharmacologically by the starvation-mimicking drug rapamycin

Aneuploidy imposes strong cellular fitness defects, including dysregulated energy metabolism and metabolic stress, which ultimately manifest in elevated energy consumption but low biomass accumulation (Stingele et al., 2012; Torres et al., 2007; Williams et al., 2008). In budding yeast, these changes are reflected on transcriptome level, as the transcription of genes involved in carbohydrate metabolism and cell cycle progression are downregulated (Torres et al., 2007).

Due to elevated energy demands, aneuploid yeast are preferentially sensitized to the TORC1 inhibitor rapamycin (Torres et al., 2007). The proof-of-principle study in mammalian cell lines demonstrated that aneuploids are highly sensitive to energy stress inducing agent AICAR (Tang

et al., 2011). I was able to confirm these findings using X-rays adapted *rad52* mutants (Figure 23a). High sensitivity to rapamycin could potentially arise as a result of a few possible alterations: first, the activity of multiprotein complex TORC1 could be attenuated due to the aneuploidy-associated stresses; second, the activity of TORC1 could be upregulated as a compensatory mechanisms, and even slight TORC1 inhibition would invoke strong growth defect. To discriminate between these two possibilities, I have monitored the phosphorylation of a direct TORC1 target, Sch9, in X-rays adapted *rad52* mutants (Figure 23c) (Urban et al., 2007). I have observed decreased levels of phosphorylated Sch9, which indicates that the TORC1 activity is downregulated in aneuploids. The inhibition of TORC1 leads to induction of autophagy (reviewed in (Loewith and Hall, 2011)). Consistently, I observed that X-ray adapted *rad52* mutants have increased autophagy levels (Figure 23d). The nearly haploid CPT resistant *rad52* mutants displayed moderate sensitivity to rapamycin and moderate autophagy induction, which is comparable to diploid *rad52* strain (Figure 24). These results imply that the degree of TORC1 activity is inversely proportional to the degree of aneuploidy. Activation of autophagy mediates the degradation of protein aggregates in aneuploid mammalian cells (Santaguida et al., 2015). Moreover, activation of autophagy in aneuploid cells helps to counteract high ROS levels (Ariyoshi et al., 2016). Because the TORC1 kinase regulates the autophagy induction, it is tempting to speculate that low TORC1 activity is a general feature of aneuploid cells, which underlies their high rapamycin sensitivity.

My results indicate that adapted cells could be targeted pharmacologically, with proteotoxic stress inducing proteasome inhibitor MG132, and low energy mimetic rapamycin. Importantly, high TORC1 activity is shown to promote adaptation to DDC in a telomere deprotection model, *cdc13-1*. Treatment of *cdc13-1* cells with low dosages of rapamycin prevented CA, and rescued the accompanying genomic instability (Klermund et al., 2014). The inhibition of TORC1 with rapamycin also prevented adaptation in diploid *rad52* mutants (PhD thesis of Dr. Katharina Bender). Therefore, inhibiting TORC1 with rapamycin could be viewed as double-edge sword: rapamycin prevents adaptation, and at the same time, it is toxic to highly aneuploid adapted cells.

3.3.3 Potential causes and consequences of low TORC1 activity in aneuploids

What could be a potential reason for the low TORC1 activity in aneuploid cells? Although TORC1 activity is primarily regulated by the availability of nutrients, the activity of the complex is additionally regulated by environmental and cellular stresses (reviewed in (Wullschleger et al., 2006)). The hypothetical model how aneuploidy-associated cellular stresses might induce low activity of TORC1 in yeast and mammalian cells is presented in Figure 33. Studies in human cells

demonstrated that proteotoxic stress, a hallmark of aneuploidy, directly influences the activity of mTORC1 (Su et al., 2016). Following the proteotoxic stress induction, the constitutively formed mTORC1-JNK complex undergoes dissociation. The JNK kinase phosphorylates mTOR1 at S567 and other TORC1 component, RAPTOR, at S863, which leads to attenuation of protein biosynthesis (Su et al., 2016). The influence of proteotoxic stress on the TORC1 activity was also reported in budding and fission yeast (Beuzelin et al., 2013; Suda et al., 2019). Therefore, aneuploidy-associated proteotoxic stress is a likely source of low TORC1 activity, which allows attenuating protein biosynthesis and likely preventing further accumulation of protein aggregates by aneuploid cells (Brennan et al., 2019).

An increased ROS production, another feature of aneuploid cells, also affects TORC1 activity (Dephoure et al., 2014; Li et al., 2010). In mammalian cells, high ROS production leads to activation of the ATM checkpoint kinase, which downregulates mTORC1 activity via AMPK signaling (Alexander et al., 2010). In budding yeast, $Pbp1^{Ataxin\text{-}2}$ senses the oxidative stress via the direct oxidation of the protein, and downregulates the activity of TORC1 in response to oxidative stress (Kato et al., 2019). Importantly, the TORC1 itself regulates the endogenous ROS levels by phosphorylation of superoxide dismutase 1 (SOD1) at S39 in yeast and T40 in humans, thereby preventing accumulation of ROS in response to high nutrients (Tsang et al., 2018). It is tempting to speculate that high ROS production in aneuploids downregulate TORC1 activity, which, in turn, facilitates ROS accumulation due to low SOD activity, thereby promoting negative effects of ROS signaling on cellular physiology.

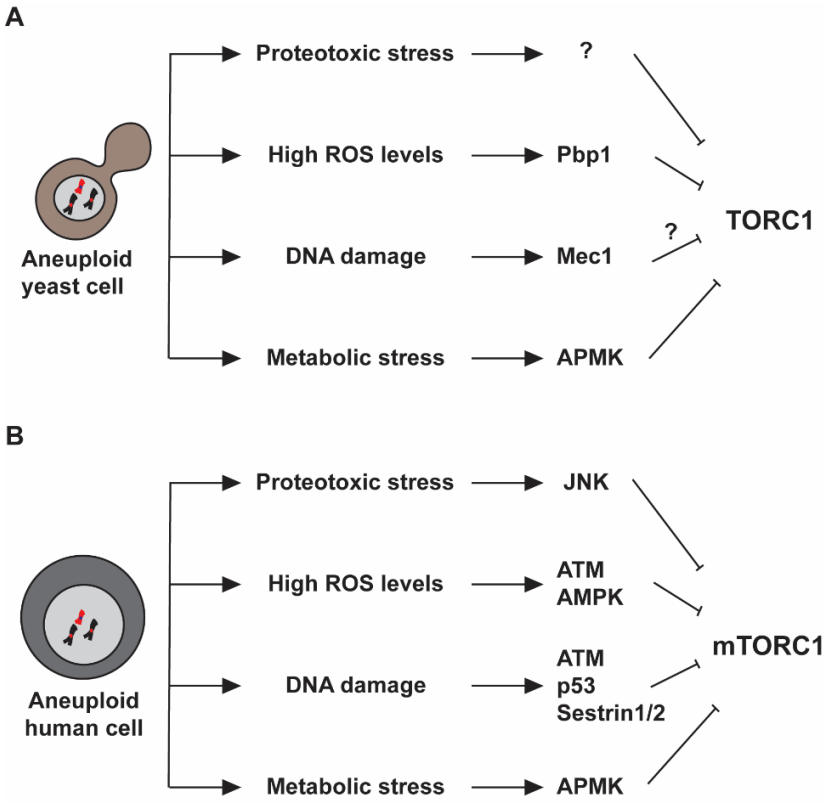

Figure 33. Aneuploidy-associated phenotypes that negatively regulate TORC1 activity in yeast and human cells. (a) In budding yeast, aneuploidy induces cellular stresses, which were shown to downregulate the activity of TORC1 via diverse signaling branches. **(b)** In human cells, aneuploidy induces a plethora of cellular stresses. Each of these stresses was shown to downregulate the activity of mTORC1 via indicated signaling pathways. Question mark- the molecular mechanism is not known.

Aneuploids suffer from elevated levels of genome instability, replication stress, and DNA damage (Passerini et al., 2016; Sheltzer et al., 2011), which also could contribute to downregulation of TORC1 signaling. In mammalian cells, activation of DNA damage signaling (similarly to high ROS production) leads to downregulation of mTORC1 via the AMPK signaling axis (Alexander et al., 2010). Additionally, activation of ATM leads to phosphorylation of the tumor suppressor p53 (Banin et al., 1998). The activated p53 targets Sestrin1/2 proteins, which target both AMPK and Rag GTPases to inhibit TORC1 ((Budanov and Karin, 2008; Peng et al., 2014), reviewed in (Su and Dai, 2017)). In budding yeast, activation of DDC leads to attenuation of TORC1 signaling and induction of autophagy (Eapen and Haber, 2013; Klermund et al., 2014). The autophagy induction requires Mec1 and is partially dependent on the mitogen-activated kinase Mpk1, yet the precise mechanism remains unclear (Ueda et al., 2019). It is likely that aneuploidy-induced replication stress and chronic DNA damage contribute to the attenuation of TORC1 signaling.

Finally, aneuploids experience dysregulation of their energy metabolism, display altered gene expression profiles for the genes involved in carbohydrate metabolism, and exhibit elevated energy demands (Tang et al., 2011; Torres et al., 2007). Moreover, aneuploids display overall dysregulation of many metabolic pathways, which manifest in metabolic stress. Particularly, aneuploids have elevated glucose uptake, which does not manifest in biomass accumulation (Torres et al., 2007). As TORC1 is a central regulator of growth in response to nutrient availability, the low levels of glucose (and therefore low ATP production) might lead to downregulation of TORC1 activity by AMPK kinase. In mammals, low levels of ATP or high AMP levels activate AMPK kinase, which phosphorylates RAPTOR at Ser722 and Ser792, leading to TORC1 inhibition (Gwinn et al., 2008). AMPK also phosphorylates TSC2 at Thr1271 and Ser1387, leading to TORC1 inactivation (Inoki et al., 2003). Additionally, the p38 kinase signaling mediates the phosphorylation of TORC1 signaling mediator Rheb, and leading to TORC1 inhibition ((Zheng et al., 2011), reviewed in (Su and Dai, 2017)). In budding yeast, glucose starvation triggers AMPK-dependent phosphorylation of Kog1 at Ser491 and Ser494, which leads to disassembly of TORC1 (Hughes Hallett et al., 2015). Therefore, aneuploidy-associated energy and metabolic stresses could potentially downregulate TORC1 activity. To summarize, aneuploidy-associated phenotypes, such as proteotoxic stress, genomic instability, high ROS production, and energy and metabolic stresses have a potential to induce low TORC1 activity.

3.3.4 The role of TOR signaling in drug resistance

The activity of TORC1 modulates the metabolic adaptation to favorable and adverse conditions (reviewed in (Loewith and Hall, 2011) and (Weisman, 2016)). The low TORC1 activity in aneuploids is likely an efficient mechanism for cellular survival under stress. For example, downregulation of TORC1 signaling by proteotoxic stress prevents further accumulation of misfolded protein aggregates, and spares energy in already energy-stressed aneuploids (Su et al., 2016; Tang et al., 2011). Paradoxically, although aneuploidy is highly disadvantageous in primary cells, cancer cells tolerate aneuploidy extremely well (reviewed in (Ben-David and Amon, 2020)). Despite often being aneuploid, cancer cells frequently display hyperactivated mTOR (reviewed in (Guri and Hall, 2016)). Therefore, it is likely that although aneuploidization leads to the low TORC1 signaling, a further selection of cells with higher TORC1 activity takes place.

TORC1 signaling has been implicated in the resistance to a variety of drugs across organisms, from yeast to humans. In lower eukaryotes, like the Fpathogenic yeast *C. albicans*, TOR activity drives resistance to antifungal drugs (Bojsen et al., 2017; Khandelwal et al., 2018). In budding yeast, TOR activity modulates adaptation of cellular metabolism to adverse conditions (Weisman,

2016). Deregulated mTOR activity in humans was implicated in the development of diabetes, obesity, and cancer (reviewed in (González and Hall, 2017)). The mTOR pathway is a major signaling pathway that underlies the resistance of a broad spectrum of human tumors to chemotherapeutics (reviewed in (Xu et al., 2020)). The signaling of mTOR confers chemoresistance in a complex manner by altering cellular metabolic pathways (reviewed in (Guri and Hall, 2016)). For example, in melanoma tumors, hyperactive mTOR signaling can compensate for the inhibition of ERK signaling by BRAF-MEK-ERK inhibitors, thereby conferring chemoresistance ((Corcoran et al., 2013; Wee et al., 2009), reviewed in (Guri and Hall, 2016)). The activity of mTOR also confers resistance to PI3K inhibitors, as was shown for human breast and thyroid cancers (Elkabets et al., 2013; Liu et al., 2009). Mechanistically, the resistance to ERK and PI3K inhibitors was attributed to the TORC-induced overexpression of the c-Myc oncogene (Guri and Hall, 2016; Hayes et al., 2016). The hyperactivation of mTOR drives the resistance to HER2 inhibitors in breast cancers (Sudhan et al., 2020). It is also important to note that the activation of mTOR drives changes in the cancer microenvironment and in the modulation of the immune system, which additionally contribute to chemoresistance (reviewed in (Bazzichetto et al., 2020)).

Because of the central role of mTOR signaling in the acquisition of chemoresistance, simultaneous administration of chemotherapeutics and mTOR inhibitors represents a promising strategy to overcome resistance in clinical studies. Even now, the mTOR inhibitor everolimus is used in combination with anti-estrogen therapy in the treatment of metastatic breast cancer (reviewed in (Guerrero-Zotano et al., 2016)). The inhibition of PI3K and mTOR leads to the re-sensitization of breast and ovarian cancer cell lines to doxorubicin (Durrant et al., 2020). The combinatorial therapy that induces DNA damage and targets mTOR was also shown to diminish drug resistance in gliomas (Jain et al., 2017). The inhibition of mTOR for cancer therapy has two potential pitfalls: first, the inhibitors of mTORC1 induce the selective activation of the AKT oncogene; second, tumors frequently develop resistance to the mTOR inhibitors (Guerrero-Zotano et al., 2016; Rodrik-Outmezguine et al., 2016). Nonetheless, the inhibition of mTOR is a promising strategy to target tumor drug resistance. My results in repair-defective *rad52* budding yeast model suggest that inhibiting TORC1 acts on two different levels: rapamycin prevent adaptation, and at the same time, it is toxic to highly aneuploid adapted cells. Therefore, the combination of TORC1 inhibitors with genotoxic drugs might be especially effective.

3.4 High levels of Cdc5 in *rad52* mutants are unlikely to explain genotoxin resistance

The yeast polo-like kinase Cdc5 is a positive regulator of CA, which I have previously shown as a factor that promotes formation of genotoxin resistant colonies. The human homologue Plk1 is

overexpressed in many tumors, and is thought to promote aggressive cell growth and resistance to anticancer drugs, including doxorubicin, gemcitabine, metformin and many other therapeutic agents ((Saatci et al., 2018; Zuco et al., 2015), reviewed in (Gutteridge et al., 2016)). Plk1 was also implicated in adaptation to ionizing radiation induced DNA damage in human cells (Syljuåsen et al., 2006). My results indicate that repair-defective *rad52* mutants display elevated but variable levels of Cdc5, which remain high and variable in both X-rays and CPT treated *rad52* mutants (Figure 25). Blank and colleagues reported that aneuploidy condition induces elevated levels of mitotic divisions with DNA damage, which might be mediated by Cdc5, although the authors never examined the Cdc5 levels in aneuploid cells directly (Blank et al., 2015). The elevated levels of Cdc5 in *rad52* mutants might indeed predispose these repair-defective cells to adaptation, as Cdc5 overexpression was shown to override DDC (Vidanes et al., 2010). I did not observe further increase in Cdc5 levels in aneuploid *rad52* mutants, which might have different explanations. First, both *rad52* mutants and aneuploid mutants accumulate in late S and G2/M phases of cell cycle (Figure 14a), in which the Cdc5 protein levels accumulate (Cheng et al., 1998). Therefore, both *rad52* mutants and aneuploids could have similar source of the elevated Cdc5 levels. Second, as the overexpression of Cdc5 is highly toxic to cells, aneuploid adapted *rad52* mutants might not tolerate even further Cdc5 levels elevation compared to the euploid *rad52* cells. My results do not exclude that Cdc5 levels are elevated in aneuploids that do not have *rad52* mutations.
Although the differences in Cdc5 protein levels between euploid *rad52* mutants and adapted *rad52* mutants are unlikely to explain the strong genotoxin resistance phenotype of the latter, they might promote adaptation and contribute to the survival in the presence of genotoxins. In human cells, Plk1 promotes resistance to genotoxic drug doxorubicin and gemcitabine ((Song et al., 2013), reviewed in (Gutteridge et al., 2016)). Moreover, high Plk1 activity promotes DNA replication and survival under the replication stress (Song et al., 2013). Therefore, therapies targeting high Plk1 levels are highly promising, and many Plk1 inhibitors enter clinical trials.

3.5 Search for the alternative DNA repair pathways that confer chemoresistance in HR and NHEJ deficient *rad52* mutants

The HR repair-defective tumors frequently gain genotoxin resistance by re-wiring their DNA repair pathways. Identifying these alterations could potentially allow targeting them, and therefore prevent DNA repair events that confer chemoresistance. Although I did not quantify directly the DNA damage load in X-rays treated and CPT-treated cells, I think the growth following 45 Gy of X-rays, and in the continuous presence of 2 μM CPT, requires active DNA repair mechanisms. Moreover, because checkpoint adapted *rad52* cells gain evident survival advantage when

repeatedly exposed to genotoxins, I anticipate that the alternative DNA repair mechanisms might be upregulated in these cells. Extensive literature data indicate multiple mechanisms that confer resistance in HR-deficient mammalian cancer cells, yet many genotoxin resistance mechanisms remain unclear (see section 1.7.2). In order to identify the DNA repair players that confer chemoresistance, I have analysed the involvement of other HDR and NHEJ repair factors. Afterwards, I have analysed the involvement of the MRX complex, and the faulty DNA repair pathway, MMEJ, in the post-adaptation repair.

3.5.1 Mitotic recombination proteins Rad51, Rad59, and Rad55 do not contribute to resistance formation in *rad52* mutants

In my yeast model for the CA, I knocked-out a key homologous recombination gene *RAD52* (Krogh and Symington, 2004). Rad52 directly interacts with RPA and Rad51, and thereby targets Rad51 to the RPA-coated ssDNA (New et al., 1998). Rad52 is required for an efficient meiotic and mitotic recombination, the latter is the preferred DSB repair mechanism in yeast. Rad52 is an essential component of two major mitotic HR pathways: the first pathway requires Rad51, Rad55, and Rad57; the second pathway requires Rad59 and the MRX complex (reviewed in (Symington et al., 2014)). Although the loss of *RAD52* induces strong defects in all HDR pathways, there were rare gene conversion events documented in diploid HR defective *rad52-1* mutants (Haber and Hearn, 1985). Another literature report indicated that following UV irradiation, the frequency of gene conversion events in *rad52* mutants increased in *RAD51*, *RAD55*, *RAD59*, and *RAD50* dependent manner (Coïc et al., 2008). It is not known how these recombination events would be produced in the absence of the Rad52 recombinase mechanistically. Human HR-defective BRCA1- and BRCA2-deficient cells frequently re-wire their DNA repair pathways in order to acquire chemoresistance (see section 1.7.2). Although the genetic reversions of BRCA2 mutations, or overexpression of the mutant protein (Park et al., 2020; Sakai et al., 2008), confer chemoresistance in human cells, I have ruled out the restoration of Rad52 function as I use complete gene deletion in my system. Rather, I wondered whether the other components of the HDR pathway compensate for the loss of Rad52. My results indicate that the *RAD51*, *RAD55* and *RAD59* genes are dispensable for the resistance to both CPT and X-rays in *rad52* mutants (Figure 26). Therefore, although the rare spontaneous Rad52-independent recombination events might have minimal contribution to the DNA repair, they play little to no role following relatively robust treatments with X-rays and CPT.

3.5.2 Restoration of NHEJ repair does not contribute to genotoxin resistance in *rad52* mutants

NHEJ is the second major DNA repair pathway, which operates in G1 in yeast, and throughout cell cycle in mammals. NHEJ does not depend on the availability of homologous template or Rad52 for the DSB repair. This pathway directly ligates DNA ends via MRX complex and Dnl4 (reviewed in (Emerson and Bertuch, 2016)). This pathway is potentially mutagenic, as it can lead to microdeletions or translocations (Ghezraoui et al., 2014). In human cells, the role of NHEJ in the genotoxin resistance greatly depends on the specific DNA repair defect in tumor cells. In wild-type BRCA1 or BRCA2 cells, for example colorectal cancer cell line HCT116, NHEJ promotes chemoresistance to genotoxins (Liu et al., 2019). NHEJ repair also confers genotoxin resistance in HR-proficient prostate cancers (Broustas et al., 2020). However, because many NHEJ pathway proteins suppress DNA ends resection, mutations in the pathway frequently promote chemoresistance due to the restoration of ssDNA formation. For example, loss of NHEJ-promoting complex Shieldin, loss of 53BP1, or loss of RIF1 all confer chemoresistance by restoration of DNA end resection in BRCA-deficient tumors (Bunting et al., 2010; Escribano-Díaz et al., 2013; Gupta et al., 2018; Jaspers et al., 2013). In actively replicating BRCA1-deficient cells, active NHEJ pathway was shown to be toxic due to its high mutagenicity (Balmus et al., 2019). Nonetheless, the restoration of NHEJ could theoretically provide a repair mechanism in the *rad52* HR-deficient cells, because event mutagenic end joining is better that the absence of DSB repair for the cell survival.

In diploid budding yeast, Nej1 actively suppresses the NHEJ pathway in a transcription-dependent manner (Frank-Vaillant and Marcand, 2001; Valencia et al., 2001). I hypothesized that following adaptation, cells could re-wire their gene regulation (for example due to the mutations in the transcriptional repressor), and therefore restore the expression of Nej1. I have observed that *rad52* mutants lacking Dnl4, a key NHEJ protein, do not display elevated sensitivity to X-rays and CPT (Figures 26 and 27). These results indicate that the NHEJ pathway does not confer chemoresistance in diploid *rad52* mutants. I have further verified this result using another NHEJ-defective mutant, *XRS2-S47A, H50A* (Figure 29d). The Xrs2 protein plays a key NHEJ repair protein. The two point mutations in the FHA domain of the *XRS2* gene, *XRS2-S47A, H50A*, lead to a defect in the NHEJ repair pathway (Matsuzaki et al., 2008). Together, using two NHEJ-defective mutants, a complete *DNL4* gene deletion, and a point *XRS2-S47A, H50A* mutant, I show that the adapted *rad52* cells do not acquire reliance on the NHEJ pathway. Therefore, some other DNA repair mechanism must confer chemoresistance.

3.5.3 MRX complex confers chemoresistance of *rad52* mutants

MRX complex plays crucial role in DSB repair by virtually all DNA repair pathways, including HR, NHEJ, and MMEJ (reviewed in (Oh and Symington, 2018)). Although the loss of *RAD50* is considered epistatic to the loss of *RAD52* due to the defect in DNA ends resection, Coïc and colleagues reported that *rad52 rad50* double mutants have further decrease in gene conversion events compared to *rad52* mutants alone (Coïc et al., 2008; Krogh and Symington, 2004). The MRX complex was shown to be important for the Rad52- and Ku- independent MMEJ, which prompted me to test whether *rad52* mutants require MRX complex for the survival following genotoxin treatment (Ma et al., 2003). Strikingly, I found that the loss of either *MRE11* or *RAD50* strongly sensitized *rad52* mutants to CPT, and moderately but not significantly to X-rays (Figure 27). These results suggest that although MRX prevalently operates in HR- and NHEJ-mediated DSB repair, the complex has additional functions that confer the genotoxin resistance of *rad52* mutants. Using an auxin-inducible degron of Mre11 (Morawska and Ulrich, 2013), I was able to demonstrate that in already CPT-resistant *rad52* mutants, MRX confers the resistance to a second round of genotoxic treatment. These data indicate that the complex remains critical for the DNA repair post-adaptation. Which function of MRX complex could potentially confer CPT resistance in HR-defective cells?

CPT treatment leads to Top1 trapping on the DNA by the stabilization of a transient Top1-cc (reviewed in (Pommier et al., 2010)). Top1-cc is removed from the DNA majorly by Tdp1-dependent hydrolysis, and Rad1-Rad10 nucleases (Liu et al., 2002; Sacho and Maizels, 2011). Mre11 nuclease activity was shown to contribute to the removal of Top1-cc from DNA ends in the absence of Tdp1 (Liu et al., 2002). It is unlikely that *mre11* cells are sensitized to CPT due to defective Top1-cc removal, because I performed my experiments in wild-type *TDP1* background. The removal of the second major Top1-cc repair gene, *RAD1*, also did not affect the viability of *rad52* mutants on CPT (Figure 30a), suggesting that the Tdp1 activity was likely sufficient for the processing of Top1-cc.

MRX mutants themselves display high sensitivity to CPT, majorly due to defects in DNA end resection and HR (Foster et al., 2011). The restoration of DNA end resection in Mre11-defective mutants rescued the mutants' viability on CPT, supporting the importance of resection in a repair of CPT-induced damage (Foster et al., 2011). Mutants expressing nuclease-dead *mre11-H125N* allele, which does not affect the integrity of MRX complex, are extremely sensitive to even low CPT dosages (Menin et al., 2018; Oh et al., 2016). I have observed that the nuclease-deficient *mre11-D56N* and *mre11-H125N* mutants still supported the viability of *rad52* cells on low CPT dosages (Figure 29c). These results could be interpreted as the DNA end resection is dispensable

for the CPT resistance formation in *rad52* mutants. It is important to note that because MRX complex, besides initiating DSB resection, has multiple roles including DNA end tethering, initiation of DDC, recruitment of cohesin, and others (reviewed in (Oh and Symington, 2018)). Therefore, mutants with the deletion of *mre11* display more severe CPT sensitivity compared to mutants that express nuclease-deficient alleles of *MRE11*. Moreover, the deletion of *MRE11* leads to more severe DNA end resection defect, due to the impaired recruitment of Exo1 and Sgs1-Dna2. MRX is also important to recruit chromatin remodelers RSC, Chd1, and Isw1, which promote chromatin remodeling at stalled forks and allow efficient resection (Delamarre et al., 2020). This function of MRX does not depend on the nuclease activity of Mre11. The nuclease-deficient alleles of *MRE11* induce a delay in initial resection steps; nevertheless, Exo1 and Sgs1-Dna2 execute DNA ends resection with a delayed kinetics (Oh and Symington, 2018; Shim et al., 2010). It is possible that during the prolonged checkpoint arrest in *rad52* mutants, the delayed DSB ends resection kinetics does not impair DNA repair.

MRX plays a dual role in activation of DDC, as Xrs2 directly recruits Tel1 to the DSB, and the initiation of DSB resection created substrate for the activation and recruitment of Mec1 (Clerici et al., 2014). The deletion of Tel1 did not further sensitize *rad52* mutants to CPT, while the checkpoint-defective *rad53-11* mutants only slightly decreased the viability of *mre11 rad52* double mutants (Figure 29a, and b). These results are in line with literature data, which show that *mre11* mutants fail to activate DDC in response to single irreparable DSB (Cassani et al., 2019). These data also support the notion that *mre11* mutants do not display defective CA (Lee et al., 1998). If the deletion of *mre11* induced adaptation defect in *rad52* mutants, the *rad53-11* allele would rescue these cells following DNA damage. Given that abrogation of the DDC in *rad52* mutants slightly but consistently decreased their viability on CPT-containing plates, checkpoint deficiency of MRX deletion mutants rather contributed to the sensitization to genotoxins.

3.5.3.1 Potential functions of MRX at the DSB that promote resistance phenotype

Which other functions of the MRX complex could be critical for the CPT resistance of *rad52* cells? Mre11 has ssDNA annealing activity *in vitro*, which might facilitate microhomology annealing in MMEJ repair (de Jager et al., 2001). MRX also allows DNA ends tethering, which is crucial for the DNA ends joining by MMEJ, and HR (Cassani et al., 2016; Seeber et al., 2016). It is tempting to speculate that the loss of DNA ends tethering greatly reduces chances for the annealing of microhomologies during MMEJ repair. Additionally, MRX participates in cohesin loading at stalled replication forks, which is crucial for their recovery (Delamarre et al., 2020). Moreover, MRX is structurally similar to cohesin itself, and plays structural role at stalled replication forks. The stabilization of replication forks by MRX does not depend of Mre11 nuclease activity (Tittel-Elmer

et al., 2009). MRX interacts with RPA, and holds sister chromatids and DNA breaks ends together (Seeber et al., 2016). The maintenance of replication fork structure is important for its further restart or repair during replication stress, as *rad50* mutants display frequent replication forks collapse events following hydroxyurea treatment (Seeber et al., 2016). It is feasible that replication forks stalled due to CPT-induced topological stress require MRX for the maintenance of fork topology. Following the hydroxyurea treatment, the deletion of *RAD51* showed an additive phenotype to the deletion of *MRE11*, indicating that during replication stress, MRX acts in a parallel pathway to the HR machinery (Tittel-Elmer et al., 2009). It is feasible that in repair-deficient *rad52* mutants, the null alleles of the MRX complex display elevated fork collapse rates due to CPT-induced topological stress, which indirectly increases the CPT-induced DNA damage load.

3.5.4 Adapted *rad52* mutants are proficient in MMEJ repair pathway

The MMEJ pathway is a backup DNA repair mechanism that does not require Yku proteins or Dnl4, and does not depend on the key HR protein Rad52 (Ma et al., 2003; Meyer et al., 2015; Sinha et al., 2016). This pathway was shown to rely on the MRX complex, which is important to initiate DNA ends resection that allows the exposure of microhomologies (Ma et al., 2003). The MRN-mediated resection is also important for the MMEJ initiation in human cells (Truong et al., 2013). The deletion of *MRE11* gene was shown to cause severe defects in MMEJ repair, which might explain the sensitization of *rad52* mutants to CPT (Ma et al., 2003; Meyer et al., 2015). The pathway relies on DNA polymerase δ subunit Pol32, the Polymerase λ (Pol4), as well as the DNA endonuclease complex Rad1-Rad10 for the fill-in DNA synthesis (Ma et al., 2003; Meyer et al., 2015). MMEJ pathway displays the strongest reliance on Pol32 (Meyer et al., 2015). Due to the synthetic lethality of *RAD52* and *POL32* deletions, I was unable to examine the role of Pol32 in the survival of *rad52* mutants on CPT directly. When I tested the involvement of the Pol4 polymerase in the survival of *rad52* mutants following genotoxin treatments, I did not see the decrease in mutants' viability (Figure 30c, and d). Using the interchromosomal MMEJ reporter construct with different microhomologies length, Meyer and colleagues demonstrated that the *rad52* diploids upregulate MMEJ rates 10 to 115 fold compared to wild type cells (Meyer et al., 2015). At the same time, the deletion of the *POL4* gene in diploid yeast caused two-fold decrease in the frequency of MMEJ events. The *rad52 pol4* double mutants displayed 16 increase in the MMEJ events over the wild types, which might still be sufficient for the survival of *rad52* mutants following DNA damage (Meyer et al., 2015). In a different study, the loss of *RAD50* was required to abolish MMEJ repair in *pol4* mutants, supporting that *POL4* knockout does not fully abolish MMEJ (Galli et al., 2015).

The Rad1-Rad10 endonuclease complex degrades the heterologous flaps once the microhomologies are annealed, which allows the polymerases to fill in the gap, and permit DNA ends re-ligation during the MMEJ repair (Bennardo et al., 2008; Ma et al., 2003). I have observed that the loss of *RAD1* gene slightly, but not significantly, sensitized *rad52* mutants to both CPT and X-rays (Figure 30a, and b). These results indicate that Rad1 contributes to the survival of *rad52* mutants, but is not strictly required. The *rad52 rad1* double mutants demonstrated a two-fold increase in MMEJ repair events compared to wild type cells, indicating that the loss of *RAD1* also does not fully abolish MMEJ-mediated DNA repair events (Meyer et al., 2015). Together, out genetic data indicate that the MMEJ proteins Pol4 and Rad1 do not have a strong contribution to the survival of *rad52* mutants following genotoxin exposure. Alternatively, while these factors might contribute to the repair *per se*, the certain redundancy in cellular DNA repair pathways allows the repair.

These genetic data might be difficult to interpret for two reasons. First, the deletion of *RAD52* drastically upregulates the MMEJ rates, which might lead to sufficient rates of DNA repair even when certain MMEJ factor are depleted. For example, the deletion of gene encoding another recombinase, *RAD51*, rescues the survival of MMEJ-deficient *srs2* strain following the DSB induction (Lee and Sang, 2007). Second, the functional redundancy of molecular players in MMEJ pathway could compensate the loss of one of the factors. In human BRCA2-deficient cells, the 5´ flap endonuclease Fen1 (a homologue of yeast Rad27) participates in MMEJ repair of DSBs (Mengwasser et al., 2019). One could hypothesize that Rad27 could compensate for the Rad1 loss in yeast. Similarly, the loss of the Pol4 could be compensated by the other MMEJ polymerases, Pol32 and Pol3, which could perform the fill-inn DNA synthesis. These data, however, do not exclude that the DNA repair in *rad52* mutants is carried out by yet another mechanism.

3.5.4.1 CPT adapted *rad52* mutants do not further upregulate their MMEJ rates

Due to difficulties in interpretation of the genetic data on the involvement of MMEJ factors in the formation of genotoxin resistance in *rad52* mutants, I set out to directly measure the MMEJ rates in adapted *rad52* cells. Therefore, I have utilized a previously published MMEJ reporter (Meyer et al., 2015). Using this reporter, I have measured the interchromosomal MMEJ rates between substrates that share 20 bp microhomologies in diploid *rad52* mutants and CPT-resistant nearly haploid *rad52* mutants (Figure 31). I did not detect significant differences in interchromosomal MMEJ rates between naïve and adapted *rad52* mutants. I was not able to measure intra-chromosomal MMEJ rates, as this type of reporter was not available. These results indicate that

the MMEJ is available for CPT resistant *rad52* mutants; however, the pathway is not upregulated. The already high MMEJ rates in *rad52* mutants might be sufficient to support the viability of these cells on CPT. Alternatively, these mutants upregulate MMEJ repair specifically at broken replication forks, which I was not able to detect with the interchromosomal MMEJ reporter.

It is not known whether the MMEJ repair efficiency differs when it happens on the same chromosome or on two different ones, as is the case with the reporter I used. Each interphase chromosome occupies a defined territory within the nucleus, and acquires defined conformation (Duan et al., 2010). The DSB induction leads to a re-localization of the break to the nuclear periphery (Oza et al., 2009). The majority of HR events occur at the nuclear periphery, where more than one DSB can be repaired simultaneously (Lisby et al., 2003; Oza et al., 2009). The efficiency of DSB repair by HR depends on the proximity of homologous template, as the breaks that are located in the same chromosome territory are repaired most efficiently (Agmon et al., 2013). The homology search was shown to be the critical rate-limiting step for DSB repair (Lee et al., 2016). Similar to HR, MMEJ preferentially utilizes microhomologies with closest proximity to the break (Lee et al., 2019). These data suggest that the interchromosomal MMEJ rates might not directly reflect repair rates when microhomologies are localized on the same chromosome, a scenario I expect to occur at the CPT-induced DSB. I did not detect chromosomal translocations in CPT-resistant *rad52* mutants when I analyzed them using whole-genome sequencing (Figure 14), supporting the idea that these mutants likely used microhomologies located on the same chromosome.

The MMEJ repair is differentially might be differentially regulated depending on the type of DSBs induced. The vast majority of studies utilize endonuclease-induced DSBs to measure MMEJ rates (Bennardo et al., 2008; Ma et al., 2003; Meyer et al., 2015). CPT induces DSBs that are different in their structure and genomic context, as they are produced by the collision of replication or transcription machinery with trapped Top1, or by a Mus81-mediated cleavage of a stalled replication fork ((Regairaz et al., 2011), reviewed in (Pommier, 2006)). The MMEJ repair at stalled replication forks was shown to confer chemoresistance in BRCA2-deficient cells, which indicates that replication forks are a relevant genomic context for the MMEJ repair (Kais et al., 2016). The DNA polymerase θ (POLQ) is critical for MMEJ repair of DSBs in HR-deficient cells (Ceccaldi et al., 2015; Mateos-Gomez et al., 2015). Curiously, the depletion of POLQ sensitized BRCA1-mutated breast cancer cells to topoisomerases poisons CPT and Etoposide, suggesting that MMEJ is involved in the repair of CPT-induced DNA damage (Wang et al., 2019). The sensitivity to CPT was also observed in $POLQ^{-/-}$ bone marrow cells, which utilize the MMEJ-mediated DSB repair for immunoglobulin class-switch recombination (Yousefzadeh et al., 2014).

How would MMEJ occur when the TOP1-cc collides with replication machinery? I envision two possible scenarios (Figure 34). First, when the collision of a leading-strand replication machinery with a CPT-trapped Top1 generates one-ended DSB, which is converted to two-ended DSB by a converging replication fork (Figure 34a). Alternatively, the break is produced by a Mus81-mediated cleavage of a stalled replication fork. The resection of DSB ends exposes microhomologies, which are repaired by MMEJ. Second, the CPT-induced DSB could be repaired at the fork directly (Figure 34b). Following the Top1-cc removal, the single-ended DSB is resected, which exposes microhomologies. The replication fork is unwound by a helicase, which allows the exposure and alignment of microhomologies. These structures are repaired by MMEJ pathway, which allows the resumption of DNA replication. These mechanisms were proposed to operate at collapsed replication forks following the hydroxyurea treatment (Truong et al., 2013). The treatment with hydroxyurea produces long stretches of ssDNA at stalled replication forks, which are converted to a DSB when the fork is cleaved with Mus81, ARTEMIS, or XPF (Bétous et al., 2018). The structurally different CPT-induced DSBs rather require the removal of Top1-cc complex. Yet both treatments potentially induce DSBs at the replication forks. It is therefore tempting to speculate that the MMEJ-mediated repair of collapsed replication forks is similar in hydroxyurea- and CPT-treated cells, which allowed me to build a hypothetical model of MMEJ-mediated repair of CPT-induced DNA damage.

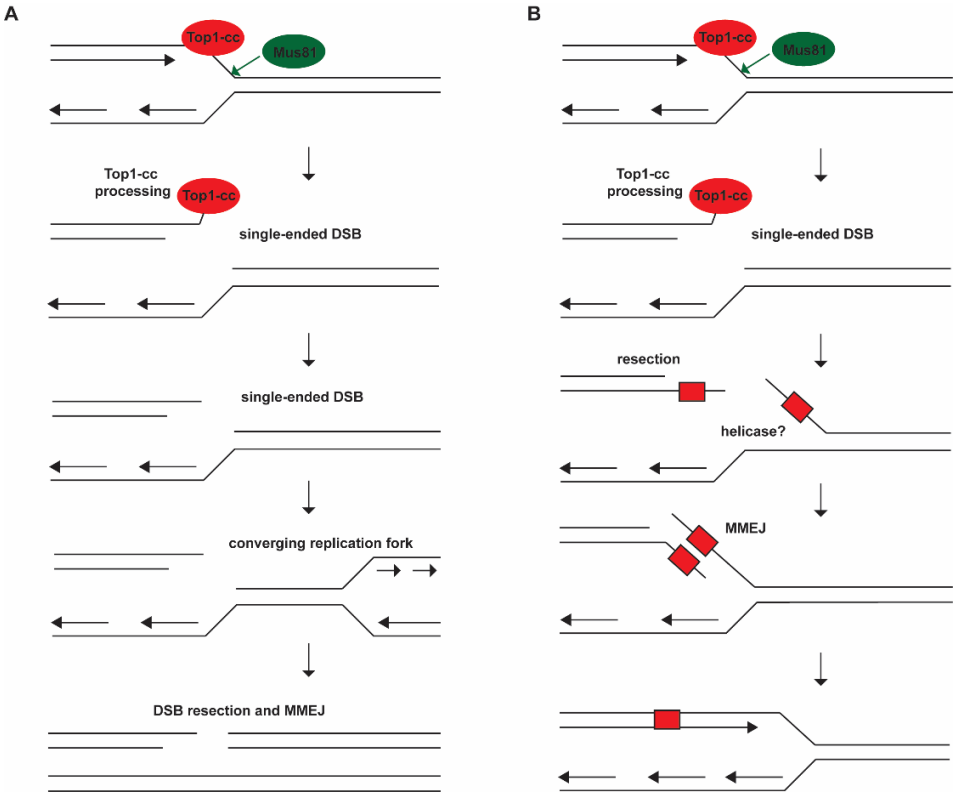

Figure 34. Hypothetical models of MMEJ repair of CPT-induced DSB. (a) The collision of the leading strand with Top1-cc, or a cleavage of stalled replication fork with Mus81, lead to a DSB. The Top1-cc is processed in order to create DSB ends that are compatible with repair. The converging replication fork (that originates from a neighboring origin of replication) converts single-ended DSB into two-ended DSB. This break could be repaired by MMEJ. **(b)** Following the DSB formation, Top1-cc complex is processed, creating DNA ends compatible with DSB repair. This one-ended DSB is resected, exposing microhomologies. At the same time, the replication fork is unwound by an unknown helicase. Following the alignment of microhomologies, the break is repaired by MMEJ. Red square box- microhomology. This figure is created using models from (Truong et al., 2013) and (Wang et al., 2019).

3.5.4.2 Potential reasons for high MMEJ rates in naïve and adapted *rad52* mutants

The rates of MMEJ seem to be directly controlled by the HR machinery (Ahrabi et al., 2016). The HR proteins Rad51 and Rad52 in yeast, and BRCA1 and BRCA2 in mammals suppress the MMEJ-mediated repair (Ahrabi et al., 2016; Meyer et al., 2015). In budding yeast, the deletion of *RAD52* gene leads to 200-fold increase in MMEJ via an unknown mechanism (Meyer et al., 2015). RPA suppresses MMEJ repair, because the complex coats ssDNA and prevents the exposure of microhomologies (Deng et al., 2014). In mammals, the MMEJ pathway is upregulated in cells deficient for BRCA2, because the RPA-coated ssDNA is destabilized in these cells. The ssDNA instability results in defective HR, and the DNA ends are repaired by the error-prone end-joining

(Han et al., 2017). The upregulated MMEJ pathway in BRCA2-deficient cells have is a source of genomic instability in these cells (Han et al., 2017).

In human cancer cells, high activity of mitotic kinases Plk1, Aurora A, and CDK1 promote MMEJ repair (Wang et al., 2018). Mechanistically, CtIP is initially phosphorylated at S723 by Plk1, and further phosphorylated by CDK1-Aurora A and PLK1, which results in suppression of DSB resection (Wang et al., 2018). In budding yeast, CtIP homologue Sae2 is also phosphorylated by Plk1 homologue Cdc5, which results in DSB resection slow down (Donnianni et al., 2010). Therefore, high Cdc5 protein levels in *rad52* mutants (Figure 25) could potentially explain high MMEJ rates in *rad52* mutants.

Adaptation to DDC was associated with an increased usage of faulty repair pathways and acquisition of genomic re-arrangements, particularly via BIR (Galgoczy and Toczyski, 2001). Authors also reported that adaptation was frequently accompanied by a deletion of a large fragment of chromosome VII, which was flanked by two identical tRNA sequences. The deletions flanked by two homologous sequences are a signature of BIR or MMEJ repair. CA is driven by high activity of Cdc5; curiously, adaptation-defective *cdc5-ad* mutants demonstrated significantly lower numbers of faulty BIR events (Galgoczy and Toczyski, 2001). It is tempting to speculate that during adaptation, Cdc5 targets certain DNA repair factors that allow switch to mutagenic DNA repair events. In mitosis, phosphorylation of Mus81-Mms4 complex by Cdc5 leads to cleavage joined DNA molecules (Gritenaite et al., 2014; Princz et al., 2017). The cleavage of stalled replication forks during adaptation course creates a potential MMEJ substrate. In human cells, Plk1 phosphorylation of CtIP not only promotes MMEJ, but also drives the suppression of G2/M checkpoint (Wang et al., 2018). The phosphorylation of CtIP by Plk3 in G1 phase also promotes alternative end-joining events that are highly mutagenic (Barton et al., 2014). The activation of faulty DSB repair pathways during adaptation could potentially allow the repair of the break in expense of acquisition of genomic aberrations. Yet, the relationship between adaptation and MMEJ repair remains to be determines experimentally.

3.5.4.3 The role of MMEJ in genotoxin resistance in cancer cells

Cancer cells frequently rely on the MMEJ pathway for DSB repair, which allows the repair of genotoxin-induced DNA damage, thereby conferring chemoresistance. In HR deficient BRCA2-mutated tumors, DNA polymerase θ (POLQ) interacts with Rad51 and suppresses HR-mediated DSB repair (Ceccaldi et al., 2015; Mateos-Gomez et al., 2015). The MMEJ repair is promoted by PARP1, which recruits POLQ to the DNA damage sites (Mateos-Gomez et al., 2015). While BRCA2 functions as a suppressor of MMEJ pathway, mitotic kinases Plk1, Aurora A, and CDK1

promote MMEJ repair (Wang et al., 2018). These kinases are frequently overexpressed in cancer cells, which likely contributes to the high MMEJ rates in many cancer cells (Gutteridge et al., 2016; Ke et al., 2003; Strebhardt and Ullrich, 2006).

BRCA1 and BRCA2 proteins are important for the stabilization of replication forks, and BRCA-deficient cells suffer from replication stress (Lomonosov et al., 2003; Pathania et al., 2014). The activity of POLQ is important to sustain replication stress in BRCA2-deficient cells, and promote replication forks recovery (Ceccaldi et al., 2015). FANCD2, a Fanconi anemia pathway protein, protects stalled replication forks from nucleolitic degradation (Lossaint et al., 2013). In BRCA2-deficient cells, FANCD2 localizes to stalled replication forks and recruits POLQ and CtIP, which facilitates MMEJ pathway (Kais et al., 2016). The mutations in BRCA2-interacting partner PALB2 also leads to an increase in MMEJ repair pathway (Obermeier et al., 2016). The upregulation of the MMEJ pathway was reported to confer resistance to PARPi in BRCA2-deficient tumors. The pathway is upregulated due to the increased expression of aldehyde dehydrogenase ALDH1A1, which increases the DNA repair capacity by MMEJ in an unknown way (Liu et al., 2020).

HR deficient tumors demonstrate high reliance on the MMEJ pathway for their DNA repair, and targeting MMEJ components is a promising strategy to overcome tumor resistance. BRCA2-deficient cell display synthetic lethality with multiple MMEJ pathway proteins, including polymerase POLQ, 5´ flap endonuclease Fen1, and FANCD2 (Ceccaldi et al., 2015; Kais et al., 2016; Mengwasser et al., 2019).

The repair with MMEJ pathway is highly mutagenic, and generates random insertions or deletions at the break point (Mateos-Gomez et al., 2015). The pathway also leads to generation of chromosomal translocations in a CtIP-dependent manner (Zhang and Jasin, 2011). These data indicate that DNA repair with MMEJ has a potential to promote tumorigenesis by generation of oncogenic translocations, or other types of mutations in tumor suppressor genes (Zhang and Jasin, 2011). In malignant cells, highly mutagenic DNA repair events allow the generation and selection of therapy-resistant mutations.

3.6 Model

In my model, I connect adaptation, aneuploidization, and acquisition of genotoxin resistance in HR-defective cells in response to genotoxins (Figure 35). Moreover, I suggest that adaptation itself, and adapted cells are vulnerable to pharmacological targeting. Because adaptation precedes the re-growth following irreparable DNA damage, preventing adaptation specifically sensitizes only repair-defective cells. In repair-proficient cells, preventing adaptation does not

induce the sensitivity to genotoxins, because these cells repair DNA damage before the adaptation occurs (Figure 35a).

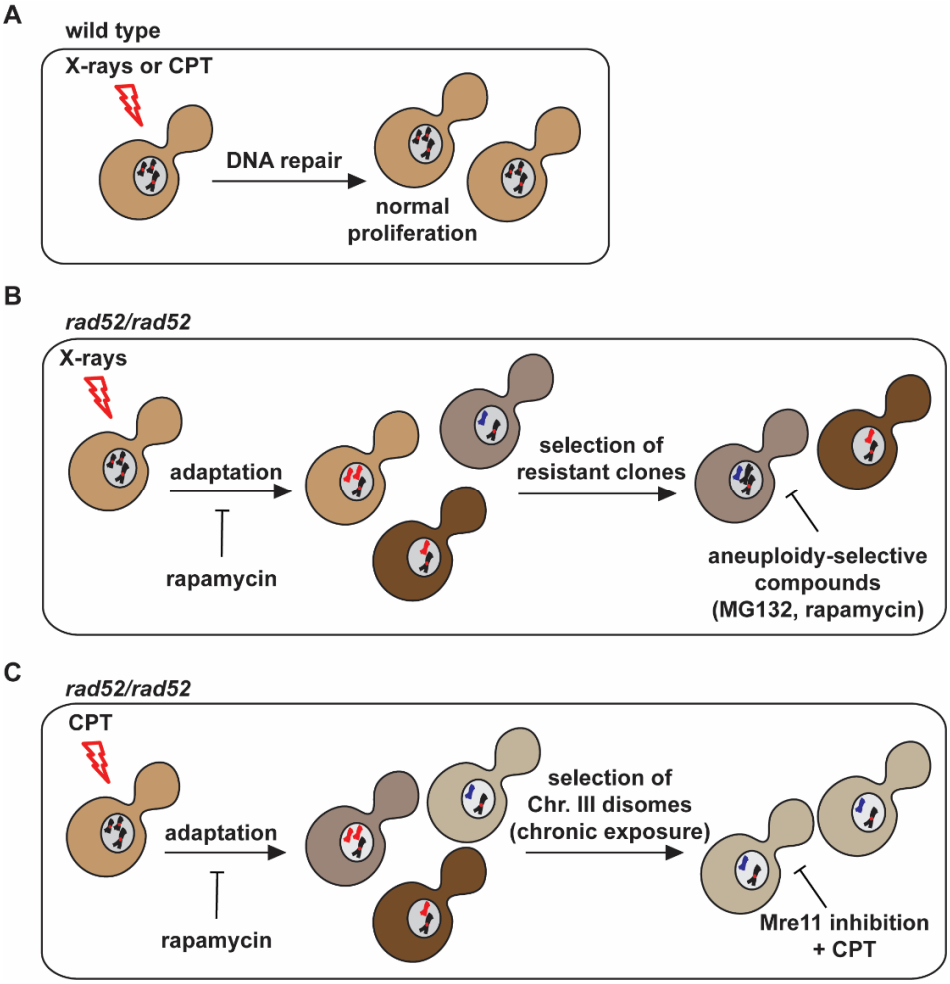

Figure 35. Genotoxin resistant cells can be targeted pharmacologically. (a) Repair-profficient wild type cells are able to execute successful DNA repair following treatment with genotoxins, X-rays or CPT. These cells resume normal proliferation once the DNA damage is repaired, and do not undergo aneuploidization. **(b)** HR defective *rad52* cells udergo CA following treatment with X-rays. Adaptation leads to genomic instability, which creates genetically heterogeneous population of aneuploid cells (depicted in different shades of beige), from which genotoxin resistant mutants are selected. CA in response to X-rays treatment could be prevented by the TORC1 inhibitor rapamycin. The genotoxin resistant aneuploids can be targeted by aneuploidy-selective antiproliferation compounds, MG132 or rapamycin. **(c)** *rad52* mutants undergo adaptation following treatment with CPT. Adaptation to chronic CPT-induced DNA damage leads to drastic chromosome loss events and also generates genetically heterogeneous population (depicted in different shades of beige), and results in selection of nearly-haploid chromosome III disomes. The adaptation to acute CPT exposure generates genetically heterogeneous population that is not followed by the selection of Chr. III disomes. CA in response to CPT-induced damage could be prevented by rapamycin. The *rad52* chromosome III disomes cells are sensitive to Mre11 depletion combined with genotoxic CPT treatment.

HR-defective *rad52* cells undergo CA following treatment with X-rays (as previously shown in (Galgoczy and Toczyski, 2001)) and CPT, which allows them to re-grow despite their inability to repair the damage. It was previously demonstrated that high TORC1 activity promotes adaptation, and treatment of cells with TORC1 inhibitor rapamycin prevents it (Klermund et al., 2014). Using adaptation-defective *cdc5-ad*, *ckb2*, and *sae2* mutants, and rapamycin treatment, I was able to confirm that preventing adaptation sensitizes HR defective *rad52* cells to genotoxins. Adaptation leads to high levels of genomic instability (Galgoczy and Toczyski, 2001; Klermund et al., 2014), and eventually results in aneuploidization. As X-rays induce DNA damage in random genomic loci, during adaptation cells acquire versatile aneuploidies and create genetically diverse population (Figure 35b). Due to karyotype diversity, this highly heterogeneous aneuploid population could have an increased potential to adapt to different environments and stresses, including genotoxic treatment (Chen et al., 2015). Therefore, adapted cells become resistant to X-rays via aneuploidization. These aneuploid adapted cells suffer from aneuploidy-associated stresses, which allows pharmacological targeting post adaptation with proteasome inhibitor MG132 and TORC1 inhibitor rapamycin. According to my model, lowering TORC1 activity with rapamycin is beneficial in two ways: first, by preventing CA, it decreases the occurrence of genotoxin-resistant colonies; second, it is toxic to checkpoint-adapted aneuploids.

I have also demonstrated that *rad52* mutants undergo adaptation following CPT treatment, which also induces genomic instability accompanied by drastic chromosome loss (Figure 35c). Similarly to X-rays, adaptation to CPT-induced DNA damage could be prevented by TORC1 inhibition with rapamycin. Once repair-defective cells adapt to CPT, they undergo aneuploidization. However, CPT treatment leads to the selection of one particular aneuploid karyotype, a chromosome III disome, which is not vulnerable to aneuploidy-selective compounds. Instead, I find that the loss of MRX complex function sensitizes both naïve and checkpoint adapted *rad52* mutants to CPT. These results indicate that the combination of CPT treatment and an impairment of MRX function selectively eliminates *rad52* repair-defective cells.

4. Materials and Methods

4.1 Materials

4.1.1 Yeast strains used in this study

All yeast strains used in this thesis are derivatives of S288C background, specifically BY4743 (*MATa/MATalpha his3Δ1 / his3Δ1 leu2Δ0/ leu2Δ0 ura3Δ0 / ura3Δ0 MET15 / met15Δ0 LYS2 / lys2Δ0*), and BY4741 (*MATa his3Δ1 leu2Δ0 met15Δ0 ura3Δ0*) (Winston et al., 1995), unless indicated otherwise. The *rad52 / rad52* strains that were treated with X-rays and 2 μM CPT were not frozen as a cryostock, because they have rapidly undergone chromosome loss events and therefore had unstable genotype.

Table 4.1.1. List of yeast strains used in this study.

Database name	Genotype	Source
YBL1	MATa/MATalpha his3Δ1 / his3Δ1 leu2Δ0/ leu2Δ0 ura3Δ0 / ura3Δ0 MET15 / met15Δ0 LYS2 / lys2Δ0	Euroscarf
YBL7	MATa his3Δ1 leu2Δ0 ura3Δ0 met15Δ0 lys2Δ0	This study
YBL8	MATa *lys1 cry1*	Matthias Peter
YBL9	MATalpha *lys1*	Matthias Peter
YJK1052	MATa/MATalpha *CDC5::cdc5-ad (URA) / CDC5::cdc5-ad (URA)*	Julia Klermund
YJK1056	MATa/MATalpha *RAD52::KAN CDC5::cdc5-ad (URA) / RAD52::KAN CDC5::cdc5-ad (URA)*	Julia Klermund
YKB262	MATa/MATalpha *RAD52::KAN CDC5::cdc5-ad (URA) / RAD52::KAN CDC5::cdc5-ad (URA)*	Katharina Bender
YKB258	MATa/MATalpha *RAD52::KAN / RAD52::KAN*	Katharina Bender
YKB262	MATa/MATalpha *RAD52::KAN CDC5::cdc5-ad (URA) / RAD52::KAN CDC5::cdc5-ad (URA)*	Katharina Bender
YOV22	MATa *Hsp104-GFP HIS PDR5::NAT*	(Miller et al., 2015)
YOV54	MATa/MATalpha *Hsp104-GFP HIS / Hsp104-GFP HIS*	This study
YOV58	MATa/MATalpha *RAD52::KAN Hsp104-GFP HIS / RAD52::KAN Hsp104-GFP HIS*	This study
YOV61	MATa/MATalpha *PDR5::NAT / PDR5::NAT*	This study
YOV64	MATa/MATalpha *RAD52::KAN PDR5::NAT / RAD52::KAN PDR5::NAT*	This study
YOV36	MATa *PDR5::NAT*	This study
YOV40	MATa *RAD52::KAN PDR5::NAT*	This study
YOV233	MATa/MATalpha	This study
YOV234	MATa/MATalpha *RAD52::KAN / RAD52::KAN*	This study
YOV346	MATa/MATalpha	This study

Database name	Genotype	Source
YOV347	MATa/MATalpha *RAD52::NAT / RAD52::NAT*	This study
YOV349	MATa/MATalpha *RAD52::NAT ATG1::KAN / RAD52::NAT ATG1::KAN*	This study
YOV260	MATa/MATalpha	This study
YOV261	MATa/MATalpha *RAD52::KAN / RAD52::KAN*	This study
YOV262	MATa/MATalpha *MRE11::HIS / MRE11::HIS*	This study
YOV263	MATa/MATalpha *DNL4::HYG / DNL4::HYG*	This study
YOV264	MATa/MATalpha *RAD52::KAN DNL4::HYG / RAD52::KANN DNL4::HYG*	This study
YOV265	MATa/MATalpha *RAD52::KAN MRE11::HIS / RAD52::KAN MRE11::HIS*	This study
YOV266	MATa/MATalpha *MRE11::HIS DNL4::HYG / MRE11::HIS DNL4::HYG*	This study
YOV267	MATa/MATalpha *RAD52::KAN MRE11::HIS DNL4::HYG / RAD52::KAN MRE11::HIS DNL4::HYG*	This study
YOV235	MATa/MATalpha *RAD50::HIS / RAD50::HIS*	This study
YOV236	MATa/MATalpha *DNL4::HYG / DNL4::HYG*	This study
YOV237	MATa/MATalpha *RAD52::KAN RAD50::HIS / RAD52::KAN RAD50::HIS*	This study
YOV238	MATa/MATalpha *RAD52::KAN DNL4::HYG / RAD52::KAN DNL4::HYG*	This study
YOV239	MATa/MATalpha *RAD52::KAN RAD50::HIS DNL4::HYG / RAD52::KAN RAD50::HIS DNL4::HYG*	This study
YOV243	MATa/MATalpha *RAD51::NAT / RAD51::NAT*	This study
YOV245	MATa/MATalpha *RAD51::NAT DNL4::HYG / RAD51::NAT DNL4::HYG*	This study
YOV247	MATa/MATalpha *RAD52::KAN RAD51::NAT / RAD52::KAN RAD51::NAT*	This study
YOV249	MATa/MATalpha *RAD52::KAN RAD51::NAT DNL4::HYG / RAD52::KAN RAD51::NAT DNL4::HYG*	This study
YOV277	MATa/MATalpha	This study
YOV278	MATa/MATalpha *RAD52::KAN / RAD52::KAN*	This study
YOV279	MATa/MATalpha *RAD59::NAT / RAD59::NAT*	This study
YOV280	MATa/MATalpha *DNL4::HYG / DNL4::HYG*	This study
YOV281	MATa/MATalpha *RAD59::NAT DNL4::HYG / RAD59::NAT DNL4::HYG*	This study
YOV282	MATa/MATalpha *RAD52::KAN RAD59::NAT DNL4::HYG / RAD52::KAN RAD59::NAT DNL4::HYG*	This study
YOV283	MATa/MATalpha *RAD52::KAN DNL4::HYG / RAD52::KAN DNL4::HYG*	This study
YOV284	MATa/MATalpha *RAD52::KAN RAD59::NAT / RAD52::KAN RAD59::NAT*	This study
YOV299	MATa/MATalpha	This study
YOV300	MATa/MATalpha *RAD52::KAN / RAD52::KAN*	This study
YOV301	MATa/MATalpha *RAD55::NAT / RAD55::NAT*	This study

Database name	Genotype	Source
YOV302	MATa/MATalpha *DNL4::HYG / DNL4::HYG*	This study
YOV303	MATa/MATalpha *RAD52::KAN DNL4::HYG / RAD52::KAN DNL4::HYG*	This study
YOV304	MATa/MATalpha *RAD52::KAN RAD55::NAT / RAD52::KAN RAD55::NAT*	This study
YOV305	MATa/MATalpha *RAD55::NAT DNL4::HYG / RAD55::NAT DNL4::HYG*	This study
YOV306	MATa/MATalpha *RAD52::KAN RAD55::NAT DNL4::HYG / RAD52::KAN RAD55::NAT DNL4::HYG*	This study
YOV317	MATa/MATalpha	This study
YOV318	MATa/MATalpha *RAD1::NAT / RAD1::NAT*	This study
YOV319	MATa/MATalpha *RAD52::KAN / RAD52::KAN*	This study
YOV320	MATa/MATalpha *DNL4::HYG / DNL4::HYG*	This study
YOV321	MATa/MATalpha *RAD1::NAT DNL4::HYG / RAD1::NAT DNL4::HYG*	This study
YOV322	MATa/MATalpha *RAD52::KAN DNL4::HYG / RAD52::KAN DNL4::HYG*	This study
YOV323	MATa/MATalpha *RAD52::KAN RAD1::NAT / RAD52::KAN RAD1::NAT*	This study
YOV324	MATa/MATalpha *RAD52::KAN RAD1::NAT DNL4::HYG / RAD52::KAN RAD1::NAT DNL4::HYG*	This study
YOV326	MATa/MATalpha	This study
YOV327	MATa/MATalpha *RAD52::KAN / RAD52::KAN*	This study
YOV328	MATa/MATalpha *POL4::HIS / POL4::HIS*	This study
YOV329	MATa/MATalpha *DNL4::HYG / DNL4::HYG*	This study
YOV330	MATa/MATalpha *RAD52::KAN DNL4::HYG / RAD52::KAN DNL4::HYG*	This study
YOV331	MATa/MATalpha *POL4::HIS DNL4::HYG / POL4::HIS DNL4::HYG*	This study
YOV332	MATa/MATalpha *RAD52::KAN POL4::HIS / RAD52::KAN POL4::HIS*	This study
YOV333	MATa/MATalpha *RAD52::KAN POL4::HIS DNL4::HYG / RAD52::KAN POL4::HIS DNL4::HYG*	This study
YOV356	MATa/MATalpha *GDP-AFB2 LEU / GDP-AFB2 LEU*	This study
YOV357	MATa/MATalpha *RAD52::KAN GDP-AFB2 LEU / RAD52::KAN GDP-AFB2 LEU*	This study
YOV358	MATa/MATalpha *Mre11-AID* HYG GDP-AFB2 LEU / Mre11-AID* HYG GDP-AFB2 LEU*	This study
YOV359	MATa/MATalpha *RAD52::KAN Mre11-AID* HYG GDP-AFB2 LEU / RAD52::KAN Mre11-AID* HYG GDP-AFB2 LEU*	This study
YOV394	MATa his3Δ1 leu2Δ0 ura3Δ0 met15Δ0	(Pavelka et al., 2010)
YOV395	MATa/MATa his3Δ1 / his3Δ1 leu2Δ0 / leu2Δ0 ura3Δ0 / ura3Δ0 MET15 / met15Δ0 LYS2 / lys2Δ0	Rong Li

Database name	Genotype	Source
YOV396	MATa/MATalpha his3Δ1 / his3Δ1 leu2Δ0 / leu2Δ0 ura3Δ0 / ura3Δ0 MET15 / met15Δ0 LYS2 / lys2Δ0	(Pavelka et al., 2010)
YOV397	MATa/MATa his3Δ1 leu2Δ0 ura3Δ0 met15Δ0 lys2Δ0 disome for Chr. III	this study
YOV399	MATa/MATalpha his3Δ1 leu2Δ0 ura3Δ0 met15Δ0 lys2Δ0 disome for Chr. III and Chr.XII	(Mulla et al., 2017)
YOV415	Mata-inc/MATalpha *ade2-1 /- can1-100 /- his3Δ3'(20bp)-HOcs(117) / his3Δ200 leu2::his3Δ5'-HOcs(117) / leu2-3,112/- trp1-1/trp1::KANMX-GALHO* URA3 / *URA3::TRP1 RAD52::LEU2 / RAD52::LEU2*	(Meyer et al., 2015)
YOV420	MATa/MATa his3Δ1 leu2Δ0 ura3Δ0 met15Δ0 lys2Δ0 *RAD52::HIS* disome for Chr. III	this study
YOV425	MATa/MATalpha his3Δ1 leu2Δ0 ura3Δ0 met15Δ0 lys2Δ0 *RAD52::HIS* disome for Chr. III	this study
YOV435	MATa/MATalpha *CKB2::HYG / CKB2::HYG*	this study
YOV436	MATa/MATalpha *RAD52::KAN CKB2::HYG / RAD52::KAN CKB2::HYG*	this study
YOV490	MATa/MATalpha	this study
YOV492	MATa/MATalpha *TEL1::HYG / TEL1::HYG*	this study
YOV493	MATa/MATalpha *RAD52::KAN / RAD52::KAN*	this study
YOV494	MATa/MATalpha *MRE11::HIS / MRE11::HIS*	this study
YOV497	MATa/MATalpha *RAD52::KAN TEL1::HYG / RAD52::KAN TEL1::HYG*	this study
YOV498	MATa/MATalpha *MRE11::HIS TEL1::HYG / MRE11::HIS TEL1::HYG*	this study
YOV500	MATa/MATalpha *RAD52::KAN MRE11::HIS TEL1::HYG / RAD52::KAN MRE11::HIS TEL1::HYG*	this study
YOV501	MATa/MATalpha *RAD52::KAN MRE11::HIS / RAD52::KAN MRE11::HIS*	this study
YOV503	MATa/MATalpha *rho*$^-$	this study
YOV505	MATa/MATalpha *RAD52::KAN / RAD52::KAN rho*$^-$	this study
YOV514	MATa/MATalpha	this study
YOV515	MATa/MATalpha *RAD52::NAT / RAD52::NAT*	this study
YOV516	MATa/MATalpha *SAE2::KAN / SAE2::KAN*	this study
YOV518	MATa/MATalpha *RAD52::NAT SAE2::KAN / RAD52::NAT SAE2::KAN*	this study
YOV538	MATa/MATalpha *MRE11::HIS / MRE11::HIS* pRS315	this study
YOV540	MATa/MATalpha *MRE11::HIS / MRE11::HIS* pRS315-*MRE11*	this study
YOV542	MATa/MATalpha *MRE11::HIS / MRE11::HIS* pRS315-*mre11-D56N*	this study
YOV544	MATa/MATalpha *MRE11::HIS / MRE11::HIS* pRS315-*mre11-H125N*	this study
YOV546	MATa/MATalpha *RAD52::KAN MRE11::HIS / RAD52::KAN MRE11::HIS* pRS315	this study

Database name	Genotype	Source
YOV548	MATa/MATalpha *RAD52::KAN MRE11::HIS / RAD52::KAN MRE11::HIS* pRS315-*MRE11*	this study
YOV550	MATa/MATalpha *RAD52::KAN MRE11::HIS / RAD52::KAN MRE11::HIS* pRS315-*mre11-D56N*	this study
YOV552	MATa/MATalpha *RAD52::KAN MRE11::HIS / RAD52::KAN MRE11::HIS* pRS315-*mre11-H125N*	this study
YOV570	MATa/MATalpha pRS315-GFP-ATG8	this study
YOV571	MATa/MATalpha *RAD52::NAT / RAD52::NAT* pRS315-GFP-ATG8	this study
YOV572	MATa/MATalpha *RAD52::NAT ATG1::KAN / RAD52::NAT ATG1::KAN* pRS315-GFP-ATG8	this study
YOV575	MATa/MATalpha	this study
YOV576	MATa/MATalpha *MRE11::HIS / MRE11::HIS*	this study
YOV577	MATa/MATalpha *RAD52::KAN / RAD52::KAN*	this study
YOV578	MATa/MATalpha *RAD53::rad53-11 (URA) / RAD53::rad53-11 (URA)*	this study
YOV579	MATa/MATalpha *MRE11::HIS RAD53::rad53-11 (URA) / MRE11::HIS RAD53::rad53-11 (URA)*	this study
YOV581	MATa/MATalpha *RAD52::KAN MRE11::HIS / RAD52::KAN MRE11::HIS*	this study
YOV582	MATa/MATalpha *RAD52::KAN RAD53::rad53-11 (URA) / RA52::KAN RAD53::rad53-11 (URA)*	this study
YOV583	MATa/MATalpha *RAD52::KAN MRE11::HIS RAD53::rad53-11 (URA) / RA52::KAN MRE11::HIS RAD53::rad53-11 (URA)*	this study
YOV585	MATa/MATalpha *XRS2::KAN / XRS2::KAN* pRS315	this study
YOV587	MATa/MATalpha *XRS2::KAN / XRS2::KAN* pRS315-*XRS2*	this study
YOV589	MATa/MATalpha *XRS2::KAN / XRS2::KAN* pRS315-*xrs2-S47A, H50A*	this study
YOV591	MATa/MATalpha *RAD52::NAT XRS2::KAN / RAD52::NAT XRS2::KAN* pRS315	this study
YOV593	MATa/MATalpha *RAD52::NAT XRS2::KAN / RAD52::NAT XRS2::KAN* pRS315-*XRS2*	this study
YOV595	MATa/MATalpha *RAD52::NAT XRS2::KAN / RAD52::NAT XRS2::KAN* pRS315-*xrs2-S47A, H50A*	this study

4.1.2 List of oligonucleotides

This list contains sequences of oligonucleotides used for the following purposes and abbreviated accordingly:

1. Gene knock-out: KO
2. Endogenous tagging: Tag
3. Confirmation of the knock-out: KO-confirm
4. qPCR for chromosome copy number: qPCR
5. Plasmid construction: Cloning
6. *MAT* locus PCR: MAT
7. MMEJ reporter strain confirmation: MMEJ

The FO abbreviates forward oligonucleotide; the RO abbreviates reverse oligonucleotide.

Table 4.1.2. List of oligonucleotides used in this study.

Name	Sequence (5' → 3')	Application
oBL29	ctgcagcgaggagccgtaat	KO-confirm; RO to verify *KANMX*, *HISMX*, *NATMX* cassette; binds to TEF promoter
oKB52	tttcaggatcacgagcgccatcta	pPCR; FO binds to the left arm of chromosome II
oKB53	cggcaagtgtctcactgttgcatt	pPCR; RO binds to the left arm of chromosome II
oKB54	ttgtttctgtccttgccacagctc	pPCR; FO binds to the left arm of chromosome III
oKB55	agcgcctttacctcaacctaccat	pPCR; RO binds to the left arm of chromosome III
oKB56	agccctagttgcagatcatcgtgt	pPCR; FO binds to the left arm of chromosome IV
oKB57	agaatatacggcaacagtgcccga	pPCR; RO binds to the left arm of chromosome IV
oKB58	tccgccggcaactgtaactgtaaa	pPCR; FO binds to the left arm of chromosome V
oKB59	atagtaaccaacgagagcgcgcaa	pPCR; RO binds to the left arm of chromosome V
oKB60	gcgcttatgtaaggttcctgtatggt	pPCR; FO binds to the left arm of chromosome VI
oKB61	agtgcggattcatttccaagcagc	pPCR; RO binds to the left arm of chromosome VI
oKB62	tgtgcgtcttccctaaagcagcta	pPCR; FO binds to the left arm of chromosome VII
oKB63	gcattggatgcgatgagatggcaa	pPCR; RO binds to the left arm of chromosome VII
oKB64	ttgtcggtctagccgaaaggtgtt	pPCR; FO binds to the left arm of chromosome VIII
oKB65	agttctgcggcagtaatgtagggt	pPCR; RO binds to the left arm of chromosome VIII
oKB66	aaagttggcgctgggtactttgag	pPCR; FO binds to the left arm of chromosome IX
oKB67	agaactgatggcatttgatggccg	pPCR; RO binds to the left arm of chromosome IX
oKB68	atttaccggttagtgtcagcgcca	pPCR; FO binds to the left arm of chromosome X
oKB69	cgacagagtagtttatgccgagggtt	pPCR; RO binds to the left arm of chromosome X
oKB70	agctggtgatgagccaaatgtcgt	pPCR; FO binds to the left arm of chromosome XI
oKB71	tttagagcaagcgcctttgtgagc	pPCR; RO binds to the left arm of chromosome XI

Name	Sequence (5' → 3')	Application
oKB72	tggagatgaagggttgtcgttggt	pPCR; FO binds to the left arm of chromosome XII
oKB73	acgtgtagcgtttctgctggtctt	pPCR; RO binds to the left arm of chromosome XII
oKB74	aaccgtctttcgagcagttgaagg	pPCR; FO binds to the left arm of chromosome XIII
oKB75	acaacagcgggaactaagtgcaga	pPCR; RO binds to the left arm of chromosome XIII
oKB76	gggattaacaatacggtaaaggga cg	pPCR; FO binds to the left arm of chromosome XIV
oKB77	caaccactgtcagcacaaactcct	pPCR; RO binds to the left arm of chromosome XIV
oKB78	atttaggctgcacggctcagttct	pPCR; FO binds to the left arm of chromosome XV
oKB79	ctaggttcactgctttggcacaca	pPCR; RO binds to the left arm of chromosome XV
oKB80	aagagccttgaacttctcgggtga	pPCR; FO binds to the left arm of chromosome XVI
oKB81	tgatgttcctctcgtttggcactc	pPCR; RO binds to the left arm of chromosome XVI
oOV14	atatacccagctaccgtttcttctt	KO; FO to confirm *RAD55* deletion
oOV15	tgtatgccttctaacgaattacaca	KO; RO to confirm *RAD55* deletion
oOV18	ctttattttgcgacttttcttcatc	KO; FO to confirm *RAD1* deletion
oOV19	ttggtgtagctaaaacatgcaataa	KO; RO to confirm *RAD1* deletion
oOV20	acggatgaaatcctgtatattcaaa	KO; FO to confirm *POL4* deletion
oOV21	gaaatttctcaccttcgatctcata	KO; RO to confirm *POL4* deletion
oOV52	gacggatattcttggaagtctccttgct aagaaaagaaaacgtacgctgca ggtcgac	Tag; FO for *MRE11* with Auxin-inducible degron
oOV53	gttataaataggatataatataatata gggatcaagtacaaatcgatgaatt cgagctcg	Tag; RO for *MRE11* with Auxin-inducible degron
oOV54	actgacgaagaggacgctagttatg	FO for Mre11-AID verification
oOV101	atgcaaacaaggaggttgccaaga actgctgaaggttctggtggctttggt gtgttgttgcgtacgctgcaggtcgac gga	KO; FO for *RAD52* deletion
oOV102	aggattttggagtaataaataatgatg caaatttttatttgtttcggccaggaa gcgttatcgatgaattcgagctcgtt	KO; RO for *RAD52* deletion
oOV103	gattcaacaactcccttggcgtc	KO; FO to confirm *RAD52* deletion

Name	Sequence (5' → 3')	Application
oOV104	caaccttcgatgtatgcaatcctg	KO; RO to confirm *RAD52* deletion
oOV105	agtcacatcaagatcgtttatgg	MAT; FO that binds 1695-1673 nucleotides directed towards *MAT* locus
oOV106	gcacggaatatgggactacttcg	MAT; RO that binds sequence within alpha-specific DNA
oOV107	actccacttcaagtaagagtttg	MAT; RO that binds sequence within a-specific DNA
oOV108	tccgctgcacggtcctgttccc	MMEJ; FO to amplify *HIS3Δ3* split reporter
oOV109	accagccggaatgcttggccag	MMEJ; RO to amplify *HIS3Δ3* split reporter
oOV113	atgacagagcagaaagccct	MMEJ; FO to amplify reciprocal translocation restored *HIS3* ORF
oOV114	gaacacctttggtggaggga	MMEJ; RO to amplify reciprocal translocation restored *HIS3* ORF; RO to amplify *HIS3Δ5* split reporter
oOV125	tcaggatttgcgcctttggatga	MMEJ; FO to amplify *HIS3Δ5* split reporter
oOV136	gatatcgaattcctgcagcccgggg gatcctagaggatgaacagatgtga agaagaaacg	Cloning; FO to amplify genomic *MRE11* 800 bp upstream from start codon and clone into pRS315
oOV137	gagctccaccgcggtggcggccgct ctagagctatgcatattcctatcacag ttaacg	Cloning; RO to amplify genomic *MRE11* 400 bp downstream from stop codon and clone into pRS315
oOV138	tgtacagtccggtaatctttttcacgtg aataagcctt	Cloning; FO to introduce *MRE11-D56N* mutation
oOV140	tcggcatatcaggtaataatgatgat gcgtcggg	Cloning; FO to introduce *MRE11-H125N* mutation
oOV144	taattaaaaatgataaaagtattgcc agacaggctatcacattcaaatgg	Cloning; FO to introduce *XRS2-S47A, H50A* mutations
oOV146	gctggtggaggcaaatatct	KO; FO to confirm *XRS2* deletion
oOV147	ggctactgtgtttcagatccg	KO; RO to confirm *XRS2* deletion
oOV152	ccaccgcggtggcggccgctctaga gactatgcatctctttaacaggcg	Cloning; FO to amplify genomic *XRS2* 939 bp upstream from start codon and clone into pRS315
oOV157	cgaattcctgcagcccgggggatcc gagccagcacagcttattatc	Cloning; RO to amplify genomic *XRS2* 380 bp downstream from stop codon and clone into pRS315

Name	Sequence (5' → 3')	Application
oOV158	aaggcttattcacgtgaaaaagattaccggactgtaca	Cloning; RO to introduce *MRE11-D56N* mutation
oOV159	cccgacgcatcatcattattacctgatatgccga	Cloning; RO to introduce *MRE11-H125N* mutation
oOV160	ccatttgaatgtgatagcctgtctggcaatacttttatcatttttaatta	Cloning; RO to introduce *XRS2-S47A, H50A* mutations

4.1.3 Plasmids

Plasmid name	Description	Source
pBL186	pRS423-GAL-HIS3, empty vector	(Mumberg et al., 1995)
pBL211	pRS425-GAL-LEU2, empty vector	(Mumberg et al., 1995)
pBL299	pRS41-hygB, empty vector	(Taxis and Knop, 2006)
pBL303	pRS42-KAN, empty vector	(Taxis and Knop, 2006)
pBL304	pRS42-NAT, empty vector	(Taxis and Knop, 2006)
pJK34	pRS315-GFP-ATG8	(Klermund et al., 2014)
pBL454	pSM409-pHyg-AID*-9MYC	(Morawska and Ulrich, 2013)
pBL252	pFA6A-HIS3MX6	(Longtine et al., 1998)
pBL95	pRS315-LEU2, empty vector	(Sikorski and Hieter, 1989)
pBL623	pRS315-MRE11	this study
pBL625	pRS315-MRE11-D56N	this study
pBL626	pRS315-MRE11-H125N	this study
pBL629	pRS315-XRS2	this study
pBL631	pRS315-XRS2-S47A,H50A	this study

4.1.4 Liquid media composition

Medium	Composition
Lysogeny broth medium (LB)	1 % (w/v) sodium chloride 1 % (w/v) bacto tryptone 0.5 % (w/v) bacto yeast extract 100 µg/mL carbenicillin
Yeast peptone dextrose medium (YPD)	2 % (w/v) peptone 1 % (w/v) bacto yeast extract 2 % (w/v) glucose
Yeast peptone raffinose (2 % Raff-YP)	2 % (w/v) peptone 1 % (w/v) yeast extract 2.36 % (w/v) raffinose pentahydrate
Yeast peptone galactose raffinose (2 % Gal1 % Raff-YP)	2 % (w/v) peptone 1 % (w/v) Bacto yeast extract 1.18 % (w/v) raffinose pentahydrate 2 % (w/v) galactose
Synthetic complete w/o aminoacid (SC-AA)	0.192 % (w/v) yeast synthetic dropout w/o aminoacid 0.67 % (w/v) yeast nitrogen base without amino acids 2 % (w/v) glucose
Sporulation medium (SPO)	1 % potassium acetate 0.005 % zinc acetate

4.1.5 Agar plates

Plate	Compostion
Yeast peptone dextrose (YPD) plates	6.5 % (w/v) YPD agar
Synthetic complete w/o aminoacid (SC-AA) plates	0.192 % (w/v) yeast synthetic dropout w/o amino acid 0.67 % (w/v) yeast nitrogen base without amino acids 2 % (w/v) glucose 2.4 % (w/v) agar
Synthetic complete w/o aminoacid (SC-AA) plus antibiotic plates	0.192 % (w/v) yeast synthetic dropout w/o amino acid 0.17 % (w/v) yeast nitrogen base without amino acids and ammonium sulfate 0.1 % (w/v) monosodium glutamate 2 % (w/v) glucose 2 % (w/v) agar Antibiotic (see table 5.1.6)
Presporulation plates	3 % (w/v) standard nutrient broth 1 % (w/v) bacto yeast extract 2 % (w/v) agar 5 % (w/v) glucose
Lysogeny broth medium plates	1 % (w/v) tryptone 0.5 % (w/v) bacto yeast extract 1 % (w/v) sodium chloride 1.5 % (w/v) agar

4.1.6 Antibiotics and other plate add-inns

Substance	Concentration
G418 disulfate solution	250 µg/mL
Nourseothricin-dihydrogen sulfate	100 µg/mL
Hygromycin B	300 µg/mL
Carbenicillin	100 µg/mL
Phloxine B	8 µg/mL

4.1.7 Buffers and solutions

Buffer or Solution	Composition	Application
Solution 1	1.85 M NaOH, 1.09 M 2-mercaptoethanol	Protein extraction
Solution 2	50 % trichloroacetic acid (TCA)	Protein extraction
Solution 3	100 % Acetone	Protein extraction
Urea buffer	120 mM Tris-HCl pH 6.8, 5 % glycerol, 8 M urea, 143 mM 2-mercaptoethanol, 8 % SDS, bromophenol blue	Protein extraction
SDS running buffer (10x)	25 mM Tris, 192 mM glycine, 0.1 % SDS, pH 8.3	Western blotting
Blotting buffer	25 mM Tris, 192 mM glycine	Western blotting
PBS (10x)	1.37 M NaCl, 0.03 M KCl, 0.08 M Na_2HPO_4 x 2 H_2O, 0.02 M KH_2PO4, pH 7.4	Western blotting
PBST (10x)	1 x PBS, 0.1 % Tween-20	Western blotting
Milk blocking buffer	5 % (w/v) skim milk powder in 1 x PBST	Western blotting
BSA blocking buffer	3 % (w/v) bovine serum albumin (BSA) in 1 x PBST	Western blotting
LiAC mix	0.1 M lithium acetate, 1 x TE solution	Transformation
PEG mix	40 % (w/v) PEG 400, dissolved in LiAc mix	Transformation
Potassium phosphate buffer 6.4	28 mM K_2HPO_4, 72 mM KH_2PO_4, pH 6.4	Microscopy
Potassium phosphate buffer 6.6	38 mM K_2HPO_4, 62 mM KH_2PO_4, pH 6.6	Microscopy
Potassium phosphate buffer 7.4	82 mM K_2HPO_4, 18 mM KH_2PO_4, pH 7.4	Microscopy

Buffer or Solution	Composition	Application
Formaldehyde fixation solution	2.5 % (w/v) Formaldehyde in potassium phosphate buffer 6.4	Microscopy
Cytometry solution	50 mM Tris-Cl, pH 7.5	Flow cytometry
DNA loading buffer (6x)	15 % Ficoll, 10 mM EDTA pH 8.0, Orange G	Loading buffer
TE (10x)	0.1 M Tris-HCl pH 7.5, 10 mM EDTA pH 8.0	other
TBE (10x)	0.89 M Tris base, 0.89 M boric acid, 0.02 M EDTA pH 8.0	other

4.1.8 Commercially available reagents

Reagent	Supplier
1 kb DNA ladder	New England Biolabs
100 bp DNA ladder	New England Biolabs
3-Indoleacetic acid	Sigma-Aldrich
4′,6-Diamidino-2-phenylindole dihydrochloride (DAPI)	Sigma-Aldrich
Agar	Sigma-Aldrich
Agarose	Sigma-Aldrich
Bacto Yeast	BD Biosciences
Bovine Serum Albumin (BSA)	Sigma-Aldrich
Bromphenol blue	Sigma-Aldrich
Camptothecin (CPT)	Sigma-Aldrich
Carbenicillin disodium	Sigma-Aldrich
Concanavalin A	Sigma-Aldrich
Dimethyl sulfoxide (DMSO)	Sigma-Aldrich
Ethanol, absolute	Sigma-Aldrich
Formaldehyde 37 %	AppliChem
G418 disulfate solution	AppliChem
Glucose (D+)	AppliChem
Glycerol	Thermo Scientific
Hygromycin B	InvivoGen

Reagent	Supplier
L-glutamic acid monosodium salt hydrate	Sigma-Aldrich
MG132	Sigma-Aldrich
Mini-Protean TGX stain free precast gels (7.5/10/4-15 %)	Bio-Rad
Nitrocellulose membrane	GE Healthcare
Nourseothricin dihydrogen sulfate (ClonNaT)	WERNER BioAgents
Peptone	Sigma-Aldrich
Ploxine B	Sigma-Aldrich
Poly(ethylenglycol) 400 (PEG)	Sigma-Aldrich
Ponceau S	Sigma-Aldrich
Potassium phosphate dibasic	Sigma-Aldrich
Potassium phosphate monobasic	Sigma-Aldrich
Prestained Protein Marker, Broad range (11-190 kDa)	New England Biolabs
Radicicol	Apex Bio
Raffinose x 5 H2O (D+)	AppliChem
Rapamycin	Selleckchem
Skim milk powder	Sigma-Aldrich
Sodium acetate (NaAc)	Sigma-Aldrich
Sodium dodecyl sulfate (SDS)	AppliChem
Sodium hydroxide	Sigma-Aldrich
SuperSignal West Pico Chemiluminescent Substrate	Thermo Scientific
SYBR Safe DNA gel stain	Thermo Scientific
Sytox Green	Thermo Scientific
Trichloroacetic acid (TCA)	Sigma-Aldrich
Tris (Trizma base)	Sigma-Aldrich
Tween-20	Sigma-Aldrich
Urea	Sigma-Aldrich
Yeast nitrogen base w/o amino acids	Difco
Yeast nitrogen base without amino acids and ammonium sulfate	Difco

Reagent	Supplier
Yeast synthetic dropout medium supplement without amino acid (SC or SD)	MP Biomedicals
Yeastmarker carrier DNA	Clontech
β-Mercaptoethanol	Sigma-Aldrich

4.1.9 Enzymes, commercially available kits and other small equipment

Reagent	Supplier	Catalogue number
2x Phusion® HF Mastermix GC buffer	New England Biolabs	M0532S
2x Q5® High-Fidelity Master Mix	New England Biolabs	M0492L
2x Taq Mastermix	New England Biolabs	M0270L
2x Gibson assembly enzyme mix	CF Protein production, IMB	N/A
Lyticase	Sigma-Aldrich	L4025-25KU
RNAse A	Thermo Scientific	10753721
Proteinase K	NeoLab	1151ML010
XbaI restriction enzyme	New England Biolabs	R0145S
BamHI restriction enzyme	New England Biolabs	R0136S
DyNAmo Flash SYBR Green qRT-PCR Kit	Thermo Scientific	10334009
QIAprep Spin Miniprep Kit	Qiagen	27106
QIAquick PCR Purification Kit	Qiagen	28106
Gentra Puregene Yeast/Bacterial Kit	Qiagen	158567
Trans-Blot® Turbo™ RTA Midi Nitrocellulose Transfer Kit	Bio-Rad	1704271
Hard-Shell® 384-Well PCR plates	Bio-Rad	HSP3805
Neubauer cell counting chamber	Assistent Germany	40442
CellCarrier™ 96 well plate	Perkin Elmer	6005550
Tissue culture plate, 96 well	Falcon	353072

4.1.10 Antibodies

Antibodies	Dilution	Source
Primary antibodies		
mouse anti-Rad53 EL7.E1	1:16	Gift from M. Foiani
mouse anti-Rad53 EL7.E1	1:1000	Abcam, ab166859
mouse anti-Pgk1	1:200 000	Invitrogen, #459250
rabbit anti-Rnr3	1:300	Agrisera, #AS09 574
mouse anti-actin	1:2000	Millipore, MAB1501R
rabbit anti-tubulin	1:3000	Abcam, ab184970
rabbit anti-Sch9	1:20000	Gift from R. Loewith
mouse anti-phospho Sch9	1:10000	Gift from R. Loewith
mouse anti-GFP	1:1000	Roche Diagnostics via Sigma-Aldrich, # 11814460001
mouse anti-Cdc5	1:300	Gift from E. Schiebel
Secondary antibodies		
goat anti-mouse (HRP conjugate)	1:3000	Bio-Rad, #170-5047
goat anti-rabbit (HRP conjugate)	1:3000	Bio-Rad, #170-5046
goat anti-rabbit and anti-mouse IRDye 680	1:10 000	Licor, #926-68071 and #926-68070
goat anti-rabbit and anti-mouse IRDye 800	1:10 000	Licor, #926-32211 and #926-32210

4.1.11 Electronic equipment

Device	Supplier
BD FACSVerse	Becton Dickinson
BioRuptor Pico	Diagenode
ChemiDoc Touch Imaging System	BioRad
Dissection Microscope MSM 400	Singer Instruments
Faxitron CellRad	Faxitron
NanoDrop 2000	Thermo Scientific
Odyssey CLx Imaging system	Licor
Opera Phenix High-Content Screening System	PerkinElmer
Real Time PCD Detection System CFX384 Touch	BioRad
Sonifier 450	Branson

Device	Supplier
Spark® microplate reader	TECAN
Spectrophotometer Ultraspec 2100 pro	Biochrom
Thermal Cycler C1000 Touch	BioRad
Western blot equipment and PowerPac Basic	BioRad

4.1.12 Software

Software	Supplier
Adobe Illustrator 2020	Adobe
CFX Manager™	Bio-Rad
Excel 2016	Microsoft
FACSuite 1.0.5	Becton Dickinson
FileMaker Pro 10	FileMaker Inc
GraphPadPrism 8	GraphPad
Harmony High-Content Imaging and Analysis Software	PerkinElmer
ImageJ 1.52g	open source
Image Lab V5	BioRad
ImageStudio	LI-COR
Mendeley Desktop	Elsevier
Word 2016	Microsoft

4.2 Methods

4.2.1 Yeast strains culture and construction procedures

Yeast background. Almost all yeast strains used in this study are derived from S288C (*SUC2 gal2 mal2 mel flo1 flo8-1 hap1 ho bio1 bio6*) yeast background, specifically BY4741 (*MATa his3Δ1 leu2Δ0 met15Δ0 ura3Δ0*), and BY4743 (*MATa/MATalpha his3Δ1 / his3Δ1 leu2Δ0/ leu2Δ0 ura3Δ0 / ura3Δ0 MET15 / met15Δ0 LYS2 / lys2Δ0*) (Winston et al., 1995). The exception is yOV415 strain obtained from Wolf-Dieter Heyer lab (Meyer et al., 2015), which is a derivative from W303 yeast background (*MATa/MATalpha leu2-3,112 trp1-1 can1-100 ura3-1 ade2-1 his3-11,15* [phi+]). All strains in this study are homozygous diploid unless indicated otherwise.

Genotoxin treatment procedures. Treatment with X-rays was performed using Faxitron CellRad (Faxitron) system. Cells were plated onto YPD agar plates, and irradiated in ADC mode with the following settings: 0.9 Gy / min at 130 kV and 5 mA. The 0.5 mM Aluminum filter was used to filter lower energy X-rays. Plates were incubated at 30°C for 4 to 5 days.
Chronic treatment with 2 μM Camptothecin (CPT) was performed as following: cells were plated onto CPT-containing plates, and incubated at 30°C for 7 to 8 days. Afterwards, in order to recover all the viable cells, single colonies were patched onto YPD plates and incubated at 30°C for 5 days.

Yeast culture procedures. Yeast strains were inoculated from single colonies or patches (when indicated), and grown overnight at 30°C in liquid yeast YPD or SC-AA media with orbital shaking. For the experiments with the X-ray treated *rad52* mutants, single colonies were always used. The CPT treated *rad52* mutants were always inoculated from patch, with exceptions (Figure 2e, Figure 20).

Tetrad dissection. Heterozygous diploid strains that have desired gene knock-outs or alleles were patched onto Presporulation plates and grown for 24 h at 30°C. Then cells were transferred into liquid Sporulation medium (SPO culture), and sporulated for 3 to 7 days at 23°C. To prepare the cultures for the tetrad dissection, 15 μL of SPO culture was mixed with 15 μL of Lyticase enzyme mix, and incubated for 15 minutes at room temperature. The tetrads were dissected on YPD plates using MSM 400 dissection microscope, and grown for 3 days at 30°C.

Creation of homozygous diploid strains. Isogenic haploids of *MATa* and *MATα* were mixed in liquid YPD medium at 30 °C for 5 h. Diploids were picked based on morphology using MSM 400 dissection microscope (Singer Instruments), and grown on YPD plates at 30°C for 3 days. The diploid state was conformed either using flow cytometry, or with *MAT* locus PCR.

PCR based gene knock-out. The disomic *rad52* aneuploid strain was created using PCR-based knock-out strategy (Janke et al., 2004). Briefly, the *HIS3MX6* cassette was amplified from pBL252 (pFA6A-*HIS3MX6*) with oOV101 and oOV102 primer pairs. The reaction contained 1x Phusion HF master mix, 200 ng of DNA template, and 500 nM of each primer in a final volume of 50 µL. The following PCR cycling conditions were used: 3 min at 98°C; 35 cycles of 30 sec at 98°C, 30 sec at 58°C, 60 sec at 72°C; the final extension of 5 min at 72°C. The correct size of the PCR product was verified on the1% agarose gel containing 1:20000 of SYBR Safe. The competent yeast strains were transformed with 5 µL of the PCR product using LiAc yeast transformation protocol (see below). The positive *rad52* knock-outs were selected with oOV101 and oBL29 primer pair using colony PCR technique (see below).

Creation of strains with an Auxin inducible degron. The strains were created as described in (Morawska and Ulrich, 2013). Briefly, AID*-9MYC-HYGMX cassette was amplified from pBL454 (pSM409-pHyg-AID*-9MYC) with oOV52 and oOV53 primer pairs. The reaction contained 1x Phusion HF master mix, 100 ng of DNA template, and 500 nM of each primer in a final volume of 50 µL. The following PCR cycling conditions were used: 3 min at 98°C; 35 cycles of 30 sec at 98°C, 60 sec at 58°C, 2 min 40 sec at 72°C; the final extension of 5 min at 72°C. The correct size of the PCR product was verified on the 1% agarose gel containing 1:20000 of SYBR Safe. The competent yeast strains were transformed with 5 µL of the PCR product using LiAc yeast transformation protocol (see below). In order to select positive mutants, I verified the presence of the degron tag with oOV54 and oBL29 primer pair using colony PCR technique (see below). I additionally verified that the Mre11 protein is degraded upon the addition of 1 mM IAA (auxin) using western blotting.

Yeast transformation using LiAc mix. Yeast cells were grown to exponential cultures (0.6 to 0.8 O.D.600) in total volume of 30 mL in liquid YPD medium at 30°C. Cultures were centrifuged at 4000 g, washed once with 5 mL of LiAc mix, and resuspended in 250 µL of LiAc mix. The transformation reaction contained 100 µL of cells in LiAc mix, 700 µL of PEG mix, 10 µL of Yeastmaker Carrier DNA, 7 µL DMSO, and 100-200 ng of plasmid DNA, or 5 µL of PCR reaction. The transformation reaction was incubated for 30 min at room temperature with rotation, and subsequently heat shocked for 15 min at 42°C. To recover the transformants, cells were pelleted at 4000 g, and resuspended in 300 µL YPD. To recover the clones after a transformation with a plasmid, cells were incubated for 2 h at 30°C, and plated on a selective media for 3 days. To recover mutants transformed for an endogenous genome modifications, cells were plated onto YPD plate and incubated overnight at 30°C. In the morning, cells were replica-plated onto the selective plate, and incubated for 3 days at 30°C.

Bacterial transformation. The competent Escherichia coli in DH5α background were mixed on ice with 100 ng of plasmid DNA, and incubated for 30 min. Afterwards, the bacteria were heat shocked for 60 sec at 42 °C, and put on ice. To recover positive transformants, bacteria were mixed with 300 µL of LB media (w/o antibiotic) and incubated at 37°C for 30 min. To select the successful transformants, cells were disposed onto LB plates containing antibiotic, and grown overnight at 37°C.

Yeast and bacterial cryostocks. In order to store the mutants long-term at -80°C, cryostock yeast cultures were created by mixing a colony of a desired yeast mutant with 730 µL of YPD media and 270 µL of 70% glycerol. The bacterial cryostocks were created by mixing 500 µL of bacterial cultures with 200 µL of 70% glycerol.

4.2.2 Plasmids construction

MRE11 was amplified by PCR from genomic DNA of a wild type strain from position -800 bp to +400 bp relative to the coding sequence with oOV136 and oOV137 primers using Q5® High-Fidelity DNA polymerase. The PCR conditions were the following: 5 min at 95°C; 35 cycles of 10 sec at 95°C, 10 sec at 66°C, 3 min 40 sec at 72°C; the final extension of 5 min at 72°C. In order to introduce *mre11-D56N* mutation, *MRE11* gene was amplified using oOV136 plus oOV158, and oOV138 plus oOV137 primer pairs, yielding two PCR products with overlapping sequences that contain the mutation. In order to introduce *mre11-H125N* mutation, *MRE11* gene was amplified using oOV136 plus oOV159, and oOV140 plus oOV137 primer pairs, producing overlapping PCR products. The PCR conditions for all the reactions above were the following: 5 min at 95°C; 35 cycles of 10 sec at 95°C, 10 sec at 63°C, 2 min at 72°C; the final extension of 5 min at 72°C. *XRS2* gene was amplified by PCR from genomic DNA from position -939 bp to +380 bp relative to the coding sequence with oOV152 and oOV157 primers. The PCR conditions were the following: 5 min at 95°C; 35 cycles of 10 sec at 95°C, 10 sec at 63°C, 3 min 40 sec at 72°C; the final extension of 5 min at 72°C. In order to introduce *xrs2-S47A, H50A* mutations, *XRS2* gene was amplified using oOV152 plus oOV160, and oOV144 plus oOV157 primer pairs, yielding two PCR products with overlapping sequences that contain the mutation. The PCR conditions were the following: 5 min at 95°C; 35 cycles of 10 sec at 95°C, 10 sec at 63°C, 2 min at 72°C; the final extension of 5 min at 72°C. All PCR reactions contained 1x Q5® High-Fidelity DNA polymerase (New England Biolabs) Master Mix, 500 nM each primer, and 100 ng of genomic DNA template. Centromeric vector pRS315 was linearized with XbaI and BamHI restriction enzymes. PCR products were purified using QIAquick PCR Purification Kit according to the manufacturer's instructions. PCR products were cloned into linearized pRS315 vector using enzymatic assembly (Gibson et al.,

2009) (Gibson enzymatic assembly master mix was produced *in house* by Protein Production Core Facility). To do so, 50 ng of linearized vector was mixed with an appropriate amount of the desired insert in 1:5 molar ratio, with an addition of 1x of Gibson enzymatic assembly master mix in total volume of 10 µL. The reaction was incubated at 50°C for 30 minutes, and transformed into DH5α bacteria. The presence of desired mutations was verified with Sanger sequencing.

4.2.3 Colony PCR

Colony PCR for mutant verification. A fraction of single colony was boiled in 0.02 M NaOH solution at 100 °C for 10 min. The cell debris was pelleted using table-top centrifuge. The PCR reaction contained 1x Taq polymerase master mix, 2 µL of colony supernatant, 1 µL of each primer (500 nM final concentration), and water in total volume of 20 µL. The cycling conditions were the following: 3 min at 98°C; 35 cycles of 30 sec at 98°C, 30 sec at 58°C, 60 sec at 72°C; the final extension of 5 min at 72°C. To determine whether the PCR products have correct size, they were separated on the1% agarose gel containing 1:20000 of SYBR Safe.

Colony PCR to determine *MAT* type. The colony was boiled in 0.02 M NaOH solution at 100 °C for 10 min. The cell debris was pelleted using table-top centrifuge. Each PCR reaction contained 1x Q5® High-Fidelity DNA polymerase master mix, 2 µL of colony supernatant, 1 µL of oOV105, 1 µL of oOV106, and 1 µL of oOV107 primers (500 nM each), in total volume of 20 µL. The cycling conditions were the following: 3 min at 98°C; 35 cycles of 10 sec at 98°C, 30 sec at 61°C, 60 sec at 72°C; the final extension of 5 min at 72°C. To determine whether the PCR products have correct size, they were separated on the 1% agarose gel containing 1:20000 of SYBR Safe. PCR with the *MATa* template DNA generates 544 bp product, and PCR with *MATalpha* template DNA generates 404 bp product. The PCR on DNA from diploid *MATa / MATalpha* cells generates both products. This assay was performed using a previously published oligonucleotides (Huxley et al., 1990).

Colony PCR to select for *his3Δ3* and *his3Δ5* MMEJ substrates. To select *rad52* mutants that retained *his3Δ3* MMEJ substrate, single colonies were boiled in 0.02 M NaOH solution at 100 °C for 10 min. The cell debris was pelleted using table-top centrifuge. Each PCR reaction contained 1x Q5® High-Fidelity DNA polymerase master mix, 2 µL of colony supernatant, 1 µL of oOV108, 1 µL of oOV109 primers (500 nM each), in total volume of 20 µL. The cycling conditions were the following: 3 min at 98°C; 35 cycles of 10 sec at 98°C, 30 sec at 65°C, 60 sec at 72°C; the final extension of 5 min at 72°C.

To select *rad52* mutants that retained *his3Δ5* MMEJ substrate, similar colony PCR procedure was performed. Each PCR reaction contained 1x Q5® High-Fidelity DNA polymerase master mix, 2 µL of colony supernatant, 1 µL of oOV125, 1 µL of oOV114 primers (500 nM each), in total volume

of 20 µL. The cycling conditions were identical to the ones for *his3Δ3* MMEJ substrate. To determine whether the PCR products were of correct size, they were separated on the 1% agarose gel containing 1:20000 of SYBR Safe.

4.2.4 qPCR to determine chromosome copy numbers

The qPCR assay was performed using previously published oligonucleotide pairs as described (Pavelka et al., 2010). Briefly, the primers in the study were designed to bind non-coding regions in the areas proximal to the centromere (≤25 kb) on each arm of each of the 16 yeast chromosomes. In this analysis I have used primers that bound to the left arm of each of the 16 chromosomes. The chromosome I was excluded from the analysis, as unfortunately the primer pair designed for this chromosome produced multiple unspecific products in our PCR conditions. The amplicon size was restricted to 75-150 bp, and the optimal Tm was 60°C.

To prepare samples for the qPCR, the genomic DNA was extracted from the exponential cultures using Gentra Puregene Yeast/Bacterial Kit according to the manufacturer's instructions. The qPCR reactions were set up in Hard-Shell® 384-Well PCR plates in a Real Time PCD Detection System CFX384 qPCR machine. Each PCR reaction was carried out in a technical triplicate. Each reaction contained 1x SYBR Green qRT-PCR master mix, 1 µL of each of oligo from a primer set for a single chromosome (500 mM final concentration), and 50 ng of genomic DNA in a total volume of 10 µL. The cycling conditions were the following: 95 °C for 5 min followed by 40 cycles of 95 °C for 15 seconds and 60 °C for 1 min. Dissociation curves were performed to verify that no unspecific product was generated.

The data analysis was performed in CFX Manager™ software. Ct values were determined automatically in a regression mode. To determine Chromosome copy numbers, the modified version of a classical ΔΔCt method was used (Livak and Schmittgen, 2001). First, I have excluded the Ct values that showed strong deviation in a technical triplicate. Then, I have averaged Ct values within the technical triplicate using the following formula:

$$Ct_{i,j,k} = \frac{\sum_{l=1}^{N_{i,j,k}} Ct_{i,j,k}}{N_{i,j,k}}$$

in which: i - the biological sample

j - the chromosome,

k - the qPCR assay,

l - the technical replicate,

$N_{i,j,k}$ - the number of technical replicates available for sample I chromosome j and assay k.

I have compared the Ct values of wild type controls with the Ct values of the aneuploid for each respective chromosome. This first ΔCt was obtained according to the formula:

$$\Delta Ct_{i,j,k} = Ct_{i,j,k} - Ct_{wt,j,k}$$

in which $Ct_{wt,j,k}$ is a mean Ct value of wild type control sample that was measured in the same experiment on the same plate. Afterwards, I have calculated the ΔΔCt values, which allowed us to normalize the measurement for the loading differences:

$$\Delta\Delta Ct = \Delta Ct_{i,j,k} - median(\Delta Ct)$$

in which $median(\Delta Ct)$ is the median value of $Ct_{i,j,k}$. Finally, I have calculated an absolute chromosome copy number using the following formula:

$$ACN_{i,j,k} = 2^{-\Delta\Delta Cti,j,k} * ploidy_i$$

in which $ploidy_i$ was determined using flow cytometry.

4.2.5 Colony formation assay and statistical analysis

Single colonies were inoculated in 5 mL of liquid YPD media and grown overnight at 30°C. The cell count in the overnight culture was determined using a Neubauer counting chamber. Briefly, 10 µL of cells were diluted in 990 µL of water, applied into the chamber, and manually counted using a light field microscope at 10x magnification. The average number of 4 quadrants counted was multiplied by a dilution factor. I have plated 300 cells onto YPD and 2 µM CPT plates in a technical duplicate. For the mutants that are extremely sensitive to X-rays, I plated 3000 cells per plate that was irradiated (or 300 for a control untreated plate). I have incubated plates at 30°C for 3 to 8 days, as described in section 5.2.1 (genotoxin treatment procedures). To calculate the % survival upon the genotoxic treatment conditions, I divided the average number of colonies formed on treated plates to the average number of colonies formed on control YPD plate within the same genotype.

Statistical analysis was performed in two steps. First, I confirmed that the data are normally distributed using Shapiro-Wilk test, and have comparale heterogeneity of variances using Brown-Forsythe test. Next, I performed the statistical analysis with one-way ANOVA test with Tukey's post-hoc test using GraphPadPrism 9 software. If the genotype and treatment represented two different factors (Figure 17d), I have applied two-way ANOVA test with Tukey's post-hoc instead.

4.2.6 MMEJ reporter assay

The MMEJ reporter assay was performed as described (Meyer et al., 2015) with minor modifications. I first selected CPT resistant *rad52* mutants that retained both *his3Δ3* and *his3Δ5* split reporter sequences using colony PCR described in section 5.2.3. I inoculated single colonies in 5 mL of 2% Raff-YP media and grew them overnight at 30°C. In the morning, the media was exchanged to 2%Gal1%Raff-YP to induce the expression of HO nuclease. After 4 h of induction, cells were resuspended in 2 mL of 2% Raff-YP and plated onto SD-His plates to select for histidine prototrophs. The 1:10 000 dilution of cultures were plated on YPD to estimate the total number of viable cells. Plates were incubated at 30 °C for 4 to 6 days. MMEJ rates were calculated by dividing the number of histidine prototrophs by the number of viable cells. The median frequency of interchromosomal MMEJ was estimated based on 24 to 30 independent colonies.

4.2.7 Growth curve assay and statistical analysis

Single colonies were inoculated, and overnight cultures were grown in 5 mL of liquid YPD media at 30 °C. The OD600nm of the overnight culture was measured in 100 µL culture volume in 96 well plate (Tissue culture plate, Falcon®) using Spark® microplate reader (TECAN). The cultures were diluted to 0.05 OD600nm units in 100 µL YPD with the addition of either DMSO, or respective drugs. Each measurement was repeated in technical triplicate. Cultures were grown at 30 °C overnight with orbital shaking in a 96 well plate (Tissue culture plate, Falcon®) in the Spark® microplate reader. The growth dynamics of the cultures was monitored by measuring OD600nm every hour, with a prior orbital shaking to ensure the even cells distribution. The population doubling time was calculated from an average values of technical replicates at the exponential part of the growth curve using an algorithm from (Roth V, 2006), Doubling Time Computing. The formula for the doubling time calculation was the following:

$$Doubling\ time = \frac{duration * \log(2)}{\log(C_{final}) - \log(C_{initial})}$$

in which C_{final} is the final O.D.600nm in which the culture is still exponential, and $C_{initial}$ is the initial O.D.600nm in which the culture is exponential. The $duration$ means the time frame in which the culture was in an exponential growth phase.

For the statistical analysis, all groups were randomly downsampled to the size of the smallest group. The normality of the data was tested using the Shapiro-Wilk test, and to test for homogeneity of variances, the Fligner-Killeen test was applied. Because the data were neither normally distributed nor had equal variances, the Scheirer-Ray-Hare test (an extension of the Kruskal-Wallis test and, thus, a non-parametric alternative to the two-way ANOVA (Scheirer et al.,

1976) was applied and followed by Dunn's post-hoc test. For all pairwise comparisons between the groups, the Mann-Whitney U test with Bonferroni correction was applied.

4.2.8 Spot assay

Cultures were inoculated in 10 mL of liquid YPD media and grown at 30°C overnight. In the morning, the O.D.600nm was measured using a spectrophotometer. The culture volume corresponding to 0.5 units at OD600nm were diluted in sterile water, and later diluted in a serial manner in 1:10 proportion. Afterwards, 4 µL of the diluted cultures were spotted onto agar plates, and grown at 30°C for 2 to 6 days, unless indicated otherwise. The images of the plates were taken with ChemiDoc™ Touch Imaging System. The images were processed using Image Lab V5 software.

4.2.9 High throughput fluorescence microscopy and data analysis

Overnight cultures were grown in 5 mL of liquid YPD media at 25 °C. In the morning, cultures were diluted to 0.2 OD600nm units in 5 mL YPD media, and grown to exponential phase for 3 h at 25 °C and afterwards shifted to 37 °C. The heat stress response was monitored during 3 h at 37°C, during which one mL of liquid culture was collected per time point. Cells were pelleted by centrifugation at 4,000 g for 3 minutes. Afterwards, cells were fixed for 10 min at room temperature in formaldehyde fixation solution, washed twice with potassium phosphate buffer pH6.6, and stored in potassium phosphate buffer pH7.4 at 4 °C for maximum of 4 weeks. Prior to microscopy, cells were permeabilized with 80 % ethanol for 10 min at room temperature, and resuspended in 500 µL potassium phosphate buffer pH7.4 containing 0.5 µg/mL DAPI. Samples were loaded onto 96-well plates (CellCarrier®, PerkinElmer) pre-coated with concanavalin A.

Imaging was performed using High-Content Screening Opera PhenixTM microscope (PerkinElmer) in confocal mode, using a water objective with 63x magnification. Fifteen independent fields with five planes each were imaged for each sample. Acquired images were analysed with Harmony High-Content Imaging and Analysis Software (version 4.4, PerkinElmer) using standard building blocks. First, nuclei were identified with algorithm M based on the DAPI signal. Second, cytoplasm was identified with algorithm A based on GFP signal. Cellular morphology properties were calculated with standard built-in algorithm, and cell roundness was set to 65 %. Spot detection of GFP foci was performed in the cytoplasm region of the cell with algorithm C. Cells on the periphery of images were excluded from analysis. I have analysed data on the single cell level, with at least 3,000 cells per sample. The percentage of cell population that had one or more Hsp104-GFP foci was calculated using a custom script in Microsoft Excel 2017.

The data were visualized with the GraphPadPrism software package. Representative images were processed using ImageJ 1.52g software.

4.2.10 SDS-PAGE and western blot analysis

Proteins were extracted using TCA extraction protocol. Briefly, cell amount corresponding to 1 or 2 units of O.D.600nm were collected from liquid cultures by centrifugation at 17000g for 2 minutes. Cell pellets were stored at -20°C prior to the extraction procedure. The pellets were resuspended in 150 µL of solution 1 and kept on ice for 10 minutes. After the addition of 150 µL of solution 2, samples were vigorously mixed by vortexing, and incubated for 10 more minutes on ice. The samples were cleared by centrifugation at 17000g for 2 minutes at 4°C. The pellets were washed with 1 mL of solution 3, and resuspended in 100 µL of urea buffer. Proteins were denatured at 75°C for 5 minutes.

Proteins were separated on 7.5 % or 4-15 % Mini-PROTEAN® TGX Stain-Free™ precast polyacrylamide gels (Bio-Rad) in 1x SDS running buffer using Mini-PROTEAN® electrophoresis chambers (Bio-Rad). The stain-free images of the gels were obtained using ChemiDoc™ Touch Imaging System in 45 seconds UV light activation and autoexposure image acquisition mode. Gels were blotted onto 0.45 µm pore size nitrocellulose membrane by semi-dry blot using the Trans-Blot® Turbo™ Transfer System (Bio-Rad) with the pre-set 10 min blotting program for high molecular weight proteins. The blotting efficiency was verified using Ponceau S staining. The membranes were blocked in milk blocking buffer for 1 hour at room temperature. The membranes were incubated with primary antibodies solutions overnight at 4°C, with the exception of anti Cdc5 antibody, which was incubated for 1.5 h at room temperature. The primary antibodies were diluted in milk blocking solution, with the exception of anti-Sch9, anti-phospho-Sch9, and anti Cdc5 antibodies, which were diluted in 3% BSA in PBST solution. After three washes for 15 minutes at room temperature with PBST, the membranes were incubated with the secondary antibodies for 1.5 h at room temperature. The supplementary table 5.1.10 contains the information about primary and secondary antibodies dilutions.

Proteins were visualized by chemiluminescence using SuperSignal West Pico Chemiluminescent Substrate on a ChemiDoc™ Touch imaging system (Bio-Rad). Alternatively, proteins were detected on an Odyssey CLx Imaging system (Licor).

Western blot quantification. Images taken with the ChemiDoc™ Touch Imaging System (Bio-Rad) were quantified using the Image Lab software (version 5.2.1) (Bio-Rad). The chemiluminescence signal (defined as area under the curve) from the membrane incubated with Cdc5 antibody was normalized to the corresponding total lane signal from the Mini-PROTEAN®

TGX Stain-Free™ precast polyacrylamide gels (Bio-Rad) that were activated for 45 seconds with UV light. Afterwards, in order to calculate the relative Cdc5p levels in each mutant tested, the relative signal of wild type clone “a” from each independent gel was set to one.

4.2.11 DNA content analysis using flow cytometry

Cells in amounts equivalent to 0.18 OD600nm units were harvested by centrifugation at 17000g for 1 minute. Cells were washed once in 1 mL water, and resuspended in 1 mL of 70% ethanol. The pellets were stored in ethanol at 4°C prior to the analysis. Afterwards, samples were centrifuged at 17000g for 1 minute, and washed in 1 mL water. Pellets were resuspended in 500 µL 50 mM Tris-HCl pH 7.5 containing 10 mg/mL RNase A and incubated at 37 °C for 3 h or overnight. Sfterwards, 25 µL of 1 mg/mL Proteinase K was added to samples, and incubated at 50 °C for 45 min. In order to break apart cell aggregates, samples were sonified with ultrasound for 2 cycles 30 sec each using Bioruptor Pico (Diagenode). Subsequently, 500 µL 50 mM Tris-HCl pH 7.5 containing 2 µM Sytox Green was added (final concentration 1 µM), cells were transferred to round bottom tubes (Falcon) and analysed on a FACSVerse flow cytometer (BD) using FACS Suite software (BD).

References

Abreu, C.M., Kumar, R., Hamilton, D., Dawdy, A.W., Creavin, K., Eivers, S., Finn, K., Balsbaugh, J.L., O'Connor, R., Kiely, P.A., et al. (2013). Site-Specific Phosphorylation of the DNA Damage Response Mediator Rad9 by Cyclin-Dependent Kinases Regulates Activation of Checkpoint Kinase 1. PLoS Genet. *9*, e1003310.

Agmon, N., Liefshitz, B., Zimmer, C., Fabre, E., and Kupiec, M. (2013). Effect of nuclear architecture on the efficiency of double-strand break repair. Nat. Cell Biol. *15*, 694–699.

Ahrabi, S., Sarkar, S., Pfister, S.X., Pirovano, G., Higgins, G.S., Porter, A.C.G., and Humphrey, T.C. (2016). A role for human homologous recombination factors in suppressing microhomology-mediated end joining. Nucleic Acids Res. *44*, 5743–5757.

Alcasabas, A.A., Osborn, A.J., Bachant, J., Hu, F., Werler, P.J.H., Bousset, K., Furuya, K., Diffley, J.F.X., Carr, A.M., and Elledge, S.J. (2001). Mrc1 transduces signals of DNA replication stress to activate Rad53. Nat. Cell Biol. *3*, 958–965.

Alexander, A., Cai, S.L., Kim, J., Nanez, A., Sahin, M., MacLean, K.H., Inoki, K., Guan, K.L., Shen, J., Person, M.D., et al. (2010). ATM signals to TSC2 in the cytoplasm to regulate mTORC1 in response to ROS. Proc. Natl. Acad. Sci. U. S. A. *107*, 4153–4158.

Alexander, J.L., Beagan, K., Orr-Weaver, T.L., and McVey, M. (2016). Multiple mechanisms contribute to double-strand break repair at rereplication forks in Drosophila follicle cells. Proc. Natl. Acad. Sci. U. S. A. *113*, 13809–13814.

Alexandru, G., Uhlmann, F., Mechtler, K., Poupart, M.A., and Nasmyth, K. (2001). Phosphorylation of the cohesin subunit Scc1 by Polo/Cdc5 kinase regulates sister chromatid separation in yeast. Cell *105*, 459–472.

Allen, J.B., Zhou, Z., Siede, W., Friedberg, E.C., and Elledge, S.J. (1994). The SAD1/RAD53 protein kinase controls multiple checkpoints and DNA damage-induced transcription in yeast. Genes Dev. *8*, 2401–2415.

Anand, R., Ranjha, L., Cannavo, E., and Cejka, P. (2016). Phosphorylated CtIP Functions as a Co-factor of the MRE11-RAD50-NBS1 Endonuclease in DNA End Resection. Mol. Cell *64*, 940–950.

Anand, R.P., Lovett, S.T., and Haber, J.E. (2013). Break-induced DNA replication. Cold Spring Harb. Perspect. Biol. *5*, a010397–a010397.

Anand, R.P., Tsaponina, O., Greenwell, P.W., Lee, C.S., Du, W., Petes, T.D., and Haber, J.E. (2014). Chromosome rearrangements via template switching between diverged repeated sequences. Genes Dev. *28*, 2394–2406.

Andor, N., Graham, T.A., Jansen, M., Xia, L.C., Aktipis, C.A., Petritsch, C., Ji, H.P., and Maley, C.C. (2016). Pan-cancer analysis of the extent and consequences of intratumor heterogeneity. Nat. Med. *22*, 105–113.

Andreassen, P., and Ren, K. (2009). Fanconi Anemia Proteins, DNA Interstrand Crosslink Repair Pathways, and Cancer Therapy. Curr. Cancer Drug Targets *9*, 101–117.

Ariyoshi, K., Miura, T., Kasai, K., Fujishima, Y., Oshimura, M., and Yoshida, M.A. (2016). Induction of genomic instability and activation of autophagy in artificial human aneuploid cells. Mutat. Res. - Fundam. Mol. Mech. Mutagen. *790*, 19–30.

Arroyo, M., Cañuelo, A., Calahorra, J., Hastert, F.D., Sánchez, A., Clarke, D.J., and Marchal, J.A. (2020). Mitotic entry upon Topo II catalytic inhibition is controlled by Chk1 and Plk1. FEBS J. febs.15280.

Asakawa, K., Yoshida, S., Otake, F., and Toh-e, A. (2001). A novel functional domain of Cdc15 kinase is required for its interaction with Tem1 GTPase in saccharomyces cerevisiae. Genetics *157*, 1437–1450.

Asano, S., Park, J.E., Sakchaisri, K., Yu, L.R., Song, S., Supavilai, P., Veenstra, T.D., and Lee, K.S. (2005). Concerted mechanism of Swe1/Wee1 regulation by multiple kinases in budding yeast. EMBO J. *24*, 2194–2204.

Awad, S., Ryan, D., Prochasson, P., Owen-Hughes, T., and Hassan, A.H. (2010). The Snf2 homolog Fun30 acts as a homodimeric ATP-dependent chromatin-remodeling enzyme. J. Biol. Chem. *285*, 9477–9484.

Bacal, J., Moriel□Carretero, M., Pardo, B., Barthe, A., Sharma, S., Chabes, A., Lengronne, A., and Pasero, P. (2018). Mrc1 and Rad9 cooperate to regulate initiation and elongation of DNA replication in response to DNA damage. EMBO J. *37*.

Baldo, V., Testoni, V., Lucchini, G., and Longhese, M.P. (2008). Dominant TEL1-hy Mutations Compensate for Mec1 Lack of Functions in the DNA Damage Response. Mol. Cell. Biol. *28*, 358–375.

Balmus, G., Pilger, D., Coates, J., Demir, M., Sczaniecka-Clift, M., Barros, A.C., Woods, M., Fu, B., Yang, F., Chen, E., et al. (2019). ATM orchestrates the DNA-damage response to counter toxic non-homologous end-joining at broken replication forks. Nat. Commun. *10*, 87.

Balzi, E., Wang, M., Leterme, S., Van Dyck, L., and Goffeau, A. (1994). PDR5, a novel yeast multidrug resistance conferring transporter controlled by the transcription regulator PDR1. J. Biol. Chem. *269*, 2206–2214.

Banin, S., Moyal, L., Shieh, S.Y., Taya, Y., Anderson, C.W., Chessa, L., Smorodinsky, N.I., Prives, C., Reiss, Y., Shiloh, Y., et al. (1998). Enhanced phosphorylation of p53 by ATM in response to DNA damage. Science (80-.). *281*, 1674–1677.

Barazas, M., Annunziato, S., Pettitt, S.J., de Krijger, I., Ghezraoui, H., Roobol, S.J., Lutz, C., Frankum, J., Song, F.F., Brough, R., et al. (2018). The CST Complex Mediates End Protection at Double-Strand Breaks and Promotes PARP Inhibitor Sensitivity in BRCA1-Deficient Cells. Cell Rep. *23*, 2107–2118.

Barbet, N.C., Schneider, U., Helliwell, S.B., Stansfield, I., Tuite, M.F., and Hall, M.N. (1996). TOR controls translation initiation and early G1 progression in yeast. Mol. Biol. Cell *7*, 25–42.

Barton, O., Naumann, S.C., Diemer-Biehs, R., Künzel, J., Steinlage, M., Conrad, S., Makharashvili, N., Wang, J., Feng, L., Lopez, B.S., et al. (2014). Polo-like kinase 3 regulates CtIP during DNA double-strand break repair in G1. J. Cell Biol. *206*, 877–894.

Bashkirov, V.I., Bashkirova, E. V., Haghnazari, E., and Heyer, W.-D. (2003). Direct Kinase-to-Kinase Signaling Mediated by the FHA Phosphoprotein Recognition Domain of the Dun1 DNA Damage Checkpoint Kinase. Mol. Cell. Biol. *23*, 1441–1452.

Bazzichetto, C., Conciatori, F., Falcone, I., and Ciuffreda, L. (2020). Translational Landscape of mTOR Signaling in Integrating Cues Between Cancer and Tumor Microenvironment. In Advances in Experimental Medicine and Biology, pp. 69–80.

Beach, R.R., Ricci-Tam, C., Brennan, C.M., Moomau, C.A., Hsu, P. hsin, Hua, B., Silberman,

R.E., Springer, M., and Amon, A. (2017). Aneuploidy Causes Non-genetic Individuality. Cell *169*, 229-242.e21.

Beaupere, C., Dinatto, L., Wasko, B.M., Chen, R.B., VanValkenburg, L., Kiflezghi, M.G., Lee, M.B., Promislow, D.E.L., Dang, W., Kaeberlein, M., et al. (2018). Genetic screen identifies adaptive aneuploidy as a key mediator of ER stress resistance in yeast. Proc. Natl. Acad. Sci. U. S. A. *115*, 9586–9591.

Beck, T., and Hall, M.N. (1999). The TOR signalling pathway controls nuclear localization of nutrient- regulated transcription factors. Nature *402*, 689–692.

Ben-David, U., and Amon, A. (2020). Context is everything: aneuploidy in cancer. Nat. Rev. Genet. *21*, 44–62.

Ben-David, U., and Benvenisty, N. (2012). High prevalence of evolutionarily conserved and species-specific genomic aberrations in mouse pluripotent stem cells. Stem Cells *30*, 612–622.

Ben-David, U., Ha, G., Khadka, P., Jin, X., Wong, B., Franke, L., and Golub, T.R. (2016). The landscape of chromosomal aberrations in breast cancer mouse models reveals driver-specific routes to tumorigenesis. Nat. Commun. *7*, 12160.

Ben-David, U., Ha, G., Tseng, Y.Y., Greenwald, N.F., Oh, C., Shih, J., McFarland, J.M., Wong, B., Boehm, J.S., Beroukhim, R., et al. (2017). Patient-derived xenografts undergo mouse-specific tumor evolution. Nat. Genet. *49*, 1567–1575.

Ben-David, U., Siranosian, B., Ha, G., Tang, H., Oren, Y., Hinohara, K., Strathdee, C.A., Dempster, J., Lyons, N.J., Burns, R., et al. (2018). Genetic and transcriptional evolution alters cancer cell line drug response. Nature *560*, 325–330.

Bender, K. (2018) Understanding the differential consequences of checkpoint adaptation following DNA damage in repair-proficient and repair-deficient cells. Doctoral dissertation, Ruperto-Carola University of Heidelberg, Germany.

Bennardo, N., Cheng, A., Huang, N., and Stark, J.M. (2008). Alternative-NHEJ is a mechanistically distinct pathway of mammalian chromosome break repair. PLoS Genet. *4*, e1000110.

Berchtold, D., and Walther, T.C. (2009). TORC2 plasma membrane localization is essential for cell viability and restricted to a distinct domain. Mol. Biol. Cell *20*, 1565–1575.

Berens, T.J., and Toczyski, D.P. (2012). Colocalization of Mec1 and Mrc1 is sufficient for Rad53 phosphorylation in vivo. Mol. Biol. Cell *23*, 1058–1067.

Beroukhim, R., Mermel, C.H., Porter, D., Wei, G., Raychaudhuri, S., Donovan, J., Barretina, J., Boehm, J.S., Dobson, J., Urashima, M., et al. (2010). The landscape of somatic copy-number alteration across human cancers. Nature *463*, 899–905.

Bétous, R., Goullet de Rugy, T., Pelegrini, A.L., Queille, S., de Villartay, J.P., and Hoffmann, J.S. (2018). DNA replication stress triggers Rapid DNA Replication Fork Breakage by Artemis and XPF. PLoS Genet. *14*, e1007541.

Beuzelin, C., Evnouchidou, I., Rigolet, P., Cauvet-Burgevin, A., Girard, P.M., Dardalhon, D., Culina, S., Gdoura, A., van Endert, P., and Francesconi, S. (2013). Deletion of the Fission Yeast Homologue of Human Insulinase Reveals a TORC1-Dependent Pathway Mediating Resistance to Proteotoxic Stress. PLoS One *8*, e67705.

Bhargava, R., Onyango, D.O., and Stark, J.M. (2016). Regulation of Single-Strand Annealing

and its Role in Genome Maintenance. Trends Genet. *32*, 566–575.

Binda, M., Péli-Gulli, M.P., Bonfils, G., Panchaud, N., Urban, J., Sturgill, T.W., Loewith, R., and De Virgilio, C. (2009). The Vam6 GEF Controls TORC1 by Activating the EGO Complex. Mol. Cell *35*, 563–573.

Black, S.J., Ozdemir, A.Y., Kashkina, E., Kent, T., Rusanov, T., Ristic, D., Shin, Y., Suma, A., Hoang, T., Chandramouly, G., et al. (2019). Molecular basis of microhomology-mediated end-joining by purified full-length Polθ. Nat. Commun. *10*.

Blank, H.M., Sheltzer, J.M., Meehl, C.M., and Amon, A. (2015). Mitotic entry in the presence of DNA damage is a widespread property of aneuploidy in yeast. Mol. Biol. Cell *26*, 1440–1451.

Blankley, R.T., and Lydall, D. (2004). A domain of Rad9 specifically required for activation of Chk1 in budding yeast. J. Cell Sci. *117*, 601–608.

Boddy, M.N., Gaillard, P.H.L., McDonald, W.H., Shanahan, P., Yates, J.R., and Russell, P. (2001). Mus81-Eme1 are essential components of a Holliday junction resolvase. Cell *107*, 537–548.

Bojsen, R., Regenberg, B., and Folkesson, A. (2017). Persistence and drug tolerance in pathogenic yeast. Curr. Genet. *63*, 19–22.

Bolhaqueiro, A.C.F., Ponsioen, B., Bakker, B., Klaasen, S.J., Kucukkose, E., van Jaarsveld, R.H., Vivié, J., Verlaan-Klink, I., Hami, N., Spierings, D.C.J., et al. (2019). Ongoing chromosomal instability and karyotype evolution in human colorectal cancer organoids. Nat. Genet. *51*, 824–834.

Bolzán, A.D., and Bianchi, M.S. (2018). DNA and chromosome damage induced by bleomycin in mammalian cells: An update. Mutat. Res. - Rev. Mutat. Res. *775*, 51–62.

Bonetti, D., Villa, M., Gobbini, E., Cassani, C., Tedeschi, G., and Longhese, M.P. (2015). Escape of Sgs1 from Rad9 inhibition reduces the requirement for Sae2 and functional MRX in DNA end resection . EMBO Rep. *16*, 351–361.

Bonetti, D., Colombo, C.V., Clerici, M., and Longhese, M.P. (2018). Processing of DNA ends in the maintenance of genome stability. Front. Genet. *9*.

Botchkarev, V. V., and Haber, J.E. (2018). Functions and regulation of the Polo-like kinase Cdc5 in the absence and presence of DNA damage. Curr. Genet. *64*, 87–96.

Bouwman, P., and Jonkers, J. (2012). The effects of deregulated DNA damage signalling on cancer chemotherapy response and resistance. Nat. Rev. Cancer *12*, 587–598.

Brastianos, P.K., Carter, S.L., Santagata, S., Cahill, D.P., Taylor-Weiner, A., Jones, R.T., Van Allen, E.M., Lawrence, M.S., Horowitz, P.M., Cibulskis, K., et al. (2015). Genomic characterization of brain metastases reveals branched evolution and potential therapeutic targets. Cancer Discov. *5*, 1164–1177.

Brennan, C.M., Vaites, L.P., Wells, J.N., Santaguida, S., Paulo, J.A., Storchova, Z., Harper, J.W., Marsh, J.A., and Amon, A. (2019). Protein aggregation mediates stoichiometry of protein complexes in aneuploid cells. Genes Dev. *33*, 1031–1047.

Bressan, D.A., Baxter, B.K., and Petrini, J.H.J. (1999). The Mre11-Rad50-Xrs2 Protein Complex Facilitates Homologous Recombination-Based Double-Strand Break Repair inSaccharomyces cerevisiae. Mol. Cell. Biol. *19*, 7681–7687.

Broustas, C.G., Duval, A.J., Chaudhary, K.R., Friedman, R.A., Virk, R.K., and Lieberman, H.B. (2020). Targeting MEK5 impairs nonhomologous end-joining repair and sensitizes prostate cancer to DNA damaging agents. Oncogene *39*, 2467–2477.

Brush, G.S., Morrow, D.M., Hieter, P., and Kelly, T.J. (1996). The ATM homologue MEC1 is required for phosphorylation of replication protein A in yeast. Proc. Natl. Acad. Sci. U. S. A. *93*, 15075–15080.

Budanov, A. V., and Karin, M. (2008). p53 Target Genes Sestrin1 and Sestrin2 Connect Genotoxic Stress and mTOR Signaling. Cell *134*, 451–460.

Bunting, S.F., Callén, E., Wong, N., Chen, H.T., Polato, F., Gunn, A., Bothmer, A., Feldhahn, N., Fernandez-Capetillo, O., Cao, L., et al. (2010). 53BP1 inhibits homologous recombination in brca1-deficient cells by blocking resection of DNA breaks. Cell *141*, 243–254.

Butt, G., Shahwar, D., Qureshi, M.Z., Attar, R., Akram, M., Birinci, Y., Karatoprak, G.S., Gasparri, M.L., and Farooqi, A.A. (2019). Role of mTORC1 and mTORC2 in Breast Cancer: Therapeutic Targeting of mTOR and Its Partners to Overcome Metastasis and Drug Resistance. In Advances in Experimental Medicine and Biology, pp. 283–292.

Cannavo, E., and Cejka, P. (2014). Sae2 promotes dsDNA endonuclease activity within Mre11-Rad50-Xrs2 to resect DNA breaks. Nature *514*, 122–125.

Carvalho, C.M.B., and Lupski, J.R. (2016). Mechanisms underlying structural variant formation in genomic disorders. Nat. Rev. Genet. *17*, 224–238.

Carvalho, C.M.B., Ramocki, M.B., Pehlivan, D., Franco, L.M., Gonzaga-Jauregui, C., Fang, P., McCall, A., Pivnick, E.K., Hines-Dowell, S., Seaver, L.H., et al. (2011). Inverted genomic segments and complex triplication rearrangements are mediated by inverted repeats in the human genome. Nat. Genet. *43*, 1074–1081.

Casper, A.M., Nghiem, P., Arlt, M.F., and Glover, T.W. (2002). ATR regulates fragile site stability. Cell *111*, 779–789.

Cassani, C., Gobbini, E., Wang, W., Niu, H., Clerici, M., Sung, P., and Longhese, M.P. (2016). Tel1 and Rif2 Regulate MRX Functions in End-Tethering and Repair of DNA Double-Strand Breaks. PLoS Biol. *14*.

Cassani, C., Gobbini, E., Vertemara, J., Wang, W., Marsella, A., Sung, P., Tisi, R., Zampella, G., and Longhese, M.P. (2018). Structurally distinct Mre11 domains mediate MRX functions in resection, end-tethering and DNA damage resistance. Nucleic Acids Res. *46*, 2990–3008.

Cassani, C., Vertemara, J., Bassani, M., Marsella, A., Tisi, R., Zampella, G., and Longhese, M.P. (2019). The ATP-bound conformation of the Mre11–Rad50 complex is essential for Tel1/ATM activation. Nucleic Acids Res. *47*, 3550–3567.

Ceccaldi, R., Liu, J.C., Amunugama, R., Hajdu, I., Primack, B., Petalcorin, M.I.R., O'Connor, K.W., Konstantinopoulos, P.A., Elledge, S.J., Boulton, S.J., et al. (2015). Homologous-recombination-deficient tumours are dependent on Polθ -mediated repair. Nature *518*, 258–262.

Cejka, P., Cannavo, E., Polaczek, P., Masuda-Sasa, T., Pokharel, S., Campbell, J.L., and Kowalczykowski, S.C. (2010a). DNA end resection by Dna2-Sgs1-RPA and its stimulation by Top3-Rmi1 and Mre11-Rad50-Xrs2. Nature *467*, 112–116.

Cejka, P., Plank, J.L., Bachrati, C.Z., Hickson, I.D., and Kowalczykowski, S.C. (2010b). Rmi1 stimulates decatenation of double Holliday junctions during dissolution by Sgs1-Top3. Nat. Struct. Mol. Biol. *17*, 1377–1382.

Chaudhuri, A.R., Callen, E., Ding, X., Gogola, E., Duarte, A.A., Lee, J.-E., Wong, N., Lafarga, V., Calvo, J.A., Panzarino, N.J., et al. (2016). Replication fork stability confers chemoresistance in BRCA-deficient cells. Nature *535*, 382–387.

Chen, X., and Tomkinson, A.E. (2011). Yeast Nej1 is a key participant in the initial end binding and final ligation steps of nonhomologous end joining. J. Biol. Chem. *286*, 4931–4940.

Chen, C.C., Carson, J.J., Feser, J., Tamburini, B., Zabaronick, S., Linger, J., and Tyler, J.K. (2008). Acetylated Lysine 56 on Histone H3 Drives Chromatin Assembly after Repair and Signals for the Completion of Repair. Cell *134*, 231–243.

Chen, E.S.W., Weng, J.H., Chen, Y.H., Wang, S.C., Liu, X.X., Huang, W.C., Matsui, T., Kawano, Y., Liao, J.H., Lim, L.H., et al. (2017). Phospho-Priming Confers Functionally Relevant Specificities for Rad53 Kinase Autophosphorylation. Biochemistry *56*, 5112–5124.

Chen, G., Bradford, W.D., Seidel, C.W., and Li, R. (2012a). Hsp90 stress potentiates rapid cellular adaptation through induction of aneuploidy. Nature *482*, 246–250.

Chen, G., Rubinstein, B., and Li, R. (2012b). Whole chromosome aneuploidy: Big mutations drive adaptation by phenotypic leap. BioEssays *34*, 893–900.

Chen, G., Mulla, W.A., Kucharavy, A., Tsai, H.J., Rubinstein, B., Conkright, J., McCroskey, S., Bradford, W.D., Weems, L., Haug, J.S., et al. (2015). Targeting the adaptability of heterogeneous aneuploids. Cell *160*, 771–784.

Chen, H., Lisby, M., and Symington, L.S. (2013). RPA Coordinates DNA End Resection and Prevents Formation of DNA Hairpins. Mol. Cell *50*, 589–600.

Chen, X., Niu, H., Chung, W.H., Zhu, Z., Papusha, A., Shim, E.Y., Lee, S.E., Sung, P., and Ira, G. (2011). Cell cycle regulation of DNA double-strand break end resection by Cdk1-dependent Dna2 phosphorylation. Nat. Struct. Mol. Biol. *18*, 1015–1019.

Chen, Z., Shi, T., Zhang, L., Zhu, P., Deng, M., Huang, C., Hu, T., Jiang, L., and Li, J. (2016). Mammalian drug efflux transporters of the ATP binding cassette (ABC) family in multidrug resistance: A review of the past decade. Cancer Lett. *370*, 153–164.

Cheng, L., Hunke, L., and Hardy, C.F.J. (1998). Cell cycle regulation of the Saccharomyces cerevisiae polo-like kinase cdc5p. Mol Cell Biol *18*, 7360–7370.

Chunduri, N.K., and Storchová, Z. (2019). The diverse consequences of aneuploidy. Nat. Cell Biol. *21*, 54–62.

Chung, W.H., Zhu, Z., Papusha, A., Malkova, A., and Ira, G. (2010). Defective resection at DNA double-strand breaks leads to de Novo telomere formation and enhances gene targeting. PLoS Genet. *6*, 24.

Cimini, D., Tanzarella, C., and Degrassi, F. (1999). Differences in malsegregation rates obtained by scoring ana-telophases or binucleate cells. Mutagenesis *14*, 563–568.

Clémenson, C., and Marsolier-Kergoat, M.C. (2009). DNA damage checkpoint inactivation: Adaptation and recovery. DNA Repair (Amst). *8*, 1101–1109.

Clerici, M., Paciotti, V., Baldo, V., Romano, M., Lucchini, G., and Longhese, M.P. (2001). Hyperactivation of the yeast DNA damage checkpoint by TEL1 and DDC2 overexpression. EMBO J. *20*, 6485–6498.

Clerici, M., Baldo, V., Mantiero, D., Lottersberger, F., Lucchini, G., and Longhese, M.P. (2004). A

Tel1/MRX-Dependent Checkpoint Inhibits the Metaphase-to-Anaphase Transition after UV Irradiation in the Absence of Mec1. Mol. Cell. Biol. *24*, 10126–10144.

Clerici, M., Mantiero, D., Lucchini, G., and Longhese, M.P. (2006). The Saccharomyces cerevisiae Sae2 protein negatively regulates DNA damage checkpoint signalling. EMBO Rep. *7*, 212–218.

Clerici, M., Mantiero, D., Guerini, I., Lucchini, G., and Longhese, M.P. (2008). The Yku70-Yku80 complex contributes to regulate double-strand break processing and checkpoint activation during the cell cycle. EMBO Rep. *9*, 810–818.

Clerici, M., Trovesi, C., Galbiati, A., Lucchini, G., and Longhese, M.P. (2014). Mec1/ATR regulates the generation of single-stranded DNA that attenuates Tel1/ATM signaling at DNA ends. EMBO J. *33*, 198–216.

Coïc, E., Feldman, T., Landman, A.S., and Haber, J.E. (2008). Mechanisms of Rad52-independent spontaneous and UV-induced mitotic recombination in Saccharomyces cerevisiae. Genetics *179*, 199–211.

Colombo, C.V., Menin, L., Ranieri, R., Bonetti, D., Clerici, M., and Longhese, M.P. (2019). Uncoupling SAE2 functions in downregulation of tel1 and RAD53 signaling activities. Genetics *211*, 515–530.

Di Como, C.J., and Arndt, K.T. (1996). Nutrients, via the Tor proteins, stimulate the association of Tap42 with type 2A phosphatases. Genes Dev. *10*, 1904–1916.

Di Como, C.J., Chang, H., and Arndt, K.T. (1995). Activation of CLN1 and CLN2 G1 cyclin gene expression by BCK2. Mol. Cell. Biol. *15*, 1835–1846.

Coopera, T.J., Garcia, V., and Neale, M.J. (2016). Meiotic DSB patterning: A multifaceted process. Cell Cycle *15*, 13–21.

Corbett, K.D. (2017). Molecular Mechanisms of Spindle Assembly Checkpoint Activation and Silencing. Prog. Mol. Subcell. Biol. *56*, 429–455.

Corcoran, R.B., Rothenberg, S.M., Hata, A.N., Faber, A.C., Piris, A., Nazarian, R.M., Brown, R.D., Godfrey, J.T., Winokur, D., Walsh, J., et al. (2013). TORC1 suppression predicts responsiveness to RAF and MEK inhibition in BRAF-mutant melanoma. Sci. Transl. Med. *5*, 196ra98-196ra98.

Cortez, D. (2005). Unwind and slow down: Checkpoint activation by helicase and polymerase uncoupling. Genes Dev. *19*, 1007–1012.

Costanzo, M., Nishikawa, J.L., Tang, X., Millman, J.S., Schub, O., Breitkreuz, K., Dewar, D., Rupes, I., Andrews, B., and Tyers, M. (2004). CDK activity antagonizes Whi5, an inhibitor of G1/S transcription in yeast. Cell *117*, 899–913.

Costelloe, T., Louge, R., Tomimatsu, N., Mukherjee, B., Martini, E., Khadaroo, B., Dubois, K., Wiegant, W.W., Thierry, A., Burma, S., et al. (2012). The yeast Fun30 and human SMARCAD1 chromatin remodellers promote DNA end resection. Nature *489*, 581–584.

Coutelier, H., Xu, Z., Morisse, M.C., Lhuillier-Akakpo, M., Pelet, S., Charvin, G., Dubrana, K., and Teixeira, M.T. (2018). Adaptation to DNA damage checkpoint in senescent telomerase-negative cells promotes genome instability. Genes Dev. *32*, 1499–1513.

Cristini, A., Ricci, G., Britton, S., Salimbeni, S., Huang, S. yin N., Marinello, J., Calsou, P., Pommier, Y., Favre, G., Capranico, G., et al. (2019). Dual Processing of R-Loops and

Topoisomerase I Induces Transcription-Dependent DNA Double-Strand Breaks. Cell Rep. *28*, 3167-3181.e6.

Cussiol, J.R., Jablonowski, C.M., Yimit, A., Brown, G.W., and Smolka, M.B. (2015). Dampening DNA damage checkpoint signalling via coordinated BRCT domain interactions . EMBO J. *34*, 1704–1717.

D'Amore, C., Salizzato, V., Borgo, C., Cesaro, L., Pinna, L.A., and Salvi, M. (2019). A Journey through the Cytoskeleton with Protein Kinase CK2. Curr. Protein Pept. Sci. *20*, 547–562.

Darieva, Z., Bulmer, R., Pic-Taylor, A., Doris, K.S., Geymonat, M., Sedgwick, S.G., Morgan, B.A., and Sharrocks, A.D. (2006). Polo kinase controls cell-cycle-dependent transcription by targeting a coactivator protein. Nature *444*, 494–498.

Deans, B., Griffin, C.S., O'Regan, P., Jasin, M., and Thacker, J. (2003). Homologous Recombination Deficiency Leads to Profound Genetic Instability in Cells Derived from Xrcc2-Knockout Mice. Cancer Res. *63*, 8181–8187.

Delamarre, A., Barthe, A., de la Roche Saint-André, C., Luciano, P., Forey, R., Padioleau, I., Skrzypczak, M., Ginalski, K., Géli, V., Pasero, P., et al. (2020). MRX Increases Chromatin Accessibility at Stalled Replication Forks to Promote Nascent DNA Resection and Cohesin Loading. Mol. Cell *77*, 395-410.e3.

Deng, S.K., Gibb, B., De Almeida, M.J., Greene, E.C., and Symington, L.S. (2014). RPA antagonizes microhomology-mediated repair of DNA double-strand breaks. Nat. Struct. Mol. Biol. *21*, 405–412.

Dephoure, N., Hwang, S., O'Sullivan, C., Dodgson, S.E., Gygi, S.P., Amon, A., and Torres, E.M. (2014). Quantitative proteomic analysis reveals posttranslational responses to aneuploidy in yeast. Elife *3*, e03023.

Deshmukh, R.R., Kim, S., Elghoul, Y., and Dou, Q.P. (2017). P-Glycoprotein Inhibition Sensitizes Human Breast Cancer Cells to Proteasome Inhibitors. J. Cell. Biochem. *118*, 1239–1248.

Deshpande, R.A., Williams, G.J., Limbo, O., Williams, R.S., Kuhnlein, J., Lee, J.H., Classen, S., Guenther, G., Russell, P., Tainer, J.A., et al. (2014). ATP-driven Rad50 conformations regulate DNA tethering, end resection, and ATM checkpoint signaling. EMBO J. *33*, 482–500.

Diethelm-Varela, B., Ai, Y., Liang, D., and Xue, F. (2019). Nitrogen Mustards as Anticancer Chemotherapies: Historic Perspective, Current Developments and Future Trends. Curr. Top. Med. Chem. *19*, 691–712.

Donnelly, N., and Storchová, Z. (2015). Aneuploidy and proteotoxic stress in cancer. Mol. Cell. Oncol. *2*, e976491.

Donnelly, N., Passerini, V., Durrbaum, M., Stingele, S., and Storchova, Z. (2014). HSF1 deficiency and impaired HSP90-dependent protein folding are hallmarks of aneuploid human cells. EMBO J. *33*, 2374–2387.

Donnianni, R.A., and Symington, L.S. (2013). Break-induced replication occurs by conservative DNA synthesis. Proc. Natl. Acad. Sci. U. S. A. *110*, 13475–13480.

Donnianni, R.A., Ferrari, M., Lazzaro, F., Clerici, M., Nachimuthu, B.T., Plevani, P., Muzi-Falconi, M., and Pellicioli, A. (2010). Elevated levels of the polo kinase Cdc5 override the Mec1/ATR checkpoint in budding yeast by acting at different steps of the signaling pathway. PLoS Genet. *6*, 1–14.

Dotiwala, F., Eapen, V. V., Harrison, J.C., Arbel-Eden, A., Ranade, V., Yoshida, S., and Haber, J.E. (2013). DNA damage checkpoint triggers autophagy to regulate the initiation of anaphase. Proc. Natl. Acad. Sci. U. S. A. *110*.

Downs, J.A., Lowndes, N.F., and Jackson, S.P. (2000). A role for Saccharomyces cerevisiae histone H2A in DNA repair. Nature *408*, 1001–1004.

Duan, Z., Andronescu, M., Schutz, K., McIlwain, S., Kim, Y.J., Lee, C., Shendure, J., Fields, S., Blau, C.A., and Noble, W.S. (2010). A three-dimensional model of the yeast genome. Nature *465*, 363–367.

Dunham, M.J., Badrane, H., Ferea, T., Adams, J., Brown, P.O., Rosenzweig, F., and Botstein, D. (2002). Characteristic genome rearrangements in experimental evolution of Saccharomyces cerevisiae. Proc. Natl. Acad. Sci. U. S. A. *99*, 16144–16149.

Durkin, S.G., Arlt, M.F., Howlett, N.G., and Glover, T.W. (2006). Depletion of CHK1, but not CHK2, induces chromosomal instability and breaks at common fragile sites. Oncogene *25*, 4381–4388.

Durrant, D.E., Das, A., Dyer, S., and Kukreja, R.C. (2020). A dual PI3 kinase/mTOR inhibitor BEZ235 reverses doxorubicin resistance in ABCB1 overexpressing ovarian and pancreatic cancer cell lines. Biochim. Biophys. Acta - Gen. Subj. *1864*, 129556.

Dürrbaum, M., and Storchová, Z. (2015). Consequences of aneuploidy in cancer: Transcriptome and beyond. In Chromosomal Instability in Cancer Cells, pp. 195–224.

Dürrbaum, M., and Storchová, Z. (2016). Effects of aneuploidy on gene expression: Implications for cancer. FEBS J. *283*, 791–802.

Dürrbaum, M., Kuznetsova, A.Y., Passerini, V., Stingele, S., Stoehr, G., and Storchová, Z. (2014). Unique features of the transcriptional response to model aneuploidy in human cells. BMC Genomics *15*.

Eapen, V. V., and Haber, J.E. (2013). DNA damage signaling triggers the cytoplasm-to-vacuole pathway of autophagy to regulate cell cycle progression. Autophagy *9*, 440–441.

Eapen, V. V., Sugawara, N., Tsabar, M., Wu, W.-H., and Haber, J.E. (2012). The Saccharomyces cerevisiae Chromatin Remodeler Fun30 Regulates DNA End Resection and Checkpoint Deactivation. Mol. Cell. Biol. *32*, 4727–4740.

Eapen, V. V., Waterman, D.P., Bernard, A., Schiffmann, N., Sayas, E., Kamber, R., Lemos, B., Memisoglu, G., Ang, J., Mazella, A., et al. (2017). A pathway of targeted autophagy is induced by DNA damage in budding yeast. Proc. Natl. Acad. Sci. U. S. A. *114*, E1158–E1167.

van Echten-Arends, J., Mastenbroek, S., Sikkema-Raddatz, B., Korevaar, J.C., Heineman, M.J., van der Veen, F., and Repping, S. (2011). Chromosomal mosaicism in human preimplantation embryos: A systematic review. Hum. Reprod. Update *17*, 620–627.

Edwards, S.L., Brough, R., Lord, C.J., Natrajan, R., Vatcheva, R., Levine, D.A., Boyd, J., Reis-Filho, J.S., and Ashworth, A. (2008). Resistance to therapy caused by intragenic deletion in BRCA2. Nature *451*, 1111–1115.

Elkabets, M., Vora, S., Juric, D., Morse, N., Mino-Kenudson, M., Muranen, T., Tao, J., Campos, A.B., Rodon, J., Ibrahim, Y.H., et al. (2013). MTORC1 inhibition is required for sensitivity to PI3K p110α inhibitors in PIK3CA-mutant breast cancer. Sci. Transl. Med. *5*.

Elserafy, M., Šarić, M., Neuner, A., Lin, T.C., Zhang, W., Seybold, C., Sivashanmugam, L., and

Schiebel, E. (2014). Molecular mechanisms that restrict yeast centrosome duplication to one event per cell cycle. Curr. Biol. *24*, 1456–1466.

Emerson, C.H., and Bertuch, A.A. (2016). Consider the workhorse: Nonhomologous end-joining in budding yeast1. Biochem. Cell Biol. *94*, 396–406.

Eng, W.K., Faucette, L., Johnson, R.K., and Sternglanz, R. (1988). Evidence that DNA topoisomerase I is necessary for the cytotoxic effects of camptothecin. Mol. Pharmacol. *34*, 755–760.

Enoiu, M., Jiricny, J., and Schärer, O.D. (2012). Repair of cisplatin-induced DNA interstrand crosslinks by a replication-independent pathway involving transcription-coupled repair and translesion synthesis. Nucleic Acids Res. *40*, 8953–8964.

Escribano-Díaz, C., Orthwein, A., Fradet-Turcotte, A., Xing, M., Young, J.T.F., Tkáč, J., Cook, M.A., Rosebrock, A.P., Munro, M., Canny, M.D., et al. (2013). A Cell Cycle-Dependent Regulatory Circuit Composed of 53BP1-RIF1 and BRCA1-CtIP Controls DNA Repair Pathway Choice. Mol. Cell *49*, 872–883.

Eykelenboom, J.K., Harte, E.C., Canavan, L., Pastor-Peidro, A., Calvo-Asensio, I., Llorens-Agost, M., and Lowndes, N.F. (2013). ATR Activates the S-M Checkpoint during Unperturbed Growth to Ensure Sufficient Replication Prior to Mitotic Onset. Cell Rep. *5*, 1095–1107.

Ferrari, E., Bruhn, C., Peretti, M., Cassani, C., Carotenuto, W.V., Elgendy, M., Shubassi, G., Lucca, C., Bermejo, R., Varasi, M., et al. (2017). PP2A Controls Genome Integrity by Integrating Nutrient-Sensing and Metabolic Pathways with the DNA Damage Response. Mol. Cell *67*, 266-281.e4.

Ferrari, M., Nachimuthu, B.T., Donnianni, R.A., Klein, H., and Pellicioli, A. (2013). Tid1/Rdh54 translocase is phosphorylated through a Mec1- and Rad53-dependent manner in the presence of DSB lesions in budding yeast. DNA Repair (Amst). *12*, 347–355.

Foster, S.S., Balestrini, A., and Petrini, J.H.J. (2011). Functional Interplay of the Mre11 Nuclease and Ku in the Response to Replication-Associated DNA Damage. Mol. Cell. Biol. *31*, 4379–4389.

Frank-Vaillant, M., and Marcand, S. (2001). NEHJ regulation by mating type is exercised through a novel protein, Lif2p, essential to the Ligase IV pathway. Genes Dev. *15*, 3005–3012.

Fricke, W.M., and Brill, S.J. (2003). Slx1 - Slx4 is a second structure-specific endonuclease functionally redundant with Sgs1 - Top3. Genes Dev. *17*, 1768–1778.

Fried, A.A., Kiechle, M., Maxeiner, H.G., Schiestl, R.H., and Eckardt-Schupp, F. (2010). Ty1 integrase overexpression leads to integration of non-Ty1 DNA fragments into the genome of Saccharomyces cerevisiae. Mol. Genet. Genomics *284*, 231–242.

Fry, R.C., DeMott, M.S., Cosgrove, J.P., Begley, T.J., Samson, L.D., and Dedon, P.C. (2006). The DNA-damage signature in Saccharomyces cerevisiae is associated with single-strand breaks in DNA. BMC Genomics *7*.

Furnari, B., Rhind, N., and Russell, P. (1997). Cdc25 mitotic inducer targeted by Chk1 DNA damage checkpoint kinase. Science (80-.). *277*, 1495–1497.

Furnari, B., Blasina, A., Boddy, M.N., McGowan, C.H., and Russell, P. (1999). Cdc25 inhibited in vivo and in vitro by checkpoint kinases Cds1 and Chk1. Mol. Biol. Cell *10*, 833–845.

Gaillard, H., García-Muse, T., and Aguilera, A. (2015). Replication stress and cancer. Nat. Rev.

Cancer *15*, 276–280.

Galgoczy, D.J., and Toczyski, D.P. (2001). Checkpoint adaptation precedes spontaneous and damage-induced genomic instability in yeast. Mol Cell Biol *21*, 1710–1718.

Galli, A., Chan, C.Y., Parfenova, L., Cervelli, T., and Schiestl, R.H. (2015). Requirement of POL3 and POL4 on non-homologous and microhomology-mediated end joining in rad50/xrs2 mutants of Saccharomyces cerevisiae. Mutagenesis *30*, 841–849.

Ganguly, S., Home, T., Yacoub, A., Kambhampati, S., Shi, H., Dandawate, P., Padhye, S., Saluja, A.K., McGuirk, J., and Rao, R. (2015). Targeting HSF1 disrupts HSP90 chaperone function in chronic lymphocytic leukemia. Oncotarget *6*, 31767–31779.

Gao, C., Su, Y., Koeman, J., Haak, E., Dykema, K., Essenberg, C., Hudson, E., Petillo, D., Khoo, S.K., and Vande Woude, G.F. (2016). Chromosome instability drives phenotypic switching to metastasis. Proc. Natl. Acad. Sci. U. S. A. *113*, 14793–14798.

García-Muse, T., and Aguilera, A. (2016). Transcription-replication conflicts: How they occur and how they are resolved. Nat. Rev. Mol. Cell Biol. *17*, 553–563.

Gasch, A.P., Spellman, P.T., Kao, C.M., Carmel-Harel, O., Eisen, M.B., Storz, G., Botstein, D., and Brown, P.O. (2000). Genomic expression programs in the response of yeast cells to environmental changes. Mol. Biol. Cell *11*, 4241–4257.

Gasch, A.P., Huang, M., Metzner, S., Botstein, D., Elledge, S.J., and Brown, P.O. (2001). Genomic expression responses to DNA-damaging agents and the regulatory role of the yeast ATR Homolog Mec1p. Mol. Biol. Cell *12*, 2987–3003.

Gasch, A.P., Hose, J., Newton, M.A., Sardi, M., Yong, M., and Wang, Z. (2016). Further support for aneuploidy tolerance in wild yeast and effects of dosage compensation on gene copy-number evolution. Elife *5*, 1–12.

Gates, K.S. (2009). An overview of chemical processes that damage cellular DNA: Spontaneous hydrolysis, alkylation, and reactions with radicals. Chem. Res. Toxicol. *22*, 1747–1760.

Gaubitz, C., Oliveira, T.M., Prouteau, M., Leitner, A., Karuppasamy, M., Konstantinidou, G., Rispal, D., Eltschinger, S., Robinson, G.C., Thore, S., et al. (2015). Molecular Basis of the Rapamycin Insensitivity of Target Of Rapamycin Complex 2. Mol. Cell *58*, 977–988.

Georis, I., Feller, A., Vierendeels, F., and Dubois, E. (2009). The Yeast GATA Factor Gat1 Occupies a Central Position in Nitrogen Catabolite Repression-Sensitive Gene Activation. Mol. Cell. Biol. *29*, 3803–3815.

Geymonat, M., Spanos, A., Smith, S.J.M., Wheatley, E., Rittinger, K., Johnston, L.H., and Sedgwick, S.G. (2002). Control of mitotic exit in budding yeast: In vitro regulation of Tem1 GTPase by Bub2 and Bfa1. J. Biol. Chem. *277*, 28439–28445.

Ghezraoui, H., Piganeau, M., Renouf, B., Renaud, J.B., Sallmyr, A., Ruis, B., Oh, S., Tomkinson, A.E., Hendrickson, E.A., Giovannangeli, C., et al. (2014). Chromosomal Translocations in Human Cells Are Generated by Canonical Nonhomologous End-Joining. Mol. Cell *55*, 829–842.

Giannattasio, M., Lazzaro, F., Plevani, P., and Muzi-Falconi, M. (2005). The DNA damage checkpoint response requires histone H2B ubiquitination by Rad6-Bre1 and H3 methylation by Dot1. J. Biol. Chem. *280*, 9879–9886.

Gibson, D.G., Young, L., Chuang, R.Y., Venter, J.C., Hutchison, C.A., and Smith, H.O. (2009).

Enzymatic assembly of DNA molecules up to several hundred kilobases. Nat. Methods *6*, 343–345.

Gilchrist, C., and Stelkens, R. (2019). Aneuploidy in yeast: Segregation error or adaptation mechanism? Yeast *36*, 525–539.

Gobbini, E., Cassani, C., Villa, M., Bonetti, D., and Longhese, M. (2016). Functions and regulation of the MRX complex at DNA double-strand breaks. Microb. Cell *3*, 329–337.

Gobbini, E., Cassani, C., Vertemara, J., Wang, W., Mambretti, F., Casari, E., Sung, P., Tisi, R., Zampella, G., and Longhese, M.P. (2018). The MRX complex regulates Exo1 resection activity by altering DNA end structure . EMBO J. *37*.

Gogola, E., Duarte, A.A., de Ruiter, J.R., Wiegant, W.W., Schmid, J.A., de Bruijn, R., James, D.I., Guerrero Llobet, S., Vis, D.J., Annunziato, S., et al. (2018). Selective Loss of PARG Restores PARylation and Counteracts PARP Inhibitor-Mediated Synthetic Lethality. Cancer Cell *33*, 1078-1093.e12.

González, A., and Hall, M.N. (2017). Nutrient sensing and TOR signaling in yeast and mammals . EMBO J. *36*, 397–408.

Gordon, D.J., Resio, B., and Pellman, D. (2012). Causes and consequences of aneuploidy in cancer. Nat. Rev. Genet. *13*, 189–203.

Greenberg, P., Cox, C., LeBeau, M.M., Fenaux, P., Morel, P., Sanz, G., Sanz, M., Vallespi, T., Hamblin, T., Oscier, D., et al. (1997). International scoring system for evaluating prognosis in myelodysplastic syndromes. Blood *89*, 2079–2088.

Gregan, J., Polakova, S., Zhang, L., Tolić-Nørrelykke, I.M., and Cimini, D. (2011). Merotelic kinetochore attachment: Causes and effects. Trends Cell Biol. *21*, 374–381.

Grinberg-Rashi, H., Cytron, S., Gelman-Kohan, Z., Litmanovitch, T., and Avivi, L. (2010). Replication timing aberrations and aneuploidy in peripheral blood lymphocytes of breast cancer patients. Neoplasia *12*, 668–674.

Gritenaite, D., Princz, L.N., Szakal, B., Bantele, S.C.S., Wendeler, L., Schilbach, S., Habermann, B.H., Matos, J., Lisby, M., Branzei, D., et al. (2014). A cell cycle-regulated Slx4-Dpb11 complex promotes the resolution of DNA repair intermediates linked to stalled replication. Genes Dev. *28*, 1604–1619.

Guang, M.H.Z., Kavanagh, E.L., Dunne, L.P., Dowling, P., Zhang, L., Lindsay, S., Bazou, D., Goh, C.Y., Hanley, C., Bianchi, G., et al. (2019). Targeting proteotoxic stress in cancer: A review of the role that protein quality control pathways play in oncogenesis. Cancers (Basel). *11*, 66.

Guerrero-Zotano, A., Mayer, I.A., and Arteaga, C.L. (2016). PI3K/AKT/mTOR: role in breast cancer progression, drug resistance, and treatment. Cancer Metastasis Rev. *35*, 515–524.

Guillemain, G., Ma, E., Mauger, S., Miron, S., Thai, R., Guérois, R., Ochsenbein, F., and Marsolier-Kergoat, M.-C. (2007). Mechanisms of checkpoint kinase Rad53 inactivation after a double-strand break in Saccharomyces cerevisiae. Mol. Cell. Biol. *27*, 3378–3389.

Gupta, R., Somyajit, K., Narita, T., Maskey, E., Stanlie, A., Kremer, M., Typas, D., Lammers, M., Mailand, N., Nussenzweig, A., et al. (2018). DNA Repair Network Analysis Reveals Shieldin as a Key Regulator of NHEJ and PARP Inhibitor Sensitivity. Cell *173*, 972-988.e23.

Guri, Y., and Hall, M.N. (2016). mTOR Signaling Confers Resistance to Targeted Cancer Drugs. Trends in Cancer *2*, 688–697.

Gutteridge, R.E.A., Ndiaye, M.A., Liu, X., and Ahmad, N. (2016). Plk1 inhibitors in cancer therapy: From laboratory to clinics. Mol. Cancer Ther. *15*, 1427–1435.

Gwinn, D.M., Shackelford, D.B., Egan, D.F., Mihaylova, M.M., Mery, A., Vasquez, D.S., Turk, B.E., and Shaw, R.J. (2008). AMPK Phosphorylation of Raptor Mediates a Metabolic Checkpoint. Mol. Cell *30*, 214–226.

Haber, J.E., and Hearn, M. (1985). Rad52-independent mitotic gene conversion in Saccharomyces cerevisiae frequently results in chromosomal loss. Genetics *111*, 7–22.

Han, J., Ruan, C., Huen, M.S.Y., Wang, J., Xie, A., Fu, C., Liu, T., and Huang, J. (2017). BRCA2 antagonizes classical and alternative nonhomologous end-joining to prevent gross genomic instability. Nat. Commun. *8*.

Hanahan, D., and Weinberg, R.A. (2011). Hallmarks of cancer: The next generation. Cell *144*, 646–674.

Hardie, D.G. (2014). AMPK - Sensing energy while talking to other signaling pathways. Cell Metab. *20*, 939–952.

Hassold, T., and Hunt, P. (2001). To err (meiotically) is human: The genesis of human aneuploidy. Nat. Rev. Genet. *2*, 280–291.

Hatakeyama, R., and De Virgilio, C. (2016). Unsolved mysteries of Rag GTPase signaling in yeast. Small GTPases *7*, 239–246.

Hayes, T.K., Neel, N.F., Hu, C., Gautam, P., Chenard, M., Long, B., Aziz, M., Kassner, M., Bryant, K.L., Pierobon, M., et al. (2016). Long-Term ERK Inhibition in KRAS-Mutant Pancreatic Cancer Is Associated with MYC Degradation and Senescence-like Growth Suppression. Cancer Cell *29*, 75–89.

Heitman, J., Movva, N.R., and Hall, M.N. (1991). Targets for cell cycle arrest by the immunosuppressant rapamycin in yeast. Science (80-.). *253*, 905–909.

Helliwell, S.B., Wagner, P., Kunz, J., Deuter-Reinhard, M., Henriquez, R., and Hall, M.N. (1994). TOR1 and TOR2 are structurally and functionally similar but not identical phosphatidylinositol kinase homologues in yeast. Mol. Biol. Cell *5*, 105–118.

Hernández-Vargas, H., Von Kobbe, C., Sánchez-Estévez, C., Julián-Tendero, M., Palacios, J., and Moreno-Bueno, G. (2007). Inhibition of paclitaxel-induced proteasome activation influences paclitaxel cytotoxicity in breast cancer cells in a sequence-dependent manner. Cell Cycle *6*, 2662–2668.

Heselmeyer, K., Schröck, E., Du Manoir, S., Blegen, H., Shah, K., Steinbeck, R., Auer, G., and Ried, T. (1996). Gain of chromosome 3q defines the transition from severe dysplasia to invasive carcinoma of the uterine cervix. Proc. Natl. Acad. Sci. U. S. A. *93*, 479–484.

Hicks, W.M., Kim, M., and Haber, J.E. (2010). Increased mutagenesis and unique mutation signature associated with mitotic gene conversion. Science (80-.). *329*, 82–85.

Hieronymus, H., Murali, R., Tin, A., Yadav, K., Abida, W., Moller, H., Berney, D., Scher, H., Carver, B., Scardino, P., et al. (2018). Tumor copy number alteration burden is a pan-cancer prognostic factor associated with recurrence and death. Elife *7*.

Hohl, M., Kwon, Y., Galván, S.M., Xue, X., Tous, C., Aguilera, A., Sung, P., and Petrini, J.H.J. (2010). The Rad50 coiled-coil domain is indispensable for Mre11 complex functions. Nat. Struct. Mol. Biol. *18*, 1124–1131.

Holohan, C., Van Schaeybroeck, S., Longley, D.B., and Johnston, P.G. (2013). Cancer drug resistance: an evolving paradigm. Nat. Rev. Cancer *13*, 714–726.

Hopfner, K.P., Karcher, A., Craig, L., Woo, T.T., Carney, J.P., and Tainer, J.A. (2001). Structural biochemistry and interaction architecture of the DNA double-strand break repair Mre11 nuclease and Rad50-ATPase. Cell *105*, 473–485.

Hopfner, K.P., Craig, L., Moncalian, G., Zinkel, R.A., Usui, T., Owen, B.A.L., Karcher, A., Henderson, B., Bodmer, J.L., McMurray, C.T., et al. (2002). The Rad50 zinc-hook is a structure joining Mre11 complexes in DNA recombination and repair. Nature *418*, 562–566.

Hornig, N.C.D., and Uhlmann, F. (2004). Preferential cleavage of chromatin-bound cohesin after targeted phosphorylation by Polo-like kinase. EMBO J. *23*, 3144–3153.

Hose, J., Escalante, L.E., Clowers, K.J., Dutcher, H.A., Robinson, D., Bouriakov, V., Coon, J.J., Shishkova, E., and Gasch, A.P. (2020). The genetic basis of aneuploidy tolerance in wild yeast. Elife *9*.

Hsiang, Y.H., Lihou, M.G., and Liu, L.F. (1989). Arrest of Replication Forks by Drug-stabilized Topoisomerase I-DNA Cleavable Complexes as a Mechanism of Cell Killing by Camptothecin. Cancer Res. *49*, 5077–5082.

Hu, F., Wang, Y., Liu, D., Li, Y., Qin, J., and Elledge, S.J. (2001). Regulation of the Bub2/Bfa1 GAP complex by Cdc5 and cell cycle checkpoints. Cell *107*, 655–665.

Huang, J.C., Svoboda, D.L., Reardon, J.T., and Sancar, A. (1992). Human nucleotide excision nuclease removes thymine dimers from DNA by incising the 22nd phosphodiester bond 5' and the 6th phosphodiester bond 3' to the photodimer. Proc. Natl. Acad. Sci. U. S. A. *89*, 3664–3668.

Huang, M., Zhou, Z., and Elledge, S.J. (1998). The DNA replication and damage checkpoint pathways induce transcription by inhibition of the Crt1 repressor. Cell *94*, 595–605.

Huber, A., French, S.L., Tekotte, H., Yerlikaya, S., Stahl, M., Perepelkina, M.P., Tyers, M., Rougemont, J., Beyer, A.L., and Loewith, R. (2011). Sch9 regulates ribosome biogenesis via Stb3, Dot6 and Tod6 and the histone deacetylase complex RPD3L. EMBO J. *30*, 3052–3064.

Huehls, A.M., Huntoon, C.J., Joshi, P.M., Baehr, C.A., Wagner, J.M., Wang, X., Lee, M.Y., and Karnitz, L.M. (2016). Genomically incorporated 5-fluorouracil that escapes ung-initiated base excision repair blocks dna replication and activates homologous recombination. Mol. Pharmacol. *89*, 53–62.

Huertas, P., Cortés-Ledesma, F., Sartori, A.A., Aguilera, A., and Jackson, S.P. (2008). CDK targets Sae2 to control DNA-end resection and homologous recombination. Nature *455*, 689–692.

Hughes Hallett, J.E., Luo, X., and Capaldi, A.P. (2015). Snf1/AMPK promotes the formation of Kog1/raptor-bodies to increase the activation threshold of TORC1 in budding yeast. Elife *4*.

Hurley, L.H. (2002). DNA and its associated processes as targets for cancer therapy. Nat. Rev. Cancer *2*, 188–200.

Hustedt, N., Gasser, S.M., and Shimada, K. (2013). Replication checkpoint: Tuning and coordination of replication forks in S phase. Genes (Basel). *4*, 388–434.

Illuxley, C., Green, E.D., and Dunbam, I. (1990). Rapid assessment of S. cerevisiae mating type by PCR. Trends Genet. *6*, 236.

Inoki, K., Zhu, T., and Guan, K.L. (2003). TSC2 Mediates Cellular Energy Response to Control Cell Growth and Survival. Cell *115*, 577–590.

Ip, S.C.Y., Rass, U., Blanco, M.G., Flynn, H.R., Skehel, J.M., and West, S.C. (2008). Identification of Holliday junction resolvases from humans and yeast. Nature *456*, 357–361.

Ishida, S., McCormick, F., Smith-McCune, K., and Hanahan, D. (2010). Enhancing Tumor-Specific Uptake of the Anticancer Drug Cisplatin with a Copper Chelator. Cancer Cell *17*, 574–583.

Islam, S., Paek, A.L., Hammer, M., Rangarajan, S., Ruijtenbeek, R., Cooke, L., Weterings, E., and Mahadevan, D. (2018). Drug-induced aneuploidy and polyploidy is a mechanism of disease relapse in MYC/BCL2-addicted diffuse large B-cell lymphoma. Oncotarget *9*, 35875–35890.

Ivanov, E.L., Sugawara, N., Fishman-Lobell, J., and Haber, J.E. (1996). Genetic requirements for the single-strand annealing pathway of double-strand break repair in Saccharomyces cerevisiae. Genetics *142*, 693–704.

Iwasaki, D., Hayashihara, K., Shima, H., Higashide, M., Terasawa, M., Gasser, S.M., and Shinohara, M. (2016). The MRX Complex Ensures NHEJ Fidelity through Multiple Pathways Including Xrs2-FHA–Dependent Tel1 Activation. PLoS Genet. *12*, e1005942.

Jacinto, E., Guo, B., Arndt, K.T., Schmelzle, T., and Hall, M.N. (2001). TIP41 interacts with TAP42 and negatively regulates the TOR signaling pathway. Mol. Cell *8*, 1017–1026.

Jackson, J.D. (2000). Histone H2A.Z has a conserved function that is distinct from that of the major H2A sequence variants. Nucleic Acids Res. *28*, 3811–3816.

Jaehnig, E.J., Kuo, D., Hombauer, H., Ideker, T.G., and Kolodner, R.D. (2013). Checkpoint Kinases Regulate a Global Network of Transcription Factors in Response to DNA Damage. Cell Rep. *4*, 174–188.

de Jager, M. (2001). DNA-binding and strand-annealing activities of human Mre11: implications for its roles in DNA double-strand break repair pathways. Nucleic Acids Res. *29*, 1317–1325.

Jain, P., Silva, A., Han, H.J., Lang, S.S., Zhu, Y., Boucher, K., Smith, T.E., Vakil, A., Diviney, P., Choudhari, N., et al. (2017). Overcoming resistance to single-agent therapy for oncogenic BRAF gene fusions via combinatorial targeting of MAPK and PI3K/mTOR signaling pathways. Oncotarget *8*, 84697–84713.

Jakobsen, K.P., Andersen, A.H., and Bjergbæk, L. (2019). Abortive activity of Topoisomerase I: a challenge for genome integrity? Curr. Genet. *65*, 1141–1144.

Jamal-Hanjani, M., A'Hern, R., Birkbak, N.J., Gorman, P., Grönroos, E., Ngang, S., Nicola, P., Rahman, L., Thanopoulou, E., Kelly, G., et al. (2015). Extreme chromosomal instability forecasts improved outcome in ER-negative breast cancer: A prospective validation cohort study from the TACT trial. Ann. Oncol. *26*, 1340–1346.

Janke, C., Magiera, M.M., Rathfelder, N., Taxis, C., Reber, S., Maekawa, H., Moreno-Borchart, A., Doenges, G., Schwob, E., Schiebel, E., et al. (2004). A versatile toolbox for PCR-based tagging of yeast genes: New fluorescent proteins, more markers and promoter substitution cassettes. Yeast *21*, 947–962.

Jaspers, J.E., Kersbergen, A., Boon, U., Sol, W., Van Deemter, L., Zander, S.A., Drost, R., Wientjens, E., Ji, J., Aly, A., et al. (2013). Loss of 53BP1 causes PARP inhibitor resistance in BRCA1-mutated mouse mammary tumors. Cancer Discov. *3*, 68–81.

Jiang, Y., and Broach, J.R. (1999). Tor proteins and protein phosphatase 2A reciprocally regulate Tap42 in controlling cell growth in yeast. EMBO J. *18*, 2782–2792.

Jonsdottir, A.B., Stefansson, O.A., Bjornsson, J., Jonasson, J.G., Ogmundsdottir, H.M., and Eyfjord, J.E. (2012). Tetraploidy in BRCA2 breast tumours. Eur. J. Cancer *48*, 305–310.

Jorgensen, P., and Tyers, M. (2004). How cells coordinate growth and division. Curr. Biol. *14*.

Jorgensen, P., Nishikawa, J.L., Breitkreutz, B.J., and Tyers, M. (2002). Systematic identification of pathways that couple cell growth and division in yeast. Science (80-.). *297*, 395–400.

Kais, Z., Rondinelli, B., Holmes, A., O'Leary, C., Kozono, D., D'Andrea, A.D., and Ceccaldi, R. (2016). FANCD2 Maintains Fork Stability in BRCA1/2-Deficient Tumors and Promotes Alternative End-Joining DNA Repair. Cell Rep. *15*, 2488–2499.

Kamada, Y., Yoshino, K., Kondo, C., Kawamata, T., Oshiro, N., Yonezawa, K., and Ohsumi, Y. (2010). Tor Directly Controls the Atg1 Kinase Complex To Regulate Autophagy. Mol. Cell. Biol. *30*, 1049–1058.

Karaayvaz-Yildirim, M., Silberman, R.E., Langenbucher, A., Saladi, S.V., Ross, K.N., Zarcaro, E., Desmond, A., Yildirim, M., Vivekanandan, V., Ravichandran, H., et al. (2020). Aneuploidy and a deregulated DNA damage response suggest haploinsufficiency in breast tissues of BRCA2 mutation carriers. Sci. Adv. *6*, eaay2611.

Kato, M., Yang, Y.S., Sutter, B.M., Wang, Y., McKnight, S.L., and Tu, B.P. (2019). Redox State Controls Phase Separation of the Yeast Ataxin-2 Protein via Reversible Oxidation of Its Methionine-Rich Low-Complexity Domain. Cell *177*, 711-721.e8.

Katou, Y., Kanoh, Y., Bando, M., Noguchi, H., Tanaka, H., Ashikari, T., Sugimoto, K., and Shirahige, K. (2003). S-phase checkpoint proteins Tof1 and Mrc1 form a stable replication-pausing complex. Nature *424*, 1078–1083.

Kaya, A., Mariotti, M., Tyshkovskiy, A., Zhou, X., Hulke, M.L., Ma, S., Gerashchenko, M. V., Koren, A., and Gladyshev, V.N. (2020). Molecular signatures of aneuploidy-driven adaptive evolution. Nat. Commun. *11*.

Ke, Y.W., Dou, Z., Zhang, J., and Yao, X.B. (2003). Function and regulation of Aurora/Ipl1p kinase family in cell division. Cell Res. *13*, 69–81.

Kegel, A., Sjöstrand, J.O.O., and Åström, S.U. (2001). Nej1p, a cell type-specific regulator of nonhomologous end joining in yeast. Curr. Biol. *11*, 1611–1617.

Keith, C.T., and Schreiber, S.L. (1995). PIK-Related Kinases: DNA Repair, Recombination, and Cell Cycle Checkpoints. Science (80-.). *270*, 50–50.

Keogh, M.C., Kim, J.A., Downey, M., Fillingham, J., Chowdhury, D., Harrison, J.C., Onishi, M., Datta, N., Galicia, S., Emili, A., et al. (2006). A phosphatase complex that dephosphorylates γH2AX regulates DNA damage checkpoint recovery. Nature *439*, 497–501.

Keskin, H., Shen, Y., Huang, F., Patel, M., Yang, T., Ashley, K., Mazin, A. V., and Storici, F. (2014). Transcript-RNA-templated DNA recombination and repair. Nature *515*, 436–439.

Khandelwal, N.K., Chauhan, N., Sarkar, P., Esquivel, B.D., Coccetti, P., Singha, A., Coste, A.T., Guptaa, M., Sanglard, D., White, T.C., et al. (2018). Azole resistance in a Candida albicans mutant lacking the ABC transporter CDR6/ROA1 depends on TOR signaling. J. Biol. Chem. *293*, 412–432.

Kim, H.-S., and Brill, S.J. (2001). Rfc4 Interacts with Rpa1 and Is Required for Both DNA Replication and DNA Damage Checkpoints in Saccharomyces cerevisiae. Mol. Cell. Biol. *21*, 3725–3737.

Kim, B.M., Hong, Y., Lee, S., Liu, P., Lim, J.H., Lee, Y.H., Lee, T.H., Chang, K.T., and Hong, Y. (2015). Therapeutic implications for overcoming radiation resistance in cancer therapy. Int. J. Mol. Sci. *16*, 26880–26913.

Kim, C., Gao, R., Sei, E., Brandt, R., Hartman, J., Hatschek, T., Crosetto, N., Foukakis, T., and Navin, N.E. (2018). Chemoresistance Evolution in Triple-Negative Breast Cancer Delineated by Single-Cell Sequencing. Cell *173*, 879-893.e13.

Kim, J.-A., Hicks, W.M., Li, J., Tay, S.Y., and Haber, J.E. (2011). Protein Phosphatases Pph3, Ptc2, and Ptc3 Play Redundant Roles in DNA Double-Strand Break Repair by Homologous Recombination. Mol. Cell. Biol. *31*, 507–516.

Klermund, J., Bender, K., and Luke, B. (2014). High nutrient levels and torc1 activity reduce cell viability following prolonged telomere dysfunction and cell cycle arrest. Cell Rep. *9*, 324–335.

Klionsky, D.J. (2011). For the last time, it is GFP-Atg8, not Atg8-GFP (and the same goes for LC3). Autophagy *7*, 1093–1094.

Kloosterman, W.P., Hoogstraat, M., Paling, O., Tavakoli-Yaraki, M., Renkens, I., Vermaat, J.S., van Roosmalen, M.J., van Lieshout, S., Nijman, I.J., Roessingh, W., et al. (2011). Chromothripsis is a common mechanism driving genomic rearrangements in primary and metastatic colorectal cancer. Genome Biol. *12*, R103.

Knouse, K.A., Wu, J., Whittaker, C.A., and Amon, A. (2014). Single cell sequencing reveals low levels of aneuploidy across mammalian tissues. Proc. Natl. Acad. Sci. U. S. A. *111*, 13409–13414.

Van Komen, S., Petukhova, G., Sigurdsson, S., Stratton, S., and Sung, P. (2000). Superhelicity-driven homologous DNA pairing by yeast recombination factors Rad51 and Rad54. Mol. Cell *6*, 563–572.

Konopleva, M., Contractor, R., Tsao, T., Samudio, I., Ruvolo, P.P., Kitada, S., Deng, X., Zhai, D., Shi, Y.X., Sneed, T., et al. (2006). Mechanisms of apoptosis sensitivity and resistance to the BH3 mimetic ABT-737 in acute myeloid leukemia. Cancer Cell *10*, 375–388.

Kops, G.J.P.L., Weaver, B.A.A., and Cleveland, D.W. (2005). On the road to cancer: Aneuploidy and the mitotic checkpoint. Nat. Rev. Cancer *5*, 773–785.

Kosuri, K. V., Wu, X., Wang, L., Villalona-Calero, M.A., and Otterson, G.A. (2010). An epigenetic mechanism for capecitabine resistance in mesothelioma. Biochem. Biophys. Res. Commun. *391*, 1465–1470.

Krogh, B.O., and Symington, L.S. (2004). Recombination Proteins in Yeast. Annu. Rev. Genet. *38*, 233–271.

Krogh, B.O., Llorente, B., Lam, A., and Symington, L.S. (2005). Mutations in Mre11 phosphoesterase motif I that impair Saccharomyces cerevisiae Mre11-Rad50-Xrs2 complex stability in addition to nuclease activity. Genetics *171*, 1561–1570.

Krokidis, M.G., Terzidis, M.A., Efthimiadou, E., Zervou, S.K., Kordas, G., Papadopoulos, K., Hiskia, A., Kletsas, D., and Chatgilialoglu, C. (2017). Purine 5′,8-cyclo-2′-deoxynucleoside lesions: formation by radical stress and repair in human breast epithelial cancer cells. Free Radic. Res. *51*, 470–482.

Kumar, S., and Burgers, P.M. (2013). Lagging strand maturation factor Dna2 is a component of the replication checkpoint initiation machinery. Genes Dev. *27*, 313–321.

Kunz, J., Henriquez, R., Schneider, U., Deuter-Reinhard, M., Movva, N.R., and Hall, M.N. (1993). Target of rapamycin in yeast, TOR2, is an essential phosphatidylinositol kinase homolog required for G1 progression. Cell *73*, 585–596.

Lampson, M.A., and Grishchuk, E.L. (2017). Mechanisms to avoid and correct erroneous kinetochore-microtubule attachments. Biology (Basel). *6*.

Lanz, M.C., Dibitetto, D., and Smolka, M.B. (2019). DNA damage kinase signaling: checkpoint and repair at 30 years . EMBO J. *38*.

Laubert, T., Freitag-Wolf, S., Linnebacher, M., König, A., Vollmar, B., and Habermann, J.K. (2015). Stage-specific frequency and prognostic significance of aneuploidy in patients with sporadic colorectal cancer—a meta-analysis and current overview. Int. J. Colorectal Dis. *30*, 1015–1028.

Ledermann, J.A., Drew, Y., and Kristeleit, R.S. (2016). Homologous recombination deficiency and ovarian cancer. Eur. J. Cancer *60*, 49–58.

Lee-Theilen, M., Matthews, A.J., Kelly, D., Zheng, S., and Chaudhuri, J. (2011). CtIP promotes microhomology-mediated alternative end joining during class-switch recombination. Nat. Struct. Mol. Biol. *18*, 75–80.

Lee, C.-S., and Haber, J.E. (2015). Mating-type Gene Switching in Saccharomyces cerevisiae. Microbiol. Spectr. *3*.

Lee, K., and Sang, E.L. (2007). Saccharomyces cerevisiae Sae2- and Tel1-dependent single-strand DNA formation at DNA break promotes microhomology-mediated end joining. Genetics *176*, 2003–2014.

Lee, T.H., and Kang, T.H. (2019). DNA oxidation and excision repair pathways. Int. J. Mol. Sci. *20*, 6092.

Lee, A.J.X., Endesfelder, D., Rowan, A.J., Walther, A., Birkbak, N.J., Futreal, P.A., Downward, J., Szallasi, Z., Tomlinson, I.P.M., Howell, M., et al. (2011). Chromosomal instability confers intrinsic multidrug resistance. Cancer Res. *71*, 1858–1870.

Lee, C.S., Wang, R.W., Chang, H.H., Capurso, D., Segal, M.R., and Haber, J.E. (2016). Chromosome position determines the success of double-strand break repair. Proc. Natl. Acad. Sci. U. S. A. *113*, E146–E154.

Lee, J.M., Ledermann, J.A., and Kohn, E.C. (2014). PARP inhibitors for BRCA1/2 mutation-associated and BRCA-like malignancies. Ann. Oncol. *25*, 32–40.

Lee, K., Ji, J.H., Yoon, K., Che, J., Seol, J.H., Lee, S.E., and Shim, E.Y. (2019). Microhomology selection for Microhomology mediated end joining in Saccharomyces Cerevisiae. Genes (Basel). *10*.

Lee, S.E., Moore, J.K., Holmes, A., Umezu, K., Kolodner, R.D., and Haber, J.E. (1998). Saccharomyces Ku70, Mre11/Rad50, and RPA proteins regulate adaptation to G2/M arrest after DNA damage. Cell *94*, 399–409.

Lee, S.E., Pellicioli, A., Malkova, A., Foiani, M., and Haber, J.E. (2001). The Saccharomyces recombination protein Tid1p is required for adaptation from G2/M arrest induced by a double-strand break. Curr. Biol. *11*, 1053–1057.

Lempiäinen, H., Uotila, A., Urban, J., Dohnal, I., Ammerer, G., Loewith, R., and Shore, D. (2009). Sfp1 Interaction with TORC1 and Mrs6 Reveals Feedback Regulation on TOR Signaling. Mol. Cell *33*, 704–716.

Leroy, C., Lee, S.E., Vaze, M.B., Ochsenbien, F., Guerois, R., Haber, J.E., and Marsolier-Kergoat, M.C. (2003). PP2C phosphatases Ptc2 and Ptc3 are required for DNA checkpoint inactivation after a double-strand break. Mol. Cell *11*, 827–835.

Letourneau, A., Santoni, F.A., Bonilla, X., Sailani, M.R., Gonzalez, D., Kind, J., Chevalier, C., Thurman, R., Sandstrom, R.S., Hibaoui, Y., et al. (2014). Domains of genome-wide gene expression dysregulation in Down's syndrome. Nature *508*, 345–350.

Li, J., Yan, G., Liu, S., Jiang, T., Zhong, M., Yuan, W., Chen, S., Zheng, Y., Jiang, Y., and Jiang, Y. (2017). Target of rapamycin complex 1 and Tap42-associated phosphatases are required for sensing changes in nitrogen conditions in the yeast Saccharomyces cerevisiae. Mol. Microbiol. *106*, 938–948.

Li, M., Fang, X., Baker, D.J., Guo, L., Gao, X., Wei, Z., Han, S., Van Deursen, J.M., and Zhang, P. (2010). The ATM-p53 pathway suppresses aneuploidy-induced tumorigenesis. Proc. Natl. Acad. Sci. U. S. A. *107*, 14188–14193.

Li, Y., Zhang, X., Liu, D., Gong, J., Wang, D.D., Li, S., Peng, Z., Li, Y., Wang, X., Lin, P.P., et al. (2018). Evolutionary expression of HER2 conferred by chromosome aneuploidy on circulating gastric cancer cells contributes to developing targeted and chemotherapeutic resistance. Clin. Cancer Res. *24*, 5261–5271.

Liang, F., and Wang, Y. (2007). DNA damage checkpoints inhibit mitotic exit by two different mechanisms. Mol. Cell. Biol. *27*, 5067–5078.

Liang, J., Suhandynata, R.T., and Zhou, H. (2015). Phosphorylation of Sae2 mediates Forkhead-associated (FHA) domain-specific interaction and regulates its DNA repair function. J. Biol. Chem. *290*, 10751–10763.

Lim, H.S., Kim, J.S., Park, Y.B., Gwon, G.H., and Cho, Y. (2011). Crystal structure of the Mre11-Rad50-ATPγS complex: Understanding the interplay between Mre11 and Rad50. Genes Dev. *25*, 1091–1104.

Lin, Y., Raj, J., Li, J., Ha, A., Hossain, M.A., Richardson, C., Mukherjee, P., and Yan, S. (2020). APE1 senses DNA single-strand breaks for repair and signaling. Nucleic Acids Res. *48*, 1925–1940.

Lindahl, T. (1993). Instability and decay of the primary structure of DNA. Nature *362*, 709–715.

Lindahl, T., and Barnes, D.E. (2000). Repair of endogenous DNA damage. In Cold Spring Harbor Symposia on Quantitative Biology, pp. 127–133.

Lisby, M., Mortensen, U.H., and Rothstein, R. (2003). Colocalization of multiple DNA double-strand breaks at a single Rad52 repair center. Nat. Cell Biol. *5*, 572–577.

Liu, C., Pouliot, J.J., and Nash, H.A. (2002). Repair of topoisomerase I covalent complexes in the absence of the tyrosyl-DNA phosphodiesterase Tdp1. Proc. Natl. Acad. Sci. U. S. A. *99*, 14970–14975.

Liu, D., Hou, P., Liu, Z., Wu, G., and Xing, M.M. (2009). Genetic alterations in the phosphoinositide 3-kinase/Akt signaling pathway confer sensitivity of thyroid cancer cells to therapeutic targeting of Akt and mammalian target of rapamycin. Cancer Res. *69*, 7311–7319.

Liu, J., Renault, L., Veaute, X., Fabre, F., Stahlberg, H., and Heyer, W.D. (2011). Rad51 paralogues Rad55-Rad57 balance the antirecombinase Srs2 in Rad51 filament formation. Nature *479*, 245–248.

Liu, J., Ede, C., Wright, W.D., Gore, S.K., Jenkins, S.S., Freudenthal, B.D., Washington, M.T., Veaute, X., and Heyer, W.D. (2017a). Srs2 promotes synthesis-dependent strand annealing by disrupting DNA polymerase d-extending D-loops. Elife *6*.

Liu, L., Cai, S., Han, C., Banerjee, A., Wu, D., Cui, T., Xie, G., Zhang, J., Zhang, X., McLaughlin, E., et al. (2020). ALDH1A1 contributes to PARP inhibitor resistance via enhancing DNA repair in BRCA2-/- Ovarian cancer cells. Mol. Cancer Ther. *19*, 199–210.

Liu, S., Kwon, M., Mannino, M., Yang, N., Renda, F., Khodjakov, A., and Pellman, D. (2018). Nuclear envelope assembly defects link mitotic errors to chromothripsis. Nature *561*, 551–555.

Liu, Y., Borel, C., Li, L., Müller, T., Williams, E.G., Germain, P.L., Buljan, M., Sajic, T., Boersema, P.J., Shao, W., et al. (2017b). Systematic proteome and proteostasis profiling in human Trisomy 21 fibroblast cells. Nat. Commun. *8*.

Liu, Z., Yu, M., Fei, B., Sun, J., and Wang, D. (2019). Nonhomologous end joining key factor XLF enhances both 5-florouracil and oxaliplatin resistance in colorectal cancer. Onco. Targets. Ther. *12*, 2095–2104.

Livak, K.J., and Schmittgen, T.D. (2001). Analysis of relative gene expression data using real-time quantitative PCR and the 2-ΔΔCT method. Methods *25*, 402–408.

Lloyd, J., Chapman, J.R., Clapperton, J.A., Haire, L.F., Hartsuiker, E., Li, J., Carr, A.M., Jackson, S.P., and Smerdon, S.J. (2009). A Supramodular FHA/BRCT-Repeat Architecture Mediates Nbs1 Adaptor Function in Response to DNA Damage. Cell *139*, 100–111.

Loewith, R., and Hall, M.N. (2011). Target of rapamycin (TOR) in nutrient signaling and growth control. Genetics *189*, 1177–1201.

Loewith, R., Jacinto, E., Wullschleger, S., Lorberg, A., Crespo, J.L., Bonenfant, D., Oppliger, W., Jenoe, P., and Hall, M.N. (2002). Two TOR complexes, only one of which is rapamycin sensitive, have distinct roles in cell growth control. Mol. Cell *10*, 457–468.

Lomonosov, M., Anand, S., Sangrithi, M., Davies, R., and Venkitaraman, A.R. (2003). Stabilization of stalled DNA replication forks by the BRCA2 breast cancer susceptibility protein. Genes Dev. *17*, 3017–3022.

Longtine, M.S., McKenzie, A., Demarini, D.J., Shah, N.G., Wach, A., Brachat, A., Philippsen, P., and Pringle, J.R. (1998). Additional modules for versatile and economical PCR-based gene deletion and modification in Saccharomyces cerevisiae. Yeast *14*, 953–961.

Lord, C.J., and Ashworth, A. (2017). PARP inhibitors: Synthetic lethality in the clinic. Science (80-.). *355*, 1152–1158.

Lossaint, G., Larroque, M., Ribeyre, C., Bec, N., Larroque, C., Décaillet, C., Gari, K., and Constantinou, A. (2013). FANCD2 Binds MCM Proteins and Controls Replisome Function upon Activation of S Phase Checkpoint Signaling. Mol. Cell *51*, 678–690.

Lydeard, J.R., Jain, S., Yamaguchi, M., and Haber, J.E. (2007). Break-induced replication and telomerase-independent telomere maintenance require Pol32. Nature *448*, 820–823.

Ma, J.-L., Kim, E.M., Haber, J.E., and Lee, S.E. (2003). Yeast Mre11 and Rad1 Proteins Define a Ku-Independent Mechanism To Repair Double-Strand Breaks Lacking Overlapping End

Sequences. Mol. Cell. Biol. *23*, 8820–8828.

Ma, J.L., Lee, S.J., Duong, J.K., and Stern, D.F. (2006). Activation of the checkpoint kinase Rad53 by the phosphatidyl inositol kinase-like kinase Mec1. J. Biol. Chem. *281*, 3954–3963.

MacDougall, C.A., Byun, T.S., Van, C., Yee, M.C., and Cimprich, K.A. (2007). The structural determinants of checkpoint activation. Genes Dev. *21*, 898–903.

Maciejowski, J., Li, Y., Bosco, N., Campbell, P.J., and De Lange, T. (2015). Chromothripsis and Kataegis Induced by Telomere Crisis. Cell *163*, 1641–1654.

Madaan, K., Kaushik, D., and VerM.A., T. (2012). Hydroxyurea: A key player in cancer chemotherapy. Expert Rev. Anticancer Ther. *12*, 19–29.

Majka, J., Niedziela-Majka, A., and Burgers, P.M.M.J. (2006). The Checkpoint Clamp Activates Mec1 Kinase during Initiation of the DNA Damage Checkpoint. Mol. Cell *24*, 891–901.

Majumdar, C., Nuñez, N.N., Raetz, A.G., Khuu, C., and David, S.S. (2018). Cellular Assays for Studying the Fe–S Cluster Containing Base Excision Repair Glycosylase MUTYH and Homologs. In Methods in Enzymology, pp. 69–99.

Malet-Martino, M., and Martino, R. (2002). Clinical Studies of Three Oral Prodrugs of 5-Fluorouracil (Capecitabine, UFT, S-1): A Review. Oncologist *7*, 288–323.

Malkova, A. (2018). Break-Induced Replication: The Where, The Why, and The How. Trends Genet. *34*, 518–531.

Maloisel, L., Fabre, F., and Gangloff, S. (2008). DNA Polymerase δ Is Preferentially Recruited during Homologous Recombination To Promote Heteroduplex DNA Extension. Mol. Cell. Biol. *28*, 1373–1382.

Manier, S., Salem, K.Z., Park, J., Landau, D.A., Getz, G., and Ghobrial, I.M. (2017). Genomic complexity of multiple myeloma and its clinical implications. Nat. Rev. Clin. Oncol. *14*, 100–113.

Mantiero, D., Clerici, M., Lucchini, G., and Longhese, M.P. (2007). Dual role for Saccharomyces cerevisiae Tel1 in the checkpoint response to double-strand breaks. EMBO Rep. *8*, 380–387.

Marini, F., Rawal, C.C., Liberi, G., and Pellicioli, A. (2019). Regulation of DNA Double Strand Breaks Processing: Focus on Barriers. Front. Mol. Biosci. *6*.

Marsella, A., Cassani, C., Casari, E., Tisi, R., and Longhese, M.P. (2019). Structure–function relationships of the Mre11 protein in the control of DNA end bridging and processing. Curr. Genet. *65*, 11–16.

Marsolier, M.C., Roussel, P., Leroy, C., and Mann, C. (2000). Involvement of the PP2C-like phosphatase Ptc2p in the DNA checkpoint pathways of Saccharomyces cerevisiae. Genetics *154*, 1523–1532.

Mateos-Gomez, P.A., Gong, F., Nair, N., Miller, K.M., Lazzerini-Denchi, E., and Sfeir, A. (2015). Mammalian polymerase θ promotes alternative NHEJ and suppresses recombination. Nature *518*, 254–257.

Matsuzaki, K., Shinohara, A., and Shinohara, M. (2008). Forkhead-associated domain of yeast Xrs2, a homolog of human Nbs1, promotes nonhomologous end joining through interaction with a ligase IV partner protein, Lif1. Genetics *179*, 213–225.

Mayle, R., Campbell, I.M., Beck, C.R., Yu, Y., Wilson, M., Shaw, C.A., Bjergbaek, L., Lupski, J.R., and Ira, G. (2015). Mus81 and converging forks limit the mutagenicity of replication fork

breakage. Science (80-.). *349*, 742–747.

Mazina, O.M., Keskin, H., Hanamshet, K., Storici, F., and Mazin, A. V. (2017). Rad52 Inverse Strand Exchange Drives RNA-Templated DNA Double-Strand Break Repair. Mol. Cell *67*, 19-29.e3.

Mazón, G., and Symington, L.S. (2013). Mph1 and Mus81-Mms4 prevent aberrant processing of mitotic recombination intermediates. Mol. Cell *52*, 63–74.

McClellan, A.J., Xia, Y., Deutschbauer, A.M., Davis, R.W., Gerstein, M., and Frydman, J. (2007). Diverse Cellular Functions of the Hsp90 Molecular Chaperone Uncovered Using Systems Approaches. Cell *131*, 121–135.

McDevitt, S., Rusanov, T., Kent, T., Chandramouly, G., and Pomerantz, R.T. (2018). How RNA transcripts coordinate DNA recombination and repair. Nat. Commun. *9*.

Meers, C., Keskin, H., and Storici, F. (2016). DNA repair by RNA: Templated, or not templated, that is the question. DNA Repair (Amst). *44*, 17–21.

Meggio, F., and Pinna, L.A. (2003). One-thousand-and-one substrates of protein kinase CK2? FASEB J. *17*, 349–368.

Meister, S., Schubert, U., Neubert, K., Herrmann, K., Burger, R., Gramatzki, M., Hahn, S., Schreiber, S., Wilhelm, S., Herrmann, M., et al. (2007). Extensive immunoglobulin production sensitizes myeloma cells for proteasome inhibition. Cancer Res. *67*, 1783–1792.

Memisoglu, G., Lanz, M.C., Eapen, V. V., Jordan, J.M., Lee, K., Smolka, M.B., and Haber, J.E. (2019). Mec1ATR Autophosphorylation and Ddc2ATRIP Phosphorylation Regulates DNA Damage Checkpoint Signaling. Cell Rep. *28*, 1090-1102.e3.

Mengwasser, K.E., Adeyemi, R.O., Leng, Y., Choi, M.Y., Clairmont, C., D'Andrea, A.D., and Elledge, S.J. (2019). Genetic Screens Reveal FEN1 and APEX2 as BRCA2 Synthetic Lethal Targets. Mol. Cell *73*, 885-899.e6.

Menin, L., Ursich, S., Trovesi, C., Zellweger, R., Lopes, M., Longhese, M.P., and Clerici, M. (2018). Tel1/ ATM prevents degradation of replication forks that reverse after topoisomerase poisoning . EMBO Rep. *19*.

Meyer, D., Fu, B.X.H., and Heyer, W.D. (2015). DNA polymerases δ and λ cooperate in repairing double-strand breaks by microhomology-mediated end-joining in Saccharomyces cerevisiae. Proc. Natl. Acad. Sci. U. S. A. *112*, E6907–E6916.

Migdal, I., Ilina, Y., Tamás, M.J., and Wysocki, R. (2008). Mitogen-activated protein kinase Hog1 mediates adaptation to G1 checkpoint arrest during arsenite and hyperosmotic stress. Eukaryot. Cell *7*, 1309–1317.

Millan-Zambrano, G., Santos-Rosa, H., Puddu, F., Robson, S.C., Jackson, S.P., and Kouzarides, T. (2018). Phosphorylation of Histone H4T80 Triggers DNA Damage Checkpoint Recovery. Mol. Cell *72*, 625-635.e4.

Miller, S.B., Ho, C., Winkler, J., Khokhrina, M., Neuner, A., Mohamed, M.Y., Guilbride, D.L., Richter, K., Lisby, M., Schiebel, E., et al. (2015). Compartment-specific aggregases direct distinct nuclear and cytoplasmic aggregate deposition. EMBO J. *34*, 778–797.

Millet, C., and Makovets, S. (2016). Aneuploidy as a mechanism of adaptation to telomerase insufficiency. Curr. Genet. *62*, 557–564.

Mimitou, E.P., and Symington, L.S. (2008). Sae2, Exo1 and Sgs1 collaborate in DNA double-strand break processing. Nature *455*, 770–774.

Min, J., Wright, W.E., and Shay, J.W. (2017). Alternative Lengthening of Telomeres Mediated by Mitotic DNA Synthesis Engages Break-Induced Replication Processes. Mol. Cell. Biol. *37*.

Mini, E., Nobili, S., Caciagli, B., Landini, I., and Mazzei, T. (2006). Cellular pharmacology of gemcitabine. Ann. Oncol. *17*, v7–v12.

Minois, N., Frajnt, M., Wilson, C., and Vaupel, J.W. (2005). Advances in measuring lifespan in the yeast Saccharomyces cerevisiae. Proc. Natl. Acad. Sci. U. S. A. *102*, 402–406.

Mitchell, T.J., Turajlic, S., Rowan, A., Nicol, D., Farmery, J.H.R., O'Brien, T., Martincorena, I., Tarpey, P., Angelopoulos, N., Yates, L.R., et al. (2018). Timing the Landmark Events in the Evolution of Clear Cell Renal Cell Cancer: TRACERx Renal. Cell *173*, 611-623.e17.

Miyata, Y. (2009). CK2: The kinase controlling the Hsp90 chaperone machinery. Cell. Mol. Life Sci. *66*, 1840–1849.

Mogk, A., Kummer, E., and Bukau, B. (2015). Cooperation of Hsp70 and Hsp100 chaperone machines in protein disaggregation. Front. Mol. Biosci. *2*.

Monda, J.K., and Cheeseman, I.M. (2018). The kinetochore-microtubule interface at a glance. J. Cell Sci. *131*.

Moore, J.K., and Haber, J.E. (1996). Capture of retrotransposon DNA at the sites of chromosomal double- strand breaks. Nature *383*, 644–646.

Morawska, M., and Ulrich, H.D. (2013). An expanded tool kit for the auxin-inducible degron system in budding yeast. Yeast *30*, 341–351.

Mordes, D.A., Glick, G.G., Zhao, R., and Cortez, D. (2008). TopBP1 activates ATR through ATRIP and a PIKK regulatory domain. Genes Dev. *22*, 1478–1489.

Morey, L., and Helin, K. (2010). Polycomb group protein-mediated repression of transcription. Trends Biochem. Sci. *35*, 323–332.

Morrical, S.W. (2015). DNA-pairing and annealing processes in homologous recombination and homology-directed repair. Cold Spring Harb. Perspect. Biol. *7*, a016444.

Morrish, T.A., Gilbert, N., Myers, J.S., Vincent, B.J., Stamato, T.D., Taccioli, G.E., Batzer, M.A., and Moran, J. V. (2002). DNA repair mediated by endonuclease-independent LINE-1 retrotransposition. Nat. Genet. *31*, 159–165.

Morrish, T.A., Garcia-Perez, J.L., Stamato, T.D., Taccioli, G.E., Sekiguchi, J.A., and Moran, J. V. (2007). Endonuclease-independent LINE-1 retrotransposition at mammalian telomeres. Nature *446*, 208–212.

Morrow, D.M., Tagle, D.A., Shiloh, Y., Collins, F.S., and Hieter, P. (1995). TEL1, an S. cerevisiae homolog of the human gene mutated in ataxia telangiectasia, is functionally related to the yeast checkpoint gene MEC1. Cell *82*, 831–840.

Mortensen, E.M., Haas, W., Gygi, M., Gygi, S.P., and Kellogg, D.R. (2005). Cdc28-dependent regulation of the Cdc5/Polo kinase. Curr. Biol. *15*, 2033–2037.

Mortimer, R.K., Contopoulou, R., and Schild, D. (1981). Mitotic chromosome loss in a radiation-sensitive strain of the yeast Saccharomyces cerevisiae. Proc. Natl. Acad. Sci. U. S. A. *78*, 5778–5782.

Moynahan, M.E., Pierce, A.J., and Jasin, M. (2001). BRCA2 is required for homology-directed repair of chromosomal breaks. Mol. Cell *7*, 263–272.

Mulla, W.A., Seidel, C.W., Zhu, J., Tsai, H.J., Smith, S.E., Singh, P., Bradford, W.D., McCroskey, S., Nelliat, A.R., Conkright, J., et al. (2017). Aneuploidy as a cause of impaired chromatin silencing and mating-type specification in budding yeast. Elife *6*.

Mullard, A. (2020). Stemming the tide of drug resistance in cancer. Nat. Rev. Drug Discov. *19*, 221–223.

Mumberg, D., Müller, R., and Funk, M. (1995). Yeast vectors for the controlled expression of heterologous proteins in different genetic backgrounds. Gene *156*, 119–122.

Nagaraju, G.P., Zakka, K.M., Landry, J.C., Shaib, W.L., Lesinski, G.B., and El-Rayes, B.F. (2019). Inhibition of HSP90 overcomes resistance to chemotherapy and radiotherapy in pancreatic cancer. Int. J. Cancer *145*, 1529–1537.

Nakada, D., Matsumoto, K., and Sugimoto, K. (2003). ATM-related Tel1 associates with double-strand breaks through an Xrs2-dependent mechanism. Genes Dev. *17*, 1957–1962.

Nakada, D., Hirano, Y., and Sugimoto, K. (2004). Requirement of the Mre11 Complex and Exonuclease 1 for Activation of the Mec1 Signaling Pathway. Mol. Cell. Biol. *24*, 10016–10025.

Nakada, D., Hirano, Y., Tanaka, Y., and Sugimoto, K. (2005). Role of the C terminus of Mec1 checkpoint kinase in its localization to sites of DNA damage. Mol. Biol. Cell *16*, 5227–5235.

Nakano, T., Xu, X., Salem, A.M.H., Shoulkamy, M.I., and Ide, H. (2017). Radiation-induced DNA–protein cross-links: Mechanisms and biological significance. Free Radic. Biol. Med. *107*, 136–145.

Nakashima, A., Maruki, Y., Imamura, Y., Kondo, C., Kawamata, T., Kawanishi, I., Takata, H., Matsuura, A., Lee, K.S., Kikkawa, U., et al. (2008). The yeast Tor signaling pathway is involved in G2/M transition via polo-kinase. PLoS One *3*.

Namee, N.M., and O'Driscoll, L. (2018). Extracellular vesicles and anti-cancer drug resistance. Biochim. Biophys. Acta - Rev. Cancer *1870*, 123–136.

Navadgi-Patil, V.M., and Burgers, P.M. (2009). A tale of two tails: Activation of DNA damage checkpoint kinase Mec1/ATR by the 9-1-1 clamp and by Dpb11/TopBP1. DNA Repair (Amst). *8*, 996–1003.

New, J.H., Sugiyama, T., Zaitseva, E., and Kowalczykowski, S.C. (1998). Rad52 protein stimulates DNA strand exchange by Rad51 and replication protein A. Nature *391*, 407–410.

Nicholson, J.M., Macedo, J.C., Mattingly, A.J., Wangsa, D., Camps, J., Lima, V., Gomes, A.M., Dória, S., Ried, T., Logarinho, E., et al. (2015). Chromosome mis-segregation and cytokinesis failure in trisomic human cells. Elife *4*.

Nigg, E.A. (2002). Centrosome aberrations: Cause or consequence of cancer progression? Nat. Rev. Cancer *2*, 815–825.

Nooter, K., Brutel De La Riviere, G., Look, M.P., Van Wingerden, K.E., Henzen-Logmans, S.C., Scheper, R.J., Flens, M.J., Klijn, J.G.M., Stoter, G., and Foekens, J.A. (1997). The prognostic significance of expression of the multidrug resistance-associated protein (MRP) in primary breast cancer. Br. J. Cancer *76*, 486–493.

O'Neill, B.M., Szyjka, S.J., Lis, E.T., Bailey, A.O., Yates, J.R., Aparicio, O.M., and Romesberg,

F.E. (2007). Pph3-Psy2 is a phosphatase complex required for Rad53 dephosphorylation and replication fork restart during recovery from DNA damage. Proc. Natl. Acad. Sci. U. S. A. *104*, 9290–9295.

Obermeier, K., Sachsenweger, J., Friedl, T.W.P., Pospiech, H., Winqvist, R., and Wiesmuller, L. (2016). Heterozygous PALB2 c.1592delT mutation channels DNA double-strand break repair into error-prone pathways in breast cancer patients. Oncogene *35*, 3796–3806.

Oh, J., and Symington, L.S. (2018). Role of the Mre11 complex in preserving genome integrity. Genes (Basel). *9*, 589.

Oh, J., Al-Zain, A., Cannavo, E., Cejka, P., and Symington, L.S. (2016). Xrs2 Dependent and Independent Functions of the Mre11-Rad50 Complex. Mol. Cell *64*, 405–415.

Ohashi, A., Ohori, M., Iwai, K., Nakayama, Y., Nambu, T., Morishita, D., Kawamoto, T., Miyamoto, M., Hirayama, T., Okaniwa, M., et al. (2015). Aneuploidy generates proteotoxic stress and DNA damage concurrently with p53-mediated post-mitotic apoptosis in SAC-impaired cells. Nat. Commun. *6*.

Ohouo, P.Y., Bastos De Oliveira, F.M., Liu, Y., Ma, C.J., and Smolka, M.B. (2013). DNA-repair scaffolds dampen checkpoint signalling by counteracting the adaptor Rad9. Nature *493*, 120–125.

De Oliveira, F.M.B., Harris, M.R., Brazauskas, P., De Bruin, R.A.M., and Smolka, M.B. (2012). Linking DNA replication checkpoint to MBF cell-cycle transcription reveals a distinct class of G1/S genes. EMBO J. *31*, 1798–1810.

Onozawa, M., Zhang, Z., Kim, Y.J., Goldberg, L., Varga, T., Bergsagel, P.L., Kuehl, W.M., and Aplan, P.D. (2014). Repair of DNA double-strand breaks by templated nucleotide sequence insertions derived from distant regions of the genome. Proc. Natl. Acad. Sci. U. S. A. *111*, 7729–7734.

Oromendia, A.B., Dodgson, S.E., and Amon, A. (2012). Aneuploidy causes proteotoxic stress in yeast. Genes Dev. *26*, 2696–2708.

Ovejero, S., Bueno, A., and Sacristán, M.P. (2020). Working on genomic stability: From the S-phase to mitosis. Genes (Basel). *11*.

Oza, P., Jaspersen, S.L., Miele, A., Dekker, J., and Peterson, C.L. (2009). Mechanisms that regulate localization of a DNA double-strand break to the nuclear periphery. Genes Dev. *23*, 912–927.

Ozeri-Galai, E., Lebofsky, R., Rahat, A., Bester, A.C., Bensimon, A., and Kerem, B. (2011). Failure of Origin Activation in Response to Fork Stalling Leads to Chromosomal Instability at Fragile Sites. Mol. Cell *43*, 122–131.

Palmberg, C., Koivisto, P., Hyytinen, E., Isola, J., Visakorpi, T., Kallioniemi, O.P., and Tammela, T. (1997). Androgen receptor gene amplification in a recurrent prostate cancer after monotherapy with the nonsteroidal potent antiandrogen Casodex (bicalutamide) with a subsequent favorable response to maximal androgen blockade. Eur. Urol. *31*, 216–219.

Palou, G., Palou, R., Zeng, F., Vashisht, A.A., Wohlschlegel, J.A., and Quintana, D.G. (2015). Three Different Pathways Prevent Chromosome Segregation in the Presence of DNA Damage or Replication Stress in Budding Yeast. PLoS Genet. *11*.

Panda, M., and Biswal, B.K. (2019). Cell signaling and cancer: a mechanistic insight into drug resistance. Mol. Biol. Rep. *46*, 5645–5659.

Pannunzio, N.R., Watanabe, G., and Lieber, M.R. (2018). Nonhomologous DNA end-joining for repair of DNA double-strand breaks. J. Biol. Chem. *293*, 10512–10523.

Papamichos-Chronakis, M., Krebs, J.E., and Peterson, C.L. (2006). Interplay between Ino80 and Swr1 chromatin remodeling enzymes regulates cell cycle checkpoint adaptation in response to DNA damage. Genes Dev. *20*, 2437–2449.

Park, P.H., Yamamoto, T.M., Li, H., Alcivar, A.L., Xia, B., Wang, Y., Bernhardy, A.J., Turner, K.M., Kossenkov, A. V., Watson, Z.L., et al. (2020). Amplification of the mutation-carrying BRCA2 allele promotes RAD51 loading and PARP inhibitor resistance in the absence of reversion mutations. Mol. Cancer Ther. *19*, 602–613.

Parrilla-Castellar, E.R., Arlander, S.J.H., and Karnitz, L. (2004). Dial 9-1-1 for DNA damage: The Rad9-Hus1-Rad1 (9-1-1) clamp complex. DNA Repair (Amst). *3*, 1009–1014.

Passerini, V., Ozeri-Galai, E., De Pagter, M.S., Donnelly, N., Schmalbrock, S., Kloosterman, W.P., Kerem, B., and Storchová, Z. (2016). The presence of extra chromosomes leads to genomic instability. Nat. Commun. *7*.

Pathania, S., Bade, S., Le Guillou, M., Burke, K., Reed, R., Bowman-Colin, C., Su, Y., Ting, D.T., Polyak, K., Richardson, A.L., et al. (2014). BRCA1 haploinsufficiency for replication stress suppression in primary cells. Nat. Commun. *5*, 5496.

Paull, T.T., and Gellert, M. (1998). The 3′ to 5′ exonuclease activity of Mre11 facilitates repair of DNA double-strand breaks. Mol. Cell *1*, 969–979.

Pavelka, N., Rancati, G., Zhu, J., Bradford, W.D., Saraf, A., Florens, L., Sanderson, B.W., Hattem, G.L., and Li, R. (2010). Aneuploidy confers quantitative proteome changes and phenotypic variation in budding yeast. Nature *468*, 321–325.

Payer, B., and Lee, J.T. (2008). X Chromosome Dosage Compensation: How Mammals Keep the Balance. Annu. Rev. Genet. *42*, 733–772.

Pellicioli, A., Lee, S.E., Lucca, C., Foiani, M., and Haber, J.E. (2001). Regulation of Saccharomyces Rad53 checkpoint kinase during adaptation from DNA damage-induced G2/M arrest. Mol. Cell *7*, 293–300.

Peng, M., Yin, N., and Li, M.O. (2014). Sestrins function as guanine nucleotide dissociation inhibitors for rag GTPases to control mTORC1 signaling. Cell *159*, 122–133.

Pérez-Hidalgo, L., and Moreno, S. (2017). Coupling TOR to the cell cycle by the greatwall-endosulfine-PP2A-B55 pathway. Biomolecules *7*.

Pettitt, S.J., Krastev, D.B., Brandsma, I., Dréan, A., Song, F., Aleksandrov, R., Harrell, M.I., Menon, M., Brough, R., Campbell, J., et al. (2018). Genome-wide and high-density CRISPR-Cas9 screens identify point mutations in PARP1 causing PARP inhibitor resistance. Nat. Commun. *9*.

Petukhova, G., Sung, P., and Klein, H. (2000). Promotion of Rad51-dependent D-loop formation by yeast recombination factor Rdh54/Tid1. Genes Dev. *14*, 2206–2215.

Poli, J., Tsaponina, O., Crabbé, L., Keszthelyi, A., Pantesco, V., Chabes, A., Lengronne, A., and Pasero, P. (2012). dNTP pools determine fork progression and origin usage under replication stress. EMBO J. *31*, 883–894.

Pommier, Y. (2006). Topoisomerase I inhibitors: Camptothecins and beyond. Nat. Rev. Cancer *6*, 789–802.

Pommier, Y. (2009). DNA topoisomerase I Inhibitors: Chemistry, biology, and interfacial inhibition. Chem. Rev. *109*, 2894–2902.

Pommier, Y., Leo, E., Zhang, H., and Marchand, C. (2010). DNA topoisomerases and their poisoning by anticancer and antibacterial drugs. Chem. Biol. *17*, 421–433.

Pommier, Y., Cushman, M., and Doroshow, J.H. (2018). Novel clinical indenoisoquinoline topoisomerase I inhibitors: A twist around the camptothecins. Oncotarget *9*, 37286–37288.

Prado, F. (2018). Homologous recombination: To fork and beyond. Genes (Basel). *9*, 603.

Princz, L.N., Wild, P., Bittmann, J., Aguado, F.J., Blanco, M.G., Matos, J., and Pfander, B. (2017). Dbf4-dependent kinase and the Rtt107 scaffold promote Mus81-Mms4 resolvase activation during mitosis. EMBO J. *36*, 664–678.

Pringle, J.R. (1975). Chapter 12 Induction, Selection, and Experimental Uses of Temperature-Sensitive and Other Conditional Mutants of Yeast. Methods Cell Biol. *12*, 233–272.

Prouteau, M., Desfosses, A., Sieben, C., Bourgoint, C., Mozaffari, N.L., Demurtas, D., Mitra, A.K., Guichard, P., Manley, S., and Loewith, R. (2017). TORC1 organized in inhibited domains (TOROIDs) regulate TORC1 activity. Nature *550*, 265–269.

Pusztai, L., Wagner, P., Ibrahim, N., Rivera, E., Theriault, R., Booser, D., Symmans, F.W., Wong, F., Blumenschein, G., Fleming, D.R., et al. (2005). Phase II study of tariquidar, a selective P-glycoprotein inhibitor, in patients with chemotherapy-resistant, advanced breast carcinoma. Cancer *104*, 682–691.

Rahal, R., and Amon, A. (2008). The polo-like kinase Cdc5 interacts with FEAR network components and Cdc14. Cell Cycle *7*, 3262–3272.

Rancati, G., Pavelka, N., Fleharty, B., Noll, A., Trimble, R., Walton, K., Perera, A., Staehling-Hampton, K., Seidel, C.W., and Li, R. (2008). Aneuploidy Underlies Rapid Adaptive Evolution of Yeast Cells Deprived of a Conserved Cytokinesis Motor. Cell *135*, 879–893.

Randell, J.C.W., Fan, A., Chan, C., Francis, L.I., Heller, R.C., Galani, K., and Bell, S.P. (2010). Mec1 Is One of Multiple Kinases that Prime the Mcm2-7 Helicase for Phosphorylation by Cdc7. Mol. Cell *40*, 353–363.

Raspelli, E., Cassani, C., Chiroli, E., and Fraschini, R. (2015). Budding yeast Swe1 is involved in the control of mitotic spindle elongation and is regulated by Cdc14 phosphatase during mitosis. J. Biol. Chem. *290*, 1–12.

Rass, E., Grabarz, A., Plo, I., Gautier, J., Bertrand, P., and Lopez, B.S. (2009). Role of Mre11 in chromosomal nonhomologous end joining in mammalian cells. Nat. Struct. Mol. Biol. *16*, 819–824.

Ratsima, H., Serrano, D., Pascariu, M., and D'Amours, D. (2016). Centrosome-Dependent Bypass of the DNA Damage Checkpoint by the Polo Kinase Cdc5. Cell Rep. *14*, 1422–1434.

Ravichandran, M.C., Fink, S., Clarke, M.N., Hofer, F.C., and Campbell, C.S. (2018). Genetic interactions between specific chromosome copy number alterations dictate complex aneuploidy patterns. Genes Dev. *32*, 1485–1498.

Rawal, C.C., Riccardo, S., Pesenti, C., Ferrari, M., Marini, F., and Pellicioli, A. (2016). Reduced kinase activity of polo kinase Cdc5 affects chromosome stability and DNA damage response in S. cerevisiae. Cell Cycle *15*, 2906–2919.

Redon, C., Pilch, D.R., Rogakou, E.P., Orr, A.H., Lowndes, N.F., and Bonner, W.M. (2003). Yeast histone 2A serine 129 is essential for the efficient repair of checkpoint-blind DNA damage. EMBO Rep. *4*, 678–684.

Regairaz, M., Zhang, Y.W., Fu, H., Agama, K.K., Tata, N., Agrawal, S., Aladjem, M.I., and Pommier, Y. (2011). Mus81-mediated DNA cleavage resolves replication forks stalled by topoisomerase I-DNA complexes. J. Cell Biol. *195*, 739–749.

Reginato, G., Cannavo, E., and Cejka, P. (2017). Physiological protein blocks direct the Mre11-Rad50-Xrs2 and Sae2 nuclease complex to initiate DNA end resection. Genes Dev. *31*, 2325–2330.

Rehen, S.K., McConnell, M.J., Kaushal, D., Kingsbury, M.A., Yang, A.H., and Chun, J. (2001). Chromosomal variation in neurons of the developing and adult mammalian nervous system. Proc. Natl. Acad. Sci. U. S. A. *98*, 13361–13366.

Rehen, S.K., Yung, Y.C., McCreight, M.P., Kaushal, D., Yang, A.H., Almeida, B.S.V., Kingsbury, M.A., Cabral, K.M.S., McConnell, M.J., Anliker, B., et al. (2005). Constitutional aneuploidy in the normal human brain. J. Neurosci. *25*, 2176–2180.

Reinke, A., Chen, J.C.Y., Aronova, S., and Powers, T. (2006). Caffeine targets TOR complex I and provides evidence for a regulatory link between the FRB and kinase domains of Tor1p. J. Biol. Chem. *281*, 31616–31626.

Reiter, J.G., Makohon-Moore, A.P., Gerold, J.M., Heyde, A., Attiyeh, M.A., Kohutek, Z.A., Tokheim, C.J., Brown, A., DeBlasio, R.M., Niyazov, J., et al. (2018). Minimal functional driver gene heterogeneity among untreated metastases. Science (80-.). *361*, 1033–1037.

Richter, K., Haslbeck, M., and Buchner, J. (2010). The Heat Shock Response: Life on the Verge of Death. Mol. Cell *40*, 253–266.

Robert, T., Vanoli, F., Chiolo, I., Shubassi, G., Bernstein, K.A., Rothstein, R., Botrugno, O.A., Parazzoli, D., Oldani, A., Minucci, S., et al. (2011). HDACs link the DNA damage response, processing of double-strand breaks and autophagy. Nature *471*, 74–79.

Rodina, A., Wang, T., Yan, P., Gomes, E.D., Dunphy, M.P.S., Pillarsetty, N., Koren, J., Gerecitano, J.F., Taldone, T., Zong, H., et al. (2016). The epichaperome is an integrated chaperome network that facilitates tumour survival. Nature *538*, 397–401.

Rodrik-Outmezguine, V.S., Okaniwa, M., Yao, Z., Novotny, C.J., McWhirter, C., Banaji, A., Won, H., Wong, W., Berger, M., De Stanchina, E., et al. (2016). Overcoming mTOR resistance mutations with a new-generation mTOR inhibitor. Nature *534*, 272–276.

Rondinelli, B., Gogola, E., Yücel, H., Duarte, A.A., Van De Ven, M., Van Der Sluijs, R., Konstantinopoulos, P.A., Jonkers, J., Ceccaldi, R., Rottenberg, S., et al. (2017). EZH2 promotes degradation of stalled replication forks by recruiting MUS81 through histone H3 trimethylation. Nat. Cell Biol. *19*, 1371–1378.

Rosen, D.M., Younkin, E.M., Miller, S.D., and Casper, A.M. (2013). Fragile Site Instability in Saccharomyces cerevisiae Causes Loss of Heterozygosity by Mitotic Crossovers and Break-Induced Replication. PLoS Genet. *9*.

Ross-Innes, C.S., Becq, J., Warren, A., Cheetham, R.K., Northen, H., O'Donovan, M., Malhotra, S., Di Pietro, M., Ivakhno, S., He, M., et al. (2015). Whole-genome sequencing provides new insights into the clonal architecture of Barrett's esophagus and esophageal adenocarcinoma. Nat. Genet. *47*, 1038–1046.

Roth, V. (2006). http://www.doubling-time.com/compute.php. Roth V. 2006 Doubling Time Comput. Available from Http//Www.Doubling-Time.Com/Compute.Php.

Roy, R., Chun, J., and Powell, S.N. (2012). BRCA1 and BRCA2: Different roles in a common pathway of genome protection. Nat. Rev. Cancer *12*, 68–78.

Rudin, N., and Haber, J.E. (1988). Efficient repair of HO-induced chromosomal breaks in Saccharomyces cerevisiae by recombination between flanking homologous sequences. Mol. Cell. Biol. *8*, 3918–3928.

Rutledge, S.D., Douglas, T.A., Nicholson, J.M., Vila-Casadesús, M., Kantzler, C.L., Wangsa, D., Barroso-Vilares, M., Kale, S.D., Logarinho, E., and Cimini, D. (2016). Selective advantage of trisomic human cells cultured in non-standard conditions. Sci. Rep. *6*, 22828.

Saatci, Ö., Borgoni, S., Akbulut, Ö., Durmuş, S., Raza, U., Eyüpoğlu, E., Alkan, C., Akyol, A., Kütük, Ö., Wiemann, S., et al. (2018). Targeting PLK1 overcomes T-DM1 resistance via CDK1-dependent phosphorylation and inactivation of Bcl-2/xL in HER2-positive breast cancer. Oncogene *37*, 2251–2269.

Sacho, E.J., and Maizels, N. (2011). DNA repair factor MRE11/RAD50 cleaves 3′-phosphotyrosyl bonds and resects DNA to repair damage caused by topoisomerase 1 poisons. J. Biol. Chem. *286*, 44945–44951.

Sage, E., and Shikazono, N. (2017). Radiation-induced clustered DNA lesions: Repair and mutagenesis. Free Radic. Biol. Med. *107*, 125–135.

Sakai, W., Swisher, E.M., Karlan, B.Y., Agarwal, M.K., Higgins, J., Friedman, C., Villegas, E., Jacquemont, C., Farrugia, D.J., Couch, F.J., et al. (2008). Secondary mutations as a mechanism of cisplatin resistance in BRCA2-mutated cancers. Nature *451*, 1116–1120.

Sakofsky, C.J., and Malkova, A. (2017). Break induced replication in eukaryotes: mechanisms, functions, and consequences. Crit. Rev. Biochem. Mol. Biol. *52*, 395–413.

Saldivar, J.C., Cortez, D., and Cimprich, K.A. (2017). The essential kinase ATR: Ensuring faithful duplication of a challenging genome. Nat. Rev. Mol. Cell Biol. *18*, 622–636.

Sallmyr, A., Tomkinson, A.E., and Rassool, F. V. (2008). Up-regulation of WRN and DNA ligase lllά in chronic myeloid leukemia: Consequences for the repair of DNA double-strand breaks. Blood *112*, 1413–1423.

Sampath, H., and Lloyd, R.S. (2019). Roles of OGG1 in transcriptional regulation and maintenance of metabolic homeostasis. DNA Repair (Amst). *81*, 102667.

Sanchez, Y., Desany, B.A., Jones, W.J., Liu, Q., Wang, B., and Elledge, S.J. (1996). Regulation of RAD53 by the ATM-like kinases MEC1 and TEL1 in yeast cell cycle checkpoint pathways. Science (80-.). *271*, 357–360.

Sanchez, Y., Wong, C., Thoma, R.S., Richman, R., Wu, Z., Piwnica-Worms, H., and Elledge, S.J. (1997). Conservation of the Chk1 checkpoint pathway in mammals: Linkage of DNA damage to Cdk regulation through Cdc25. Science (80-.). *277*, 1497–1501.

Sanchez, Y., Bachant, J., Wang, H., Hu, F., Liu, D., Tetzlaff, M., and Elledge, S.J. (1999). Control of the DNA damage checkpoint by Chk1 and Rad53 protein kinases through distinct mechanisms. Science (80-.). *286*, 1166–1171.

Sandell, L.L., and Zakian, V.A. (1993). Loss of a yeast telomere: Arrest, recovery, and chromosome loss. Cell *75*, 729–739.

Sansregret, L., and Swanton, C. (2017). The role of aneuploidy in cancer evolution. Cold Spring Harb. Perspect. Med. *7*, a028373.

Santaguida, S., Vasile, E., White, E., and Amon, A. (2015). Aneuploidy-induced cellular stresses limit autophagic degradation. Genes Dev. *29*, 2010–2021.

Santaguida, S., Richardson, A., Iyer, D.R., M'Saad, O., Zasadil, L., Knouse, K.A., Wong, Y.L., Rhind, N., Desai, A., and Amon, A. (2017). Chromosome Mis-segregation Generates Cell-Cycle-Arrested Cells with Complex Karyotypes that Are Eliminated by the Immune System. Dev. Cell *41*.

Scheirer, C.J., Ray, W.S., and Hare, N. (1976). The Analysis of Ranked Data Derived from Completely Randomized Factorial Designs. Biometrics *32*, 429.

Schlacher, K., Wu, H., and Jasin, M. (2012). A Distinct Replication Fork Protection Pathway Connects Fanconi Anemia Tumor Suppressors to RAD51-BRCA1/2. Cancer Cell *22*, 106–116.

Schleker, T., Shimada, K., Sack, R., Pike, B.L., and Gasser, S.M. (2010). Cell cycle-dependent phosphorylation of Rad53 kinase by Cdc5 and Cdc28 modulates checkpoint adaptation. Cell Cycle *9*, 350–363.

Schmelzle, T., and Hall, M.N. (2000). TOR, a central controller of cell growth. Cell *103*, 253–262.

Schoonen, P.M., Kok, Y.P., Wierenga, E., Bakker, B., Foijer, F., Spierings, D.C.J., and van Vugt, M.A.T.M. (2019). Premature mitotic entry induced by ATR inhibition potentiates olaparib inhibition-mediated genomic instability, inflammatory signaling, and cytotoxicity in BRCA2-deficient cancer cells. Mol. Oncol. *13*, 2422–2440.

Schubert, U., Antón, L.C., Gibbs, J., Norbury, C.C., Yewdell, J.W., and Bennink, J.R. (2000). Rapid degradation of a large fraction of newly synthesized proteins by proteasomes. Nature *404*, 770–774.

Seeber, A., Hegnauer, A.M., Hustedt, N., Deshpande, I., Poli, J., Eglinger, J., Pasero, P., Gut, H., Shinohara, M., Hopfner, K.P., et al. (2016). RPA Mediates Recruitment of MRX to Forks and Double-Strand Breaks to Hold Sister Chromatids Together. Mol. Cell *64*, 951–966.

Selmecki, A.M., Maruvka, Y.E., Richmond, P.A., Guillet, M., Shoresh, N., Sorenson, A.L., De, S., Kishony, R., Michor, F., Dowell, R., et al. (2015). Polyploidy can drive rapid adaptation in yeast. Nature *519*, 349–352.

Seol, J.H., Shim, E.Y., and Lee, S.E. (2018). Microhomology-mediated end joining: Good, bad and ugly. Mutat. Res. - Fundam. Mol. Mech. Mutagen. *809*, 81–87.

Serrano, D., and D'Amours, D. (2016). Checkpoint adaptation: Keeping Cdc5 in the T-loop. Cell Cycle *15*, 3339–3340.

Sfeir, A., and Symington, L.S. (2015). Microhomology-Mediated End Joining: A Back-up Survival Mechanism or Dedicated Pathway? Trends Biochem. Sci. *40*, 701–714.

Sheltzer, J.M., Blank, H.M., Pfau, S.J., Tange, Y., George, B.M., Humpton, T.J., Brito, I.L., Hiraoka, Y., Niwa, O., and Amon, A. (2011). Aneuploidy drives genomic instability in yeast. Science (80-.). *333*, 1026–1030.

Sheltzer, J.M., Ko, J.H., Replogle, J.M., Habibe Burgos, N.C., Chung, E.S., Meehl, C.M., Sayles, N.M., Passerini, V., Storchova, Z., and Amon, A. (2017). Single-chromosome Gains Commonly Function as Tumor Suppressors. Cancer Cell *31*, 240–255.

Shim, E.Y., Chung, W.H., Nicolette, M.L., Zhang, Y., Davis, M., Zhu, Z., Paull, T.T., Ira, G., and Lee, S.E. (2010). Saccharomyces cerevisiae Mre11/Rad50/Xrs2 and Ku proteins regulate association of Exo1 and Dna2 with DNA breaks. EMBO J. *29*, 3370–3380.

Shimada, K., Pasero, P., and Gasser, S.M. (2002). ORC and the intra-S-phase checkpoint: A threshold regulates Rad53p activation in S phase. Genes Dev. *16*, 3236–3252.

Shimada, K., Oma, Y., Schleker, T., Kugou, K., Ohta, K., Harata, M., and Gasser, S.M. (2008). Ino80 Chromatin Remodeling Complex Promotes Recovery of Stalled Replication Forks. Curr. Biol. *18*, 566–575.

Shinohara, M., Gasior, S.L., Bishop, D.K., and Shinohara, A. (2000). Tid1/Rdh54 promotes colocalization of Rad51 and Dmc1 during meiotic recombination. Proc. Natl. Acad. Sci. U. S. A. *97*, 10814–10819.

Shou, W., Azzam, R., Chen, S.L., Huddleton, M.J., Baskerville, C., Charbonneau, H., Annan, R.S., Carr, S.A., and Deshaies, R.J. (2002). Cdc5 influences phosphorylation of Net1 and disassembly of the RENT complex. BMC Mol. Biol. *3*.

Sia, R.A.L., Herald, H.A., and Lew, D.J. (1996). Cdc28 tyrosine phosphorylation and the morphogenesis checkpoint in budding yeast. Mol. Biol. Cell *7*, 1657–1666.

Sidera, K., and Patsavoudi, E. (2013). HSP90 Inhibitors: Current Development and Potential in Cancer Therapy. Recent Pat. Anticancer. Drug Discov. *9*, 1–20.

Signon, L., Malkova, A., Naylor, M.L., Klein, H., and Haber, J.E. (2001). Genetic Requirements for RAD51- andRAD54-Independent Break-Induced Replication Repair of a Chromosomal Double-Strand Break. Mol. Cell. Biol. *21*, 2048–2056.

Sikorski, R.S., and Hieter, P. (1989). A system of shuttle vectors and yeast host strains designed for efficient manipulation of DNA in Saccharomyces cerevisiae. Genetics *122*, 19–27.

Silva, E., and Ideker, T. (2019). Transcriptional responses to DNA damage. DNA Repair (Amst). *79*, 40–49.

Simsek, D., Brunet, E., Wong, S.Y.W., Katyal, S., Gao, Y., McKinnon, P.J., Lou, J., Zhang, L., Li, J., Rebar, E.J., et al. (2011). DNA ligase III promotes alternative nonhomologous end-joining during chromosomal translocation formation. PLoS Genet. *7*.

Sinha, D., Duijf, P.H.G., and Khanna, K.K. (2019). Mitotic slippage: an old tale with a new twist. Cell Cycle *18*, 7–15.

Sinha, S., Villarreal, D., Shim, E.Y., and Lee, S.E. (2016). Risky business: Microhomology-mediated end joining. Mutat. Res. - Fundam. Mol. Mech. Mutagen. *788*, 17–24.

Smail, B.A., Clifton, B.E., Mizuuchi, R., and Lehman, N. (2019). Spontaneous advent of genetic diversity in RNA populations through multiple recombination mechanisms. Rna *25*, 453–464.

Smets, B., De Snijder, P., Engelen, K., Joossens, E., Ghillebert, R., Thevissen, K., Marchal, K., and Winderickx, J. (2008). Genome-wide expression analysis reveals TORC1-dependent and -independent functions of Sch9. FEMS Yeast Res. *8*, 1276–1288.

Smith, C.E., Llorente, B., and Symington, L.S. (2007). Template switching during break-induced replication. Nature *447*, 102–105.

Smith, C.E., Lam, A.F., and Symington, L.S. (2009). Aberrant Double-Strand Break Repair Resulting in Half Crossovers in Mutants Defective for Rad51 or the DNA Polymerase δ Complex.

Mol. Cell. Biol. *29*, 1432–1441.

Smith, J., Mun Tho, L., Xu, N., and A. Gillespie, D. (2010). The ATM-Chk2 and ATR-Chk1 pathways in DNA damage signaling and cancer. In Advances in Cancer Research, pp. 73–112.

Sobinoff, A.P., and Pickett, H.A. (2020). Mechanisms that drive telomere maintenance and recombination in human cancers. Curr. Opin. Genet. Dev. *60*, 25–30.

Song, B., Liu, X.S., Rice, S.J., Kuang, S., Elzey, B.D., Konieczny, S.F., Ratliff, T.L., Hazbun, T., Chiorean, E.G., and Liu, X. (2013). Plk1 phosphorylation of Orc2 and Hbo1 contributes to gemcitabine resistance in pancreatic cancer. Mol. Cancer Ther. *12*, 58–68.

Speicher, M.R., Antonarakis, S.E., and Motulsky, A.G. (2010). Vogel and Motulsky's human genetics: Problems and approaches (fourth edition) (Berlin, Heidelberg: Springer Berlin Heidelberg).

Spiegelberg, D., Abramenkovs, A., Mortensen, A.C.L., Lundsten, S., Nestor, M., and Stenerlöw, B. (2020). The HSP90 inhibitor Onalespib exerts synergistic anti-cancer effects when combined with radiotherapy: an in vitro and in vivo approach. Sci. Rep. *10*, 5923.

St-Pierre, J., Douziech, M., Bazile, F., Pascariu, M., Bonneil, É., Sauvé, V., Ratsima, H., and D'Amours, D. (2009). Polo Kinase Regulates Mitotic Chromosome Condensation by Hyperactivation of Condensin DNA Supercoiling Activity. Mol. Cell *34*, 416–426.

Štafa, A., Donnianni, R.A., Timashev, L.A., Lam, A.F., and Symington, L.S. (2014). Template switching during break-induced replication is promoted by the mph1 helicase in Saccharomyces cerevisiae. Genetics *196*, 1017–1028.

Stephens, P.J., Greenman, C.D., Fu, B., Yang, F., Bignell, G.R., Mudie, L.J., Pleasance, E.D., Lau, K.W., Beare, D., Stebbings, L.A., et al. (2011). Massive genomic rearrangement acquired in a single catastrophic event during cancer development. Cell *144*, 27–40.

Stingele, J., Bellelli, R., and Boulton, S.J. (2017). Mechanisms of DNA-protein crosslink repair. Nat. Rev. Mol. Cell Biol. *18*, 563–573.

Stingele, S., Stoehr, G., Peplowska, K., Cox, J., Mann, M., and Storchova, Z. (2012). Global analysis of genome, transcriptome and proteome reveals the response to aneuploidy in human cells. Mol. Syst. Biol. *8*.

Stone, N.R.H., Rhodes, J., Fisher, M.C., Mfinanga, S., Kivuyo, S., Rugemalila, J., Segal, E.S., Needleman, L., Molloy, S.F., Kwon-Chung, J., et al. (2019). Dynamic ploidy changes drive fluconazole resistance in human cryptococcal meningitis. J. Clin. Invest. *129*, 999–1014.

Storchova, Z. (2014). Ploidy changes and genome stability in yeast. Yeast *31*, 421–430.

Storchova, Z. (2018). Evolution of aneuploidy: Overcoming the original CIN. Genes Dev. *32*, 1459–1460.

Storici, F., Bebenek, K., Kunkel, T.A., Gordenin, D.A., and Resnick, M.A. (2007). RNA-templated DNA repair. Nature *447*, 338–341.

Strebhardt, K., and Ullrich, A. (2006). Targeting polo-like kinase 1 for cancer therapy. Nat. Rev. Cancer *6*, 321–330.

Sturgill, T.W., Cohen, A., Diefenbacher, M., Trautwein, M., Martin, D.E., and Hall, M.N. (2008). TOR1 and TOR2 have distinct locations in live cells. Eukaryot. Cell *7*, 1819–1830.

Su, K.H., and Dai, C. (2017). mTORC1 senses stresses: Coupling stress to proteostasis.

BioEssays *39*, 1600268.

Su, K.H., Cao, J., Tang, Z., Dai, S., He, Y., Sampson, S.B., Benjamin, I.J., and Dai, C. (2016). HSF1 critically attunes proteotoxic stress sensing by mTORC1 to combat stress and promote growth. Nat. Cell Biol. *18*, 527–539.

Suda, K., Kaneko, A., Shimobayashi, M., Nakashima, A., Tatsuya, M., Hall, M.N., and Ushimaru, T. (2019). TORC1 regulates autophagy induction in response to proteotoxic stress in yeast and human cells. Biochem. Biophys. Res. Commun. *511*, 434–439.

Sudhan, D.R., Guerrero-Zotano, A., Won, H., González Ericsson, P., Servetto, A., Huerta-Rosario, M., Ye, D., Lee, K. min, Formisano, L., Guo, Y., et al. (2020). Hyperactivation of TORC1 Drives Resistance to the Pan-HER Tyrosine Kinase Inhibitor Neratinib in HER2-Mutant Cancers. Cancer Cell *37*, 183-199.e5.

Sugawara, N., Ira, G., and Haber, J.E. (2000). DNA length dependence of the single-strand annealing pathway and the role of Saccharomyces cerevisiae RAD59 in double-strand break repair. Mol. Cell. Biol. *20*, 5300–5309.

Sugawara, N., Wang, X., and Haber, J.E. (2003). In vivo roles of Rad52, Rad54, and Rad55 proteins in Rad51-mediated recombination. Mol. Cell *12*, 209–219.

Sun, Z., Fay, D.S., Marini, F., Foiani, M., and Stern, D.F. (1996). Spk1/Rad53 is regulated by Mec1-dependent protein phosphorylation in DNA replication and damage checkpoint pathways. Genes Dev. *10*, 395–406.

Sung, P. (1997). Yeast Rad55 and Rad57 proteins form a heterodimer that functions with replication protein A to promote DNA strand exchange by Rad51 recombinase. Genes Dev. *11*, 1111–1121.

Sweeney, F.D., Yang, F., Chi, A., Shabanowitz, J., Hunt, D.F., and Durocher, D. (2005). Saccharomyces cerevisiae Rad9 acts as a Mec1 adaptor to allow Rad53 activation. Curr. Biol. *15*, 1364–1375.

Swift, L.H., and Golsteyn, R.M. (2014). Genotoxic anti-cancer agents and their relationship to DNA damage, mitosis, and checkpoint adaptation in proliferating cancer cells. Int. J. Mol. Sci. *15*, 3403–3431.

Swift, L.H., and Golsteyn, R.M. (2016). Cytotoxic amounts of cisplatin induce either checkpoint adaptation or apoptosis in a concentration-dependent manner in cancer cells. Biol. Cell *108*, 127–148.

Syljuåsen, R.G. (2007). Checkpoint adaptation in human cells. Oncogene *26*, 5833–5839.

Syljuåsen, R.G., Jensen, S., Bartek, J., and Lukas, J. (2006). Adaptation to the ionizing radiation-induced G2 checkpoint occurs in human cells and depends on checkpoint kinase 1 and polo-like kinase 1 kinases. Cancer Res. *66*, 10253–10257.

Symington, L.S. (2016). Mechanism and regulation of DNA end resection in eukaryotes. Crit. Rev. Biochem. Mol. Biol. *51*, 195–212.

Symington, L.S., and Gautier, J. (2011). Double-Strand Break End Resection and Repair Pathway Choice. Annu. Rev. Genet. *45*, 247–271.

Symington, L.S., Rothstein, R., and Lisby, M. (2014). Mechanisms and regulation of mitotic recombination in saccharomyces cerevisiae. Genetics *198*, 795–835.

Syrovatkina, V., and Tran, P.T. (2015). Loss of kinesin-14 results in aneuploidy via kinesin-5-dependent microtubule protrusions leading to chromosome cut. Nat. Commun. *6*.

Talarek, N., Gueydon, E., and Schwob, E. (2017). Homeostatic control of start through negative feedback between Cln3-Cdk1 and Rim15/greatwall kinase in budding yeast. Elife *6*.

Tang, Y.C., Williams, B.R., Siegel, J.J., and Amon, A. (2011). Identification of aneuploidy-selective antiproliferation compounds. Cell *144*, 499–512.

Tao, R., Xue, H., Zhang, J., Liu, J., Deng, H., and Chen, Y.-G. (2013). Deacetylase Rpd3 Facilitates Checkpoint Adaptation by Preventing Rad53 Overactivation. Mol. Cell. Biol. *33*, 4212–4224.

Tartaglia, N.R., Howell, S., Sutherland, A., Wilson, R., and Wilson, L. (2010). A review of trisomy X (47,XXX). Orphanet J. Rare Dis. *5*.

Taxis, C., and Knop, M. (2006). System of centromeric, episomal, and integrative vectors based on drug resistance markers for Saccharomyces cerevisiae. Biotechniques *40*, 73–78.

Taylor, A.M., Shih, J., Ha, G., Gao, G.F., Zhang, X., Berger, A.C., Schumacher, S.E., Wang, C., Hu, H., Liu, J., et al. (2018). Genomic and Functional Approaches to Understanding Cancer Aneuploidy. Cancer Cell *33*.

Teng, S.C., Kim, B., and Gabriel, A. (1996). Retrotransposon reverse-transcriptase-mediated repair of chromosomal breaks. Nature *383*, 641–644.

Thorburn, R.R., Gonzalez, C., Brar, G.A., Christen, S., Carlile, T.M., Ingolia, N.T., Sauer, U., Weissman, J.S., and Amon, A. (2013). Aneuploid yeast strains exhibit defects in cell growth and passage through START. Mol. Biol. Cell *24*, 1274–1289.

Tian, T., Li, X., and Zhang, J. (2019). mTOR signaling in cancer and mtor inhibitors in solid tumor targeting therapy. Int. J. Mol. Sci. *20*.

Tittel-Elmer, M., Alabert, C., Pasero, P., and Cobb, J.A. (2009). The MRX complex stabilizes the replisome independently of the S phase checkpoint during replication stress. EMBO J. *28*, 1142–1156.

Toczyski, D.P., Galgoczy, D.J., and Hartwell, L.H. (1997). CDC5 and CKII control adaptation to the yeast DNA damage checkpoint. Cell *90*, 1097–1106.

Tomkinson, A.E., Ramos, W., Bardwell, A.J., Tappe, N., and Friedberg, E.C. (1994). Purification of Rad1 Protein from Saccharomyces cerevisiae and Further Characterization of the Rad1/Rad 10 Endonuclease Complex. Biochemistry *33*, 5305–5311.

Torres, E.M., Sokolsky, T., Tucker, C.M., Chan, L.Y., Boselli, M., Dunham, M.J., and Amon, A. (2007). Effects of Aneuploidy on Cellular Physiology and Cell Division in Haploid Yeast. Science (80-.). *317*, 916–924.

Torres, E.M., Dephoure, N., Panneerselvam, A., Tucker, C.M., Whittaker, C.A., Gygi, S.P., Dunham, M.J., and Amon, A. (2010). Identification of aneuploidy-tolerating mutations. Cell *143*, 71–83.

Torres, E.M., Springer, M., and Amon, A. (2016). No current evidence for widespread dosage compensation in S. Cerevisiae. Elife *5*, 1–19.

Travesa, A., Kuo, D., De Bruin, R.A.M., Kalashnikova, T.I., Guaderrama, M., Thai, K., Aslanian, A., Smolka, M.B., Yates, J.R., Ideker, T., et al. (2012). DNA replication stress differentially

regulates G1/S genes via Rad53-dependent inactivation of Nrm1. EMBO J. *31*, 1811–1822.

Truong, L.N., Li, Y., Shi, L.Z., Hwang, P.Y.H., He, J., Wang, H., Razavian, N., Berns, M.W., and Wu, X. (2013). Microhomology-mediated End Joining and Homologous Recombination share the initial end resection step to repair DNA double-strand breaks in mammalian cells. Proc. Natl. Acad. Sci. U. S. A. *110*, 7720–7725.

Tsai, H.J., and Nelliat, A. (2019). A double-edged sword: Aneuploidy is a prevalent strategy in fungal adaptation. Genes (Basel). *10*, 787.

Tsai, H.J., Nelliat, A.R., Choudhury, M.I., Kucharavy, A., Bradford, W.D., Cook, M.E., Kim, J., Mair, D.B., Sun, S.X., Schatz, M.C., et al. (2019). Hypo-osmotic-like stress underlies general cellular defects of aneuploidy. Nature *570*, 117–121.

Tsang, C.K., Chen, M., Cheng, X., Qi, Y., Chen, Y., Das, I., Li, X., Vallat, B., Fu, L.W., Qian, C.N., et al. (2018). SOD1 Phosphorylation by mTORC1 Couples Nutrient Sensing and Redox Regulation. Mol. Cell *70*, 502-515.e8.

Tsukamoto, Y., Mitsuoka, C., Terasawa, M., Ogawa, H., and Ogawa, T. (2005). Xrs2p regulates Mre11p translocation to the nucleus and plays a role in telomere elongation and meiotic recombination. Mol. Biol. Cell *16*, 597–608.

Tsurutani, J., Nitta, T., Hirashima, T., Komiya, T., Uejima, H., Tada, H., Syunichi, N., Tohda, A., Fukuoka, M., and Nakagawa, K. (2002). Point mutations in the topoisomerase I gene in patients with non-small cell lung cancer treated with irinotecan. Lung Cancer *35*, 299–304.

Tubbs, A., and Nussenzweig, A. (2017). Endogenous DNA Damage as a Source of Genomic Instability in Cancer. Cell *168*, 644–656.

Ueda, S., Ozaki, R., Kaneko, A., Akizuki, R., Katsuta, H., Miura, A., Matsuura, A., and Ushimaru, T. (2019). TORC1, Tel1/Mec1, and Mpk1 regulate autophagy induction after DNA damage in budding yeast. Cell. Signal. *62*, 109344.

Urban, J., Soulard, A., Huber, A., Lippman, S., Mukhopadhyay, D., Deloche, O., Wanke, V., Anrather, D., Ammerer, G., Riezman, H., et al. (2007). Sch9 Is a Major Target of TORC1 in Saccharomyces cerevisiae. Mol. Cell *26*, 663–674.

Valencia-Burton, M., Oki, M., Johnson, J., Seier, T.A., Kamakaka, R., and Haber, J.E. (2006). Different mating-type-regulated genes affect the DNA repair defects of saccharomyces RAD51, RAD52 and RAD55 mutants. Genetics *174*, 41–55.

Valencia, M., Bentele, M., Vaze, M.B., Herrmann, G., Kraus, E., Lee, S.E., Schär, P., and Haber, J.E. (2001). NEJ1 controls non-homologous end joining in Saccharomyces cerevisiae. Nature *414*, 666–669.

Valerio-Santiago, M., de los Santos-Velázquez, A.I., and Monje-Casas, F. (2013). Inhibition of the Mitotic Exit Network in Response to Damaged Telomeres. PLoS Genet. *9*.

Vaze, M.B., Pellicioli, A., Lee, S.E., Ira, G., Liberi, G., Arbel-Eden, A., Foiani, M., and Haber, J.E. (2002). Recovery from checkpoint-mediated arrest after repair of a double-strand break requires Srs2 helicase. Mol. Cell *10*, 373–385.

Venkitaraman, A.R. (2019). How do mutations affecting the breast cancer genes BRCA1 and BRCA2 cause cancer susceptibility? DNA Repair (Amst). *81*.

Vernieri, C., Chiroli, E., Francia, V., Gross, F., and Ciliberto, A. (2013). Adaptation to the spindle checkpoint is regulated by the interplay between Cdc28/Clbs and PP2ACdc55. J. Cell Biol. *202*,

765–778.

Vidanes, G.M., Sweeney, F.D., Galicia, S., Cheung, S., Doyle, J.P., Durocher, D., and Toczyski, D.P. (2010). CDC5 inhibits the hyperphosphorylation of the checkpoint kinase Rad53, leading to checkpoint adaptation. PLoS Biol. *8*.

Voordeckers, K., Kominek, J., Das, A., Espinosa-Cantú, A., De Maeyer, D., Arslan, A., Van Pee, M., van der Zande, E., Meert, W., Yang, Y., et al. (2015). Adaptation to High Ethanol Reveals Complex Evolutionary Pathways. PLoS Genet. *11*, e1005635.

Wall, M.E., and Wani, M.C. (1995). Camptothecin and Taxol: Discovery to Clinic—Thirteenth Bruce F. Cain Memorial Award Lecture. Cancer Res. *55*, 753–760.

Wang, H., Liu, D., Wang, Y., Qin, J., and Elledge, S.J. (2001). Pds1 phosphorylation in response to DNA damage is essential for its DNA damage checkpoint function. Genes Dev. *15*, 1361–1372.

Wang, H., Rosidi, B., Perrault, R., Wang, M., Zhang, L., Windhofer, F., and Iliakis, G. (2005). DNA ligase III as a candidate component of backup pathways of nonhomologous end joining. Cancer Res. *65*, 4020–4030.

Wang, H., Qiu, Z., Liu, B., Wu, Y., Ren, J., Liu, Y., Zhao, Y., Wang, Y., Hao, S., Li, Z., et al. (2018). PLK1 targets CtIP to promote microhomology-mediated end joining. Nucleic Acids Res. *46*, 10724–10739.

Wang, W., Daley, J.M., Kwon, Y., Krasner, D.S., and Sung, P. (2017). Plasticity of the Mre11-Rad50-Xrs2-Sae2 nuclease ensemble in the processing of DNA-bound obstacles. Genes Dev. *31*, 2331–2336.

Wang, Z., Song, Y., Li, S., Kurian, S., Xiang, R., Chiba, T., and Wu, X. (2019). DNA polymerase (POLQ) is important for repair of DNA double-strand breaks caused by fork collapse. J. Biol. Chem. *294*, 3909–3919.

Wanke, V., Cameroni, E., Uotila, A., Piccolis, M., Urban, J., Loewith, R., and De Virgilio, C. (2008). Caffeine extends yeast lifespan by targeting TORC1. Mol. Microbiol. *69*, 277–285.

Wanrooij, P.H., and Burgers, P.M. (2015). Yet another job for Dna2: Checkpoint activation. DNA Repair (Amst). *32*, 17–23.

Warren, J.J., Forsberg, L.J., and Beese, L.S. (2006). The structural basis for the mutagenicity of O6-methyl-guanine lesions. Proc. Natl. Acad. Sci. U. S. A. *103*, 19701–19706.

Wee, S., Jagani, Z., Kay, X.X., Loo, A., Dorsch, M., Yao, Y.M., Sellers, W.R., Lengauer, C., and Stegmeier, F. (2009). PI3K pathway activation mediates resistance to MEK inhibitors in KRAS mutant cancers. Cancer Res. *69*, 4286–4293.

Wei, L., Nakajima, S., Böhm, S., Bernstein, K.A., Shen, Z., Tsang, M., Levine, A.S., and Lan, L. (2015). DNA damage during the G0/G1 phase triggers RNA-templated, Cockayne syndrome B-dependent homologous recombination. Proc. Natl. Acad. Sci. U. S. A. *112*, E3495–E3504.

Weinert, T.E.D.A., and Hartwell, L.H. (1988). The RAD9 Gene Controls the Cell Cycle Response to DNA Damage in Saccharomyces cerevisiae. Science (80-.). *241*, 317–241.

Weinert, T.A., Kiser, G.L., Hartwell, L.H., Kiset, G.L., and Hartwelp, L.H. (1994). Mitotic checkpoint eenes in budding yeast and the dependence of mitosis on DNA replication and repair. Genes Dev. *8*, 652–665.

Weisman, R. (2016). Target of Rapamycin (TOR) Regulates Growth in Response to Nutritional Signals. In Microbiology Spectrum, (American Society of Microbiology), pp. 535–548.

Welty, S., Teng, Y., Liang, Z., Zhao, W., Sanders, L.H., Greenamyre, J.T., Rubio, M.E., Thathiah, A., Kodali, R., Wetzel, R., et al. (2018). RAD52 is required for RNA-templated recombination repair in post-mitotic neurons. J. Biol. Chem. *293*, 1353–1362.

Weyburne, E.S., Wilkins, O.M., Sha, Z., Williams, D.A., Pletnev, A.A., de Bruin, G., Overkleeft, H.S., Goldberg, A.L., Cole, M.D., and Kisselev, A.F. (2017). Inhibition of the Proteasome β2 Site Sensitizes Triple-Negative Breast Cancer Cells to β5 Inhibitors and Suppresses Nrf1 Activation. Cell Chem. Biol. *24*, 218–230.

Williams, B.R., Prabhu, V.R., Hunter, K.E., Glazier, C.M., Whittaker, C.A., Housman, D.E., and Amon, A. (2008). Aneuploidy affects proliferation and spontaneous immortalization in mammalian cells. Science (80-.). *322*, 703–709.

Wilson, M.A., Kwon, Y., Xu, Y., Chung, W.H., Chi, P., Niu, H., Mayle, R., Chen, X., Malkova, A., Sung, P., et al. (2013). Pif1 helicase and Polδ promote recombination-coupled DNA synthesis via bubble migration. Nature *502*, 393–396.

Wilson, T.E., Grawunder, U., and Lieber, M.R. (1997). Yeast DNA ligase IV mediates non-homologous DNA end joining. Nature *388*, 495–498.

Winston, F., Dollard, C., and Ricupero-Hovasse, S.L. (1995). Construction of a set of convenient saccharomyces cerevisiae strains that are isogenic to S288C. Yeast *11*, 53–55.

Workman, J.J., Chen, H., and Nicholas Laribee, R. (2016). Saccharomyces cerevisiae TORC1 controls histone acetylation by signaling through the sit4/PP6 phosphatase to regulate sirtuin deacetylase nuclear accumulation. Genetics *203*, 1733–1746.

Wullschleger, S., Loewith, R., and Hall, M.N. (2006). TOR signaling in growth and metabolism. Cell *124*, 471–484.

Xie, A., Kwok, A., and Scully, R. (2009). Role of mammalian Mre11 in classical and alternative nonhomologous end joining. Nat. Struct. Mol. Biol. *16*, 814–818.

Xie, X., Hu, H., Tong, X., Li, L., Liu, X., Chen, M., Yuan, H., Xie, X., Li, Q., Zhang, Y., et al. (2018). The mTOR-S6K pathway links growth signalling to DNA damage response by targeting RNF168. Nat. Cell Biol. *20*, 320–331.

Xu, G., Chapman, J.R., Brandsma, I., Yuan, J., Mistrik, M., Bartkova, J., Gogola, E., Warmerdam, D., Barazas, M., Celie, N., et al. (2015). REV7 counteracts DNA double-strand break resection and impacts PARP inhibition.

Xu, Z., Han, X., Ou, D., Liu, T., Li, Z., Jiang, G., Liu, J., and Zhang, J. (2020). Targeting PI3K/AKT/mTOR-mediated autophagy for tumor therapy. Appl. Microbiol. Biotechnol. *104*, 575–587.

Yang, F., Teoh, F., Tan, A.S.M., Cao, Y., Pavelka, N., Berman, J., and Malik, H. (2019). Aneuploidy Enables Cross-Adaptation to Unrelated Drugs. Mol. Biol. Evol. *36*, 1768–1782.

Yeap, L.S., and Meng, F.L. (2019). Cis- and trans-factors affecting AID targeting and mutagenic outcomes in antibody diversification. In Advances in Immunology, pp. 51–103.

Yelamanchi, S.K., Veis, J., Anrather, D., Klug, H., and Ammerer, G. (2014). Genotoxic Stress Prevents Ndd1-Dependent Transcriptional Activation of G2/M-Specific Genes in Saccharomyces cerevisiae. Mol. Cell. Biol. *34*, 711–724.

Yeung, M.T., and Durocher, D. (2011). Srs2 enables checkpoint recovery by promoting disassembly of DNA damage foci from chromatin. DNA Repair (Amst). *10*, 1213–1222.

Yona, A.H., Manor, Y.S., Herbst, R.H., Romano, G.H., Mitchell, A., Kupiec, M., Pilpel, Y., and Dahan, O. (2012). Chromosomal duplication is a transient evolutionary solution to stress. Proc. Natl. Acad. Sci. U. S. A. *109*, 21010–21015.

Yoo, H.Y., Kumagai, A., Shevchenko, A., Shevchenko, A., and Dunphy, W.G. (2004). Adaptation of a DNA replication checkpoint response depends upon inactivation of Claspin by the Polo-like kinase. Cell *117*, 575–588.

Yorimitsu, T., Zaman, S., Broach, J.R., and Klionsky, D.J. (2007). Protein kinase A and Sch9 cooperatively regulate induction of autophagy in Saccharomyces cerevisiae. Mol. Biol. Cell *18*, 4180–4189.

Yorimitsu, T., He, C., Wang, K., and Klionsky, D.J. (2009). Tap42-associated protein phosphatase type 2A negatively regulates induction of autophagy. Autophagy *5*, 616–624.

Yoshida, S., Kono, K., Lowery, D.M., Bartolini, S., Yaffe, M.B., Ohya, Y., and Pellman, D. (2006). Polo-like kinase Cdc5 controls the local activation of Rho1 to promote cytokinesis. Science (80-.). *313*, 108–111.

Young, J.C., Agashe, V.R., Siegers, K., and Hartl, F.U. (2004). Pathways of chaperone-mediated protein folding in the cytosol. Nat. Rev. Mol. Cell Biol. *5*, 781–791.

Yousefzadeh, M.J., Wyatt, D.W., Takata, K. ichi, Mu, Y., Hensley, S.C., Tomida, J., Bylund, G.O., Doublié, S., Johansson, E., Ramsden, D.A., et al. (2014). Mechanism of Suppression of Chromosomal Instability by DNA Polymerase POLQ. PLoS Genet. *10*.

Yu, X., and Gabriel, A. (1999). Patching broken chromosomes with extranuclear cellular DNA. Mol. Cell *4*, 873–881.

Zack, T.I., Schumacher, S.E., Carter, S.L., Cherniack, A.D., Saksena, G., Tabak, B., Lawrence, M.S., Zhang, C.Z., Wala, J., Mermel, C.H., et al. (2013). Pan-cancer patterns of somatic copy number alteration. Nat. Genet. *45*, 1134–1140.

Zaim, J., Speina, E., and Kierzek, A.M. (2005). Identification of new genes regulated by the Crt1 transcription factor, an effector of the DNA damage checkpoint pathway in Saccharomyces cerevisiae. J. Biol. Chem. *280*, 28–37.

Zalcberg, J., Hu, X.F., Slater, A., Parisot, J., El-Osta, S., Kantharidis, P., Chou, S.T., and Parkin, J.D. (2000). MRP1 not MDR1 gene expression is the predominant mechanism of acquired multidrug resistance in two prostate carcinoma cell lines. Prostate Cancer Prostatic Dis. *3*, 66–75.

Zeman, M.K., and Cimprich, K.A. (2014). Causes and consequences of replication stress. Nat. Cell Biol. *16*, 2–9.

Zeng, Y., Forbes, K.C., Wu, Z., Moreno, S., Piwnica-Worms, H., and Enoch, T. (1998). Replication checkpoint requires phosphorylation of the phosphatase Cdc25 by Cds1 or Chk1. Nature *395*, 507–510.

Zhang, Y., and Jasin, M. (2011). An essential role for CtIP in chromosomal translocation formation through an alternative end-joining pathway. Nat. Struct. Mol. Biol. *18*, 80–85.

Zhang, C., Xu, Y., Wang, H., Li, G., Yan, H., Fei, Z., Xu, Y., and Li, W. (2018). Curcumin reverses irinotecan resistance in colon cancer cell by regulation of epithelial-mesenchymal

transition. Anticancer. Drugs *29*, 334–340.

Zhang, T., Nirantar, S., Lim, H.H., Sinha, I., and Surana, U. (2009). DNA Damage Checkpoint Maintains Cdh1 in an Active State to Inhibit Anaphase Progression. Dev. Cell *17*, 541–551.

Zhang, T., Péli-Gulli, M.P., Yang, H., De Virgilio, C., and Ding, J. (2012). Ego3 functions as a homodimer to mediate the interaction between Gtr1-Gtr2 and Ego1 in the EGO complex to activate TORC1. Structure *20*, 2151–2160.

Zhang, X., Linder, S., and Bazzaro, M. (2020). Drug development targeting the ubiquitin-proteasome system (UPS) for the treatment of human cancers. Cancers (Basel). *12*, 902.

Zhang, Y., Hefferin, M.L., Chen, L., Shim, E.Y., Tseng, H.M., Kwon, Y., Sung, P., Lee, S.E., and Tomkinson, A.E. (2007). Role of Dnl4-Lif1 in nonhomologous end-joining repair complex assembly and suppression of homologous recombination. Nat. Struct. Mol. Biol. *14*, 639–646.

Zhao, X., and Rothstein, R. (2002). The Dun1 checkpoint kinase phosphorylates and regulates the ribonucleotide reductase inhibitor Sml1. Proc. Natl. Acad. Sci. U. S. A. *99*, 3746–3751.

Zheng, M., Wang, Y.H., Wu, X.N., Wu, S.Q., Lu, B.J., Dong, M.Q., Zhang, H., Sun, P., Lin, S.C., Guan, K.L., et al. (2011). Inactivation of Rheb by PRAK-mediated phosphorylation is essential for energy-depletion-induced suppression of mTORC1. Nat. Cell Biol. *13*, 263–272.

Zhou, Z., and Elledge, S.J. (1993). DUN1 encodes a protein kinase that controls the DNA damage response in yeast. Cell *75*, 1119–1127.

Zhu, J., Pavelka, N., Bradford, W.D., Rancati, G., and Li, R. (2012). Karyotypic determinants of chromosome instability in Aneuploid budding yeast. PLoS Genet. *8*.

Zhu, J., Tsai, H.J., Gordon, M.R., and Li, R. (2018). Cellular Stress Associated with Aneuploidy. Dev. Cell *44*, 420–431.

Zinzalla, V., Graziola, M., Mastriani, A., Vanoni, M., and Alberghina, L. (2007). Rapamycin-mediated G1 arrest involves regulation of the Cdk inhibitor Sic1 in Saccharomyces cerevisiae. Mol. Microbiol. *63*, 1482–1494.

Zou, L., and Elledge, S.J. (2003). Sensing DNA damage through ATRIP recognition of RPA-ssDNA complexes. Science (80-.). *300*, 1542–1548.

Zuco, V., De Cesare, M., Zaffaroni, N., Lanzi, C., and Cassinelli, G. (2015). PLK1 is a critical determinant of tumor cell sensitivity to CPT11 and its inhibition enhances the drug antitumor efficacy in squamous cell carcinoma models sensitive and resistant to camptothecins. Oncotarget *6*, 8736–8749.

References

Acknowlegdement

Curriculum Vitae